TESIS DE LA UNIVERSIDAD DE ZARAGOZA

2024

200

Guillermo Landa Baila

Development of Nanosystems Based on Molecules of Biological Origin for the Monitoring and Treatment of Bacterial Infections

Director/es

Arruebo Gordo, Manuel

Mendoza Cantos, Gracia María

ISSN 2254-7606

Prensas de la Universidad Universidad Zaragoza

Universidad de Zaragoza
Servicio de Publicaciones

ISSN 2254-7606

Universidad Zaragoza
1542

Tesis Doctoral

DEVELOPMENT OF NANOSYSTEMS BASED ON MOLECULES OF BIOLOGICAL ORIGIN FOR THE MONITORING AND TREATMENT OF BACTERIAL INFECTIONS

Autor

Guillermo Landa Baila

Director/es

Arruebo Gordo, Manuel
Mendoza Cantos, Gracia María

UNIVERSIDAD DE ZARAGOZA
Escuela de Doctorado

Programa de Doctorado en Ingeniería Química y del Medio Ambiente

2024

Universidad Zaragoza
1542

Tesis Doctoral

Development of Nanosystems Based on Molecules of Biological Origin for the Monitoring and Treatment of Bacterial Infections

Autor

Guillermo Landa Baila

Directores

Manuel Arruebo Gordo
Gracia María Mendoza Cantos

Universidad de Zaragoza
2023

"Development of Nanosystems Based on Molecules of Biological Origin for the Monitoring and Treatment of Bacterial Infections"

A thesis conducted in the framework of a national research project funded by the Spanish Ministry of Economy, Industry and Competitiveness (grant number CTQ2017-84473-R) and carried out at the University of Zaragoza, Department of Chemical Engineering and Environmental Technologies

The author also acknowledges the financial support from the FPI program (PRE2018-085769) of the Spanish Ministry of Science, Innovation and Universities

Departamento de Ingeniería Química y Tecnologías del Medio Ambiente
Universidad Zaragoza

Supervisors

Dr. Manuel Arruebo Gordo, Professor in the Department of Chemical Engineering and Environmental Technologies, University of Zaragoza, Spain.

Dr. Gracia María Mendoza Cantos, Miguel Servet Researcher, Aragon Institute of Health Research (IIS Aragon), Zaragoza, Spain.

Dr. Manuel Arruebo Gordo,

Professor at the University of Zaragoza in the Department of Chemical Engineering and Environmental Technologies, and member of the Institute of Nanoscience of Aragon,

and **Dr. Gracia Mendoza Cantos**, Miguel Servet Researcher and member of the Aragon Institute of Health Research,

certify that,

the Doctoral thesis entitled:

"Development of Nanosystems Based on Molecules of Biological Origin for the Monitoring and Treatment of Bacterial Infections"

has been written by Mr. Guillermo Landa Baila under our supervision and has not been submitted in support of any other application for obtaining another official degree at this or at any other University. The research for this thesis was conducted at the laboratories of the Institute of Nanoscience and Materials of Aragon and the Biomedical Research Centre of Aragon, with the financial support from a national research project funded by the Spanish Ministry of Economy, Industry and Competitiveness (grant number CTQ2017-84473-R) and by the FPI program (PRE2018-085769) of the Spanish Ministry of Science, Innovation and Universities.

As so, we authorize and approve the presentation of this dissertation, in Zaragoza on November 06, 2023

Dr. Manuel Arruebo Gordo **Dr. Gracia María Mendoza Cantos**

Dr. Manuel Arruebo Gordo,

Catedrático en la Universidad de Zaragoza en el Departamento de Ingeniería Química y Tecnologías del Medio Ambiente, y miembro del Instituto de Nanociencia y Materiales de Aragón,

y la **Dra. Gracia Mendoza Cantos**,

Investigadora Miguel Servet y miembro del Instituto de Investigación Sanitaria de Aragón,

CERTIFICAN

Que la presente memoria titulada:

" Development of Nanosystems Based on Molecules of Biological Origin for the Monitoring and Treatment of Bacterial Infections "

ha sido escrita por D. Guillermo Landa Baila bajo nuestra supervisión y no ha sido presentada en apoyo de ninguna otra solicitud de grado en esta u otra universidad. La investigación para esta tesis se llevó a cabo en los laboratorios del Instituto de Nanociencia y Materiales de Aragón y el Centro de Investigación Biomédica de Aragón, con el respaldo económico de un proyecto de investigación nacional financiado por el Ministerio de Economía, Industria y Competitividad de España (número de subvención CTQ2017-84473-R) y gracias al apoyo del programa FPI (PRE2018-085769) del Ministerio de Ciencia, Innovación y Universidades.

Y para que así conste, firmamos este certificado en Zaragoza a 06 de noviembre de 2023.

Dr. Manuel Arruebo Gordo **Dra. Gracia María Mendoza Cantos**

Agradecimientos

Me gustaría dedicar unas palabras de profunda gratitud a las personas excepcionales que han hecho posible este trabajo.

A Manuel Arruebo, Gracia Mendoza y Silvia Irusta, por haber confiado en mí y haberme brindado esta inestimable oportunidad. Su generosidad y orientación han sido absolutamente esenciales en cada etapa de este viaje.

A mis compañeros de AMIB y del NFP por su dedicación y compañerismo, claves para haber alcanzado este logro juntos.

A mis padres, Víctor José y María Aránzazu, cuyo constante cariño y apoyo han sido fundamentales en todas las etapas de mi vida.

A cada uno de ustedes, les expreso mi más sincero agradecimiento por su contribución invaluable y su apoyo inquebrantable.

INDEX

Abbreviations

Abs	Absorbance
AMR	Antimicrobial Resistance
AuNPs	Gold Nanoparticles
BSA	Bovine Serum Albumin
CFU	Colony Forming Unit
CHXD	Chlorhexidine
CNPs	Colistin Nanoparticles
DCM	Dichloromethane
DDS	Drug Delivery Systems
DL	Drug Loading
DLS	Dynamic Light Scattering
DMEM	Dulbecco's Modified Eagle Medium
DMF	N, N-Dimethylformamide
EDS	Energy Dispersive Spectroscopy
EE	Encapsulation Efficiency
FAR NPs	Farnesol Nanoparticles
FTIR	Fourier-transform Infrared Spectroscopy
GFP	Green Fluorescent Protein
HAADF	High-Angle Annular Dark-Field Imaging
HPMC	Hydroxypropyl Methylcellulose
LPS	Lipopolysaccharide
LYS	Lysostaphin
MBC	Minimum Bactericidal Concentration
MHA	Mueller-Hinton Agar
MHB	Mueller-Hinton Broth
MIC	Minimum Inhibitory Concentration
MNPs	Metallic Nanoparticles
MRSA	Methicillin-resistant Staphylococcus aureus
NPs	Nanoparticles

PAH	Poly (allylamine hydrochloride)
PBS	Phosphate-Buffered Saline
PEG	Polyethylene glycol
PFA	Paraformaldehyde
PLGA	Poly (lactic-co-glycolic acid)
PNPs	Polymeric Nanoparticles
PSI	Post-Surgery and Infection
S100	EUDRAGIT® S 100
SA	Sialic Acid
SEM	Scanning Electron Microscopy
STEM	Scanning Transmission Electron Microscopy
TEM	Transmission Electron Microscopy
TFE	Tri-Fluoroethanol
THY	Thymol
TSA	Tryptic Soy Agar
TSB	Tryptic Soy Broth

Summary and objectives

The current doctoral thesis, entitled "*Development of nanosystems based on molecules of biological origin for the monitoring and treatment of bacterial infections*", has been conducted in the Department of Chemical Engineering and Environmental Technologies at the University of Zaragoza, Spain, within the Advanced Materials in Biomedicine (AMiB) research group. The research and experimental work were carried out at the Biomedical Research Center of Aragon (CIBA) and the Institute of Nanoscience and Materials of Aragón (INMA). Additionally, a predoctoral internship lasting 7 months was completed in the INSERM U1070 "Pharmacology of Antimicrobial Agents and Antibiotic Resistance" research group at the University of Poitiers (France). The doctoral studies and research conducted received support from a FPI predoctoral fellowship funded by the Spanish Ministry of Economy, Industry and Competitiveness (CTQ2017-84473-R).

In response to the relentless increase in bacterial resistance and the growing ineffectiveness of current antibiotics, a significant portion of contemporary research is ceaselessly dedicated to finding innovative antimicrobial therapies. Within this context, the primary goal of this thesis was to explore the potential of naturally occurring molecules with antimicrobial properties as an alternative to traditional antibiotics. The focus of this research is extended to the encapsulation of these molecules within nanostructured formulations, as well as their assessment for treating bacterial infections caused by *Staphylococcus aureus* and *Pseudomonas aeruginosa*. The selected antimicrobials, both in their free and encapsulated forms, were tested in a variety of scenarios. This included *in vitro* experiments involving planktonic cultures and bacterial biofilms, intracellular infection models within eukaryotic cells, and *in vivo* studies using a murine model of infected topical wound.

The secondary objective of this thesis was to develop effective methods for the detection and monitoring of pathogenic bacteria within the established models. Fluorescent and bioluminescent bacterial strains were utilized to obtain valuable insights into bacterial growth dynamics and the efficacy of treatments. This effort culminated in the development of a biosensor utilizing the unique optical properties of gold nanoparticles, enabling the detection, typing and quantification of bacteria in various biological samples.

The thesis is organized into several chapters, each of which presents a different part of the work conducted:

Chapter I provides a general introduction to the subject, presenting the background in which the thesis is framed. It introduces several key aspects, starting with bacterial infections. Next, it delves into the growing problem of rising antibiotic resistances, highlighting their potential alternatives. Lastly, it discusses the importance of drug delivery systems and the emerging field of nanotechnology developing promising applications in the context of bacterial infection treatments.

Chapter II presents a study on the bactericidal and antibiofilm effects of the natural antiseptic terpenes thymol and farnesol. These phytochemicals were tested individually and in combination with the standard antiseptic chlorhexidine, both *in vitro* and *in vivo*. To enhance their effectiveness and to apply it in a real setting, thymol was encapsulated within electrospun Eudragit® S100, a synthetic anionic copolymer, with the goal of developing an effective antimicrobial wound dressing. Conversely, farnesol was encapsulated in lipid micelles. *In vitro* studies revealed a significantly improved antibacterial efficacy when these compounds were utilized in combination, rather than separately. *In vivo* studies using an infected wound splinting murine model further validated the superior bactericidal effects of the proposed combination treatments. Infection progression and the evaluation of antimicrobial treatment outcomes were continuously monitored in real-time by making use of the bioluminescent *S. aureus* strain Xen36. The results of this chapter are included in the recently accepted article entitled "*Real-time in vivo monitoring of the antimicrobial action of combination therapies in the management of infected topical wounds***"** (**Landa, G.**; Miranda-Calderón, L.G.; Gómez, A.; Pérez, M.; Sebastián, V.; Arruebo, M.; Lamarche, I.; Tewes, F.; Irusta, S.; Mendoza, G. International Journal of Pharmaceutics, 2023, Volume 646, 123502, https://doi.org/10.1016/j.ijpharm.2023.123502).

Chapter III presents the establishment of an *in vitro* model of polymicrobial biofilms involving *S. aureus* and *P. aeruginosa*. This chapter highlights how the initial conditions of co-cultured bacteria had an enormous impact on the growth kinetics and on the inhibitory role of *P. aeruginosa* over *S. aureus* proliferation and metabolism. Once a satisfactory experimental model was developed, the antimicrobial activity of thymol and chlorhexidine was compared against both species in planktonic state, as well as in single and polymicrobial biofilms. Notably, it was observed lower bactericidal activity of chlorhexidine and thymol against *S. aureus* in the polymicrobial biofilm. This phenomenon was attributed to two key factors: the formation of a thicker mixed biofilm, which exceeds the total biomass of biofilms formed solely by *S. aureus* or *P. aeruginosa*, and a significant reduction in the metabolic activity of *S. aureus* induced by the presence of antimicrobial molecules produced by *P. aeruginosa*. The results of this chapter are included in a scientific article that will be submitted for publication soon, under the title "*Impact of mixed Staphylococcus aureus-Pseudomonas aeruginosa biofilms formation on resistance to antimicrobial treatment of chronically infected wounds*".

Chapter IV focused on the development of aerosolizable polymeric nanoparticulated carriers loaded with colistin, exploring four different methodologies for their synthesis: (i) the use of polylactic-co-glycolic (PLGA) nanoparticles prepared by single emulsion-solvent evaporation method as encapsulating matrix; (ii) encapsulation through nanoprecipitation with miscible solvents, utilizing PLGA-poly(ethylene glycol) (PEG) as the encapsulating matrix; (iii) colistin nanocoacervation in hydroxypropyl methylcellulose (HPMC) using the antisolvent precipitation method, followed by encapsulation within PLGA nanoparticles; and (iv) colistin encapsulation within PLGA microparticles using electrospraying. The most successful approach was

the antisolvent precipitation method (iii), which achieved the highest drug loading at 55 wt.% and produced particles with optimal aerodynamic properties (3-5 µm) for efficient pulmonary delivery. *In vitro* testing revealed a rapid release of colistin from this formulation. Furthermore, these particles exhibited enhanced antimicrobial efficacy in a biofilm model of the *Pseudomonas aeruginosa* PAO1 strain compared to equivalent doses of the free drug. The results of this chapter are included in the published article entitled "*Colistin-loaded aerosolizable particles for the treatment of bacterial respiratory infections*" (**Landa, G.**; Alejo, T.; Sauzet, T.; Laroche, J.; Sebastian, V.; Tewes, F.; Arruebo, M. International Journal of Pharmaceutics, 2023, Volume 635, 122732, https://doi.org/10.1016/j.ijpharm.2023.122732).

Chapter V introduces a novel antimicrobial formulation by encapsulating lysostaphin (LYS), an anti-staphylococci bacteriocin, within PLGA nanoparticles. The chapter assesses the antimicrobial activity of free LYS and LYS-loaded PLGA nanoparticles against different strains of *S. aureus* in planktonic, biofilm, and in an intracellular infection model. GFP-expressing *S. aureus* was employed to facilitate traceability. The results demonstrated a significant reduction in bacterial viability, both in planktonic and biofilm states, and in some cases, the complete eradication of bacteria. Notably, the *in vitro* intracellular infection model showcased the enhanced efficiency of the developed nanoparticles compared to free bacteriocin-based treatment. The content of this chapter is included in the recently submitted article entitled "*PLGA nanoparticle-encapsulated lysostaphin for the targeted treatment of Staphylococcus aureus Infections***"** (**Landa, G.**; Aguerri, L.; Irusta, S.; Mendoza, G.; Arruebo, M. Journal of Colloid and Interface Science. Submitted 2023).

Chapter VI details the development of a rapid optical whole-cell bacterial biosensor. This system utilized sialic acid-functionalized gold nanoparticles, taking advantage of the ability of pathogenic bacteria to integrate exogenous sialic acid. The interaction with bacteria caused the gold nanoparticles to aggregate. This was a result of the bacterial uptake of sialic acid for cell walls synthesis, resulting in a detectable change in their surface plasmon resonance and optical spectra. This system allowed for the selective screening of Gram-positive wild type *S. aureus* (ATCC 25923) and Methicillin-Resistant *S. aureus* (MRSA) USA300, as well as Gram-negative bacteria (*P. aeruginosa* ATCC 15442), by selecting the appropriate media. Discrimination of bacterial pathogens was conducted in different media, including water, two independent buffers, bacterial culture media, human serum, and human urine. High bacterial loads were required to provide a statistically significant optical pathogen identification in human serum, whereas it was not possible to detect the presence of bacteria at clinically relevant levels in urine. The content of this chapter has been adapted from the published article titled "*Selective point-of-care detection of pathogenic bacteria using sialic acid functionalized gold nanoparticles*" (**Landa, G.**; Miranda-Calderón, L.G.; Sebastián, V.; Irusta, S.; Mendoza, G.; Arruebo, M. Talanta, 2021, Volume 234, 122644, https://doi.org/10.1016/j.talanta.2021.122644).

Chapter VII summarizes the most relevant conclusions obtained during this doctoral thesis, presented in both English and Spanish.

Appendix I presents supplemental figures which are referenced during the presentation of results throughout the different chapters of this thesis.

Appendix II comprises a structured summary, organized by chapters, of the materials, reagents, and suppliers, essential for the completion of all experimental procedures.

Appendix III contains a compilation of the bibliographic sources referenced in the completion of this thesis.

Appendix IV highlights the scientific papers published derived from this thesis and the participation in conferences during the course of this thesis.

Resumen y objetivos

La presente tesis doctoral, titulada "Desarrollo de nanosistemas basados en moléculas de origen biológico para la monitorización y tratamiento de infecciones bacterianas", se llevó a cabo en el Departamento de Ingeniería Química y Tecnologías del Medio Ambiente de la Universidad de Zaragoza, España, en el seno del grupo de investigación de Materiales Avanzados en Biomedicina (AMiB). La investigación y el trabajo experimental se llevaron a cabo en el Centro de Investigación Biomédica de Aragón (CIBA) y en el Instituto de Nanociencia y Materiales de Aragón (INMA). Además, parte de la investigación se realizó en una estancia predoctoral de 7 meses en el grupo de investigación INSERM U1070 "*Pharmacology of Antimicrobial Agents and Antibiotic Resistance*" de la Universidad de Poitiers (Francia). Los estudios doctorales y la investigación realizada recibieron el respaldo de una beca predoctoral FPI financiada por el Ministerio de Economía, Industria y Competitividad de España (CTQ2017-84473-R).

En respuesta al constante aumento de la resistencia bacteriana y la creciente ineficacia de los antibióticos actuales, una parte significativa de la investigación contemporánea se dedica en exclusividad a desarrollar nuevas terapias antimicrobianas. En este contexto, el objetivo principal de esta tesis fue explorar el potencial de una selección de moléculas de origen natural con propiedades antimicrobianas como alternativa a los antibióticos tradicionales. Esta investigación se centró en la encapsulación de estas moléculas en formulaciones nanoestructuradas y en su evaluación para el tratamiento de infecciones bacterianas causadas por *Staphylococcus aureus* y *Pseudomonas aeruginosa*. Los antimicrobianos seleccionados, tanto en sus formas libres como encapsuladas, se evaluaron en diversos escenarios, incluyendo modelos *in vitro* de cultivos planctónicos y biofilms bacterianos, modelos de infección intracelular en células eucariotas, y estudios *in vivo* empleando un modelo murino de herida tópica infectada.

El segundo objetivo de esta tesis fue desarrollar métodos efectivos para la detección y monitorización de bacterias patógenas en los modelos experimentales. Se utilizaron cepas bacterianas fluorescentes y bioluminiscentes para extraer información sobre la dinámica de crecimiento bacteriano y la eficacia de los tratamientos. Este esfuerzo culminó en el desarrollo de un biosensor que, haciendo uso de las propiedades ópticas únicas de las nanopartículas de oro, permitió la detección, selección y cuantificación de bacterias en distintas muestras de origen biológico.

La presente tesis se organiza en varios capítulos, cada uno de los cuales aborda una sección distinta del trabajo realizado:

En el **Capítulo I**, se desarrolla una introducción general, presentando la temática y el contexto en el que se enmarca la tesis. Se introducen varios aspectos clave, comenzando con un análisis del estado del arte de las infecciones bacterianas. A continuación, se profundiza en el creciente problema de las resistencias a los

antibióticos, destacando sus posibles alternativas. Por último, se discute la importancia de los sistemas de administración de fármacos y el campo emergente de la nanotecnología, el cual desarrolla aplicaciones prometedoras en el contexto del tratamiento de infecciones bacterianas.

El **Capítulo II** presenta un estudio sobre los efectos bactericidas y antibiofilm de dos terpenos naturales con actividad antimicrobiana: el timol y el farnesol. Estos compuestos se evaluaron tanto de forma individual como en combinación con el antiséptico clorhexidina en experimentos *in vitro* e *in vivo*. Con el objetivo de mejorar su eficacia y su aplicabilidad en la práctica clínica, se encapsuló el timol en Eudragit® S100 (copolímero aniónico sintético), con el fin de desarrollar un apósito antimicrobiano. Por otro lado, el farnesol se encapsuló en micelas lipídicas. Los estudios *in vitro* revelaron una mejora significativa en la eficacia antibacteriana cuando estos compuestos se utilizaron en combinación comparado con su uso de forma individual. Los estudios *in vivo*, utilizando un modelo murino de herida infectada, validaron los efectos bactericidas superiores de los tratamientos combinados propuestos frente a la monoterapia. La progresión de la infección y la evaluación de los resultados del tratamiento antimicrobiano se monitorearon continuamente en tiempo real mediante el uso de la cepa de *S. aureus* bioluminiscente Xen36. Los resultados de este capítulo se incluyen en el artículo recientemente publicado titulado "*Real-time in vivo monitoring of the antimicrobial action of combination therapies in the management of infected topical wounds*" (**Landa, G.**; Miranda-Calderón, L.G.; Gómez, A.; Pérez, M.; Sebastián, V.; Arruebo, M.; Lamarche, I.; Tewes, F.; Irusta, S.; Mendoza, G. International Journal of Pharmaceutics, 2023, Volume 646, 123502, https://doi.org/10.1016/j.ijpharm.2023.123502).

El **Capítulo III** aborda el desarrollo de un modelo *in vitro* de biofilms polimicrobianos formados por *S. aureus* y *P. aeruginosa*. En este estudio se destaca cómo las condiciones iniciales de las bacterias en co-cultivo influyen en la cinética de crecimiento, y como *P. aeruginosa* afecta a la proliferación y metabolismo de *S. aureus*. Una vez establecido el modelo experimental, se procedió a comparar la actividad antimicrobiana del timol y de la clorhexidina frente a ambas especies, tanto en estado planctónico como en biofilms individuales y polimicrobianos. En este contexto, se observó una menor toxicidad de la clorhexidina y del timol sobre *S. aureus* cuando se encontraba en el biofilm polimicrobiano. Este fenómeno se atribuyó a dos factores fundamentales: la formación de un biofilm mixto de mayor biomasa y grosor que los formados exclusivamente por *S. aureus* o *P. aeruginosa*, y una notable reducción en la actividad metabólica de *S. aureus* inducida por la presencia de moléculas secretadas por *P. aeruginosa*. Los resultados de este capítulo se incluyen en un artículo científico que será enviado próximamente para su publicación, con el título "*Impact of mixed Staphylococcus aureus-Pseudomonas aeruginosa biofilms formation on resistance to antimicrobial treatment of chronically infected wounds*".

El **Capítulo IV** se centra en el desarrollo de partículas poliméricas aerosolizables cargadas con colistina, explorando cuatro metodologías diferentes para su síntesis.

Estas técnicas incluyeron la síntesis de nanopartículas de poli(ácido láctico-co-glicólico) (PLGA) mediante el método de evaporación de solvente en emulsión simple, la encapsulación mediante nanoprecipitación con solventes miscibles utilizando PLGA-polietilenglicol (PEG), la coacervación de colistina en hidroxipropil metilcelulosa (HPMC) utilizando el método de precipitación en solventes no-miscibles y, por último, la encapsulación de colistina en micropartículas de PLGA mediante la técnica del electrosprayado. La metodología de mayor éxito fue la de precipitación en solventes no-miscibles, logrando una carga del fármaco muy alta (55 % del peso de las partículas), y produciendo partículas con propiedades aerodinámicas adecuadas (3-5 µm) para su potencial administración pulmonar. Los ensayos *in vitro* revelaron una liberación rápida de la colistina en esta formulación. Además, estas partículas demostraron mejorar la eficacia antimicrobiana de la colistina en un modelo de biofilm de *P. aeruginosa* PAO1, en comparación con dosis equivalentes del fármaco libre. Los resultados de este capítulo se incluyen en el artículo publicado titulado "*Colistin-loaded aerosolizable particles for the treatment of bacterial respiratory infections*" (**Landa, G.**; Alejo, T.; Sauzet, T.; Laroche, J.; Sebastian, V.; Tewes, F.; Arruebo, M. International Journal of Pharmaceutics, 2023, Volumen 635, 122732, https://doi.org/10.1016/j.ijpharm.2023.122732)

El **Capítulo V** introduce una nueva formulación antimicrobiana mediante la encapsulación de lisostafina (LYS), una bacteriocina antiestafilocócica, en nanopartículas de PLGA. En este trabajo se evalúa la actividad antimicrobiana tanto de LYS libre como de las nanopartículas de PLGA cargadas con LYS contra diferentes cepas de *S. aureus* en estado planctónico, en biofilms, y en un modelo de infección intracelular. Se empleó una cepa de *S. aureus* que expresaba GFP para facilitar el análisis y la adquisición de imágenes mediante microscopía confocal. Los resultados evidenciaron una disminución significativa en la viabilidad de las bacterias, tanto en estado planctónico como en forma sésil, y en ocasiones, lograron su erradicación total. En un modelo de infección intracelular de células eucariotas *in vitro*, la formulación de LYS encapsulada demostró mayor eficacia en comparación con el tratamiento de la bacteriocina libre. El contenido de este capítulo se incluye en el artículo pendiente de publicación titulado "*PLGA nanoparticle-encapsulated lysostaphin for the targeted treatment of Staphylococcus aureus Infections*" (**Landa, G.**; Aguerri, L.; Irusta, S.; Mendoza, G.; y Arruebo, M. Journal of Colloid and Interface Science. En revisión.)

El **Capítulo VI** detalla el desarrollo de un rápido y sencillo sensor óptico de bacterias. Este sistema utiliza nanopartículas de oro funcionalizadas con ácido siálico. Debido a la capacidad de las bacterias patógenas para integrar ácido siálico exógeno, se observó como la acción de éstas causaba la agregación de las nanopartículas de oro. Esta agregación provocaba un cambio en la resonancia de plasmón superficial y en la alteración del espectro óptico de las nanopartículas. Este sistema permitió la detección selectiva de bacterias, pudiendo discriminar entre Gram-negativas (*P. aeruginosa* ATCC 15442) y Gram-positivas (*S. aureus* ATCC 25923), así como entre una cepa de *S. aureus wild type* y una resistente a la meticilina (MRSA USA300). La discriminación de patógenos bacterianos se evaluó en diferentes medios, incluyendo agua, dos

disoluciones tampón independientes, medios de cultivo bacteriano, suero y orina. Se precisó de una presencia bacteriana elevada en las muestras para proporcionar una identificación óptica estadísticamente significativa de patógenos en suero humano, mientras que no fue posible detectar la presencia de bacterias a niveles clínicamente relevantes en la orina. El contenido de este capítulo se ha adaptado del artículo publicado titulado "*Selective point-of-care detection of pathogenic bacteria using sialic acid functionalized gold nanoparticles*" (**Landa, G.**; Miranda-Calderón, L.G.; Sebastián, V.; Irusta, S.; Mendoza, G.; Arruebo, M. Talanta, 2021, Volume 234, 122644, https://doi.org/10.1016/j.talanta.2021.122644).

El **Capítulo VII** resume las conclusiones más relevantes obtenidas durante esta tesis doctoral.

El **Apéndice I** presenta figuras suplementarias. las cuales son citadas durante la presentación de resultados a lo largo de los capítulos.

El **Apéndice II** comprende una lista, organizada por capítulos, de los materiales, reactivos y proveedores que han sido necesarios para la realización de todos los experimentos.

El **Apéndice III** contiene una recopilación de las referencias bibliográficas consultadas durante la elaboración de esta tesis.

El **Apéndice IV** destaca los artículos científicos publicados y la participación en conferencias durante el transcurso de la tesis.

CHAPTER I

General Introduction

Table of contents

I.1. Infectious diseases

Infectious diseases are illnesses caused by microorganisms, including viruses, bacteria, fungi, and parasites, that can be transmitted from one person to another, from animals to humans, or through environmental sources such as water and soil. These microorganisms can enter the body through various routes such as ingestion, inhalation, and contact with infected individuals or with contaminated objects. Once inside the body, they can cause a range of symptoms depending on the type of microorganism and the immunological status of the host. Infectious diseases can be acute or chronic, and some can be life-threatening if left untreated. They represent a major global health concern and can have significant economic and social impacts [1, 2].

As observed by the World Health Organization (WHO), infectious diseases are a significant distress in impoverished nations and developing countries [3–5]. The prevalence of these diseases is notably high in regions with limited resources and inadequate healthcare infrastructure. The interplay of socio-economic factors, environmental conditions, and limited access to healthcare services creates fertile ground for the spread and persistence of infectious agents. Unfortunately, the focus on diseases prevalent in developed countries, such as cancer and cardiovascular diseases, often leads to the oversight of infectious diseases in low-income countries. The lack of research and attention towards these diseases hinders the efforts to combat them effectively where it is specially needed. **Figure I.1** illustrates the top ten causes of mortality according to WHO [5], both globally and within low-income countries.

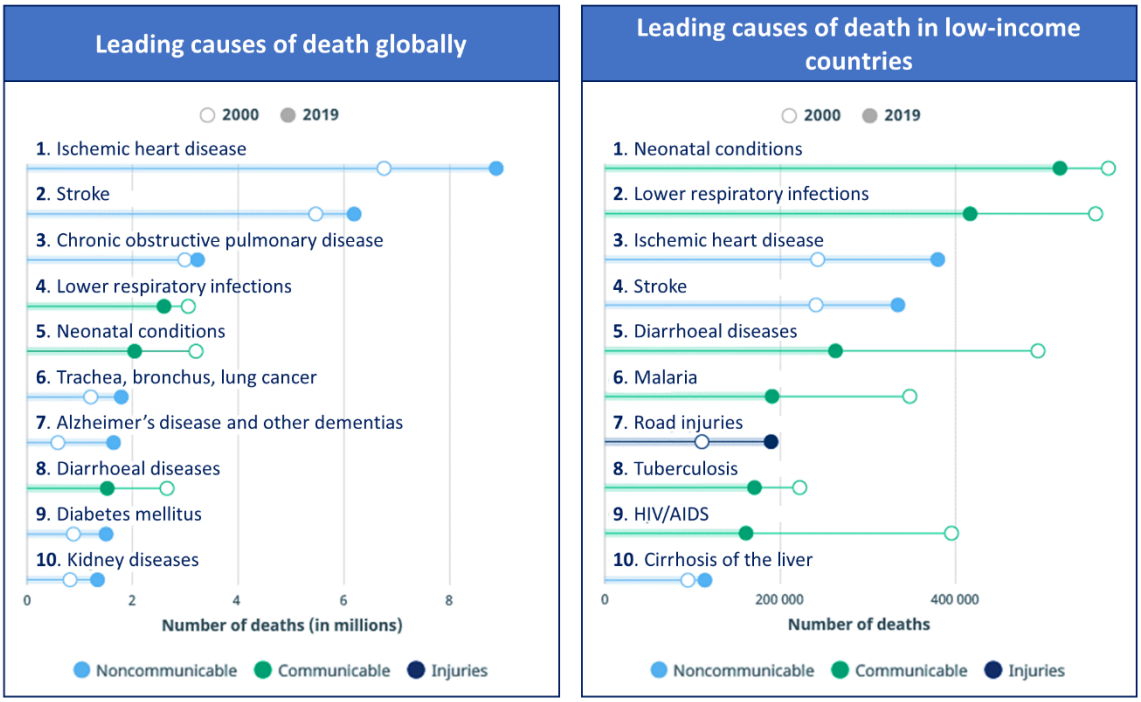

Figure I.1: Top 10 causes of death in the world and in low-income countries [5].

Effective prevention and control measures, including public health education, vaccination, early diagnosis, antimicrobial therapy, and public health interventions, are essential for minimizing the impact of infectious diseases on individuals and society. Despite all efforts, they remain as a major public health challenge worldwide. The emergence of new pathogens, the re-emergence of previously controlled infections, and the increasing resistance of microorganisms to antimicrobial agents are significant challenges that require ongoing attention and research [6]. Understanding the nature, transmission, and mechanisms of infectious diseases is critical for developing effective strategies to prevent and control their spread.

I.1.1. Bacterial infectious diseases

Bacterial infectious diseases are caused by the invasion and proliferation of harmful bacteria within the human body. These microorganisms can reproduce rapidly and release toxins that can disrupt normal body functions. Bacterial infections can manifest in various ways, ranging from mild to severe, depending on the type of bacteria involved, the site of colonization and the body's immune response [7]. Infectious diseases include pneumonia, urinary tract infections, tuberculosis, and foodborne illnesses, among others. **Figure I.2** highlights the most significant examples along with the primary microorganisms responsible.

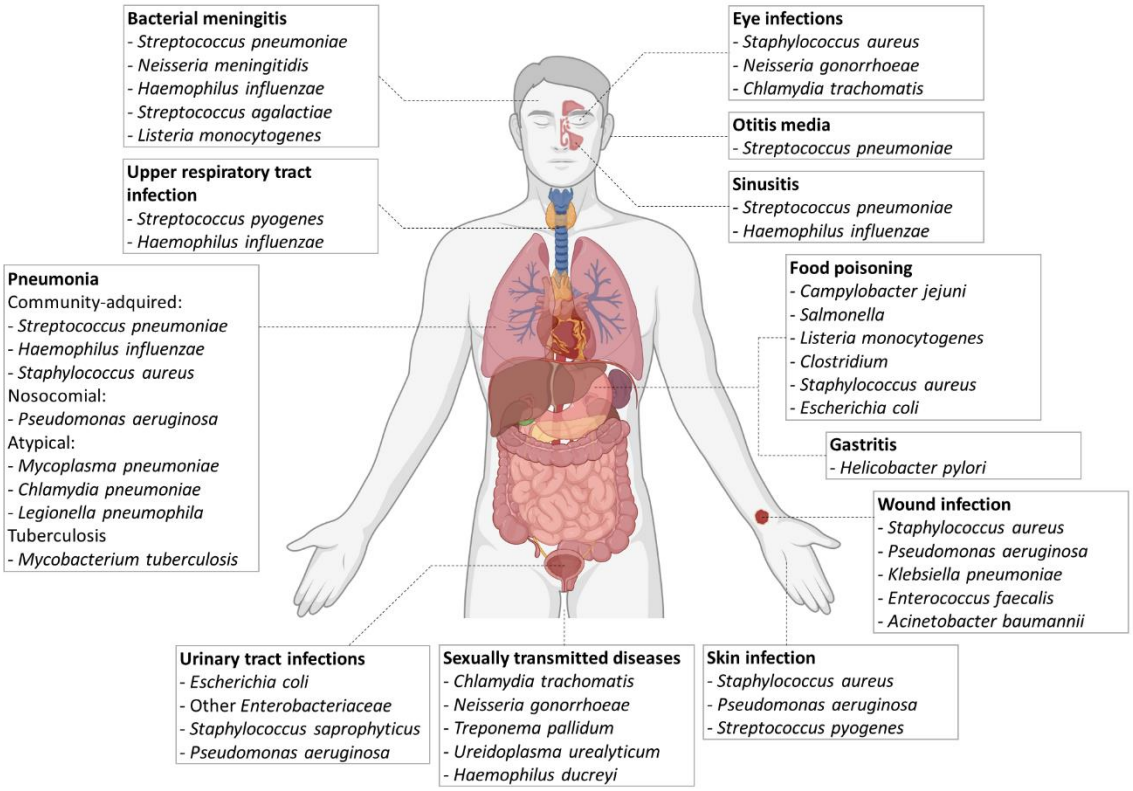

Figure I.2: Main infectious diseases and the microorganisms responsible.

In 2019, approximately 7.7 million deaths were found to be linked to bacterial infections, accounting for 13.6% or 1 in 8 of all global deaths [8]. This number ranks

bacterial infections as the second-leading cause of death globally. Surprisingly, more than half of these deaths (54.9 %) were attributed to just five types of bacteria: *Staphylococcus aureus*, *Escherichia coli*, *Streptococcus pneumoniae*, *Klebsiella pneumoniae*, and *Pseudomonas aeruginosa*. Among the deaths caused by bacterial infections, three types of infections account for more than 75% of the fatalities: lower respiratory infections (such as pneumonia), bloodstream infections, and peritoneal and intra-abdominal infections. There are significant variations in the significance and distribution of bacterial pathogens among different regions. Sub-Saharan Africa bears the highest mortality rate, with 230 deaths per 100,000 population, while high-income countries exhibit the lowest rate at 52 deaths per 100,000 population.

Proper hygiene practices, vaccination, and timely administration of antibiotic and antimicrobials are crucial in preventing and treating bacterial infections. However, the emergence of antibiotic-resistant bacteria poses a significant challenge in the management of these diseases, highlighting the need for ongoing research and the development of alternative strategies**.**

I.1.1.1. *Staphylococcus aureus*

Staphylococcus aureus, a Gram-positive bacterium, typically exists as a commensal organism on the human skin and mucous membranes. Humans are the major reservoir of these organisms, with an estimated colonization rate up to 50% in adults, and approximately 15% of the population carrying *S. aureus* persistently in the anterior nares [9]. Interestingly, about ~30% of healthy individuals colonized by *S. aureus* do not exhibit any pathological symptoms [10]. However, this bacterium possesses the capacity to become pathogenic under certain circumstances, leading to millions of severe and potentially life-threatening infections and toxin-mediated diseases worldwide [11].

S. aureus employs various mechanisms to avoid the host immune defences. These mechanisms include the development of an anti-phagocytic capsule, hiding from host antibodies using Protein A, forming biofilms, surviving inside host cells, and hindering the movement of immune cells through chemotaxis [12]. Other virulence factors of *S. aureus* include the production of toxins, such as adhesins, leucocidin, coagulase, haemolysin, and the superantigen toxic shock syndrome toxin 1 [13]. The combination of these mechanisms allows *S. aureus* to manifest in a wide variety of diseases, including foodborne toxin infections, skin and soft tissue infections, urinary tract infections, pneumonia, endocarditis, and meningitis, among others [9, 12, 14]. Infections related to prosthetic devices are frequently influenced by the capacity of *S. aureus* strains to create biofilms and communicate through quorum sensing, a mechanism that relies on bacterial cell density [15]. Lastly, *S. aureus* is a highly prevalent microorganism in nosocomial infections, especially in cases of central line-associated bloodstream infections, surgical site infections, and hospital-acquired pneumonia [16].

Based on a 2019 study, *S. aureus* was identified as a leading cause of bacterial-related fatalities in 135 countries. It was directly linked to over 1 million deaths and stood out for being responsible for the highest number of infection-related fatalities worldwide among individuals aged 15 and older [17].

In **Chapter II** of this thesis, phytochemicals with antimicrobial activity (thymol and farnesol), in combination with the antiseptic chlorhexidine, were used to treat an *in vivo* murine model of *S. aureus*-infected topical wound. Additionally, in **Chapter V**, a model of *S. aureus* intracellular infection in macrophages was treated with a PLGA-encapsulated bacteriocin (lysostaphin). Lastly, the gold nanoparticle-based biosensor detailed in **Chapter VI** achieved successful detection and typing of *S. aureus* and its methicillin-resistant variant.

I.1.1.2. *Pseudomonas aeruginosa*

Pseudomonas aeruginosa, is a Gram-negative bacterium commonly found in the natural environment. Unlike commensal organisms, *P. aeruginosa* typically does not exist as part of the human microbiota. However, it poses a significant threat as an opportunistic human pathogen, as it has the capacity to trigger a diverse range of severe infections [18]. These infections, which can be acute or chronic, are particularly problematic in individuals with compromised immune systems, including those with conditions like chronic obstructive pulmonary disease, cystic fibrosis, cancer, and cases associated with COVID-19 [19].

Additionally, *P. aeruginosa* ranks among the top nosocomial pathogens, significantly impacting healthcare systems and hospitalized individuals. It is the most prevalent microorganism in cases of ventilator-associated pneumonia, while playing a substantial role in urinary catheter-related infections, central line-associated bloodstream infections, and infections associated with surgeries or transplants [20]. This bacterium is commonly found in healthcare environments due to its presence among patients receiving medical treatment, as well as its ability to persist on both living and non-living surfaces, including medical equipment. When in a biofilm state, it demonstrates the ability to survive in highly challenging environments, such as hypoxic conditions [18]. This resilience enables it to withstand disinfection procedures and facilitates transmission from one patient to another. Lastly, *P. aeruginosa* has shown significant intrinsic resistance to a wide range of antibiotics [21]. This resistance is primarily attributed to factors such as limited outer membrane permeability, active efflux systems, and the production of antibiotic-inactivating enzymes.

In a cohort study, it was found that *P. aeruginosa* had the highest prevalence of healthcare-acquired infections among patients in European intensive care units [22]. According to a 2016 study made by the Spanish Society of Public Health and Health Management, *P. aeruginosa* constituted 10.5% of clinically isolated bacterial nosocomial infections in Spain [23].

Chapter IV of this thesis involved the incorporation of *P. aeruginosa* into a bacterial biofilm model, where the bacteria were encapsulated within agar microparticles. This *in vitro* model was treated with an encapsulated colistin formulation intended for pulmonary delivery. Furthermore, *P. aeruginosa* was the selected Gram-negative bacterial model to assess the discrimination capability of the sensor developed in **Chapter VI**.

I.2. Antimicrobial resistance

Antimicrobial resistance (AMR) refers to the ability of bacteria to resist the effects of antibiotics and other antimicrobial drugs that were once effective in treating infections at specific doses. AMRs can be classified as either innate or acquired [24, 25]. Innate resistance is a naturally occurring trait that arises from the organism's biology. On the other hand, acquired resistance occurs when previously susceptible bacteria develops resistance through mechanisms like spontaneous genetic mutations or acquisition of external DNA. The process by which bacteria acquire AMR is depicted in **Figure I.3**.

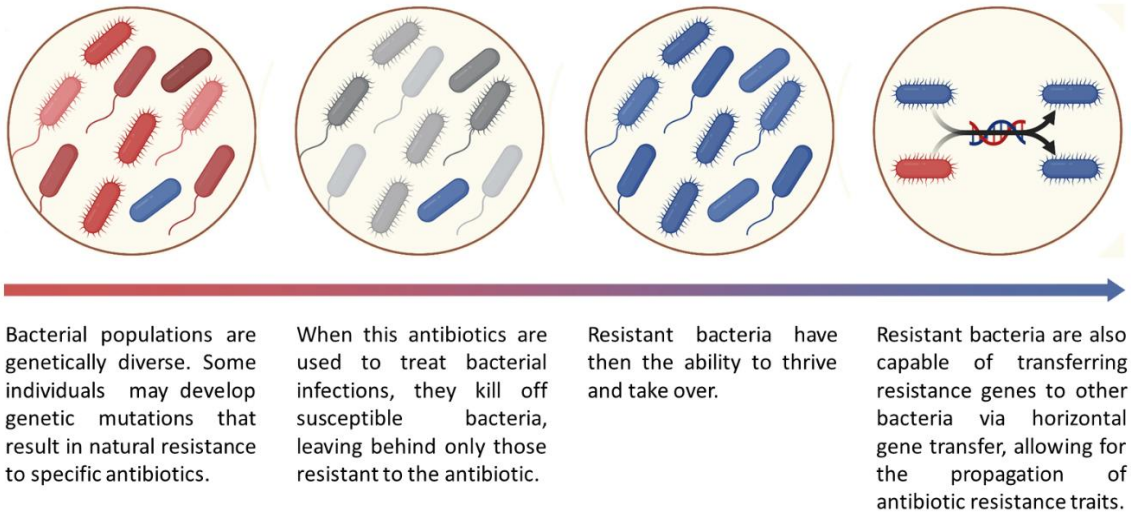

Figure I.3: Mechanism of AMR acquisition in bacterial populations.

AMR has become a significant global concern in recent years. It has profound consequences to public health, both in developed and low-income countries, as it can lead to longer hospital stays, higher healthcare costs, and increased mortality rates [26, 27]. A recent report indicated that there may have been more than one million deaths worldwide due to AMR in 2019 [6]. It is also predicted that by 2050, bacterial AMRs could be responsible for 10 million deaths and result in the loss of 100 trillion USD in global economic output if significant efforts are not undertaken to address this threat [28].

Nevertheless, the development of new antibiotics has not kept pace with the increasing prevalence of antibiotic-resistant bacteria, which exacerbates the problem

[29]. Over the years, the WHO has emphasized the urgency of investing in research and development for the discovery of new drugs to combat bacterial resistance [30]. Despite this, the development and approval of new antibiotic classes by international drug agencies, such as the US Food and Drug Administration and the European Medicines Agency, have been sparse in the past two decades: The quinolones, which emerged in 1962, were the latest significant antimicrobial compounds discovered in the field. Since 1987, with lipopeptides, there have effectively been no new classes of antibiotics discovered. In 2017, there were 44 antibiotics awaiting approval, out of which 9 had advanced to phase 3 clinical trials [31].

The declining interest among pharmaceutical companies in antibiotic development in recent years is attributed to the multiple challenges in clinical research, as well as scientific, regulatory, and economic factors. Identifying new classes of antibiotics that demonstrate high activity, favourable pharmacokinetic properties, and satisfactory safety profiles is a complex task. On top of that, conducting clinical trials to evaluate the efficacy of these new antibiotics can also be particularly difficult when focusing on multidrug-resistant bacteria, due to the lack of diagnostic tools that make possible patient recruitment. Lastly, antibiotics are not as profitable as other drugs like the those prescribed to treat chronic illnesses such as diabetes or hypertension. Any new antibiotic would likely be saved as a last-resort treatment with a very short prescription length [32].

I.2.1. Mechanism of bacterial resistance

Bacteria have developed various mechanisms to acquire AMR. These mechanisms can be categorized into four main groups:

- Antibiotic uptake reduction: Antibiotics must overcome the bacterial wall and enter the cell to exert their therapeutic action. Transmembrane proteins such as porins play a crucial role in bacterial wall transit, permeability, and antibiotic entry [33]. Changes in porins gene expression that affect their quantity or structure can significantly impact antimicrobial activity [34]. Additionally, alterations in the bacterial cell wall structure and the outer membrane and lipopolysaccharide (LPS) of Gram-negative bacteria may affect antibiotic uptake [35, 36].
- Antibiotic target modification: Molecular and structural alterations in antibiotic targets can lead to reduced affinity and subsequent loss of functionality. For example, alterations in penicillin-binding proteins (PBPs) also contribute to resistance in MRSA and other penicillin-resistant bacteria [37].
- Antibiotic inactivation: Enzymes like β-lactamases can hydrolyse β-lactam antibiotics such as penicillin G in penicillin-resistant bacteria [38], while chemical modifications such as acetylation, phosphorylation, or adenylation are common mechanisms to endure the action of aminoglycosides [39].

- Antibiotic efflux: Efflux pumps are transmembrane transporters that actively pump out antibiotics from the bacterial cells, maintaining intracellular concentration of antibiotics below the level needed to exert their action [40].

In addition, a less common resistance mechanism may involve the modification of metabolic and protein biosynthesis processes. As an example, some bacteria can bypass the need for para-aminobenzoic acid, a crucial precursor in the synthesis of folic acid and nucleic acids, and evade the inhibitory effects of sulphonamides [41]. All these mechanisms are represented schematically in **Figure I.4**.

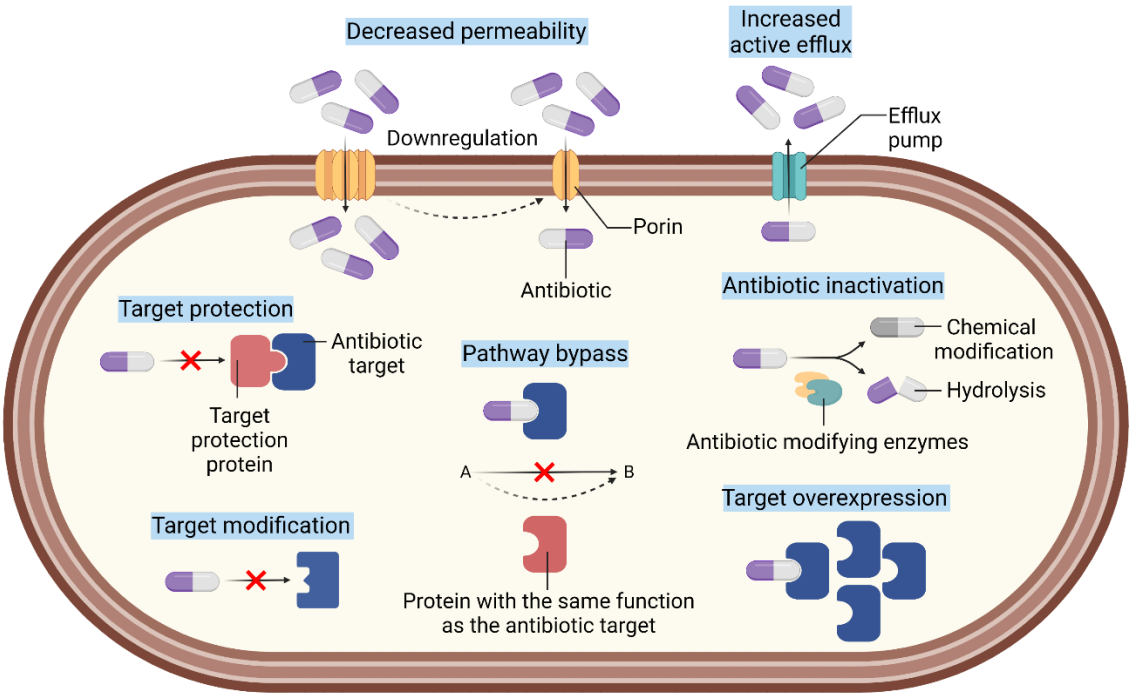

Figure I.4: Mechanisms of bacterial resistance to antibiotics.

Innate AMR in bacteria may involve limiting antibiotic uptake, inactivation, and efflux, while acquired resistance mechanisms may include antibiotic target modification, inactivation, and efflux. Notably, Gram-negative bacteria commonly utilize all four main mechanisms, whereas Gram-positive bacteria are less likely to restrict antibiotic uptake (due to the absence of an LPS outer membrane) and may lack certain efflux mechanisms due to their bacterial wall structure [42].

I.2.2. *The Rise of the Superbugs*

Bacteria can acquire multiple resistance traits over time, leading to resistance against many classes of antibiotics, a condition known as "multi-drug resistant" (MDR). A subset of MDR bacteria are classified as "extensively drug-resistant" (XDR), which means they are resistant to multiple classes of antibiotics but may still be susceptible to a limited number of them. However, the most concerning category is "pan drug-resistant" (PDR) bacteria, as they are resistant to all available antibiotics, leaving no

viable treatment options [43]. Colloquially, these categories of bacteria are commonly referred to as "superbugs".

In 2017, in response to the growing global recognition of the need for new antimicrobials, WHO created a priority list of MDR bacteria [44]. The purpose of this list was to guide the research and development on the search of new and effective antimicrobials. The report emphasized the danger to humanity from various under-researched antibiotic-resistant bacteria and underscored the urgent need for enhanced research and development to effectively address this threat. This list was ratified in 2022 and categorizes microorganisms into three levels of alert: Critical, High, and Medium Priority (**Figure I.5**).

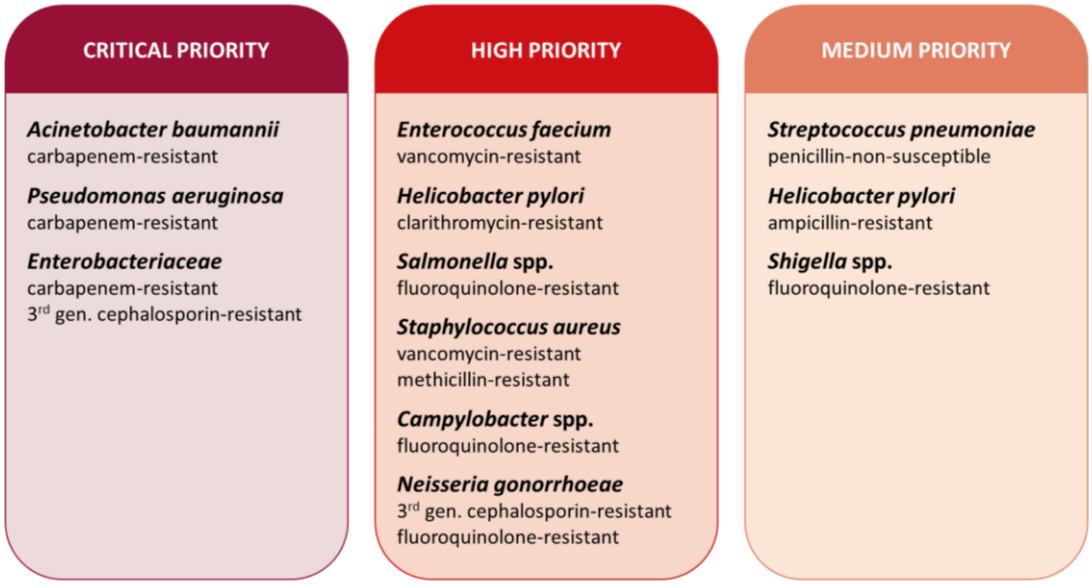

Figure I.5: Priority groups established by the WHO, the microorganisms they consist of, and the antibiotics they are resistant to [44].

These bacterial species are known by the acronym "ESKAPE" which comes from the first letter of the included species (*Enterococcus faecium*, *Staphylococcus aureus*, *Klebsiella pneumoniae*, *Acinetobacter baumannii*, *Pseudomonas aeruginosa* and *Enterobacter spp*.). These bacteria have gained notoriety for their ability to evade the effects of broad-spectrum antibiotics, making them responsible for most nosocomial infections [45]. They are often associated with high mortality rates and prolonged hospital stays, leading to significant healthcare costs [46, 47]. The implications for public health are far-reaching: The emergence and spread of these MDR microorganisms threaten the ability to treat infections and could lead to a future where routine medical procedures, such as surgeries and chemotherapy, would be too risky to perform.

Particularly noteworthy is the case of MRSA, whose emergence of has been alarming since it was first reported in the 1960s. Since then, MRSA has become increasingly prevalent in clinical settings while remaining as a significant pathogen in healthcare-associated infections [48]. Studies based on pan-European surveys indicate

that MRSA affects over 150,000 patients each year within the European Union (EU) and contributes to an additional 380 million EUR in in-hospital costs for healthcare systems across the EU [49]. In a study conducted within the United States population, it was observed that the mortality rate for hospital-acquired MRSA bloodstream infections is 29%, while for those originating in the community, the mortality rate is 18% [50].

In **Chapters V** and **VI** of this thesis, the MRSA USA300 strain was included in the experimental work to evaluate potential differences, particularly in terms of treatment resistance and variations in detection methods when compared to the *S. aureus* wild type.

I.2.3. Biofilm formation

In addition to the AMR mechanisms explained earlier, bacteria can also develop resistance to antimicrobial therapies through the formation of biofilms. Biofilms are complex microbial communities that attach to surfaces and are enclosed within a protective matrix. This matrix is formed by an extracellular polymeric substance (EPS) which is secreted by bacteria themselves [51]. The formation of biofilms is recognized as an adaptive strategy employed by bacteria to thrive and survive in challenging environmental conditions: when faced with unfavourable or fluctuating settings such as nutrient scarcity, changes in pH, or exposure to antimicrobial agents, bacteria form biofilms as a protective response [52, 53].

Biofilms can be composed of either a single bacterial specie or multiple microorganisms, including non-bacterial ones. The metabolic status of the bacterial species within these biofilms is also diverse, encompassing both metabolically active bacteria and those in a dormant state [54]. Furthermore, it is important to note that the state of the biofilm is dynamic and can vary over time.

Bacterial biofilm formation is a multi-step process that begins with reversible attachment, where bacterial cells initially adhere to a surface through adhesins [53, 55]. This is followed by a strong attachment, as the cells produce EPS to firmly anchor themselves. The biofilm then matures, developing complex three-dimensional channel structures that enable the flow of liquid through the community, allowing for the exchange of nutrients and removal of waste products. Eventually, dispersal or detachment may occur, allowing bacteria to colonize new surfaces, as depicted in **Figure I.6**.

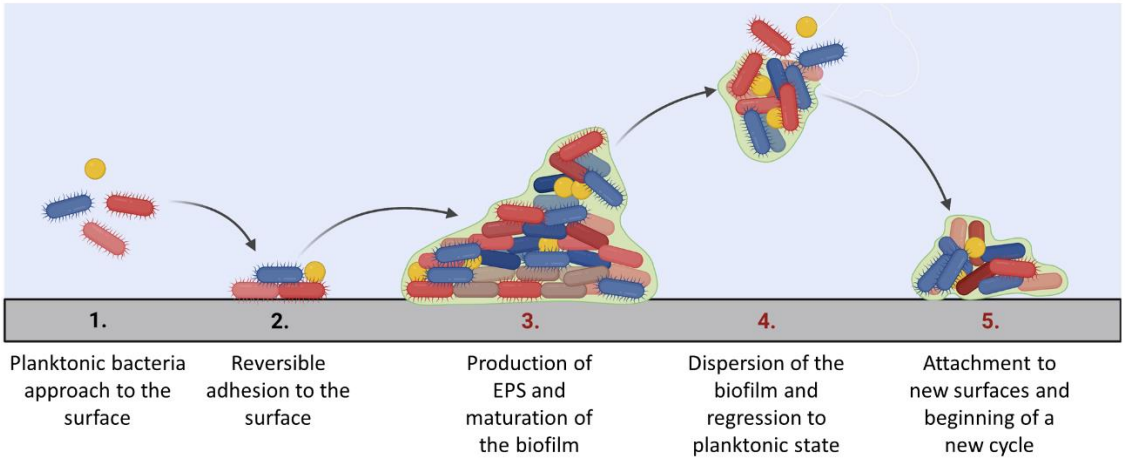

Figure I.6: Mechanism of biofilm formation. Inspired by the graphical representation in [56].

However, it is important to highlight that the traditional 5-step-model of biofilm formation may be an oversimplification of the real processes that take place and therefore is being challenged [56].

Bacteria within the biofilm produce and release intercellular signaling molecules [57]. These molecules enable bacteria to sense the presence and density of other bacteria in the community. In response to these signals, bacteria can coordinate their activities, modulate the growth pattern of the biofilm, and alter their phenotype, including the expression of virulence factors [58–60]. As it was mentioned before, this phenomenon of cell-cell communication is known as quorum sensing.

Biofilms play a crucial role in promoting bacterial resistance to antimicrobials through several key mechanisms. Firstly, the biofilm matrix acts as a physical barrier, reducing the penetration of antimicrobial agents into the biofilm. This limited penetration hinders the effective concentration of antibiotics reaching the bacterial cells. The biofilm matrix may also contain enzymes secreted by bacteria, such as beta-lactamases, which can hydrolyse or modify antimicrobial compounds and render them ineffective [61–63].

Secondly, the heterogeneous bacterial metabolic state in biofilm can lead to the presence of bacteria in a quiescent state, known as persister cells [54, 64, 65]. These dormant cells exhibit a reduced susceptibility to antimicrobials due to their low metabolic activity, specially to the ones that target actively dividing cells. Furthermore, other bacteria within the biofilm that are not in the quiescent state may exhibit other stress-driven changes like altered membrane physiology or alternative regulatory pathways, enhancing their AMR [66]. Lastly, biofilms provide an environment conducive to the transfer of resistance genes between bacterial cells. The proximity and physical interactions among bacteria within the biofilm facilitate the horizontal gene transfer [67]. This genetic exchange contributes to the dissemination and spread of resistance traits within the biofilm community.

It is reported that bacteria within a biofilm exhibit a notably increased resistance, ranging from 10 to 1,000 times, against antimicrobial agents compared to their planktonic counterparts [68].

Biofilms pose significant challenges in clinical practice due to a variety of reasons. In clinical settings, biofilms have been shown to be formed on medical device surfaces such as catheters, implants, prosthetics, and others [69, 70]. The presence of biofilms on these devices not only increases the risk of device-related infections but also provides a reservoir for continuous release of bacteria. The ability of bacteria within biofilms to resist immune clearance and withstand antimicrobial treatments can lead to recurrent infections and the chronicity of the disease [71]. This persistence often necessitates more aggressive and prolonged therapies and patient morbidity. Moreover, the bacteria within biofilms may also express increased levels of virulence factors [72], making the infection more severe and difficult to manage. It has been estimated that biofilms are present in more than 65% of nosocomial infections, approximately 80% of chronic infections, and 60% of all human bacterial infections [73].

In all the chapters of this thesis, there is a consistent focus on incorporating *in vitro* bacterial biofilm models and evaluating the anti-biofilm properties of the developed antimicrobial formulations.

I.2.4. Antibiotics against AMRs

As mentioned earlier, the emergence of AMRs is a natural adaptation of bacteria in response to the widespread and sometimes excessive use of antibiotics in clinical practice. However, antibiotics remain the primary treatment option for bacterial infections in clinical settings due to their unmatched reliability. Therefore, various strategies have been devised to revitalize antibiotics that are losing their effectiveness.

The first option is to consider what is known as antibiotic stewardship. Antibiotic stewardship programs (ASPs) are a set of strategies aimed at optimizing antibiotic use to improve treatment outcomes and prevent antimicrobial resistance [74]. The main goal is to ensure appropriate antibiotic use by reducing unnecessary prescriptions, selecting effective options, and preserving their long-term efficacy. ASPs involve pre-prescription review and authorization for restricted antibiotics, as well as ongoing reviews of treatments based on patient condition and microbiology data [75]. These programs are essential for improving clinical outcomes, reducing hospital stays, and cutting healthcare costs [75, 76].

Another significant and extensively explored approach involves combination therapies. Combination therapies refer to the use of two or more antimicrobial agents together to treat bacterial infections [77]. The goal of combination therapies is to achieve a synergistic or additive effect, where the combined action of the drugs is more effective than using each drug individually. Combination therapies in antimicrobial treatments can involve the utilization of not only two different

antimicrobials but also non-antimicrobial molecules (adjuvants). While these molecules may lack direct antimicrobial activity, they can serve to modify bacterial targets, metabolism, or microenvironment to enhance the effectiveness of the antibiotic [78].

Traditionally, various antibiotic combinations have been utilized to combat AMR infections. Notably, the combination of β-lactam antibiotics with aminoglycosides is well-studied and widely used against Gram-negative bacterial infections [79–81]. Another commonly employed clinical antibiotic combination include β-lactam/fluoroquinolone and β-lactam/tetracycline. In the context of antimicrobial and non-antimicrobial combinations, β-lactam antibiotics combined with β-lactamase inhibitors (BLBLI combinations) have been well-documented for their effectiveness in targeting infections resistant to β-lactam antibiotics [82]. Emerging combination therapies also involve the implementation of efflux pump inhibitors [83–85], histidine kinase inhibitors [86, 87], and quorum sensing molecule inhibitors [88, 89]. However, the true efficacy of these combinations is still uncertain as resistance mechanisms evolve [90, 91].

In **Chapter II** of this thesis, the combination therapy of natural origin phytochemicals with antimicrobial and anti-inflammatory properties, along with the commonly used antiseptic chlorhexidine, was explored for the treatment of infected topical wounds.

I.2.5. Post-antibiotics era: alternatives

Despite ongoing efforts to improve the current usage of antibiotics in clinical settings, researchers have also focused towards identifying novel compounds that have the potential to augment or supplant the antibiotics therapeutic role. Next, the most significant examples are introduced:

I.2.5.1. Phytochemicals and essential oils

Plants have naturally developed various defense mechanisms against microorganisms, including the synthesis of phytochemicals. These secondary metabolites can be found in various parts of the plant, such as fruit, seeds, leaves, flowers, and roots. Plant extracts and essential oils containing these metabolites have been utilized in traditional medicine for centuries, providing therapeutic benefits for a wide range of illnesses [92, 93]. The role of phytochemicals in plants defense against microorganisms has raised the interest on them for their potential as antibacterial and antibiotic resistance-modifying drug candidates [94–96].

Phytochemicals with the highest antimicrobial activity include alkaloids, phenolic compounds, terpenes and organosulfurs [97]. These substances have demonstrated antibacterial effects against a wide range of bacteria, including MDR strains [98]. Their mechanisms of action involve disrupting bacterial cell wall synthesis, inhibition of bacterial physiology, increasing antibiotic susceptibility, inhibiting biofilm formation

and inhibiting efflux pumps [83, 99]. For instance, alkaloids and phenolic compounds have been found to inhibit efflux pumps in *E. coli* and *S. aureus* [83, 100], while terpenes disrupt the cell membranes of *S. aureus*, *P. aeruginosa*, *E. coli*, and *H. pylori* [101].

Phytochemicals are considered environmentally friendly and show great promise as alternatives to the conventional antibiotic growth promoters utilized by livestock farming [102, 103].

In **Chapter III**, different nanostructured formulations were employed to encapsulate two distinct phytochemicals: thymol, a monoterpenoid phenol known for its antimicrobial activity derived from thyme essential oil, and farnesol, a sesquiterpene alcohol with anti-inflammatory properties found in various plant-derived essential oils. As stated earlier, these compounds were investigated for their potential in treating infected topical wounds, both individually and in combination with the antiseptic chlorhexidine.

I.2.5.2. Antimicrobial peptides

Antimicrobial peptides (AMPs) can be ubiquitously found in diverse natural environments, serving as components of the innate immune system from microorganisms to humans [104]. In the case of bacterial AMPs, they serve as a defense mechanism against harmful agents like bacteriophages and competing microorganisms. These peptides typically consist of 10 to 50 amino acids, carry an overall positive charge, and they generally possess amphipathic properties [105]. AMPs display similar or improved antimicrobial activity compared to antibiotics. They can target a broad spectrum of bacteria, including both Gram-positive and Gram-negative species, using mechanisms like those of conventional antibiotics [106–108].

However, their short plasma half-life due to proteolytic enzymes and their potential toxicity are common limitations [109]. Various strategies are being explored to improve their stability, including encapsulated AMPs, AMP conjugates, AMP mimetics, and immobilized AMPs. Conjugating AMPs with traditional antibiotics is promising leading to potential synergistic effects and effective targeting of pathogenic-resistant bacteria. For example, the combination of the AMP magainin with vancomycin demonstrated enhanced results against vancomycin-resistant *Enterococci* [110]. In this study the minimum inhibitory concentration (MIC) of the AMP-vancomycin combination was eightfold lower compared to that of vancomycin alone. Lastly, AMPs are widely used as targeting ligands for drug delivery systems to improve their specificity and efficacy [111].

AMPs like LL-37 are being investigated for their antimicrobial capabilities in clinical trials. Meanwhile, colistin, a last-resort polypeptide antibiotic for the treatment of infections caused by MDR *P. aeruginosa*, is already used in clinical settings [112, 113]. In **Chapter IV**, colistin was selected for its encapsulation in polymeric particles to enable its pulmonary administration.

I.2.5.3. Bacteriocins

Bacteriocins are lytic enzymes of bacterial origin. They serve as natural antimicrobial agents and play a crucial role in microbial competition and in the formation of bacterial populations [114]. They are produced by certain bacterial species in a complex polymicrobial environment against competing microorganisms. These proteins can kill or inhibit the growth of bacteria closely related to the ones producing them without harming the latter, thanks to specific immunity proteins.

Bacteriocins exhibit a wide diversity of structures and functions. As a result, they demonstrate antimicrobial potential against a variety of microorganisms, including different bacterial, fungal, and viral species [115–117]. For example, lysostaphin, a well-studied bacteriocin, is a naturally occurring endopeptidase derived from *Staphylococcus simulans*. It possesses exceptional enzymatic activity in cleaving polyglycine bridges that serve as cross-links in the cell wall structure of *Staphylococci* [118]. Studies have demonstrated its potent bactericidal efficacy against *S. aureus* biofilms and MRSA [119, 120].

However, like AMPs, they encounter stability challenges related to their proteinaceous nature when exposed to physiological environments. Considering this, **Chapter V** explores the encapsulation of lysostaphin within polymeric PLGA nanoparticles, aimed at safeguarding the protein from degradation and prolonging its activity. This formulation was assessed against *S. aureus* in various contexts, including planktonic cultures, biofilms, and in an intracellular infection model.

I.2.5.4. Immunotherapies

Monoclonal antibody (mAb) therapy is gathering attention as a promising approach for treating infectious diseases, offering significant benefits with its precise selection of antibody targets and high specificity. Unlike traditional small-molecule antibiotics, mAbs work through unique mechanisms and are less susceptible to drug resistance [121]. These mechanisms can be categorized into two main types: anti-virulence mechanisms, which involve toxin neutralization, and bactericidal mechanisms [122]. To achieve bactericidal effects, mAbs depend on the phagocytic cells and complement activation of the host's immune system.

Similar to AMPs, the high specificity of mAb has led to their consideration as targeting ligands in combination with antibiotics or nanocarriers [123]. Among these combinations, mAbs conjugated with rifamycin-type antibiotics have shown particular success. For instance, DSTA4637A is a mAb-antibiotic conjugate currently undergoing clinical trials for the elimination of intracellular *S. aureus*. It consists of a monoclonal human immunoglobulin antibody targeting bacterial wall teichoic acids, a rifamycin-family novel antibiotic (dmDNA31) effective against MRSA, and a protease-cleavable linker. The mechanism involves binding to bacteria, promoting opsonization, and subsequently releasing the antibody inside host cells [124].

As of 2021, there are 14 therapeutic mAbs in different stages of development for the treatment of bacterial infections, and three mAbs have been licensed for preventing or treating infections caused by *Bacillus anthracis* and *Clostridium difficile* [125, 126]. However, challenges remain, such as their high cost of production and issues related to systemic administration.

I.2.5.5. Metallic nanoparticles

Metallic nanoparticles (MNPS) are among the most popular nanostructured materials for antimicrobial applications. Nanoparticles (NPs) are extremely small particles or structures that have at least one dimension in the nanometer range, typically between 1 and 100 nanometers. They exhibit unique physico-chemical and biological properties due to the size and high surface area-to-volume ratio. MNPs exhibit multimodal bactericidal capabilities, ease of synthesis, functionalization, and plasmonic characteristics, making them candidates for the next generation of antibiotics [127]. MNPs composed of various elements such as silver (Ag), gold (Au), copper (Cu), zinc (Zn) or selenium (Se) have been studied as bactericidal agents.

MNPs positively charged establish strong bonds with membranes, leading to cell wall disruption and increased permeability [128]. Moreover, MNPs can release metal ions into the extracellular space, which can penetrate the cells and disrupt biological processes. Within the cell, both metal ions and MNPs can induce the production of reactive oxygen species (ROS), causing oxidative stress. The released metal ions can also interact with cellular structures, such as proteins, membranes, and DNA, disrupting normal cell functions. The synergy between MNPs and antibiotics has been extensively researched to revitalize the efficacy of antibiotics against multidrug-resistant strains [129–131]. Out of all MNPs, silver nanoparticles (AgNPs) have received significant attention and have been explored as coatings for medical devices and as active agents to treat infected topical wounds [132, 133]. However, continuous research is needed to develop more sustainable synthesis methods and to better understand and reduce their toxicological effects on eukaryotic cells [134].

Besides their enhanced antimicrobial capabilities, MNPs also hold promise for use in detecting and imaging bacterial pathogens due to their unique optical properties. One such property is local surface plasmon resonance (SPR). SPR is a phenomenon that occurs when the conduction band electrons of MNPs collectively oscillate in resonance with incident light [135]. In recent decades, this property has garnered significant attention in the field of diagnostics and theragnostics due to its unique characteristics. The SPR of metal nanostructures is highly influenced by factors such as particle size, shape, composition, interparticle interactions, and the dielectric properties of the surrounding medium [136]. The SPR of MNPs enables the creation of various optical methods, including colorimetric, fluorescent, and nonlinear techniques, for detecting bacterial pathogens [137].

In **Chapter VI**, the optical properties of gold NPs were leveraged to develop a system for the detection of pathogenic bacteria in biological samples. This involved

surface functionalization of the NPs with N-acetylneuraminic acid (i.e., sialic acid). In addition, it was observed that, by changing their surface functionalization, these nanoparticles could exert antimicrobial action.

I.2.5.6. Probiotics

Probiotics are living microorganisms that, when consumed in adequate amounts, confer health benefits to the host. They work through various mechanisms, such as competition for ecological space, colonization resistance, nutrient competition, and production of AMPs with specific bactericidal activity [138]. These actions effectively reduce the pathogenic bacteria ability to cause infections and prevent selective pressure from antibiotics.

Studies have found that probiotics help maintaining a healthy and balanced microbiota composition, contributing to optimal health and lowering the risk of opportunistic infections [139, 140]. Their use has also been associated with a significant reduction in antibiotic usage and the selective pressure associated with conventional therapies. Among the most common probiotic microorganisms are *Lactobacilli* and *Bifidobacterium* which have shown the ability to adhere to intestinal epithelial cells, survive in acidic environments and fluids, and exhibit antibacterial activity against various pathogens [141]. Probiotics have emerged as an alternative to antibiotics in the treatment of conditions like *Clostridium difficile*-associated diarrhoea [142]. Notably, faecal microbiota transplant has proven highly successful in managing recurrent *C. difficile* infections by restoring a healthy human donor flora and rebalancing the body's microbiota [143].

Despite their health advantages, probiotics also carry potential risks. They may transfer AMR traits through various mechanisms and trigger non-genetically determined resistance in the endogenous microflora [143].

I.2.5.7. Bacteriophages

Bacteriophages are viruses that specifically infect bacteria. Phage therapy, which uses bacteriophages to treat bacterial infections, has a long history dating back to the early 1900s. While its interest declined with the advent of antibiotics, it is now regaining interest due to the emergence of AMRs [144]. Bacteriophages have shown versatility in combating various infections, such as colistin-only-sensitive *P. aeruginosa* septicemia, burn wound infections and relapsing *S. aureus* prosthetic-joint infections [145–147]. Additionally, extensive research has been conducted on the potential efficacy of phage therapy in farm animals, poultry, and pet animals, particularly for zoonoses and economically significant animal diseases [148].

Lastly, it is worth noting that bacteriophages carry lytic proteins, such as endolysins and virion-associated peptidoglycan hydrolases, which are essential for breaking down phage-infected bacteria and releasing new phage particles. Lytic

proteins derived from phages are currently under investigation as potential antimicrobial treatments [149].

I.3. Drug delivery systems

Drug delivery systems (DDS) refer to a range of technologies designed to improve the therapeutic efficacy of drugs by transporting and releasing them (either passively or actively) to the desired site within the body. By this way, the therapeutic effect of the drug is enhanced, while the potential side effects caused by off-target distribution are reduced [150]. Strategies of DDS focus on modifying the pharmacokinetic (PK) and pharmacodynamic (PD) profiles of drugs, reducing their toxicity and immunogenicity, and increasing their accumulation on the targeted area.

DDS constitute a broad field with decades of continuous development, giving rise to a wide variety of systems that fall under its definition. These systems can vary in form, scale, and functionality, as the examples shown in **Figure I.7**.

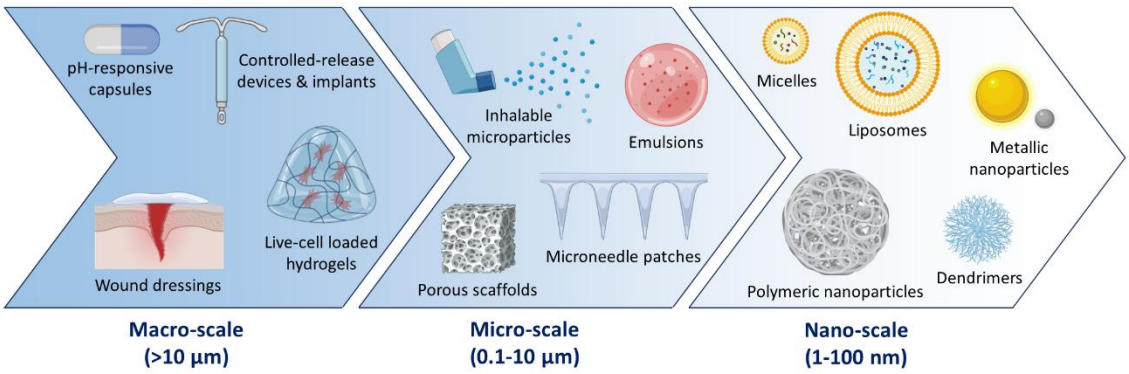

Figure I.7: Examples of some DDS varying in scale and functionality.

The history of modern drug delivery technology began in 1952 with the introduction of Spansule® sustained-release capsules, which enabled sustained drug release for 12 hours after oral administration [151, 152]. During the 1960s to 1980s, oral and transdermal formulations dominated the field, providing therapeutic effects for up to 24 hours for small molecules. In 1989, Lupron Depot®, a polymeric microsphere formulation containing leuprorelin, opened the door for polymeric long-acting injectables and implantable devices, extending drug release from days to months.

In 1990, the introduction of Adagen® marked a milestone in PEGylation, enabling long-term delivery of peptide and protein drugs. This set the stage for subsequent advancements, including the approval of Doxil® in 1995. Doxil®, featuring doxorubicin encapsulated in PEGylated liposomes, is considered the first nanomedicine formulation approved by the FDA. In the year 2000, significant landmarks were achieved with the approval of Mylotarg™, an antibody-drug conjugate, and Rapamune®, a rapamycin nanocrystal formulation. That year, the National

Nanotechnology Initiative was launched by the U.S. government, which was soon embraced globally and paved the way for extensive research in nanomedicine [153].

Nevertheless, as of 2023, the applicability of DDS for treating infectious diseases and their integration into clinical practice remains limited. The only FDA-approved DDS for the treatment of infectious diseases include AmBisome® and Abelcet® (Amphotericin B loaded liposomes used for specific fungal infections), Pegasys® and PegIntron® (PEGylated interferons used for treating hepatitis B and C), and lastly, Pfizer-BioNTech and Moderna COVID-19 vaccines [154]. These vaccines use messenger RNA (mRNA) technology encapsulated in lipid nanoparticles.

I.3.1. Drug delivery challenges

In order to develop a viable and effective DDS, it is necessary to consider several challenges that free drugs encounter upon administration in the body, hindering their therapeutic action [155, 156]. These challenges can be classified into two main categories, depending on whether they are related to the intrinsic characteristics of the drugs or to the biological barriers in the patient.

The first category is related to the physicochemical nature of the free drugs and their *in vivo* compatibility and performance. These challenges include low solubility, low bioavailability, low target specificity, toxicity, immunogenicity, rapid degradation and clearance, and every other characteristic that leads to unfavourable PK/PD profiles. The progress in DDS technologies go hand in hand with the discovery of novel drugs and therapies [150, 157]. Few decades ago, when small-molecule drugs constituted the main class of therapeutics, DDS focused on enhancing drug solubility, extending their activity, and controlling their release profile. However, over the years, new therapies based on larger molecules such as peptides, proteins, antibodies, nucleic acids and live cells have brought forth new challenges and objectives, as summarized in **Figure I.8.**

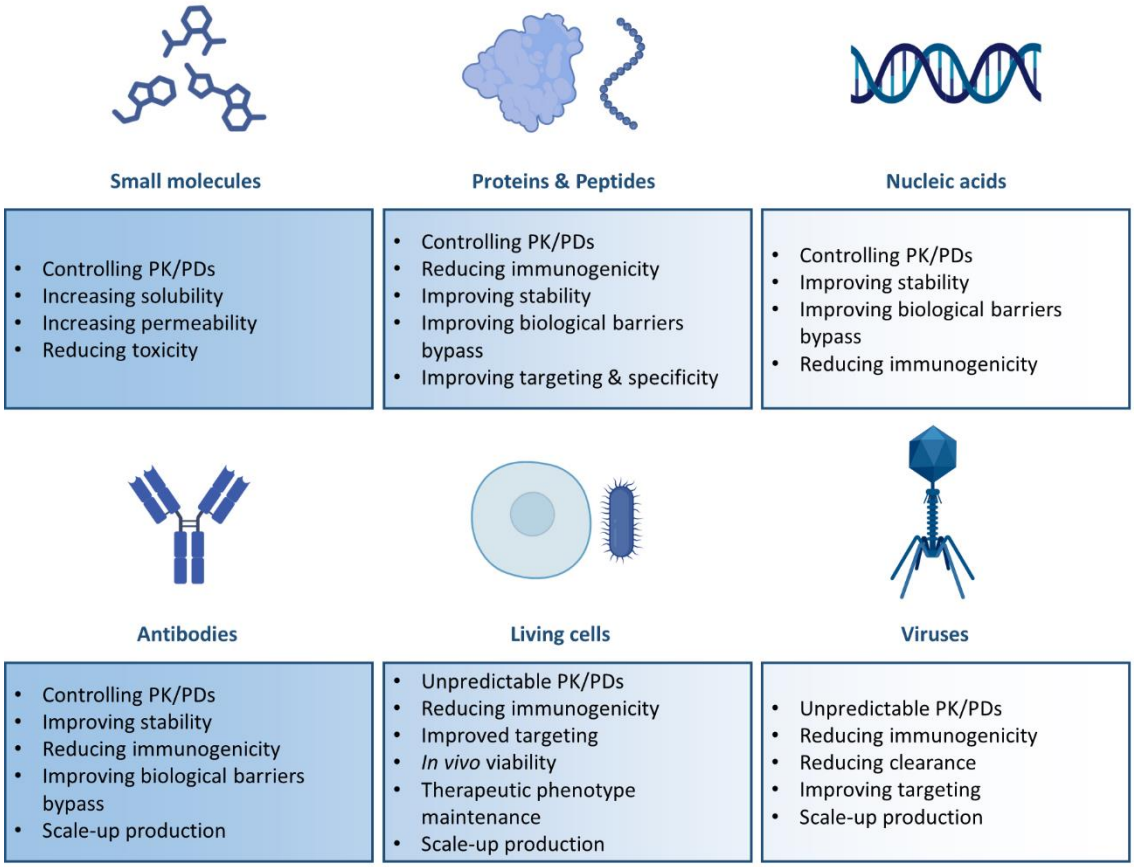

Figure I.8: DDS challenges to overcome based on the type of encapsulated drug.

In **Chapter II** of this thesis, phytochemicals with antimicrobial activity were used to treat infected topical wounds. To overcome their very low water solubility, they were encapsulated within polymeric nanofibers and lipid micelles, significantly enhancing their bioavailability. In **Chapter V**, lysostaphin, an antimicrobial enzyme, was encapsulated in polymeric particles to protect its integrity and extend its activity in complex biological environments.

The second category of challenges are those related to the existence of biological barriers, innate defense mechanisms that any drug, substance or microorganism that enters the human body must traverse [156, 158]. These barriers vary in function and scale and can be classified into organ barriers, sub-organ barriers, intercellular barriers, and intracellular barriers, as shown in **Figure I.9**. The barriers to overcome can vary depending on the administration route and the specific disease of the patient [159]. Although local drug delivery methods of administration offer a way to bypass some of the challenges associated with systemic delivery, they often involve more complex and invasive procedures, leading to their own set of limitations. Moreover, local delivery is typically applicable only in cases where the disease is localized to specific and accessible sites.

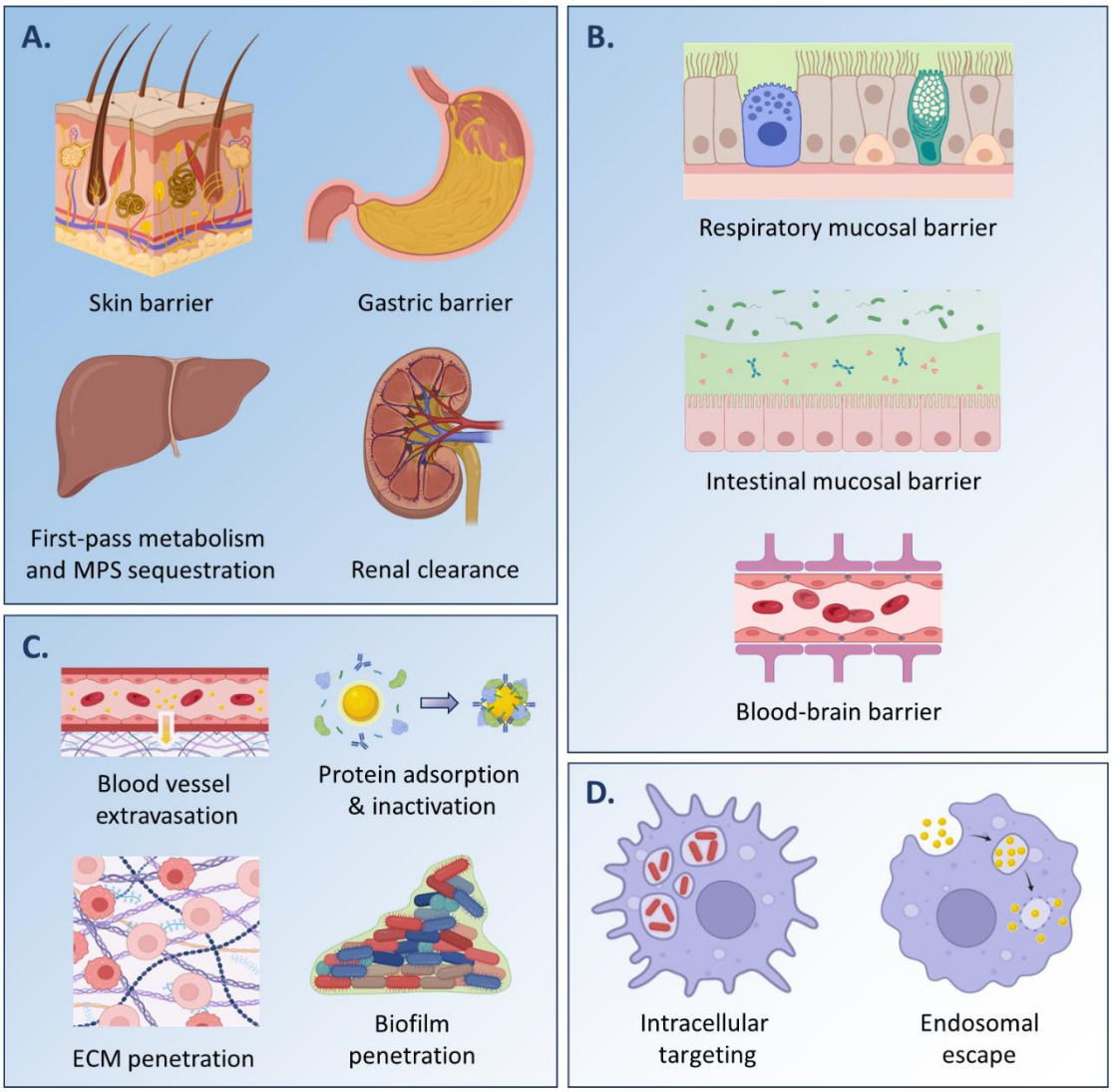

Figure I.9: Examples of biological barriers, classified as A: Organ level, B: Sub-organ level, C: Intercellular level and D: Intracellular level. MPS: Mononuclear Phagocyte System. ECM: Extracellular Matrix. Inspired by the graphical depictions in [150, 155].

In **Chapter IV**, colistin was encapsulated in polymeric particles of the appropriate size for aerosolization, to potentially allow the delivery of the drug to the pulmonary epithelium and avoiding the problems and inefficiencies associated with its intravenous administration. The encapsulated lysostaphin formulation detailed in **Chapter V** was tested against an *in vitro* model of intracellular infection in macrophages, demonstrating its effectiveness in targeting this type of infection and facilitating endosomal escape. Lastly, all formulations developed throughout the chapters considered the need to penetrate biofilm matrices and were assessed against *in vitro* models of such biofilms.

I.3.2. Drug delivery systems and nanomedicine

The term nanomedicine refers to a multidisciplinary field that comprises the application of nanotechnology to medicine, aiming to revolutionize the treatment,

diagnosis, and prevention of diseases. Operating at the nanoscale, ranging from 1 to 100 nanometers, nanomedicine seeks for innovative solutions for healthcare challenges [160, 161]. The unique properties of nanomaterials, such as their large surface area-to-volume ratio, quantum effects, and size-and-morphology dependent behavior, grant them distinct physicochemical and biological characteristics that are not observed at larger scales.

Nanomedicine applied to drug delivery relies on the development of nanocarriers such as liposomes, micelles, polymeric nanoparticles and mesoporous materials, among others [162, 163]. The objective of these nanometric systems is to enhance the therapeutic efficacy of drugs by improving their PK/PD profiles and allowing them to surpass biological barriers. Additionally, nanocarriers can be functionalized with targeting ligands [164], enabling selective accumulation at diseased sites through receptor-mediated interactions, a phenomenon known as active targeting. As a result, DDS based on nanocarriers represent the bulk of all state-of-the-art on the field [157, 165]. Nevertheless, the implementation of nanomedicine in clinical practice still requires careful consideration of biocompatibility, biodistribution, long-term safety, scale-up production, and economic viability. Although research efforts persist in addressing these challenges, as of today, there are currently no FDA-approved nanomedicine-based DDS specifically designed for treating bacterial infections.

DDS utilizing nanocarriers can be categorized based on the primary nature of their components. These categories include lipid-based, polymer-based, and inorganic-based nanocarriers. **Figure I.10** illustrates the most significant examples in each category.

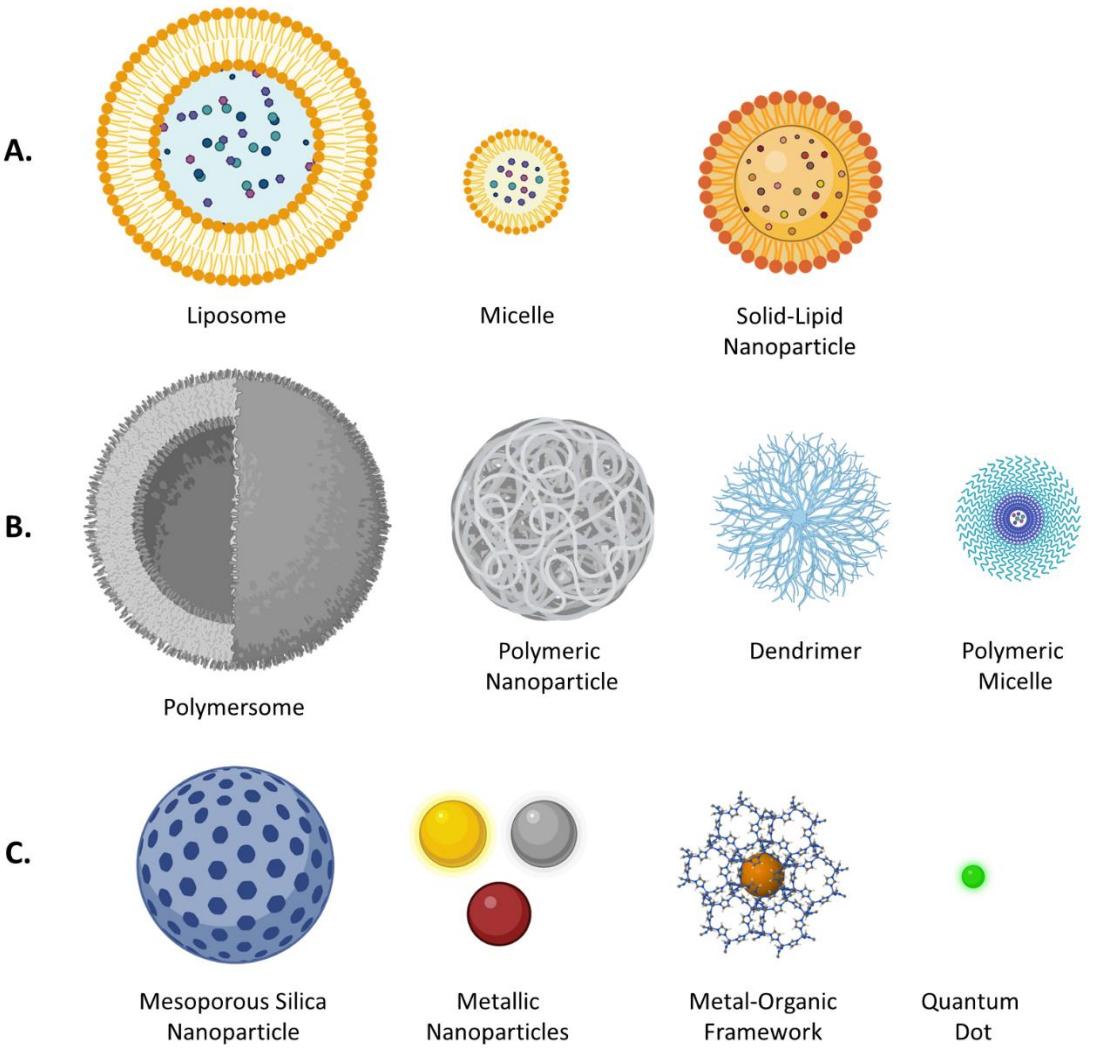

Figure I.10: Nanostructured DDS: **A.** Lipid based carriers. **B.** Polymeric carriers. **C.** Inorganic materials-based carriers.

In the next subsections, each type of nanocarrier will be explained, and their suitability regarding antimicrobial therapies will be discussed.

I.3.2.1. Lipid-based carriers

Lipid-based nanocarriers can be divided into two groups: lipid vesicles, which include micelles and liposomes, and solid-lipid nanoparticles.

Micelles are spherical aggregates of surfactant molecules, with a hydrophilic head group and a hydrophobic tail group. On the other hand, liposomes are spherical vesicles formed by phospholipids, which make up one or more bilayers that surround an aqueous compartment [166, 167]. Just as micelles can only encapsulate hydrophobic drugs in their oil-phase core, liposomes facilitate the encapsulation of drugs of a broad nature: hydrophilic compounds in the aqueous interior and hydrophobic or amphiphilic in the lipid bilayer. Furthermore, the loading capacity of liposomes tends to be higher than that of micelles.

Lipid vesicles are recognized as the most widely used drug nanocarriers present in the clinical practice [168]. As a DDS, they significantly influence the PK/PD profiles, offering a possibility of gradual and sustained release during the circulation of the drug in the body. Similarly, these formulations protect the drug from degradation and inactivation, expanding its bioavailability, as well as reducing toxic side effects [169]. For the case of antimicrobial DDS, lipid vesicles have been intensively studied with a wide spectrum of antimicrobial compounds against chronic bacterial infections. Bacterial strains resistant to a specific antibiotic have increased their susceptibility to the antibiotic when it was included in a lipid vesicle formulation, compared to its administration in its free form [170–173]. While some have suggested that this effect may be attributed to the protection provided by liposomal encapsulation against enzymatic deactivation, it is important to note that the fusogenicity of liposomes can also significantly enhance the antibacterial activity of antibiotics. Liposomes exhibit a bilayer structure like that of cell membranes, thereby contributing to their fusogenicity [174]. This distinctive ability allows liposomes to fuse with bacterial cell membranes, enabling the direct release of their antimicrobial content into the bacterial cells [175, 176].

Solid lipid nanoparticles (SLNPs) are highly stable emulsions made from lipids with a high melting point [177]. Unlike other lipid vesicles, they are solid at room temperature. They represent an alternative to the instability of lipid vesicles and the limited ability of liposomes to encapsulate hydrophobic drugs [40]. On the other hand, these formulations are not suitable for encapsulating hydrophilic drugs as the drugs are embedded in the lipid matrix. SLNPs have been used in conjunction with antimicrobials with low solubility and permeability, such as ciprofloxacin, rifampicin, or tobramycin [178]. As lipid vesicles, SLNPs have been shown to increase the bioavailability of drugs, reduce retention in the mononuclear phagocytic system**,** protect drugs from degradation and improve their overall efficacy [179]. Furthermore, their biocompatibility and the scalability of their syntheses are advantageous.

A common feature shared by all lipid-based nanocarriers is that the diameter is decisive to avoid the mononuclear phagocytic system and infiltrate the tissues [180], as well as in bacterial biofilms. Formulations designed for drug delivery of antimicrobial compounds are estimated to have diameters ranging up to a maximum of 200 to 500 nm [181]. Additionally, the most common surface modification for all lipid nanocarriers is PEGylation, the process of attaching PEG chains to carriers and molecules to improve their PK/PD profiles. Other functional groups that have been employed as targeting ligands are immunoglobulins [182, 183] or antimicrobial peptides [184], among others.

Despite their numerous advantages, lipid-based formulations have drawbacks both during their synthesis and in their *in vivo* performance. These drawbacks include low encapsulation efficiency, loss of encapsulated drug, and instability, which can lead to unwanted vesicle or particle rupture or aggregation. The stability of lipid carriers is determined by lipid composition, as well as pH and temperature. Under physiological conditions, vesicle stability is much more compromised [185].

In **Chapter II** of this thesis, farnesol was encapsulated in lipid micelles for the treatment of infected topical wounds.

I.3.2.2. Polymeric nanoparticles

Polymeric nanoparticles (PNPs) are nano-sized colloids (10-1,000 nm) designed to encapsulate drugs within a polymeric matrix [186]. These particles offer numerous possibilities for achieving controlled drug release and enhanced targeting against specific tissues or biofilms, thanks to their straightforward design, production processes, biocompatibility, and the wide range of available polymers. PNPs have been extensively studied for drug stabilization and drug delivery [187]. In comparison to free drugs, loaded PNPs have many advantages including improved drug bioavailability, protection against enzymatic degradation, controlled drug release and adaptability to various routes of administration [188].

PNPs can be classified into two main groups, nanocapsules and nanospheres [189]. Nanocapsules, or Polymersomes, resemble a vesicular system featuring a polymeric shell entrapping an aqueous core. On the other hand, nanospheres are solid spherical nanoparticles in which drugs are embedded. Within these two main groups, PNPs can be further classified based on their morphology into polymersomes, polymeric micelles, and dendrimers.

Polymersomes are similar to liposomes as their fundamental components are amphiphilic in nature, enabling them to encapsulate hydrophilic drugs. However, they show better stability and a higher cargo retention [190]. On the other hand, polymeric micelles are nanoscale carriers comprising a hydrophobic core and a hydrophilic coating, often made from smart co-polymers based on PEG or poly(dimethylsiloxane) (PDMS).

Lastly, dendrimers are well-structured polymeric macromolecules characterized by a core from which branch-like units extend outward. The term "dendrimer" does not specify a particular chemical composition or polymer but rather refers to a radially symmetrical branching molecular arrangement, consisting of three key elements: nucleus, branches, and surface functional groups [191]. Owing to their nanometric dimensions, low polydispersity, morphological uniformity, and substantial surface area-to-volume ratio, dendrimers hold promise as potential DDS, allowing for high drug loadings. Additionally, it has been reported that some dendrimers have antimicrobial activity on their own [192]. Dendrimers can encapsulate both hydrophobic drugs within their internal cavities and hydrophilic drugs in the functional groups near to the surface. Polymers like polyamidoamine (PAMAM) feature amino functional groups that enable the binding of antimicrobials to the dendrimer surface, such as vancomycin [193]. In addition, antibiotics can be a structural part of the dendrimer [194], as well as antimicrobial peptides with efficacy against bacteria in planktonic [195] or biofilm state [196].

The physicochemical characteristics of PNPs are mostly determined by their method of synthesis and the polymer(s) of which they are composed. The latter can be separated into two main groups: polymers of natural origin (chitosan, gelatin, alginate) or synthetic polymers (PLGA, PLA, polycaprolactone), among others [197]. In both cases, it is mandatory that the polymers are biocompatible and biodegradable. The polymer composition is considered to be the most important determinant for the drug release profile in the body. Additionally, there are certain polymers that already have a bactericidal capacity on their own [198], like chitosan [198]. As with other nanocarriers, PNPs offers themselves as a platform for active targeting strategies, as they can be PEGylated to reduce recognition and incorporate active targeting ligands [199]. Lastly, biodegradable polymers can be found in multiple studies in combination with other nanocomposites, working as capping agents for mesoporous materials [86] or metallic nanoparticles [200].

In **Chapter II**, thymol was encapsulated in a nanofibrous polymeric wound dressing fabricated by electrospinning. In **Chapters IV** and **V**, different methodologies were explored for the encapsulation of antimicrobial peptidic molecules in PLGA PNPs. PLGA is a synthetic copolymer present in several FDA and EMA-approved drug delivery systems and medical devices due to its remarkable biocompatibility and biodegradability, being extensively employed as a controlled drug-release polymer. Its utilization, particularly when formulated into micro or nano-sized particles, finds broad applications *in vitro* and *in vivo* for the targeted delivery of antibiotics, proteins, nucleic acids and so on [201].

I.3.2.3. Inorganic materials

Among nanocarriers based on inorganic materials, we can find mesoporous silica materials, metal-organic frameworks, and metallic nanoparticles, among others.

Mesoporous silica nanoparticles (MSNPs) are particles with well-ordered and regular interior pores, typically ranging from 2 to 50 nanometers. They possess several advantageous properties, such as high surface area, tunable surface charge, uniform porosity, inertness, robustness, and the ability to serve as gated DDS. MSNPs have been extensively studied for drug delivery, including antimicrobials [202]. By altering the synthesis conditions, their pore size can be adjusted, enabling them to entrap a wide range of molecules, from small compounds to large proteins [203, 204]. Drug loading and release are influenced by interactions between the drug and MSNPs surfaces. To enhance loading capacity, various functional groups can be grafted onto the silica internal and external surface [205]. Controlled release from MSNPs can be achieved through passive or active targeting using ligands on the external surface and by capping the pores to release cargo upon external stimuli. These gated MSNPs show promise for controlled drug release in bactericidal applications, with formulations responsive to bacteria, pH changes, enzymes, toxins, temperature, or light [206–208]. Additionally, MSNPs can be combined with other materials, such as gold or silver

nanoparticles, quantum dots, polymers, or other molecules, to create multifunctional applications with synergistic effects alongside regular antimicrobials [209].

Metal-organic frameworks (MOFs) are crystalline materials formed by transition metal ions bound to organic ligands through coordination bonds, hydrogen bonds, or electrostatic interactions [210]. Their characteristics include high porosity, high surface area, high carrier capacity, tuneability and biodegradability. As a result, MOFs have been considered good candidates for functioning as carriers and platforms for the sustained release of antimicrobials [211]. MOFs can encapsulate molecules of varying sizes, ranging from small molecules to larger ones like DNA or proteins [212–214]. Depending on the composition of MOFs, the release of entrapped drugs can be tuned by external stimuli such as pH, light, or temperature [215, 216]. Additionally, MOFs can possess inherent microbial activity due to their composition: When MOFs degrade in a physiological environment, they can release the metal ions with antimicrobial capacity [217]. Moreover, the ligands in MOFs may also possess bactericidal activity. This feature not only can complement the antimicrobial drug cargo but also have a synergistic effect, enhancing its overall effectiveness [218, 219]. Furthermore, the surface of MOFs can also be modified to increase their circulation time, prevent the release of cargo, and provide them with targeting capabilities [220–222].

As introduced in section **I.2.5.5**, metallic nanoparticles (MNPS) are one of the most popular nanomaterials for antimicrobial applications, due to their multifaceted bactericidal properties. They exert antimicrobial activity by their own through mechanisms different from those of antibiotics, making them less susceptible to the development of AMRs. Researchers are exploring the synergy between metal NPs and antibiotics to enhance their effectiveness against multidrug-resistant strains [223]. In addition, MNPs can act as physical carriers, facilitating the transportation of antibiotics to bacterial cells, thereby enhancing the bactericidal activity [224]. This enhancement is primarily attributed to the strong affinity of NPs to bind to the bacterial cell wall, leading to a localized increase in antibiotic concentration and improved bacterial targeting.

Moreover, MNPs offer various innovative strategies for combatting bacterial infections. One such strategy involves photothermal and magnetothermal therapies. In photothermal therapy, MNPs generate heat when exposed to light, which can selectively kill bacteria [225]. In magnetothermal therapy, an alternating magnetic field induces MNPs to produce heat, achieving a similar effect. Another approach is ROS production therapy, where MNPs trigger the production of ROS within bacterial cells upon external stimuli [226]. Elevated ROS levels can damage bacterial structures and DNA, contributing to bactericidal effects.

Lastly, MNPs find applications in theragnostic approaches. These nanoparticles can serve as diagnostic tools for identifying bacterial infections and simultaneously deliver therapeutic agents for treatment [227]. This dual functionality makes theragnostic applications a versatile approach in precision medicine. In this field, quantum dots are of particular significance. As semiconductor crystals of very small size (10 nm), they

show remarkable photophysical properties, such as high brightness, high quantum yield and resistance to photobleaching [228]. These characteristics make them promising for diverse diagnostic biomedical applications, as they can be conjugated with biomolecules like antibodies, nucleic acids, or small molecules to target specific biological ligands [229, 230].

CHAPTER II

Real-time in vivo monitoring of antimicrobial combination therapies in the treatment of infected topical wounds

Table of contents

Summary

The study presented in this chapter assessed the bactericidal and antibiofilm effects of two phytochemicals: thymol and farnesol. These compounds were tested individually and in combination with the standard antiseptic chlorhexidine, both *in vitro* and *in vivo*. To enhance their effectiveness and to provide with a functional medical device, thymol was encapsulated within electrospun Eudragit® S100, a synthetic anionic copolymer made of methacrylic acid and ethyl acrylate, with the goal of developing an effective antimicrobial wound dressing. Conversely, farnesol was encapsulated in lipid micelles.

In vitro studies revealed that combining these compounds significantly improved the antibacterial efficacy compared to using them alone. *In vivo* studies using infected wound splinting murine models further validated the superior bactericidal effects of the proposed combination treatments. Infection progression and the evaluation of antimicrobial treatment outcomes were continuously monitored in real-time by making use of the bioluminescent *S. aureus* strain Xen36.

This research provides promising insights into the development of treatments for non-healing infected wounds, addressing a pressing concern in clinical practice.

The content of this chapter has been adapted from the following accepted work:

Landa, G.; Miranda-Calderón, L.G.; Gómez, A.; Pérez, M.; Sebastián, V.; Arruebo, M.; Lamarche, I.; Tewes, F.; Irusta, S.; Mendoza, G.

Real-time *in vivo* monitoring of the antimicrobial action of combination therapies in the management of infected topical wounds

International Journal of Pharmaceutics, 2023, Volume 646, 123502, https://doi.org/10.1016/j.ijpharm.2023.123502

II.1. Introduction

The skin, the body's largest organ, acts as a protective barrier against pathogens and can be harmed in various ways, leading to different types of wounds. A topical wound is described as the disruption of the skin's normal structure and function. Such wounds can vary from superficial damage to the skin's surface to deeper disruptions of subcutaneous tissues, such as muscles and blood vessels. Acute skin damage, which can result from various factors like mechanical trauma, surgical procedures, burns, etc., is a very ubiquitous health issue. In such cases, failure to rapidly restore skin physiology can lead to serious systemic consequences. Therefore, promoting wound healing is essential to ensure human health and overall well-being [231].

Wound healing is a complex biological process that the body undergoes to repair the injured tissue. It initiates immediately after an injury and continues for a variable duration, influenced by factors like the severity of the wound and whether it is acute or chronic. Efficient treatments are imperative to accelerate the healing process across all its stages, aiming to rapidly restore both the structure and function of the skin tissue [232]. These stages include the initial acute inflammatory response, characterized by blood coagulation and haemostasis, followed by cell proliferation, migration and regeneration, and ultimately, connective tissue remodelling. In healthy skin, the pH is typically slightly acidic (pH=5.5), maintained by acidic keratin sebum and eccrine secretions. However, when a wound occurs, the pH shifts into an alkaline range, varying between 7 and 10 due to exposure of the underlying tissues. The rise in pH may result in complications, including the proliferation of commensal or exogenous bacteria within the wound area, an accelerated loss of transepidermal water, and alterations in the skin microbiome [233].

A crucial factor determinant of the healing process is the presence of wound infection. The intrusion and colonization of microorganisms in wounds affect the host's natural immune system and delay the natural wound healing process. The presence of bacterial biofilm further obstructs and delays the natural wound healing process. This is attributed to its role as a barrier, impeding not only external antimicrobial therapies but also the host's immune response [234]. The purpose of employing antibacterial wound dressings is to prevent infection or to diminish bacterial load and prevent the formation of biofilms when colonization occurs, ultimately leading to a shorter healing time following an injury [235–237]. A well-suited wound dressing serves as a protective barrier for the wound, preventing additional pathogen intrusion and creating a proper microenvironment to support the healing process.

Polymeric nano and microfibrous structures are extensively used as wound dressings for skin repair and regeneration. This choice is due to their high porous structure and extensive surface area, which facilitate efficient gas exchange and proper drainage of wound exudates [238]. Among the current methods for crafting nanofibrous structures, electrospinning stands out as it enables the production of

multifunctional dressings possessing improved mechanical, chemical, and physical properties. This technique enables the encapsulation of hydrophobic and hydrophilic antimicrobial drugs within the electrospun fibers, providing them with protective capabilities and the ability to release these drugs in a sustained or controlled manner [239]. These drug-loaded nanofibrous dressings can be employed either as topical applications on the wound bed or as postoperative prophylactic dressings to prevent microbial growth [240].

As noted in the previous section (**I**), in the face of the escalating problem of antibiotic resistance, the use of natural plant-derived compounds is being investigated for their therapeutic potential. These compounds exhibit various mechanisms of antimicrobial action, reducing the likelihood of phenotypic adaptations to multiple targets [241].

Thymol is a naturally occurring phenolic monoterpene found in the essential oil extracted from plants which belong to the *Lamiaceae* family, included in *Thymus*, *Lippia* and *Origanum* genera, among others. It is known for its antiseptic, antimicrobial, anti-oxidant and anti-inflammatory properties [242, 243]. Electrospun polymeric fibers loaded with active substances derived from essential oils such as thymol (THY) [244–247] have been previously developed. Polycaprolactone (PCL) electrospun wound dressings loaded with THY have demonstrated that can effectively eliminate an experimental topical infection *in vivo*. These dressings yield outcomes comparable to the conventional strong antiseptic chlorhexidine, yet they exhibit significantly reduced tissue toxicity [248].

Farnesol (FAR) is a type of acyclic sesquiterpene alcohol naturally found in various sources like vegetables, fungi, fruits, and herbs. It possesses proven antimicrobial, antiproliferative, antiallergic, and anti-inflammatory properties [249]. Prior research has indicated that FAR antibacterial effects against *S. aureus* can be attributed to two mechanisms: altering bacterial membranes and inhibiting the mevalonate pathway [250]. Notably, FAR, when used in combination with topical antibiotics at concentrations below the MIC, has been found to restore the activity of methicillin and oxacillin against *S. aureus* strains, including MRSA clinical isolates. Additionally, it enhances the effectiveness of fusidic acid, mupirocin, and gentamicin [251]. FAR has also been evaluated against biofilms formed by various microorganisms, inhibiting the formation of single or multiple biofilms of *Candida albicans* ATCC 10 231 and *Streptococcus mutans* ATCC 25 175 strains [252]. In MRSA biofilms, FAR reduces viability, disrupts the plasma membrane, and demonstrates synergy with gentamicin [253].

While many studies have reported promising results regarding FAR potential as an alternative treatment for bacterial biofilms, its clinical use is hindered by its high lipophilicity and low water solubility (logP = 4.84) [254], which limits its bioavailability. To address this limitation, various strategies have been employed. For instance, FAR has been encapsulated or loaded into different carriers, including inorganic materials like halloysite [253] and amorphous silica [255], as well as organic ones like PLGA [256]

and chitosan [252]. Non-ionic copolymer surfactants, such as Pluronic-based micelles, have also been used to enhance FAR aqueous solubility. These micelles dissolve and easily disperse the hydrophobic FAR in water, exhibiting high levels of inhibition against *Streptococcus mutans* biofilms [257]. Furthermore, Valcourt et al. [254] demonstrated that FAR, when formulated as lipid nanoparticles (NPs), restores the sensitivity of *E. coli* MCR-1 to colistin. This allows for the use of a reduced concentration of this last-resort antibiotic to achieve bactericidal effects. Additionally, FAR may offer benefits for wound healing by reducing oxidative stress and inflammation [258].

The management of pathogenic surface microorganisms includes not only the use of active compounds derived from essential oils but also antiseptics, which have a broad spectrum of antimicrobial activity, including bacteria, fungi, viruses, protozoa, and even spores [259]. Chlorhexidine (CHXD) is considered the "gold standard" antiseptic due to its effectiveness against various types of microorganisms such as Gram-positive and Gram-negative bacteria, facultative anaerobes, aerobes, molds, yeasts, and viruses. It provides both immediate and long-lasting antimicrobial effects, preventing the re-colonization of microorganisms on the skin [260]. In some cases, it has been used in combination therapy, like combining CHXD with the antibiotic ciprofloxacin, which has shown synergistic effects [261], or with the tea tree oil, which demonstrated significant antimicrobial activity against *E. coli* [261]. However, as of the current literature review, there are no reports describing the *in vivo* synergy between CHXD and THY or FAR in the treatment of infected topical wounds.

II.2. Objectives

The aim of this study was to evaluate the bactericidal and antibiofilm activity of natural compounds, including THY and FAR-based nanoparticles (NPs), and the antiseptic CHXD against bioluminescent *S. aureus*. The *S. aureus* Xen36 bioluminescent bacterial strain was utilized to allow real-time *in vivo* monitoring of infection progression and antimicrobial treatment outcomes through an IVIS® bioluminescence imaging system.

The hypothesis was that the combination of different agents with distinct antimicrobial mechanisms might act synergistically by targeting different bacterial targets, thus broadening the spectrum of antibacterial action. In this context, combinations of CHXD with THY, CHXD with FAR NPs, and THY with FAR NPs were tested against both planktonic and sessile forms of the bacterium. Moreover, THY-loaded electrospun Eudragit® S100-based dressings (S100-THY) were also assessed *in vitro* and *in vivo* against an experimental topical infection model with *S. aureus* Xen36. The use of a bioluminescent bacterial strain allowed for the observation on how the bacterial community colonized the wound and how treatments reduced their viability by measuring their bioluminescence in both planktonic and sessile bacterial growth modes. A novel clinical protocol was evaluated in which the regular treatment of

infected wounds with a topical antiseptic (e.g., CHXD) would be combined with a terpene-loaded formulation to achieve complete bacterial eradication and successful wound care.

II.3. Experimental

II.3.1. Synthesis and characterization of S100-THY

A 30% (w/v) S100 solution was prepared by dissolving the polymer in a mixture of DMF (dimethylformamide) and EtOH (ethanol) in a proportion of 4:1. To prepare THY-loaded fibers, THY was added to the previous solution to achieve a concentration of 20 wt.% (relative to the polymer weight). The solution was then loaded into a syringe connected to a Yflow 2.2 D500 electrospinner (Electrospinning Machines/R&D Microencapsulation, Málaga, Spain). The distance between the needle's tip and the collector was maintained at 15 cm, and the solution flow rate was set at 1.0 mL/h. The negative voltage applied ranged from -3.02 to -3.69 kV, and the positive voltage varied from +13.15 to +15.07 kV. A schematic diagram of the electrospinning synthesis process and a SEM image of one of the fibrous products appears in **Figure II.1**.

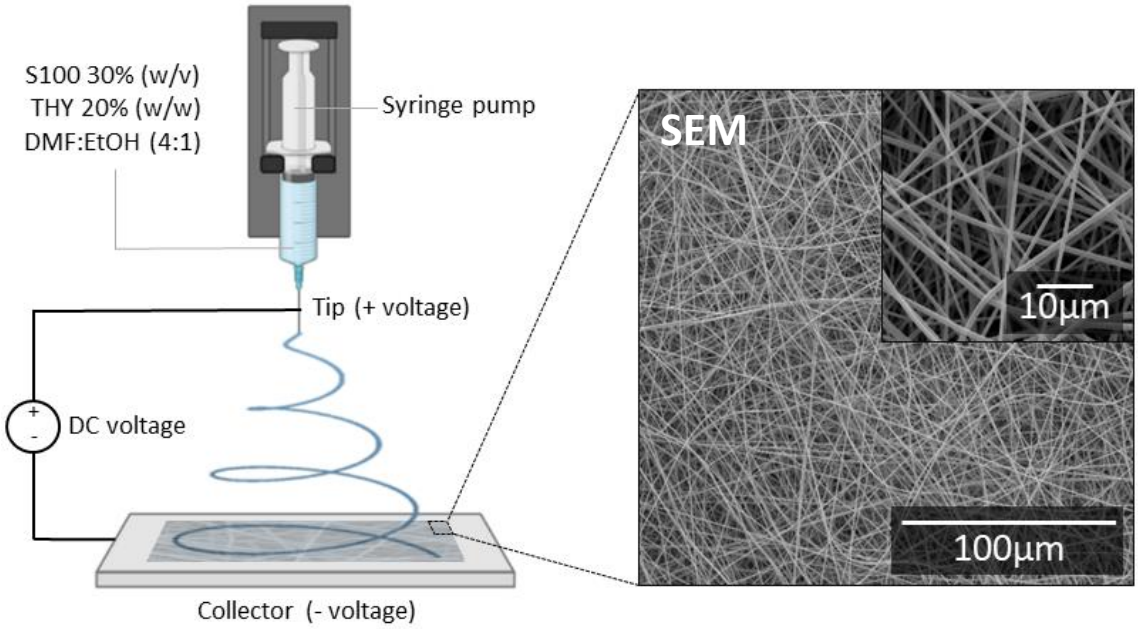

Figure II.1: Scheme depicting the S100 and S100-THY fibers synthesis by electrospinning: A polymeric solution (S100 in DMF:EtOH) containing an antimicrobial agent (THY) is pumped through a syringe and exposed to an electrical potential. As result of hydrodynamic and electrostatic forces involved, the organic solvent evaporates, leaving a dry and fibrous polymeric material in the collector in which the antimicrobial is encapsulated.

The morphology of the synthesized fibers was analysed using scanning electron microscopy (SEM) with an Inspect F50 FEG scanning electron microscope (FEI company, Hillsboro, USA). Nanofiber diameters (N=200) were measured using

DigitalMicrograph® software (Version 2.31.734.0; Gatan, Pleasanton, USA). The mechanical properties of both S100 and S100-THY fibers were evaluated through a tensile test conducted at room temperature using an Instron Microtester 5548 and a video extensometer laser (1 mm/min, 1 KN load cell; Instron, Norwood, USA). The tested samples (N = 5) followed the ISO 527-1:2012 standard for plastics, specifically the determination of tensile properties, and samples were cut into strips measuring 50 mm x 5 mm. A full-scale load of 20 N and a maximum extension of 100 mm were applied.

THY drug loading was determined by GC-MS, utilizing a Shimadzu 2010SE GC-MS chromatograph (Kyoto, Japan) equipped with a Zebron ZB-50 capillary (Phenomenex, Torrance, USA). The encapsulation efficiency (EE) and drug loading (DL) were calculated using equations (**1**) and (**2**), respectively:

(1) $$EE\ (\%) = \frac{mass\ of\ entraped\ colistin\ (mg)}{mass\ of\ added\ colistin\ (mg)} x100$$

(2) $$DL\ (\%) = \frac{mass\ of\ entraped\ colistin\ (mg)}{total\ mass\ of\ colistin\ loaded\ particles\ (mg)} x100$$

Fourier-transform infrared (FTIR) spectra were recorded using a Bruker VERTEX 70 FTIR spectrometer (Bruker, Billerica, USA) equipped with a Golden Gate® diamond ATR accessory. Spectra were recorded by averaging 40 scans in the 4,000−600 cm^{-1} wavenumber range at a resolution of 4 cm^{-1} after baseline correction and water vapor subtraction.

II.3.2. Thymol release studies

THY release from the S100-THY fibers was carried out using an orbital shaker inside an incubator (37 °C). 5 mg of S100-THY (N=5) were immersed in 5 mL of PBS (pH 7.4) during 24 hours under orbital stirring (60 rpm). At predetermined time intervals, 1 mL of the supernatant was collected, and an equal volume of fresh solution was replenished. The collected samples were analyzed in an Acquity UPLC Waters liquid chromatography system (Waters, Milford, USA). An Acquity UPLC Waters BEH C18 column was employed for the THY detection. As internal standard, 25 ppm of naproxen were included in the samples.

II.3.3. Synthesis and characterization of farnesol loaded nanoparticles

Farnesol lipidic nanoparticles (FAR NPs) were prepared following the method previously reported by Valcourt et al. [254]. In brief, the oily phase made of FAR (460 g) and caprylic/capric acid triglycerides (69 wt.%) was mixed under magnetic stirring with a 0.5 M NaCl aqueous solution containing two surfactants, Solutol® HS15 (28,4% [w/v]) and Phospholipon® HS90 (2.52% [w/v]). The initial oil-in-water emulsion was heated over the phase-inversion temperature (PIT, 90 °C) to obtain a water-in-oil emulsion. Then, it was cooled down below the PIT at 60 °C at which it reverted to the oil-in-water emulsion initial state. Three of those temperature cycles were completed

until the oil-in-water framework was fixed by adding 12 mL of water at 4 °C. **Figure II.2** illustrates a diagram of the synthesis procedure.

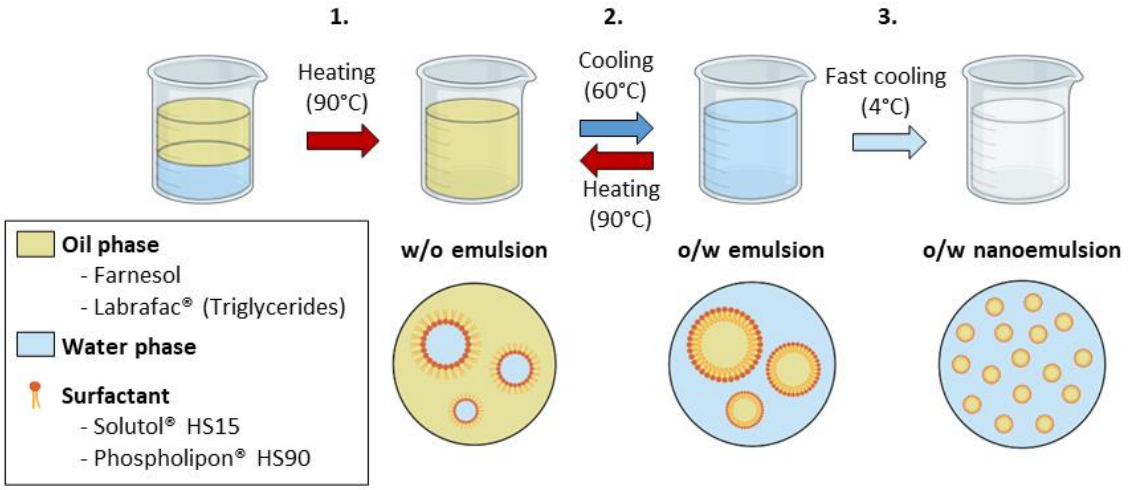

Figure II.2: Schematic representation of the FAR NPs synthesis procedure.

Size distribution of synthesized FAR NPs was determined using a NanoSight NS300 (Malvern Panalytical, Madrid, Spain). Size and morphology were also studied by transmission electron microscopy (TEM). For TEM sample preparation, 20 µL of the suspension were deposited on a carbon-coated copper grid and dried at room temperature. TEM images were recorded on a FEI Tecnai T20 transmission electron microscope (FEI, Oregon, USA) operating at 200 kV.

II.3.4. *In vitro* antimicrobial activity tests

For the antimicrobial activity tests against planktonic *S. aureus* Xen36 bacteria, 100 µL of bacterial suspension (10^7 colony forming units (CFU)/mL) were added to a 96-well microplate (Greiner®, Les Ulis, France). Bioluminescence was recorded over time using a microplate reader (Infinite M200 Pro, Tecan®, Männedorf, Switzerland) until an intensity of ≈1,000 relative light units (RLU) was achieved. At that moment, Mueller-Hinton broth (MHB) solutions with increasing concentrations of CHXD (0.4-40 µg/mL), THY and FAR NPs (0.1-1 mg/mL for both) were added to reach a final volume of 200 µL. Next, the bioluminescence was recorded every 30 minutes for 24 hours at 37 °C. Finally, cultures were serially diluted in 0.9% (w/v) NaCl aqueous solutions and cultured on Mueller-Hinton agar (MHA) plates for bacterial count by colony formation after overnight incubation at 37 °C.

For the antimicrobial activity against biofilm forming bacteria, 100 µL of bacterial suspension were dispersed in a high binding white 96-well microplate and incubated for 48 hours (37 °C, 150 rpm) to obtain mature biofilms. After incubation, MHB was discarded, and bacterial biofilms were washed with 0.9% (w/v) NaCl up to three times before adding 100 µL of fresh MHB. The bioluminescence was monitored until it reached an intensity of approximately 1,000 RLU, and the antimicrobial assay was

conducted using the same procedure as previously described for planktonic bacteria after biofilm dispersion through pipetting.

Furthermore, different combinations of the three antimicrobials (CHXD, THY and FAR NPs) were also tested against *S. aureus* Xen36 both in planktonic and sessile forms. Regarding the THY and FAR NPs combination, increasing concentrations (0.1-1 mg/mL) of both compounds were tested in the same proportions. However, in the case of the CHXD + THY and CHXD + FAR NPs, THY and FAR NPs concentrations were fixed at the MIC values obtained from the previous assays described above whereas CHXD was used in the range of 0.4-40 µg/mL.

The antimicrobial activity of the electrospun S100-THY fibrous material was tested against *S. aureus* Xen36. Disks (Ø = 12 mm) of S100-THY were cut and piled up in 24-well plates to achieve different weights. Samples were then embedded in 2 mL of bacteria-inoculated agar and incubated for 24 hours (≈10^7 CFU/mL, 37 °C). The mass of S100-THY was adjusted to test a range of concentrations in the agar (1-8 mg/mL). Control samples were also tested, including cultures without fibrous material and with unloaded (i.e., drug-free) S100 fibers. After 24 hours, the bioluminescence of the bacteria was measured using an IVIS® Lumina XR (PerkinElmer, Villebon S/Yvette, France). To obtain an accurate bacterial count in the cultures, the solid agar was collected and dissolved in 8 mL of MHB. Bacterial suspensions were then serially diluted and plated, as described above.

II.3.5. *In vivo* wound infection studies

In vivo wound infection studies were conducted in compliance with EC Directive 2010/63/EU after obtaining authorization from the Ethics Committee (COMETHEA) and registration with the French Ministry of Higher Education and Research (n° 2021022510475493). For this study, eight to twelve-week-old male SKH1 hairless mice (Charles River Laboratories, Wilmington, USA) were used. All animals were kept under specific pathogen-free conditions with access to food and water *ad libitum* in the animal facilities of the University of Poitiers (France). A murine excisional wound splinting model was developed to mimic the processes of granulation and re-epithelialization that occur during human topical wound healing, while preventing murine skin contraction by using silicone splint rings.

Sixty mice were experimentally divided into ten groups (N = 6): (I) Control group: wounds without infection or treatment; (II) Infected group without treatment; (III) Infected group treated with free THY aqueous solution (1 mg/mL); (IV) Infected group treated with free CHXD digluconate (1%); (V) Infected group treated with S100-THY dressings (16 mg); (VI) Infected group treated with unloaded S100 dressings (16 mg); (VII) Infected group treated with free THY aqueous solution (1 mg/mL) and FAR NPs suspension (10 mg/mL); (VIII) Infected group treated with FAR NPs suspension (10 mg/mL); (IX) Infected group treated with free CHXD digluconate (1%) and S100-THY dressings (16 mg); (X) Infected group treated with free CHXD digluconate (1%) and FAR NPs suspension (10 mg/mL).

Before the surgery and throughout the *in vivo* studies, the weight of the animals was monitored daily to assess potential weight loss. For surgical procedures, the animals were anesthetized using 5% isoflurane and maintained under 1-2% isoflurane in an oxygen flow of 0.5 L/min. The mice's skin was disinfected with Dakin solution (0.5% sodium hypochlorite solution, Cooper®, Melun, France). Buprenorphine (0.1 mg/kg body weight) was administered subcutaneously 30 minutes before surgery to alleviate pain. Post-surgery, buprenorphine was given two to three times a day and added to their overnight drinking water (0.009 mg/mL) until the end of the study.

Using a sterile biopsy punch (Ø = 8 mm, Eickemeyer Veterinary Equipment Ltd., Stratford, Canada), two circular incisions were made in the scapular area on each side of the medial line. Two ring-shaped silicone wound splints (14 mm OD x 10 mm ID x 0.5 mm Thick, Grace Bio-Labs, Bend, USA) were sutured to the wounds using polyamide suture (Dafilon 4/0; Braun, Germany). Following suturing, the wounds were inoculated with 25 µL of *S. aureus* Xen36 (≈10^7 CFU/mL in 0.9% [w/v] NaCl) to induce infection. The control group received an equivalent volume of saline solution. At this point, the bioluminescence signal emitted by the bacteria in the wounds was measured using an IVIS® Lumina XR instrument, with expected baseline values ranging between 10^4 and 10^5 radiance units (photons/sec/cm^2/sr) in the infection area.

Subsequently, different treatments were administered: in groups III, IV, VII, VIII, and X, 25 µL of the corresponding treatments were applied to each wound. In groups V and VI, disks (Ø = 12 mm, 16 mg) of S100-THY and unloaded S100 dressing, respectively, were placed on the wounds. For group IX, 25 µL of CHXD (1%) was administered before the application of the S100-THY dressing. All treatments were reapplied at 24 and 48 hours post-surgery and infection (PSI). Finally, sterile adhesive plasters and bandages (Hartmann, Brenz, Germany) were used to cover the wounds and splints. These materials were replaced at 24 and 48 hours PSI after microbiological evaluation of the wounds and reapplication of treatments. All wounds were left uncovered from 72 hours PSI until the end of the study, following clinical practice guidelines [234, 262]. The progression of infection, healing, weight changes, and animal welfare were monitored daily until the conclusion of the study.

II.3.6. Wound infection evaluation and pathological studies

The bioluminescence signal emitted by the bacteria in the wounds was recorded at 24, 48, 72 hours, and 7 days post-surgery and infection (PSI). In each group, three mice were euthanized at 72 hours PSI, and the remaining three at 7 days PSI using CO_2 inhalation. Microbiological samples were then collected from the wounds using swabs (Deltalab, Barcelona, Spain) and plated onto MHA plates following the streak plate method. Microbiological results for bacteria colony counting were categorized qualitatively, ranging from (+) for a low number of colonies to (++++) for massive growth. A visual representation of the procedure with the murine excisional wound splinting model is provided in Figure II.3.

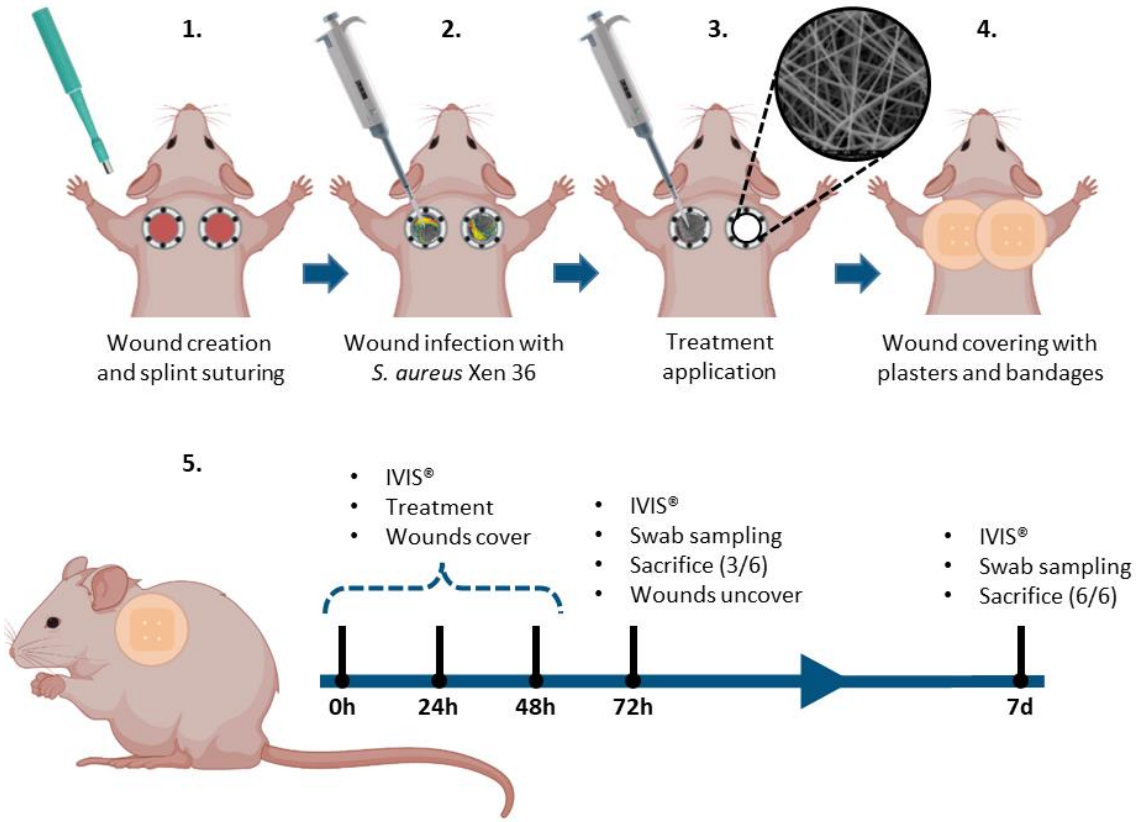

Figure II.3: Schematic overview of the murine excisional wound splinting model: (1) Surgical wounds were created using an 8 mm-diameter biopsy punch, followed by suturing the splint rings around the wounds. (2) Infection was induced by inoculating *S. aureus* Xen36 (25 µL, 10^7 CFU/mL). (3) Depending on the experimental group, different treatments were applied. (4) Wounds were covered with plasters and bandages. (5) Daily, after IVIS® measurements and treatments, the plasters and bandages were replaced to maintain wound coverage until 72 hours PSI. At this point, half of the animals in the experimental group were euthanized for swab sampling and wound extraction, while the remainder were left with uncovered and untreated wounds until 7 days PSI.

For the conduction of histological studies, wounds were collected, fixed in 4% paraformaldehyde (Alfa Aesar, Haverhill, USA) for 24 hours, and embedded in paraffin. Histological sections (5 µm thickness) were stained with haematoxylin and eosin (HE) and Gram-stained for histopathological and bacterial evaluation, respectively. Additionally, immunohistochemical evaluation of angiogenesis was performed using a rabbit polyclonal CD31 antibody (ab28364, Abcam, Cambridge, UK) on an automated immunostaining platform. Antigen retrieval was achieved through treatment with a high-pH buffer (CC1m, Roche, Basel, Switzerland). Subsequently, slides were incubated with the primary antibody (1:50, 60 minutes) followed by visualization using the corresponding horseradish peroxidase-conjugated visualization system (EnVision FLEX+, Dako, Jena, Germany). Nuclei were stained with Carazzi's haematoxylin. Lastly, the slides were then dehydrated and permanently mounted.

II.3.7. Statistical analysis

Statistics were conducted using GraphPad Prism 8 software (GraphPad Software Inc., US). Data for antimicrobial activity, drug release, and bioluminescence are presented as mean ± standard deviation. Antimicrobial activity assays were performed three times in triplicate, while *in vitro* bioluminescence studies were done in quadruplicate. Statistical analysis included the Kruskal-Wallis test, followed by Dunnett's post hoc test for multiple comparisons. Significant differences in bioluminescence signal means were analysed using a two-way analysis of variance (ANOVA), followed by Dunnett's multiple comparison test (* $p < 0.05$, ** $p < 0.01$, *** $p < 0.001$, **** $p < 0.0001$).

II.4. Results and discussion

II.4.1. Synthesis and characterization

Using the electrospinning technique, homogeneous and bead-free S100-THY fibers were obtained, with a mean diameter of 656 ± 93 nm. (**Figure II.4a** and **b)**. Unloaded (i.e., drug-free) S100 fibers displayed a slightly different mean diameter (822 ± 150 nm; **Figure II.4c** and **d**).

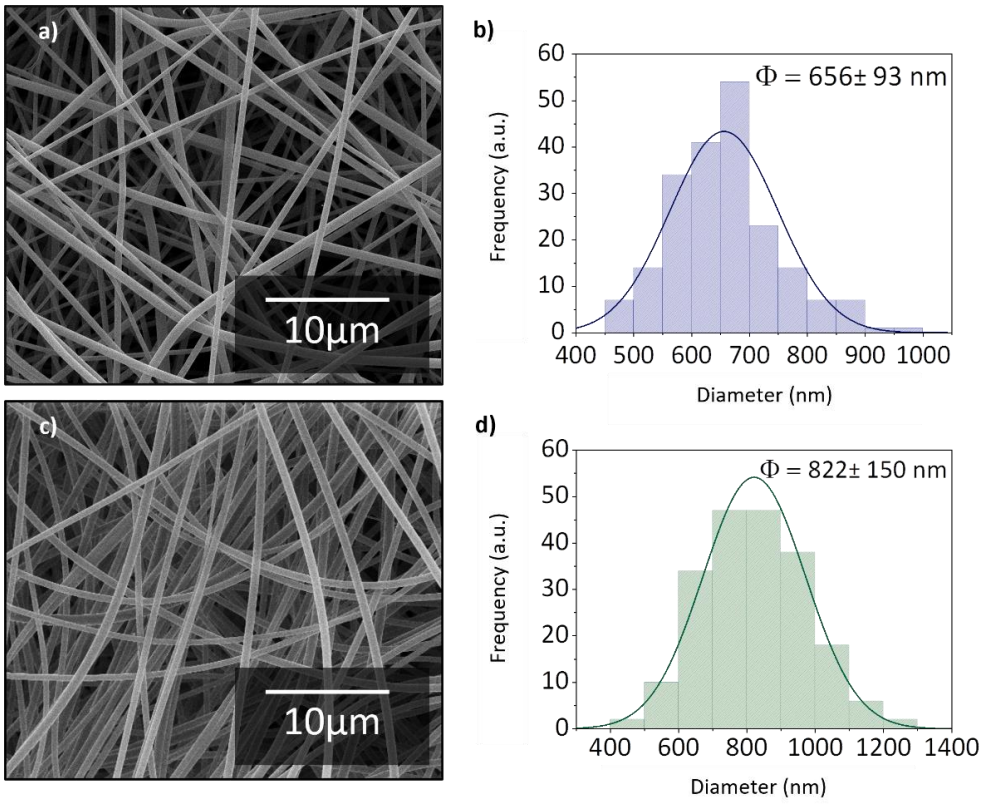

Figure II.4: Characterization of S100-THY and S100 fibers. **(a)** and **(b)**: SEM images and size distribution histogram of S100-THY fibers. **(c)** and **(d)**: SEM images and size distribution histogram of S100 fibers.

These results were consistent with those reported previously for Eudragit® S100 fibers obtained through monoaxial electrospinning and loaded with benzoic acid or 9-anthracene carboxylic acid (500-600 nm) [263] or loaded with budesonide, which also exhibited a uniform structure with a mean diameter of 660 nm [264].

The THY encapsulation efficiency achieved in the S100 fibers was 64 ± 3%, resulting in a drug loading of 11.4 ± 0.5 wt.% of THY. Burgess et al. [263] demonstrated that the encapsulation efficiency for different active compounds in electrospun S100 fibers could be higher than 85 wt.%; however, the drug loading was consistently lower than 10 wt.%. These authors attributed the decrease in loading efficiency to losses of the corresponding active compounds during the electrospinning process, such as small amounts of precipitation or adherence to the syringe walls. Additionally, due to the high volatility of THY (0.016 mm Hg at 25 °C), it is likely that a portion of the active compound evaporated along with the solvent (DMF:EtOH) in the electrosprayed jet formed from the needle tip to the collector plate.

The data presented in **Table 1** indicate that the electrospun dressings are not mechanically rigid but rather flexible and easily conformable to the wound. These characteristics are advantageous as dressings should be easy to apply, adaptable, and porous, allowing for gas exchange while preventing wound maceration. The mechanical property analysis of empty S100 fibers did not reveal significant differences compared to those observed for S100-THY fibers. However, the inclusion of THY in the dressing slightly reduces its resistance to elastic deformation. Therefore, the drug-loaded dressing is mechanically similar to its non-loaded counterpart but exhibits lower stiffness and higher elasticity. Nevertheless, this increased elasticity makes the resulting dressings soft and easily conformable to the wound contour.

Table 1: Mechanical properties of wound dressings synthesized by electrospinning.

	Tensile strength (MPa)	**Young's module (MPa)**	**Strain at break (%)**
S100	0.4 ± 0.06	3.8 ± 0.2	28.6 ± 3.4
S100-THY	0.2 ± 0.06	2.2 ± 0.3	24.8 ± 5.2

Kinetic studies (**Figure II.5a**) confirmed that 35% of the loaded THY was released in the first 5 hours. An initial burst release was observed, which could be associated with the presence of THY on the external surface of the fibers, as previously reported [247, 248, 265]. Then, controlled diffusion over 5 hours, reaching 35% of the loaded THY, was achieved, consistent with previous studies on S100 sustained delivery [266], as well as THY release from different polymeric fibers, including S100 [248, 266, 267]. Therefore, this proposed material would result in an extended duration of action, with THY being released in a controlled manner.

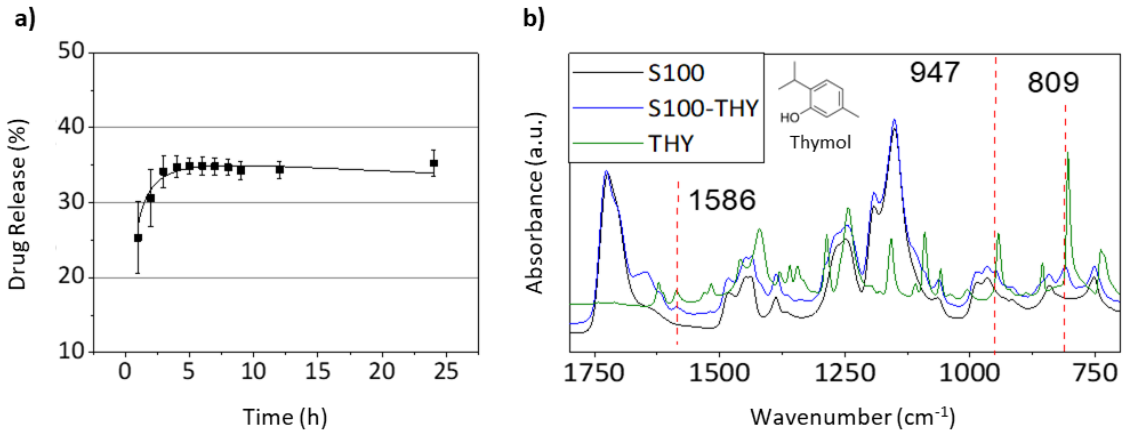

Figure II.5: Physicochemical characterization of S100-THY fibers. **a)** Kinetic release profile of THY from S100-THY fibers. **b)** FTIR spectra of THY, S100 and S100-THY fibers.

Figure II.5b displays the FTIR spectra of S100-THY, S100, and THY in the 1800-700 cm^{-1} region. The spectrum of loaded fibers exhibited all the characteristic bands of S100, while the presence of THY was confirmed by the vibrations observed at 809, 947, and 1586 cm^{-1}. This last band can be assigned to the phenol ring of THY. Meanwhile, the peaks detected at 809 and 947 cm^{-1} would be related to out-of-plane aromatic C-H wagging and bending vibrations that appear in the THY spectrum at 804 and 943 cm^{-1}, respectively [268, 269]. The observed slight blue shift in the loaded fibers could indicate some interactions between THY and the polymer, which would be beneficial as they will contribute to slowing down the release of the active compound. Considering the chemical structure, the interaction could be expected between the hydroxyl groups of THY and the carbonyl groups of the polymer. This interaction would be confirmed by the change in the intensity ratio between the characteristic C=O stretching of the S100 esterified carboxylic group observed at 1725 cm^{-1} and the shoulder due to carboxylic acid groups (1650 cm^{-1}) [270].

The synthesis of farnesol nanoparticles was successfully achieved using the cycling PIT method, as previously depicted in **Figure II.2**. TEM images of individual FAR NPs (**Figure II.6**) show a mean diameter of 47 ± 21 nm. However, most of the particles exhibit a hydrodynamic diameter of 89 ± 44 nm, although some agglomerates of more than 100 nm were observed. This hydrodynamic diameter is slightly larger than that previously reported by Valcourt et al. for the same NPs [254].

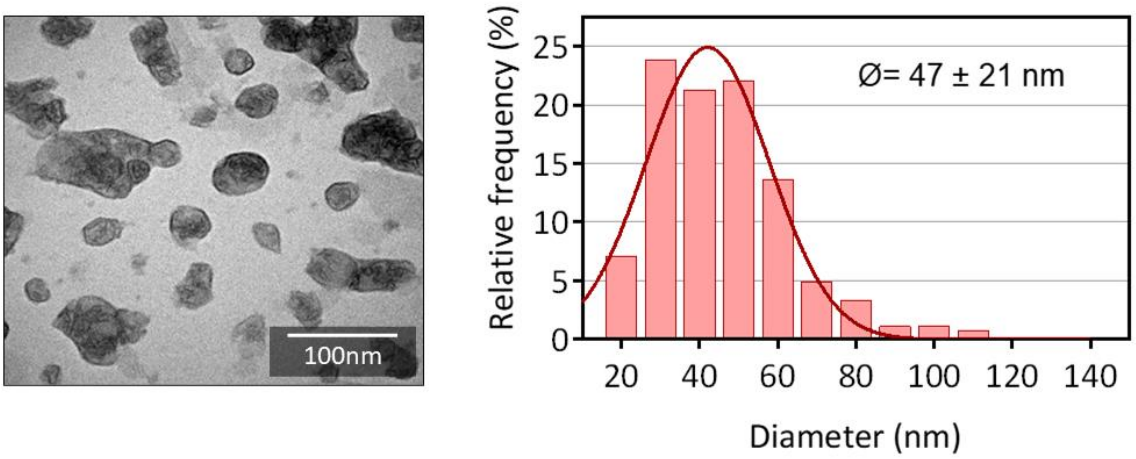

Figure II.6: TEM image of FAR NPs and particle size distribution histogram.

FTIR spectra of farnesol and FAR NPs were measured, but the overlapping signals observed for both systems, along with the vibrational signals assigned to Labrafac®, Solutol®, and Phospholipon®, made impossible to discriminate between the corresponding signals in the 4,000-500 cm^{-1} region.

II.4.2. *In vitro* bactericidal activity

The bactericidal effects of THY, FAR NPs, and CHXD in planktonic cultures demonstrated differential effects based on the treatment applied (**Figure II.7a** and **b** and **Appendix I.1** to **3**). Colony counting assays (**Figure II.7a** and **b**) revealed that CHXD was the most effective antimicrobial compound tested, showing a MIC of 2 µg/mL, whereas THY and FAR NPs significantly inhibited bacterial growth at concentrations of 0.4 and 0.9 mg/mL, respectively. In this regard, the concentration needed to reach the minimum bactericidal concentration (MBC) was higher for THY (0.6 mg/mL) than for CHXD (4 µg/mL), and planktonic cultures treated with FAR NPs were not completely eradicated even at the highest concentration tested (1 mg/mL). Indeed, at this concentration, only a 2-log reduction was observed with FAR NPs, demonstrating their reduced effectiveness compared to THY and CHXD.

Bioluminescence evaluation of the treated cultures also showed a high efficiency of the compounds tested in inhibiting bacterial growth, displaying a clear dose-dependent effect (**Appendix I.1** to **3**). The luminescence signal intensity (LSI) was depicted by normalizing the data of the relative light units (RLU) acquired from the cultures, considering the average of RLU at time zero as LSI = 1. CHXD treatment significantly decreased bioluminescence at a concentration of 1 µg/mL within the first hour after CHXD addition. On the other hand, THY and FAR NPs achieved a significant reduction in bioluminescence after the first hour of treatment at 0.6 and 0.1 mg/mL, respectively.

Surprisingly, even though FAR NPs did not reduce bacterial cell counts by more than 2-log when treated with 1 mg/mL, bioluminescence was clearly arrested at a

much lower concentration (0.1 mg/mL). This observation has also been reported by others for the same strain, where the antimicrobial pressure strongly impacts the relationship between CFU and bioluminescence [271]. Those authors concluded that in the presence of antimicrobials, bioluminescence is not controlled by luxA expression but by co-factors that affect bacterial metabolic activity. Bioluminescence depends mainly on two elements: the concentration of bacteria and their metabolic activity (since ATP is needed to produce light). Additionally, a decrease in bioluminescence without a decrease in the number of bacteria strongly suggests that FAR NPs, even at a concentration as low as 0.1 mg/mL, reduce the metabolic activity of *S. aureus*.

The effects of treating *S. aureus* Xen36 biofilm with these compounds and the different combinations tested showed promising results, particularly regarding the combined administration of these compounds (**Figure II.7c** and **d** and **Appendix I.1** to **3**). In general, eradicating biofilms required higher compound concentrations because resistance and tolerance to antimicrobials are known to be increased compared to planktonic cultures due to the extracellular polysaccharide (EPS) matrix impairing antibiotic diffusion and the reduced metabolic state (dormancy) [272]. Our results demonstrated that CHXD treatment achieved the lowest biofilm bactericidal concentration (BBC) (4 µg/mL) and minimal biofilm eradication concentration (MBEC) (40 µg/mL) values, whereas total eradication of bacterial biofilms at the highest concentrations tested for THY and FAR NPs was not achieved.

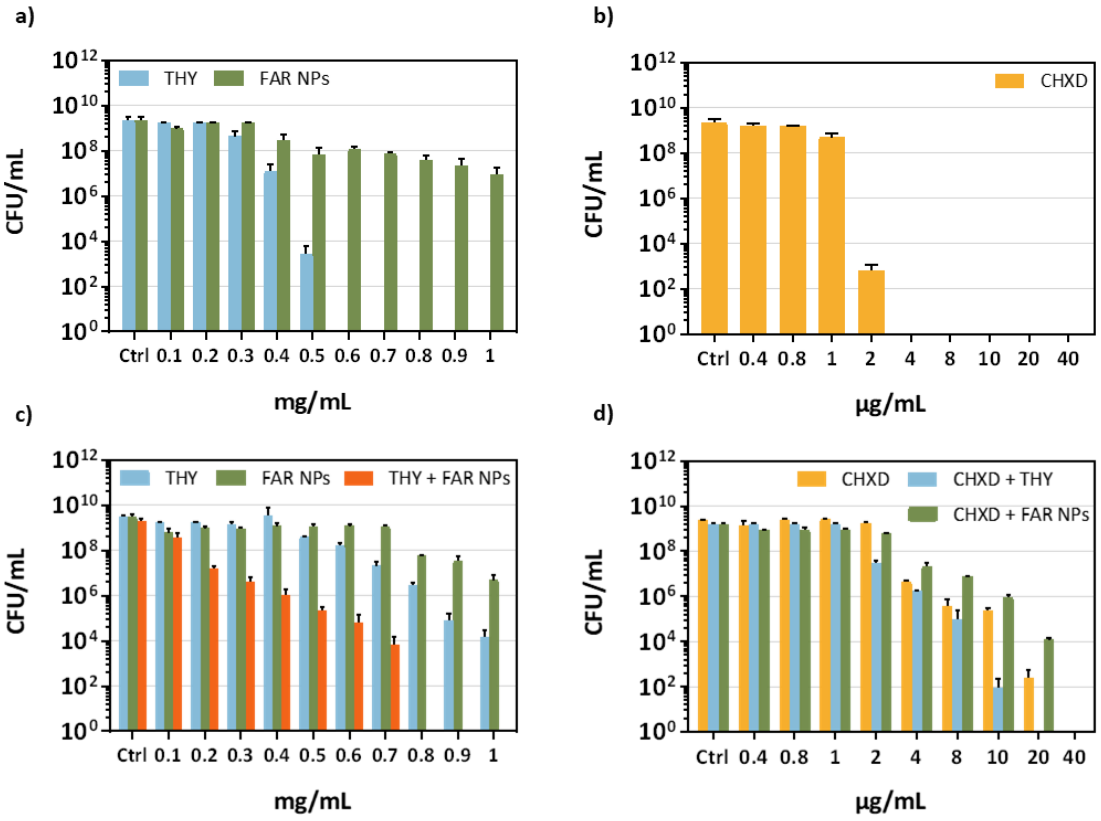

Figure II.7: *In vitro* antimicrobial activity of the different treatments evaluated. **a)** *S. aureus* Xen36 growth in planktonic state treated with free THY and FAR NPs. **b)** *S. aureus* Xen36 in planktonic state treated with CHXD. **c)** Antimicrobial activity of THY,

FAR NPs, and the combination of both at the same concentration on *S. aureus* Xen36 mature biofilms. **d)** Antimicrobial activity of CHXD alone and in the presence of a fixed concentration of THY (0.5 mg/mL) and FAR NPs (1 mg/mL) on *S. aureus* Xen36 biofilm.

Regarding the bioluminescence signal (**Appendix I.1** to **3**), biofilms treated with CHXD also displayed a significant reduction in their signal within the first hour of treatment at BBC (4 μg/mL). However, THY (≥ 0.6 mg/mL) and FAR NPs (≥ 0.1 mg/mL) were able to reduce LSI through a more sustained trend, and particularly, in the case of THY, the signal was recovered to control levels after 12 hours. Interestingly, some of the combined treatments tested (THY+FAR NPs, CHXD+THY, CHXD+FAR NPs) resulted in an enhanced bactericidal effect. Specifically, THY+FAR NPs significantly reduced the BBC value (0.2 mg/mL; >70% reduction compared to THY and FAR NPs tested independently), and the MBEC was attained at 800 μg/mL (**Figure II.7c**). The addition of THY to CHXD treatment resulted in a halving of the CHXD MIC and MBC values. However, the addition of FAR NPs to CHXD did not result in any change in the bacterial growth (**Figure II.7d**).

S100-THY fibers were also evaluated in solid cultures to elucidate their potential *in vitro* antimicrobial effects against *S. aureus* Xen36 (**Figure II.8a** and **b**). Bioluminescence measurements (**Figure II.8a**) indicated a significant effect of the electrospun loaded nanofibers, which was confirmed in the colony cell counts (**Figure II.8b**). The minimum inhibitory concentration (MIC) was attained at a concentration of 1 mg/mL, while the minimum bactericidal concentration (MBC) was attained at a concentration of 8 mg/mL. These concentrations corresponded to THY release amounts of 0.04 mg/mL and 0.32 mg/mL, respectively, within a 24-hour timeframe. These results are significantly lower than those obtained for the planktonic and biofilm experiments when free THY was added to the cultures. MIC and MBC values were reduced by more than 90% when THY was loaded into S100 fibers compared to the treatment with free THY. These promising data are consistent with previous studies [248, 273], highlighting the importance of encapsulating drugs for achieving controlled, prolonged release through polymer modification. They also underscore the significance of contact between electrospun fibers and bacteria in achieving a potent antimicrobial effect, which, in turn, reduces the necessary drug concentration. The shiny white contrast observed in the wells containing dressings at an 8 mg/mL concentration is caused by the large number of piled dressings needed to reach such a high concentration, resulting in a height increase, a change in the working distance, and the corresponding white contrast in the IVIS® equipment.

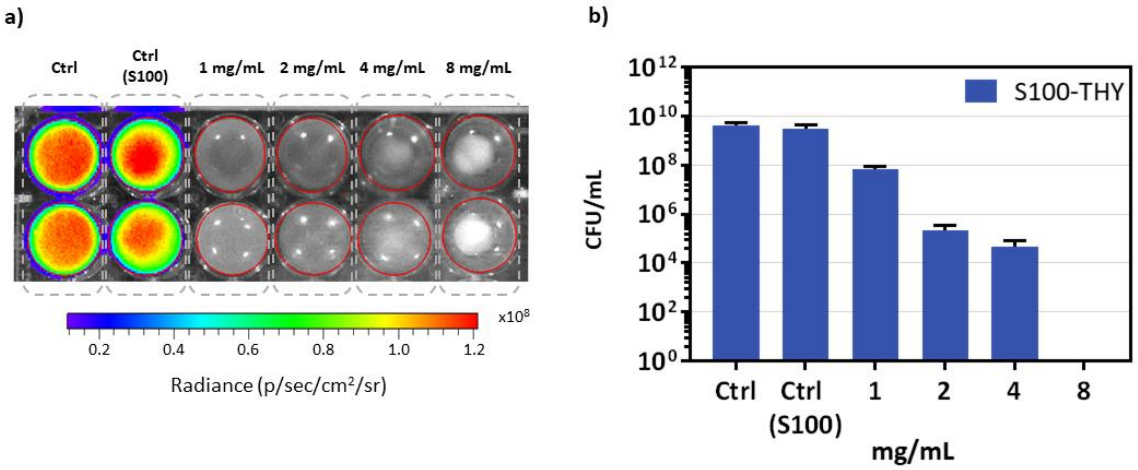

Figure II.8: Antimicrobial activity of S100-THY. **a)** Bioluminescence signal of *S. aureus* Xen36 in solid agar after 24 hours of treatment with different S100-THY concentrations. **b)** Bacterial colony counts of the cultures depicted in **(a)**.

Considering these *in vitro* studies, CHXD was the most effective treatment in reducing bacterial viability, both in planktonic and biofilm cultures. However, once the biofilm is formed, the combination of THY together with CHXD or FAR NPs produced an enhanced antimicrobial effect, resulting in a reduction in BBC and MBEC values of more than 50%. In addition, S100-THY loaded fibers also demonstrated superior *in vitro* efficiency for encapsulated THY compared to equivalent doses of the free compound.

Other authors have previously shown the higher bactericidal effects of CHXD compared to THY [274]. For instance, the MIC and MBC values obtained when CHXD was added to planktonic and biofilm cultures of *S. epidermidis* were in the range of our results (2-16 µg/mL), while THY was needed at higher concentrations (0.5-16 mg/mL) to inhibit or eliminate the same bacteria. However, their results did not demonstrate an increased antimicrobial effect with the combined use of CHXD and THY. Different studies have suggested that the enhanced antimicrobial activity of the combined treatment of CHXD with terpene-derived compounds, such as THY and farnesol, might be attributed to their combined action on the same bacterial target, i.e., the cell membrane [275]. In addition, CHXD may boost biofilm disruption due to its cationic character and the mostly negative charge of the biofilm extracellular matrix. The combination of CHXD and terpene-derived compounds would pose both hydrophobic and hydrophilic features and may modify the ionic interactions with the biofilm extracellular matrix [274].

Conversely, previous studies have suggested the potential interaction of FAR with the bacterial membrane, as well as its interference with the quorum sensing system of the bacteria [276–278], demonstrating antimicrobial activity for FAR NPs. Specifically, its hydrophobicity fosters FAR accumulation in the bacterial membrane, promoting cell leakage [277, 279]. Moreover, FAR was reported as a modifier of the synthesis of glucan, a biofilm matrix polysaccharide, inhibiting the accumulation of biofilm biomass

[280]. However, the concentrations of FAR (20-250 µg/mL) and the bacterial strains used in these previous studies vary, making it difficult to ascertain a general trend for different microorganisms and necessitating a case-by-case consideration. In this regard, some authors have highlighted the potential of FAR to be used as a sensitizer in combination with different antimicrobials by altering bacterial membrane permeability, pointing to this strategy as more efficient compared to its role in monotherapy [277, 281]. This mechanism may promote the influx of antimicrobial compounds into the cell, enhancing the interaction with intracellular targets. Therefore, the combined application of FAR NPs with THY in the treatment of established bacterial biofilms, as observed in the *in vitro* studies to reduce the MIC value by up to 70%, represents a promising strategy for effectively eradicating biofilms in the context of infected wound management.

II.4.3. *In vivo* studies

The effectiveness of the antimicrobial treatments tested in this study was assessed using a murine excisional wound splinting model, as described in **Figure II.3.** Various control and experimental groups were established, as outlined in section **II.3.5**. We evaluated the treatment effects by simultaneously measuring the bioluminescent signals emitted by the bacteria in the wounds, conducting microbiological analyses of the wounds, and performing histopathological studies.

Figure II.9 and **Appendix I.4** present the results of the bioluminescent signal, wound morphology, and microbiological analyses. These results confirmed the superior effectiveness of treatments containing CHXD, consistent with the findings from the *in vitro* experiments. At 72 hours after surgery and infection, when wounds were left uncovered and untreated for up to 7 days PSI, the groups treated daily with CHXD, CHXD+FAR NPs, and CHXD+S100-THY exhibited a significant decrease in the bioluminescent signal and a simultaneous reduction in bacterial counts. Moreover, among the other experimental groups tested, FAR NPs showed slightly higher bactericidal activity compared to that of the THY and S100-THY groups (**Figure II.9e**).

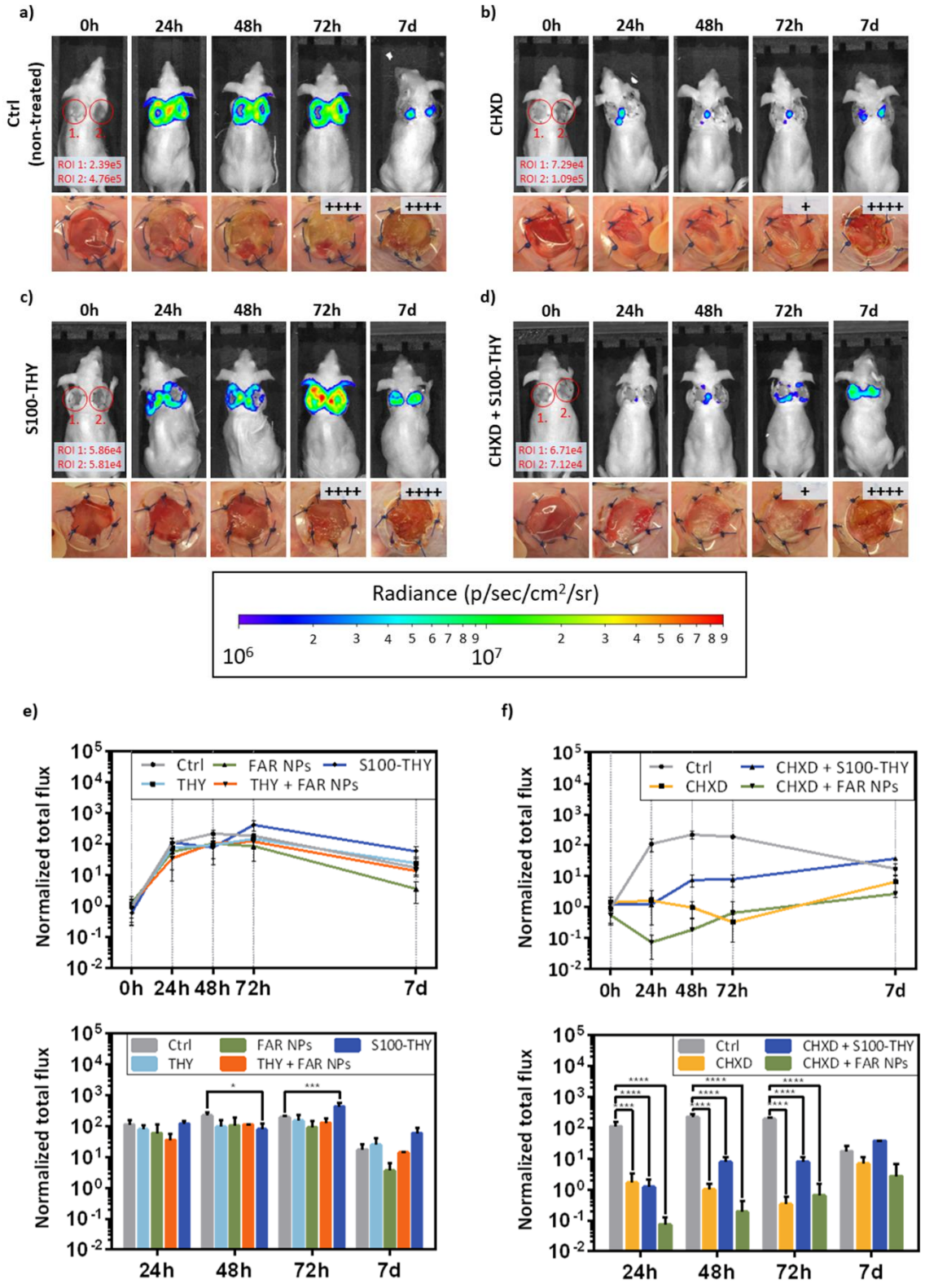

Figure II.9: *In vivo* evaluation of *S. aureus* Xen36-infected and treated wounds in SKH1 mice was conducted at 24, 48, 72 hours, and 7 days post-skin injury (PSI). The evaluation included bioluminescent signal measurements, morphological assessments, and microbiological analyses of the wounds. Each wound of every animal served as a region of interest (ROI). Values of total flux at ROIs that exceeded the scale are highlighted in red in the corresponding images. Microbiological results regarding

bacterial colony counting are presented as insets, ranging from (+) indicating a low number of colonies to (++++) representing a massive culture. **a)** Control group (infected, non-treated). **b)** Infected and treated with CHXD. **c)** Infected and treated with S100-THY dressing. **d)** Infected and treated with both CHXD and S100-THY dressing. **(e-f)** Changes in the bioluminescent signal of *S. aureus* Xen36 obtained from the different experimental groups are shown. The upper graphs display the evolution of the bioluminescent signal (total flux) at ROIs over time, with data normalized to the average initial signal (0 h PSI). The lower graphs provide data comparisons between groups at each time point. Results are expressed as Mean ± SD of three independent experiments. Statistical analyses compare each treatment group to the control group (*$p < 0.05$; **$p < 0.01$; ***$p < 0.001$; ****$p < 0.0001$).

It is important to note that by 7 days PSI, no significant differences among groups were observed due to the discontinuation of treatments and the fact that we uncovered the wounds 72 hours after infection. It is worth mentioning the substantial initial bacterial load used in the experimental infection for each wound (2.5×10^5 CFU/wound). It was noted that in the control group (non-treated), bacteria proliferated easily (**Figure II.9a**), but later on, the animal's immune system, along with the scabbing process and drying after removing the coverings, led to a reduction in bacterial burden by day 7. However, since not all bacteria were eliminated, their numbers remained relatively high.

In contrast, the initial bacterial challenge in the treated groups (**Figure II.9b** and **c**) was significantly reduced in the first few days. However, after uncovering the wounds and discontinuing treatment, bacteria continued to proliferate as expected. It is worth noting that in a real clinical setting, where aseptic conditions and surgical practices are maintained, any accidental bacterial contamination would be minimal. Consequently, the proposed treatments would effectively eliminate all present bacteria, preventing early post-wounding infections. **Figure II.9c** demonstrates that the antimicrobial wound dressing alone was unable to reduce the initial bacterial burden due to its delayed antimicrobial release. However, when combined with the immediately available antiseptic CHDX (**Figure II.9d**), the bacterial load was significantly reduced.

Histopathological and immunohistochemical evaluations were conducted to assess the wound status, including changes in tissue morphology, infection, and angiogenesis (**Figure II.10**). The groups under analysis primarily consisted of those treated with CHXD and its combinations, as these treatments demonstrated the highest efficacy in both *in vitro* and *in vivo* studies. In terms of inflammation and alterations in tissue morphology, we observed similar lesions in all groups. Additionally, coccoid bacteria were found, mainly on the surface of the wounds. Notably, CD31 immunohistochemistry revealed a slightly reduced signal in the CHXD+FAR NPs treated group, suggesting a potentially slower tissue regeneration compared to the CHXD and CHXD+S100-THY groups. The combination of CHXD with the natural terpenes tested here contributed to a successful reduction in the infective bacterial load without causing severe damage to the tissues. Additionally, the treated groups exhibited

successful granular tissue formation, re-epithelialization, remodelling, and scar tissue formation.

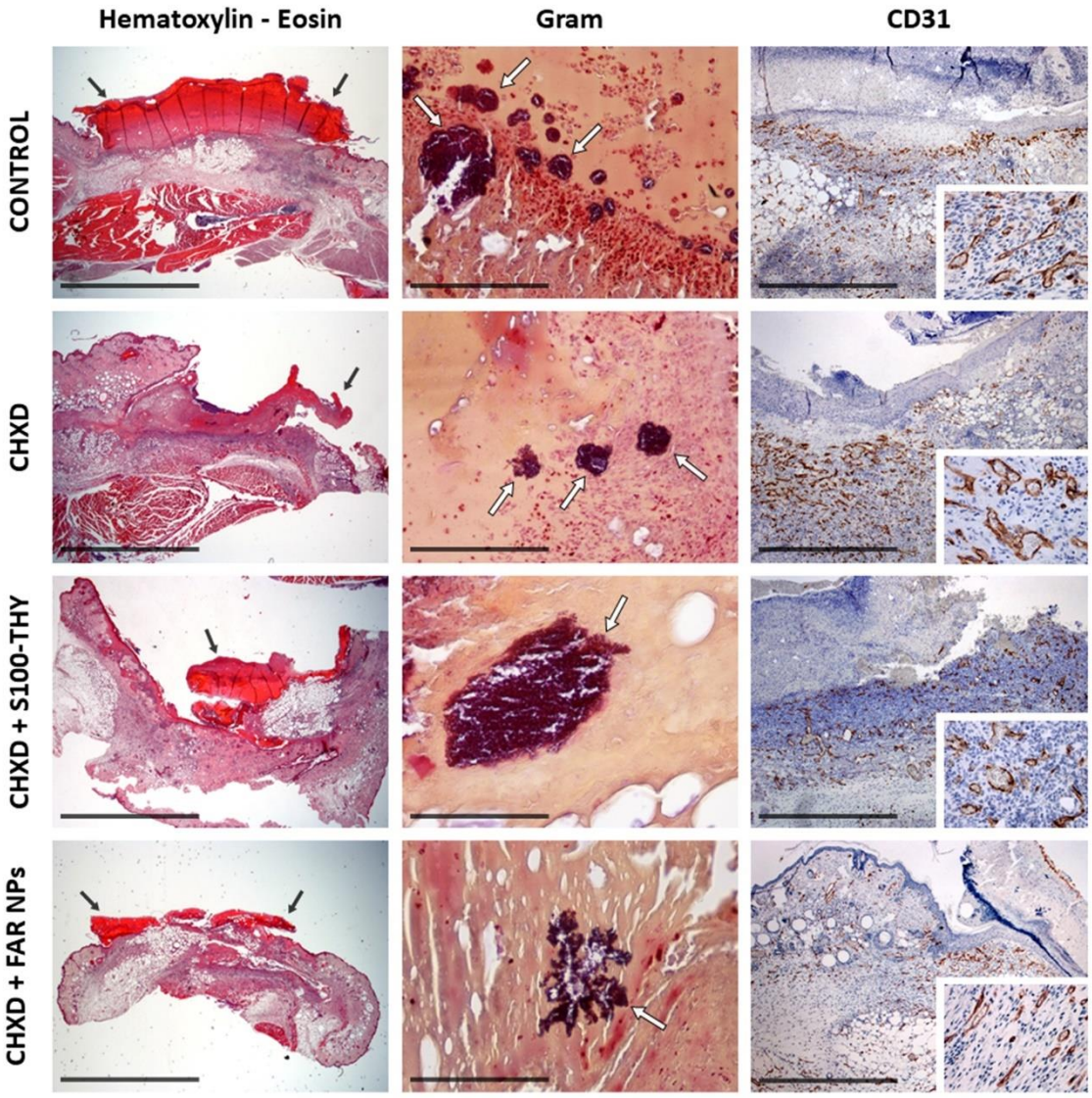

Figure II.10: Histopathology from representative mice groups: Control group (not treated), CHXD, CHXD+S100-THY, CHXD+FAR NPs. Lesions are similar in all cases, with a marked serocellular crust formation (black arrows). Bacteria are present in all groups, only within the crust (white arrows). Neovascularization (labelled in brown color in all images and insets) may be less intense in CHXD-FAR NPs group. Haematoxylin – Eosin, bar = 4 mm; Gram, bar = 100 µm; and CD31, bar = 1 mm; insets at 10x.

Considering the standard clinical practice for eliminating chronic biofilm infections, which typically involves antiseptic cleansing, debridement, and continuous administration of systemic or topical antibiotics based on wound culture results, as well as the *in vitro* and *in vivo* results of this study, the concurrent use of the proposed treatments may significantly enhance efficacy.

II.5. Conclusions

In this study, different treatments based on the bactericidal and antibiofilm abilities of the terpene compounds THY and FAR NPs, as well as the antiseptic CHXD, were extensively evaluated both *in vitro* and *in vivo*. The *in vitro* results demonstrated significant bactericidal activity in treatments that incorporated CHXD, as well as an enhanced bactericidal efficiency when combining different treatments as opposed to monotherapy. Interestingly, no direct correlation was observed between bacterial cell counts and the bioluminescence emitted by *S. aureus* Xen36 in response to antimicrobial treatments, possibly due to the influence of other co-factors on bacterial metabolic activity.

The *in vivo* study confirmed the *in vitro* results, highlighting the potential use of terpene-based compounds in conjunction with CHXD for improved wound treatment and enhanced healing. While the *in vitro* experiments showcased the superiority of combination therapies over monotherapy, the *in vivo* context revealed an initial substantial reduction in bacteria, but as not all pathogenic microorganisms were completely eradicated, bacterial regrowth occurred after treatment cessation. The exponential increase in *S. aureus* resistant infections and the prevalent presence of these biofilm-forming strains underscore the critical need for the development of novel approaches in which the combination of different bactericidal compounds may play a key role in improving current treatments for infected wound management.

CHAPTER III

Polymicrobial biofilm models for understanding the microbiome within wound infections and their successful antimicrobial treatment

Table of contents

Summary

In this chapter, bioluminescent and fluorescent strains of *S. aureus* and *P. aeruginosa* were employed to establish a study the behaviour of an *in vitro* model of a polymicrobial biofilm. In this regard, it was reported how the initial conditions of both bacteria in a co-culture determined the growth kinetics and how *P. aeruginosa* hindered the proliferation and metabolism of *S. aureus in vitro*.

Once a satisfactory experimental model was developed, the antimicrobial activity of thymol and chlorhexidine was compared against both species in planktonic state, as well as in single and polymicrobial biofilms. Notably, it was observed lower bactericidal activity of chlorhexidine and thymol against *S. aureus* in the polymicrobial biofilm. This phenomenon was attributed to two key factors: the formation of a thicker mixed biofilm, which exceeds the total biomass of biofilms formed solely by *S. aureus* or *P. aeruginosa*, and a significant reduction in the metabolic activity of *S. aureus* induced by the presence of antimicrobial molecules produced by *P. aeruginosa*. The results of this chapter are included in a scientific article that will be submitted for publication soon, under the title "*Impact of mixed Staphylococcus aureus-Pseudomonas aeruginosa biofilms formation on resistance to antimicrobial treatment of chronically infected wounds*".

III.1. Introduction

The importance of polymicrobial infections is becoming increasingly recognized, particularly in the context of biofilm formation, where various bacterial species interact and compete. In this context, *S. aureus* and *P. aeruginosa* are two commonly co-isolated bacteria in pulmonary infections and chronic wounds [282]. The interactions between these two bacteria in co-infected tissues remain unclear, but their coexistence results in treatment resistance and increased virulence. It has been reported that wounds infected with both species typically exhibit delayed closure compared to wounds infected with a single specie [283]. Alongside factors related to the host, one explanation for this phenomenon could be the increased expression of *S. aureus* virulence factors during co-infection, a pattern observed in the MRSA strain USA300 [284].

There is no consensus on whether these bacteria have an antagonistic or mutualist relationship in the complex physiological conditions. Some studies indicate that early colonisation by *P. aeruginosa* shows strong antagonism towards *S. aureus* [285], through the secretion of a variety of anti-staphylococcal molecules and proteases that inhibit *S. aureus* growth and proliferation [286, 287]. This process induces a metabolic transition of *S. aureus* from aerobic respiration to fermentation and eventually leads to a loss of *S. aureus* viability. In response to this hostile environment, *S. aureus* may adapt to *P. aeruginosa* products by increasing biofilm formation and by the presence of small colony variants inside infected eukaryotic cells [288]. In return, this would provide *S. aureus* with a greater capacity to withstand antimicrobial therapies. Other studies have shown that *S. aureus* supports colonisation and pathogenicity of *P. aeruginosa* by inhibiting its phagocytosis [289].

In multicellular communities, collective microbial dynamics generate a complex ecosystem characterised by both microbe-microbe and microbe-environment interaction. These features must somehow be present in *in vitro* models, but they are barely reproducible with liquid cultures. Co-cultures of *S. aureus* and *P. aeruginosa* have been performed using modified media in static *in vitro* conditions, anoxia, microtiter plates, Calgary biofilm devices or even directly over mammalian cells [290–292]. Nevertheless, the development of an experimental model to recreate this coexistence proves to be a challenging task, as the *in vitro* interaction between both species appears to be antagonistic at first. Interestingly, while *P. aeruginosa* strongly inhibited the growth of *S. aureus in vitro*, this effect was considerably less pronounced *in vivo* [284]. This matter adds complexity to the assessment of the effectiveness of antimicrobial treatments against these polymicrobial communities.

The co-culture of these bacteria is of extreme importance, not only because of their mutual impact on the bacterial behaviour and metabolic activity, but also because some studies have shown that their interplay contributes to antimicrobial

tolerance. Notably, it has been reported that when *S. aureus* is able to coexist with *P. aeruginosa* in a co-culture, its tolerance to antibiotics significantly increases [293, 294].

In this study, recent advances in *P. aeruginosa* and *S. aureus* molecular interactions, their physical responses, and *in vitro* and *in vivo* models are discussed. It is important to optimize growth conditions in the laboratory, determine appropriate bacterial starting ratios, and consider environmental factors when studying the coexistence of these two pathogens.

III.2. Objectives

The first aim of this study was to establish a reliable *in vitro* model of a polymicrobial biofilm of *S. aureus* and *P. aeruginosa*. The use of bioluminescent and fluorescent strains of both species was proposed to study optically the growth kinetics and metabolic state of the bacteria over time. The research investigated how the initial conditions of both bacterial species influenced their final interaction within the co-culture. Other experiments were conducted to elucidate the nature of the interaction between both species.

Once a satisfactory model was established, the antimicrobial activity of thymol and chlorhexidine was compared against both species in planktonic state, as well as in single and polymicrobial biofilms. This comparison aimed to determine whether bacteria growth changed in the polymicrobial biofilms.

III.3. Experimental

III.3.1. Development of polymicrobial co-cultures

To obtain fresh liquid cultures of bacteria, isolated colonies were dispersed in 10 mL of MHB and incubated for 24 hours under agitation at 37 °C. To produce a polymicrobial biofilm including the two bacterial species, two distinct culture strategies were used.

In the first strategy, a liquid culture of planktonic *S. aureus* was diluted with fresh MHB to obtain ~ 10^7 CFU/mL (OD_{600} ≈ 0.006). Then, 100 µL of the bacterial suspension were added to the wells of white, flat-bottomed 96-well microplates. The luminescence of wells containing *S. aureus* Xen36 was recorded over time using a microplate reader until a value of around 1,000 relative light units (RLU) was reached, which allowed an increase or decrease in RLU to be detected later with good accuracy. Next, 100 µL of bacterial suspension containing increasing concentrations (10^1 to 10^8 CFU/mL) of planktonic *P. aeruginosa* Lux or *P. aeruginosa* PAO1 were added to the wells. To ensure that the bioluminescent signal originated solely from one of the two species, *P. aeruginosa* Lux was added to non-luminescent *S. aureus* 29213, while *P.*

aeruginosa PAO1 was added to luminescent *S. aureus* Xen36. A visual representation of the experimental design is shown in **Figure III.1a** and **b**.

After the addition of *P. aeruginosa* to *S. aureus*, plates were sealed with a clear gas-permeable hydrophobic membrane (4titude Ltd, Surrey, UK) to prevent evaporation, and luminescence was recorded every 30 minutes for 48 hours at 37 °C. Finally, the wells were carefully scraped and washed with 1 mL 0.9% (w/v) NaCl to harvest the bacteria, which were serially diluted in 0.9% (w/v) NaCl and spread on two different agar media to obtain accurate bacterial counts of both species. MHA supplemented with colistin (8 µg/mL) was used for the selective growth of *S. aureus*, and normal MHA for the growth of both species.

In the second approach, 100 µL of *S. aureus* suspensions (Xen36 or ATCC 29213) at 10^7 CFU/mL were added to the wells of a white, flat-bottomed, high-binding 96-well microplates. Plates were sealed with a hydrophobic gas-permeable membrane and incubated for 48 hours at 37 °C with agitation for *S. aureus* biofilm formation. After the *S. aureus* biofilm formation, supernatants were removed, and the wells were washed 3-times with 0.9% (w/v) NaCl. Next, 100 µL of fresh MHB were added, and the bioluminescence in the wells was recorded until an intensity of around 1,000 RLU was achieved. Then, suspensions with increasing concentrations (10^1 to 10^8 CFU/mL) of *P. aeruginosa* (Lux or PAO1) were added to the wells, as depicted in **Figure III.1c** and **d**.

The microplates were then sealed with a clear gas-permeable hydrophobic membrane, and the luminescence was recorded every 30 minutes for 48 hours at 37 °C. Finally, to disperse the bacterial biofilms, the wells were carefully scraped, sonicated, and washed with 1 mL 0.9% (w/v) NaCl to harvest the bacteria, which were then serially diluted and seeded to count colonies.

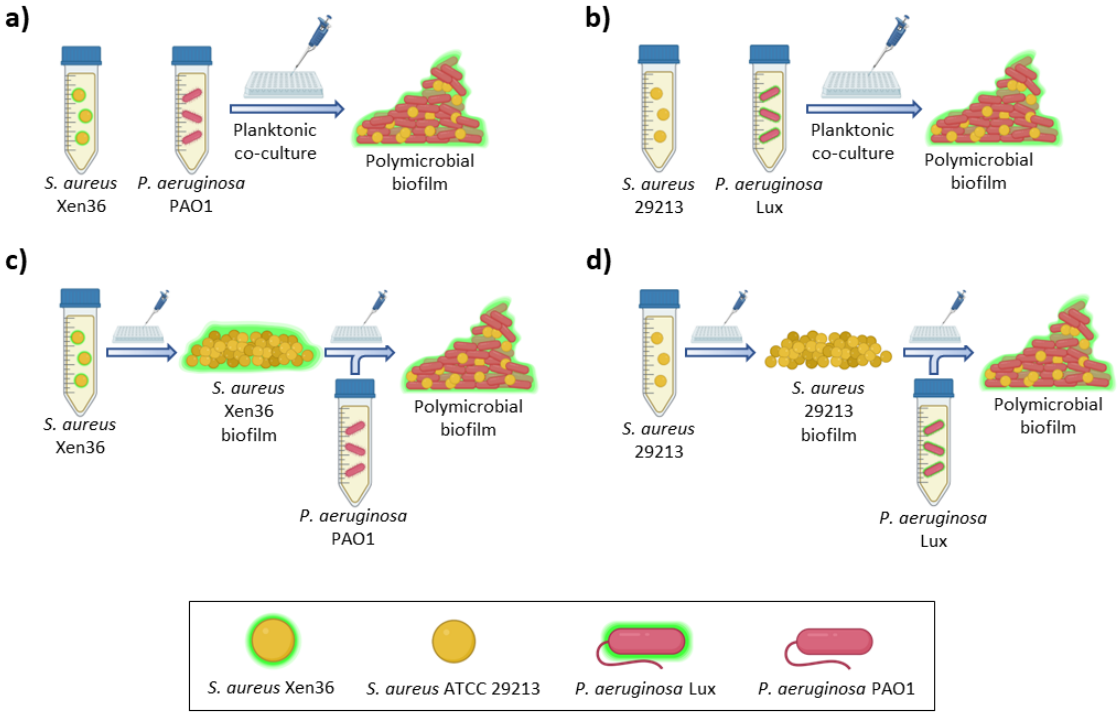

Figure III.1: Schematic overview of the strategies used to obtain polymicrobial biofilms: **(a)** and **(b)** schemes represent the first methodology, where the co-culture was established by adding the bacterial species in their planktonic state. **(c)** and **(d)** schemes depict the second methodology used, involving the addition of *P. aeruginosa* in the planktonic state to a pre-formed 48-hour *S. aureus* biofilm.

III.3.2. Study of the interaction between *S. aureus* and *P. aeruginosa*

To further investigate the interaction between *S. aureus* and *P. aeruginosa*, a Transwell® system with a 0.4 µm pore size polycarbonate membrane (Corning, France) was used to spatially separate the two species. In brief, single biofilms of bioluminescent *S. aureus* Xen36 and mixed biofilms composed of *S. aureus* Xen36 and PAO1 were established at the bottom of 24-well plates using the second strategy described in **Figure III.1c**. To form the mixed biofilms, 1 mL of *P. aeruginosa* PAO1 suspension at 10^4 CFU/mL was inoculated onto 2-day-old *S. aureus* Xen36 biofilms. In parallel, the same mixed biofilms or single PAO1 biofilms were formed in Transwell® inserts. Biofilms were then washed with 0.9% NaCl and fresh MHB was added (0.6 mL in wells and 0.1mL in insert). The inserts were placed in the wells and bioluminescence emitted by *S. aureus* at the bottom of the wells was recorded at different times over 48 h using a microplate reader. At the end of the experiments, biofilms were disrupted via sonication, diluted, and plated on MHA to quantify *S. aureus* CFUs present in the wells.

To determine whether *P. aeruginosa* was capable of secreting molecules interfering with the metabolic activity of *S. aureus* without being in direct contact or in proximity to it, a medium in which *P. aeruginosa* PAO1 had been cultured alone was recovered and placed in contact with *S. aureus* biofilms. For this study, a mutant strain

of *S. aureus* that expressed the green fluorescent protein (*S. aureus* GFP) was used. To obtain this conditioned medium (CM), 1.5 mL of *P. aeruginosa* PA01 at 10^4 CFU/mL were seeded on top of 6-well Transwell® inserts placed in wells containing 2.6 mL of MHB and incubated in a water-saturated incubator at 37 °C. Three days later, the medium under the insert was collected, centrifuged twice at 13,000 g for 5 minutes and filter through a 0.22 µm filter to remove any PAO1 potentially present. This CM was then serially diluted and deposited on 2 days-old *S. aureus* GFP biofilms grown in 96-well plates. *S. aureus* GFP fluorescence was then measured at 488 nm after excitation at 520 nm every hour for 72 hours at 37 °C using a microplate reader.

III.3.3. *In vitro* antimicrobial activity tests

Antimicrobial activity of THY and CHXD was tested against *S. aureus* Xen 36 and *P. aeruginosa* Lux in planktonic state as well as in single and mixed biofilms.

To run tests against planktonic cultures, fresh bacterial cultures were adjusted to 10^7 CFU/mL and 100 µL of the suspensions were added to the wells of white 96-well microplates. The bioluminescence of the wells was recorded over time (2-3 hours) until reaching 1,000 RLU for *S. aureus* Xen 36 and 10,000 RLU for *P. aeruginosa* Lux, which is more luminescent than *S. aureus* Xen 36. Then, MHB solutions with increasing concentrations of CHXD (0.4 to 40 µg/mL) and THY (100 to 1,000 µg/mL) were added to a final volume of 200 µL. Next, the plates were sealed with an optical clear membrane and the luminescence was recorded every 30 minutes for 24 hours at 37 °C. Finally, the cultures in the wells were seeded in MHA after serial dilution for CFU counting.

Regarding the experiments on single biofilm-forming bacteria, 100 µL of bacterial suspensions at 10^7 CFU/mL were added to the wells of high-binding 96-well white microplates, which were then sealed with a gas-permeable membrane and incubated for 48 hours at 37 °C with agitation. After incubation, MHB was removed, and biofilms were washed with 0.9% (w/v) NaCl before adding 100 µL of fresh MHB. The bioluminescence of the wells was then adjusted to the same values as for planktonic cultures (~1,000 RLU for *S. aureus* Xen 36, ~10,000 RLU for *P. aeruginosa* Lux). CHXD and THY treatments were also added to obtain the same concentrations as for the antimicrobial activity tests on planktonic bacteria (0.4 to 40 µg/mL for CHXD and 100 to 1,000 mg/mL for THY). Finally, the wells were thoroughly scraped and rinsed before serial dilution of the samples and plating them to determine the number of CFUs.

Mixed biofilm-forming bacteria assays were performed using suspensions containing 10^4 CFU/mL of planktonic *P. aeruginosa* PAO1 and *P. aeruginosa* Lux which were added to pre-formed 48 hours-old biofilms of *S. aureus* Xen36 and *S. aureus* 29213, as described in the previous section. These co-cultures were incubated again for 48 hours to form the mixed biofilms before being washed with 0.9% (w/v) NaCl and the addition of CHXD and THY treatments, as in the individual biofilm activity tests. Lastly, mixed biofilms were dispersed, serially diluted, and plated on selective (colistin-

supplemented MHA) and non-selective (regular MHA) agar plates to determine CFU numbers.

III.3.4. Confocal laser scanning microscopy studies

Single and mixed biofilms composed of the fluorescent *S. aureus* GFP and *P. aeruginosa*-BFP (Blue Fluorescent Protein) were grown on 8-well µ-slide chambers (Ibidi GmbH, Gräfelfing, Germany) enabling their spatial organization to be assessed by confocal laser scanning microscopy (CLSM). The strategy used for biofilms formation was identical to that described in **Figure III.1c**. Briefly, 300 µL of *S. aureus*-GFP at 10^7 CFU/mL were added to the chamber wells and incubated under agitation for 48 hours at 37 °C in a water-saturated atmosphere for *S. aureus* biofilm formation. *S. aureus* biofilms were then washed and supplemented with MHB or 10^4 CFU/mL of *P. aeruginosa* BFP suspension and incubated again for 48 hours under the same conditions. After the second incubation period, biofilms were washed and supplemented with different treatments (MHB, or MBH containing either CHXD 10 µg/mL or 40 µg/mL) and re-incubated for 24 hours. The wells were then washed 3 times and filled with 300 µL of 0.9% NaCl containing propidium iodide (PI) at 20 µM. In certain conditions, mixed biofilms were also labeled with 5 µM SYTO-9, a fluorescent probe that labels both live and dead bacteria in green.

At different times, bioflms were visualized on an Olympus FluoView FV-3000 with an IX83 confocal laser scanning microscope (x100 zoom). For each biofilm, samples were sequentially excited to study the fluorescence of GFP or SYTO-9 (excitation 488nm - emission 500/540nm), BFP (excitation 405nm - emission 430/470nm), and IP (excitation 561nm - emission 570/670nm). Twenty to thirty stacks of horizontal plane images (1024×1024 pixels corresponding to 127×127 µm) with a z-step of 0.5 µm were acquired for each condition. Three-dimensional biofilms projections were constructed using the Easy 3D function of the IMARIS software (Bitplane). When creating the surfaces, the same segmentation parameters (particle size, absolute intensity and absence of post-segmentation filters) were applied to all 3D constructs.

III.4. Results and discussion

III.4.1. Establishment of *S. aureus* - *P. aeruginosa* mixed biofilm

As detailed in the methods section, two different strategies were assessed for developing an *in vitro* model of a polymicrobial biofilm containing both *S. aureus* and *P. aeruginosa*. Using bioluminescent strains in conjunction with wild-type strains, the bioluminescence of both species was monitored over a 48-hour period in parallel experiments. In both cases, the *P. aeruginosa* strains were added at progressively increased concentrations. In the first approach, *S. aureus* and *P. aeruginosa* were mixed as planktonic co-cultures. The signal of the bioluminescent strains, as well as the

bacterial count in the culture at the end of the experiment, are represented in **Figure III.2**.

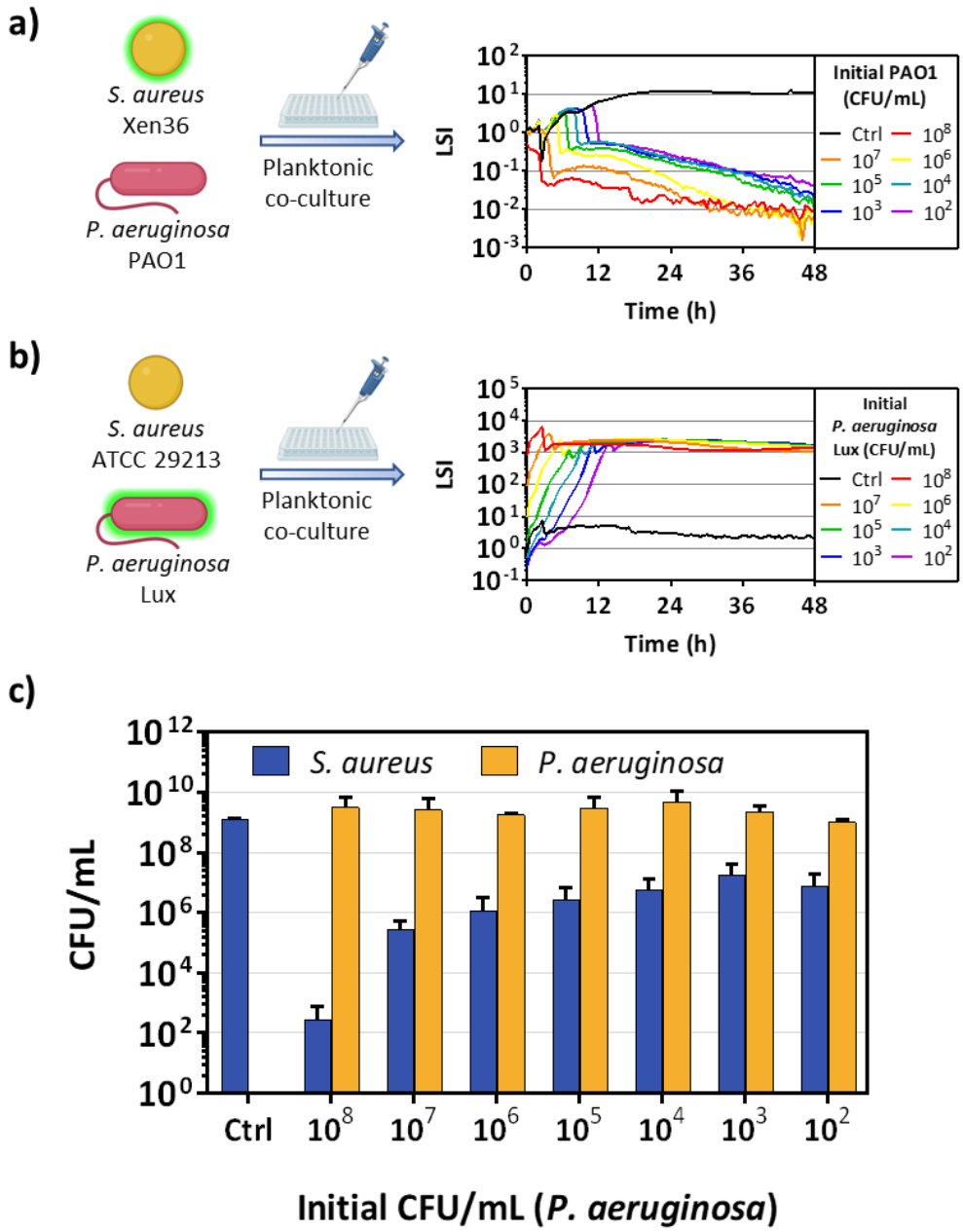

Figure III.2: Bioluminescence signals of *S. aureus* Xen36 **(a)** and *P. aeruginosa* Lux **(b)** in co-culture with either *P. aeruginosa* PAO1 or *S. aureus* 29213, respectively. The acronym LSI stands for "Luminescence Signal Intensity". The controls (Ctrl) were cultures of *S. aureus* strains to which no concentration of *P. aeruginosa* was added. **c)** Bacterial count of both species in the cultures after 48 hours. The data is represented as Mean ± SD of three independent experiments.

The bioluminescence signal of *S. aureus* Xen36 exhibited a concentration-dependent suppression when co-cultured with *P. aeruginosa* PAO1, being ultimately reduced to levels close to the background signal (**Figure III.2a**). This observation suggested a substantial influence of *P. aeruginosa* PAO1 presence on *S. aureus* Xen36 bioluminescence. Conversely, the bioluminescence signal of *P. aeruginosa* Lux

remained unaltered in the presence of *S. aureus* 29213, depending solely on its initial concentration (**Figure III.2b**).

The analysis of the bacterial counts in the culture at the end of the experiment (**Figure III.2c**) aimed to assess whether the decrease in bioluminescence resulted from a reduction in bacterial numbers, a decrease in their metabolic activity, or a combination of both factors. For *P. aeruginosa* concentrations ranging from 10^2 to 10^5 CFU/mL, *S. aureus* growth was slightly inhibited, as its concentration remained around 10^7 CFU/mL. For *P. aeruginosa* concentrations between 10^5 to 10^8 CFU/mL, *S. aureus* growth was significantly inhibited, causing its concentration to drop to 10^3 CFU/mL. Because no substrate limitation was present, *S. aureus* growth inhibition can be attributed to the presence of an anti-staphylococcal compounds released by *P. aeruginosa.*

In the second approach, the different strains of *S. aureus* were first allowed to grow into a 48-hours mature biofilm. Subsequently, a co-culture was established by introducing increasing concentrations of planktonic *P. aeruginosa.* **Figure III.3** displays both the bioluminescence of the strains and the final bacterial count in the cultures following the experiment. Similar to the previous conditions, the bioluminescence signal of *S. aureus* Xen36 exhibited a concentration-dependent suppression, while the bioluminescence signal emission of *P. aeruginosa* Lux remained unaltered (**Figure III.3a** and **b**). Nevertheless, when *S. aureus* Xen36 was already forming biofilm, the presence of planktonic *P. aeruginosa* did not inhibit its growth after 48 hours (**Figure III.3c**). Despite a one-log reduction compared to the control, both species coexisted in the culture, indicating that *S. aureus* biofilm provided some level of protection from the bactericidal and inhibitory effects caused by *P. aeruginosa* compared to those observed in the planktonic state.

It has been widely reported that when *P. aeruginosa* and *S. aureus* are grown together in co-culture, *P. aeruginosa* becomes dominant, outcompeting, and outgrowing *S. aureus* [295]. Therefore, under co-culture conditions the growth of one specie depends on the concentration of the other and on its status (sessile or planktonic).

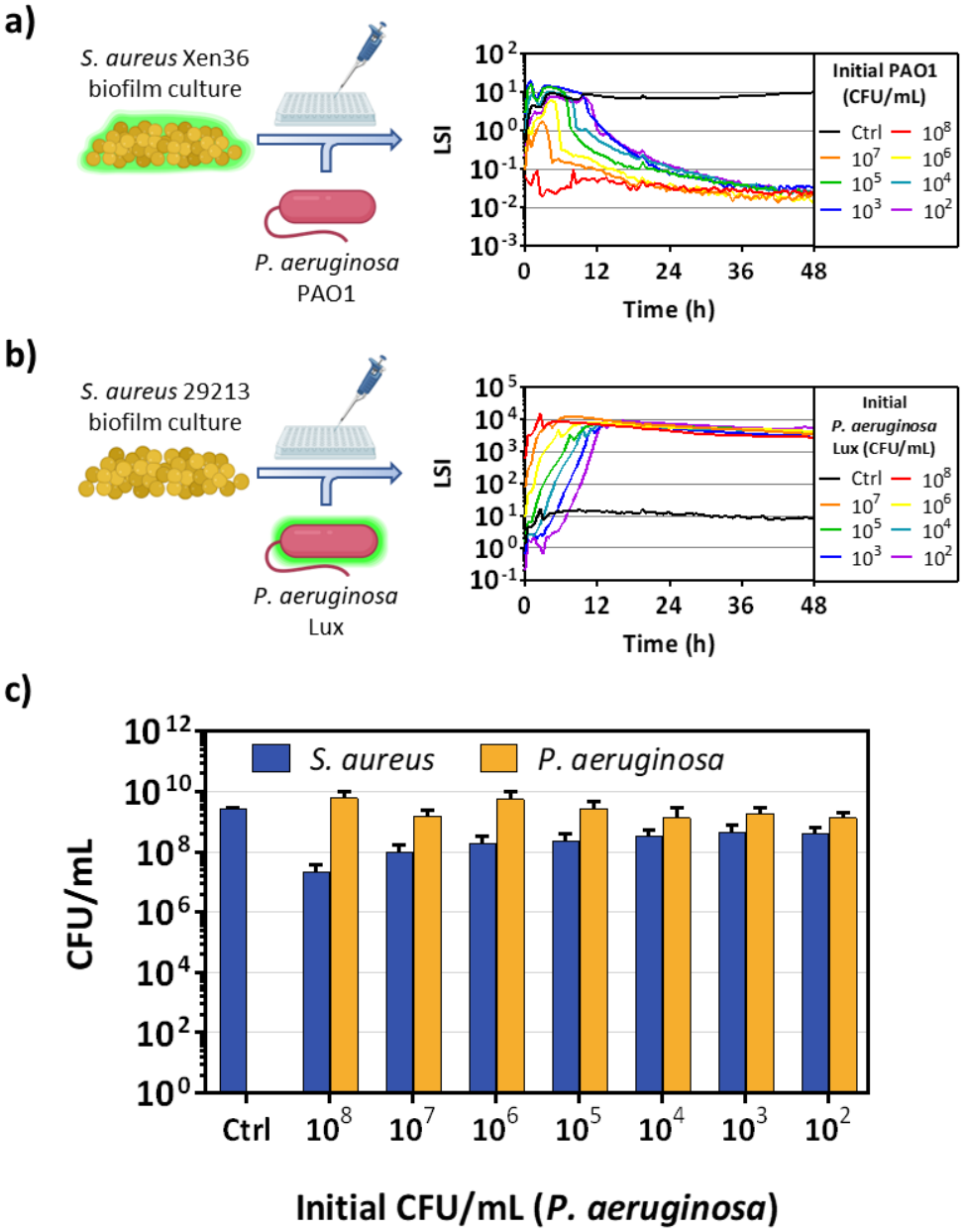

Figure III.3: Bioluminescence signals of *S. aureus* Xen36 **(a)** or *P. aeruginosa* lux **(b)** in co-culture with either *P. aeruginosa* PAO1 or *S. aureus* 29213. **c)** Bacterial count of both species in the cultures after 48 hours.

III.4.2. Study of the interaction between *S. aureus* and *P. aeruginosa*

To explore if *P. aeruginosa* requires direct contact with *S. aureus* to hinder its growth, an experiment using Transwell® inserts was conducted, in which the bacterial species shared liquid media but were not in physical contact. **Figure III.4** showcases an overview of this experiment, in addition to the measurement of the bioluminescent signal and the bacterial counting.

As observed in **Figure III.4b**, the bioluminescence signal of *S. aureus* Xen36 was only reduced after 24 hours when it was in direct physical contact with *P. aeruginosa*. In cases where *P. aeruginosa* was in the insert, the signal remained at levels similar to

those of the control culture. However, by the 48-hour mark, the signal in all cultures, except the control, had decreased to baseline levels. As depicted in **Figure III.4c**, the interaction with *P. aeruginosa* resulted in a slight reduction of approximately one logarithm in *S. aureus*. These experiments suggests that the decrease in bioluminescence may be attributed to a suppression of their metabolic activity. It is also worth mentioning that the physical proximity of *P. aeruginosa* could potentially accelerate this process.

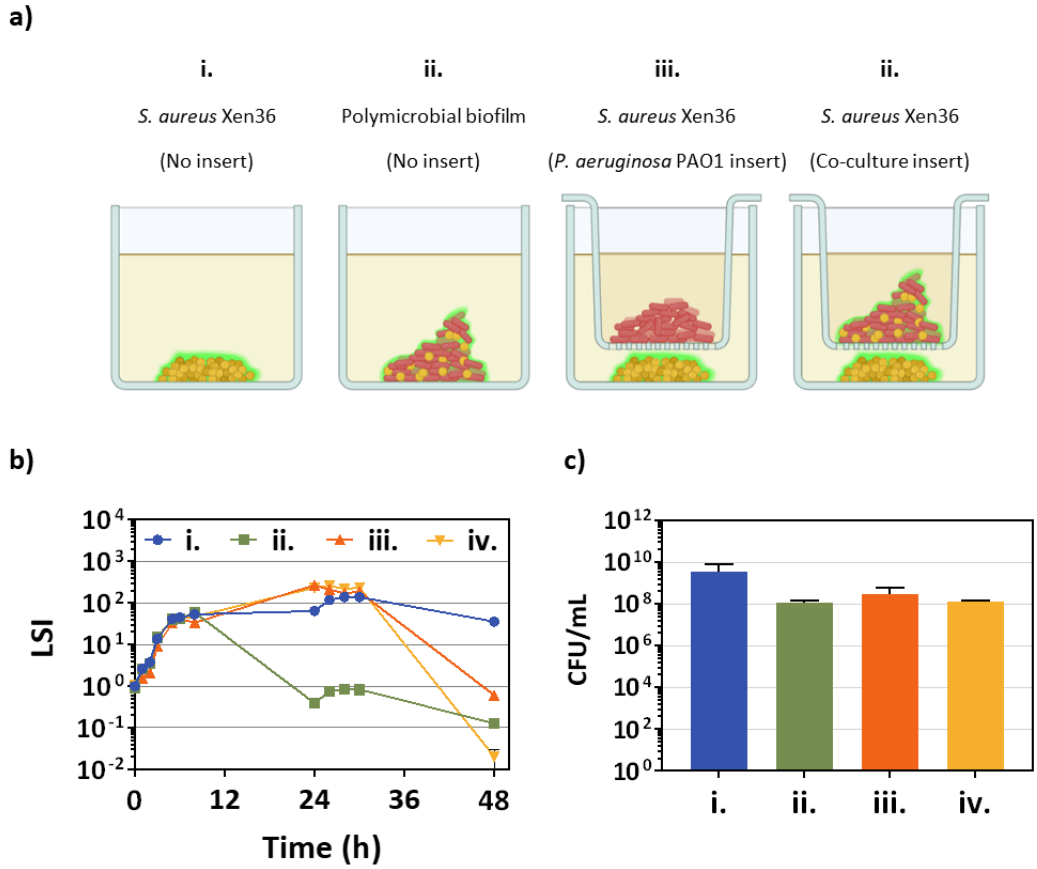

Figure III.4: a) Schematic overview of the methodology developed to evaluate the interaction between bacterial species: **i.** *S. aureus* Xen36 single biofilm culture without insert. **ii.** *S. aureus* Xen36 and *P. aeruginosa* PAO1 mixed biofilm without insert. **iii.** *S. aureus* Xen36 and *P. aeruginosa* single biofilm in the insert. **iv.** *S. aureus* Xen36 single biofilm, and *S. aureus* Xen36 and *P. aeruginosa* PAO1 mixed biofilm in the insert. **b)** bioluminescence signal of *S. aureus* Xen36 over 48 hours. **c)** *S. aureus* Xen36 counting measured after 48 hours.

To further determine whether *P. aeruginosa* needs to be in the presence of *S. aureus* to produce the molecules that interfere with *S. aureus* growth, a conditioned medium (CM) in which *P. aeruginosa* was grown was collected and added to *S. aureus* GFP biofilm. The swich from the bioluminescent strain (*S. aureus* Xen36) to the fluorescent strain (*S. aureus* GFP) was made considering its suitability for the confocal microscopy studies. The GFP fluorescence was then monitored over a period of 70 hours (**Figure III.5**).

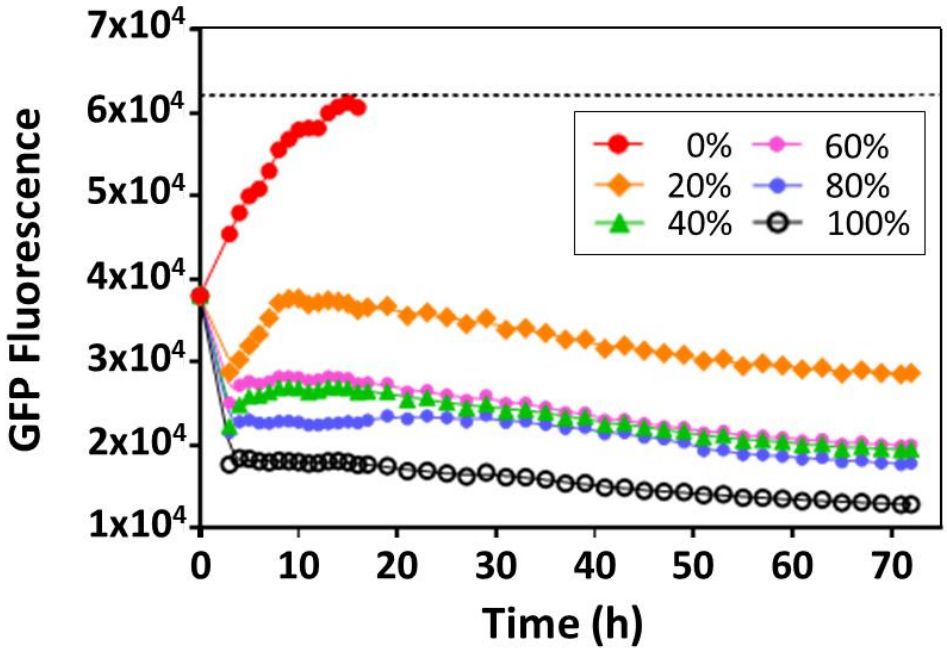

Figure III.5: *S. aureus* GFP fluorescence kinetics measured over 70 hours after the addition of different concentrations of conditioned medium (CM) obtained from an isolated culture of *P. aeruginosa* PAO1.

When *S. aureus* GFP was not exposed to CM, the GFP fluorescence intensity showed a steady increase over time, reaching a plateau after 18 hours. Conversely, when *S. aureus* was exposed to CM, a rapid and substantial decrease in GFP fluorescence intensity was observed within the first hour, followed by an overall reduction in the maximum fluorescence intensity. This suppression effect on GFP fluorescence was found to be concentration-dependent, with the degree of suppression gradually decreasing as the CM was diluted.

The anti-staphylococcal properties of *P. aeruginosa* were initially documented in the 1950s [296]. During this period, researchers identified 4-hydroxy-2-heptylquinoline N-oxide (HQNO) as a primary compound produced by *P. aeruginosa*. This compound effectively impeded the cytochrome systems of various bacteria, including *S. aureus* [297]. While HQNO is recognized as an anti-staphylococcal agent, it does not induce lysis in *S. aureus* itself; instead, it retards its growth by inhibiting oxidative respiration. Other documented anti-staphylococcal agents secreted by *P. aeruginosa* include pyocyanin [288] and the LasA protease bacteriocin [298]. Considering our results, it is worth noting that the *P. aeruginosa* may produce anti-staphylococcal agents regardless the environmental conditions. However, these agents would only have mild bactericidal effectiveness against *S. aureus* when a mature biofilm is formed.

III.4.3. Antimicrobial activity tests

In order to assess whether the polymicrobial biofilm was beneficial for the microorganisms against the action of antimicrobial agents, a 48-hour mature mixed

biofilm was prepared following the same approach as depicted in **Figure III.3a**. Results are represented in **Figure III.6**, while MIC and MBC data are summarized in **Table 2**.

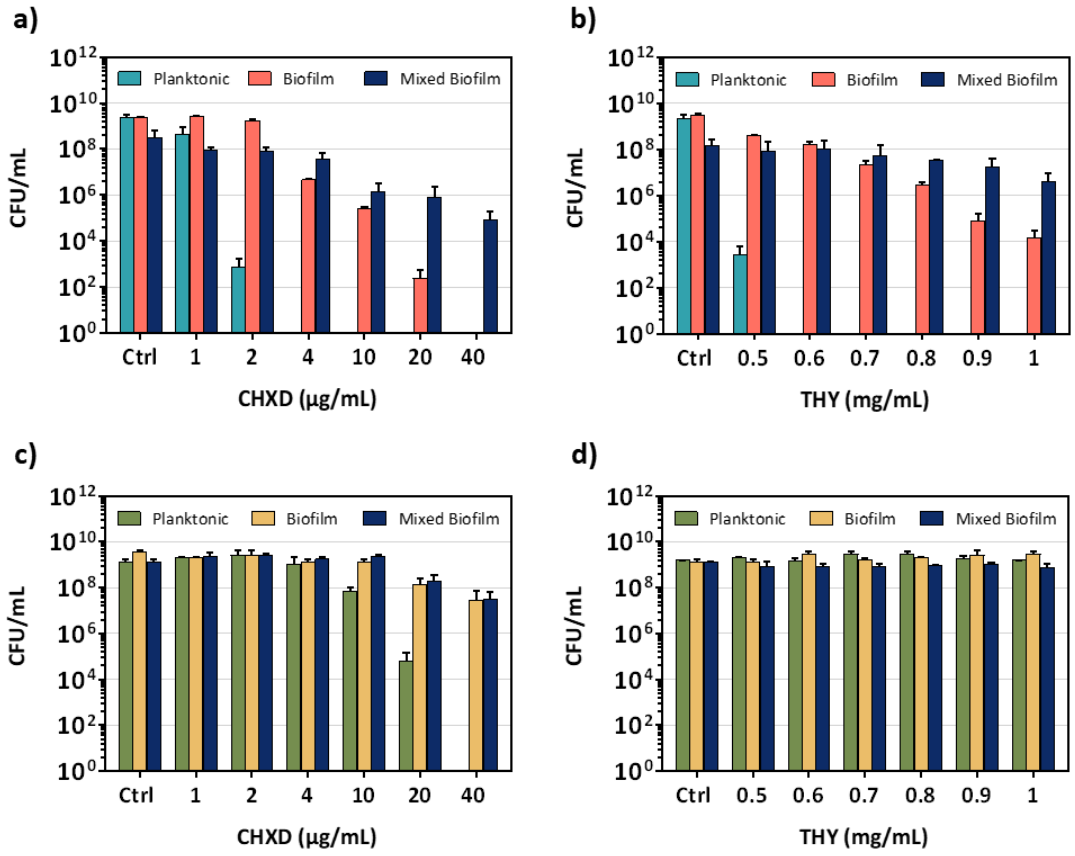

Figure III.6: Bactericidal activity of CHXD **(a)** and THY **(b)** against *S. aureus* Xen36 in planktonic, single biofilm and mixed biofilm (with *P. aeruginosa* PAO1) states after 24 hours. Bactericidal activity of CHXD **(c)** and THY **(d)** against *P. aeruginosa* Lux in planktonic, single biofilm and mixed biofilm (with *S. aureus* 29213) states after 24 hours.

Table 2: MIC and MBC obtained for CHXD and THY against *S. aureus* Xen36 and *P. aeruginosa* PAO1 in planktonic, single biofilm, and mixed biofilm states.

	***S. aureus* Xen36**				***P. aeruginosa* PAO1**			
	CHXD		**THY**		**CHXD**		**THY**	
	MIC (µg/mL)	**MBC (µg/mL)**	**MIC (mg/mL)**	**MBC (mg/mL)**	**MIC (µg/mL)**	**MBC (µg/mL)**	**MIC (mg/mL)**	**MBC (mg/mL)**
Planktonic	2	4	0.5	0.6	20	40	-	-
Biofilm	4	40	0.7	-	40	-	-	-
Mixed Biofilm	10	-	1	-	40	-	-	-

In this context, it was observed that CHXD effectively eliminated both bacterial species, with the exception of *P. aeruginosa* in its biofilm and mixed biofilm forms, as well as *S. aureus* in mixed biofilm. Notably, in the case of *S. aureus* within the mixed biofilm, its MIC against CHXD also increased by a factor of 2.5 when compared with its single biofilm form. On the other hand, THY displayed selective antimicrobial activity

against *S. aureus*, not observing bactericidal activity against *P. aeruginosa*. THY successfully eradicated *S. aureus* in its planktonic state, but it was less effective in the case of the single biofilm and the mixed biofilm. In the latter scenario, the MIC of THY increased from 0.7 to 1 mg/mL when compared with its single biofilm form.

In summary, the interaction between bacterial species within the mixed biofilm conferred a survival advantage to *S. aureus*, enabling it to withstand the bactericidal effects of CHXD and resulting in an increased MIC for both THY and CHXD. It has been reported that the presence of environmental selection pressure, such as antibiotics or the host immune system, stimulates a more synergistic relationship between different species and promotes biofilm formation. If *S. aureus* can withstand *P. aeruginosa* anti-staphylococcal activity and successfully coexists within a multi-species biofilm, it gains an advantage from the protective antimicrobial barrier created by the matrix components of *P. aeruginosa* [299].

III.4.4. Confocal microscopy studies

In order to further investigate the formation, interactions, and response to treatments within the established biofilm models, fluorescent bacterial strains (*S. aureus* GFP and *P. aeruginosa* BMP) were selected for their observation with CLSM. Single biofilms of *S. aureus* and mixed biofilms of *S. aureus* with *P. aeruginosa* were analyzed, with the latter biofilms being developed according to the strategy depicted in **Figure III.3c**. As observed in **Figure III.7a** and **b**, single *S. aureus* biofilm was established by day 2. By day 4, the scenario transformed as mixed biofilms took shape, with *P. aeruginosa* interpenetrating the existing *S. aureus* network. These mixed biofilms appeared to be thicker as their single *S. aureus* counterparts.

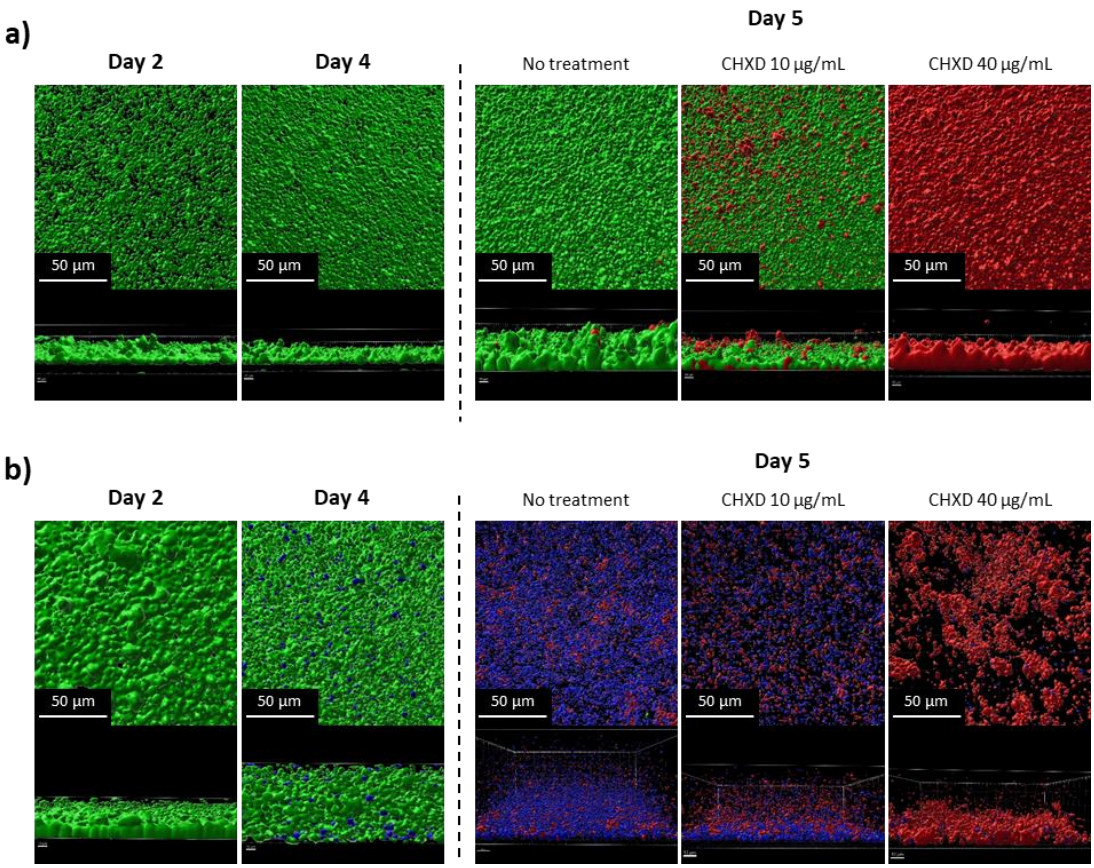

Figure III.7: CLSM visualization of biofilms. **(a)** Single *S. aureus* GFP and **(b)** Mixed *S. aureus* GFP / *P. aeruginosa* BFP. Biofilms were visualized on days 2, 4 and 5 after treatment with 10 µg/mL or 40 µg/mL of CHXD. *S. aureus* GFP is stained in green, *P. aeruginosa* BFP in blue, and dead bacteria in red, regardless of the species. Images below were constructed from the z-stack acquisition.

On day 5, single *S. aureus* biofilms exhibited a slight increase in thickness compared to day 4 and remained discernible, primarily owing to the presence of GFP fluorescence. In contrast, within the mixed biofilms, *S. aureus* GFP cells were no longer distinguishable due to the suppressive effects on GFP fluorescence.

To reveal *S. aureus* that were no more visible on the mixed biofilm of day 5 due to reduction of GFP expression, another set of untreated mixed biofilms was grown under the same conditions as in **Figure III.7b**, but with the addition of Syto9 after PI. Syto9 is a green fluorescent nucleic acid dye capable of penetrating cell membranes, enabling it to stain all bacterial cells in the biofilm non-specifically, revealing *S. aureus* that were no longer visible (**Figure III.8**).

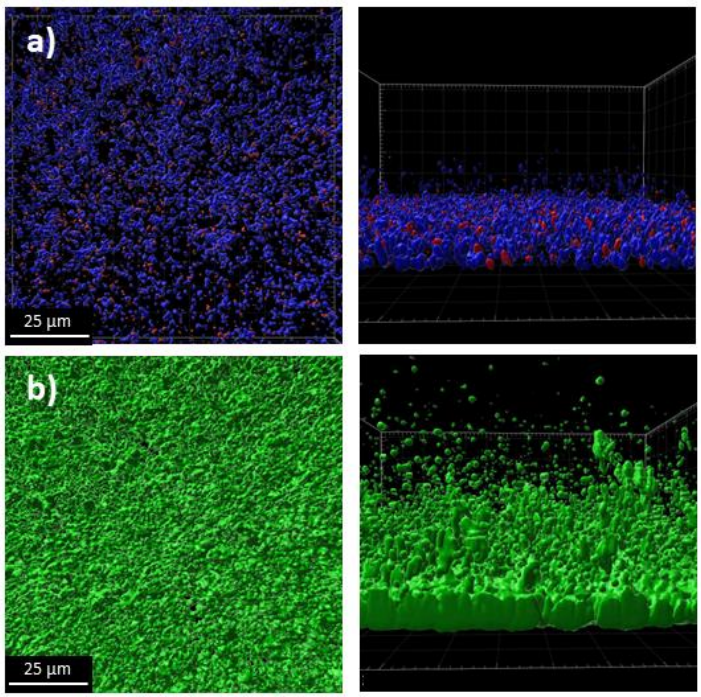

Figure III.8: CLSM images of mixed biofilms observed on day 5: a) Before the addition of SYTO-9, where *P. aeruginosa* is stained in blue, dead bacteria in red, and the signal of *S. aureus* (green) is not appreciable. b) After the addition of SYTO-9, which labels all bacteria in green, including *S. aureus*. Images below were constructed from the z-stack acquisition.

According to the images, it was found that the *P. aeruginosa* aggregates within the biofilms were located significantly further from the surface, compared to the *S. aureus* aggregates. This disparity could confirm the non-random distribution pattern of these bacteria within chronic wounds. Typically, *S. aureus* tends to colonize the superficial layers of the wound, while *P. aeruginosa* is found in the deeper regions of the wound bed. This spatial differentiation in colonization has also been reported in previous studies [300, 301]. Recent studies indicate that traditional swab culturing techniques may underestimate the presence of *P. aeruginosa* in wound infections [302]. Additionally, it aligns with the hypothesis that *P. aeruginosa* bacteria residing in the deeper regions of chronic wounds may play a pivotal role in maintaining wounds in a state characterized by inflammatory processes.

III.5. Conclusions

The monitoring of co-cultures using bioluminescent and wild type bacterial strains in order to develop a polymicrobial mixed biofilm was successful. Neither physical contact nor the presence of both bacterial species in the environment was necessary for *P. aeruginosa* to exert its anti-staphylococcal action.

Additionally, within the mixed biofilm, the interplay between bacterial species granted *S. aureus* a survival advantage, enabling it to be less susceptible to the

bactericidal action of CHXD and subsequently elevating the MIC values for both THY and CHXD. Lastly, the non-random spatial organization of the bacterial species within the mixed biofilm corresponds with previous reports on co-infected chronic wounds. This alignment with previous research reinforces the relevance and clinical implications of these findings in the context of chronic wound infections and the importance of the cross-talk between species in polymicrobial cultures.

CHAPTER IV

Colistin-loaded particles suitable for aerosolization for the treatment of *Pseudomonas aeruginosa* respiratory infections

Table of contents

Summary

In this chapter, aerosolizable polymeric nanoparticle carriers loaded with colistin were developed following four different methodologies for their synthesis: (i) PLGA nanoparticles single emulsion-solvent evaporation method; (ii) encapsulation through nanoprecipitation with miscible solvents, utilizing PLGA-poly(ethylene glycol) (PEG) as the encapsulating matrix; (iii) colistin nanocoacervation in hydroxypropyl methylcellulose (HPMC) using the antisolvent precipitation method followed by encapsulation within PLGA nanoparticles; and (iv) colistin encapsulation within PLGA microparticles using electrospraying.

The most successful approach was the antisolvent precipitation method (iii), which achieved the highest drug loading of 55 wt.% and produced particles with optimal aerodynamic properties (3-5 µm) for efficient pulmonary delivery. *In vitro* testing revealed a rapid release of colistin from this formulation. Furthermore, these particles exhibited enhanced antimicrobial efficacy in a biofilm model of the *Pseudomonas aeruginosa* PAO1 strain compared to the effect of equivalent doses of the free antibiotic.

This nanoparticulated formulation showed the potential to be a promising alternative for the treatment of pulmonary infections caused by *P. aeruginosa*, as it enhances lung deposition, and consequently improving the efficacy of colistin.

The content of this chapter has been adapted from the following published work:

Landa, G.; Alejo, T.; Sauzet, T.; Laroche, J.; Sebastian, V.; Tewes, F.; Arruebo, M.

Colistin-loaded aerosolizable particles for the treatment of bacterial respiratory infections.

International Journal of Pharmaceutics, **2023**, Volume 635, 122732, https://doi.org/10.1016/j.ijpharm.2023.122732

IV.1. Introduction

Colistin, also known as polymyxin E, is considered as a last-resort polypeptide antibiotic. It is typically utilized in combination with other antibiotics for treating infections caused by multidrug-resistant (MDR) and extensively drug-resistant (XDR) Gram-negative bacteria [303]. Colistin mechanism of action involves its binding to lipid A within the outer membrane based on lipopolysaccharides of Gram-negative bacteria. Subsequently, it disrupts the outer and inner membranes, leading to cell lysis.

In clinical practice, to mitigate its potential neuro- and nephrotoxicity, colistin is administered in the form of the prodrug colistin sodium methasulfonate (CMS). This prodrug undergoes hydrolysis following parenteral administration or inhalation, releasing its active form, colistin. However, it is worth noting that intravenous (IV) administration of CMS is also associated with a notable risk of nephrotoxicity and with limited pulmonary diffusion [304]. Currently, CMS is delivered via pulmonary administration in multiple forms, including as liquid solutions using nebulizers (i.e., PARI LC PLUS®) or as dry powders enclosed within PEG-gelatin capsules (Colobreathe®). These forms of administration are commonly used for the management of chronic pulmonary infections caused by *Pseudomonas aeruginosa* in patients diagnosed with cystic fibrosis [305].

Nevertheless, CMS is not an ideal prodrug: It lacks antimicrobial activity against *P. aeruginosa* and relies on non-enzymatic hydrolysis for its conversion into colistin, which is essential for the bactericidal action [306]. This conversion process tends to be relatively slow when compared to the rate at which CMS is absorbed in the pulmonary system. It has been observed that in patients who receive CMS through pulmonary administration, only a mere 1.4 wt.% of the CMS dose is transformed into colistin [307]. Consequently, this demands the use of relatively high concentrations of CMS to achieve the desired colistin levels in the pulmonary epithelium.

Despite these problems, the International Consensus Guidelines for the Optimal Use of the Polymyxins maintain that the potential benefits of nebulized CMS outweigh their associated risks, based on its potential to reduce nephrotoxicity, and enhance drug concentration within the lung. However, organizations such as the American College of Clinical Pharmacy or the European Society of Clinical Microbiology emphasize the need for more randomized clinical trials to establish definitive conclusions [308]. Therefore, the development of drug delivery systems for efficient pulmonary colistin administration holds promise, offering the potential to increase antibiotic concentrations locally while mitigating side effects.

Various strategies have been employed to enhance drug accumulation within the lung for the treatment of respiratory infections. One of such approaches involves the precise adjustment of drug particle sizes within the micron size range to optimize their deposition when aerosolized and prevent premature exhalation [309]. Additionally, thiolated drug delivery vehicles, known as thiomers, have been extensively used in

pulmonary drug delivery. Thiomers facilitate the binding of antibiotic-loaded carriers to lung mucus glycoproteins by forming disulfide bonds [310]. Hydrophobic interactions, often induced using hydrophobic polymers, also can contribute to this mucoadhesion [89]. PEGylation represents another common strategy, which can enhance either mucoadhesion or mucus-penetrating capabilities, depending on factors such as PEG molecular weight and structure [311]. PEGylated polymer nanoparticles can potentially avoid mucociliary clearance while improving lung retention and drug bioavailability. This enhancement is due to the diffusion of PEGylated polymeric particles through the mucus layer, enabling them to reach the underlying epithelial cells [312].

As highlighted in the general introduction, PLGA is an aliphatic polyester commonly employed for antibiotic sustained release due to its inherent hydrolytic properties, which allow to break it down into biodegradable endogenous lactic and glycolic acids. Its molecular weight and the molar ratio of its constituent monomers can be adjusted to achieve different degradation rates and, consequently, specific release profiles. Previous studies have successfully encapsulated aerosolizable colistin within PLGA, resulting in prolonged antibiofilm effects against *P. aeruginosa* with just a single application, in contrast to multiple treatments required when using its free form [313]. However, the colistin loadings achieved using the single emulsion solvent evaporation synthesis technique were relatively low (e.g., 1.27 wt.%). Similar approaches in other studies also yielded moderate drug loadings of less than 5 wt.% [314]. In contrast, Shi et al. encapsulated colistin sulphate salt in PLGA microparticles with drug loadings of up to 16 wt.% using double emulsion solvent evaporation [315]. Despite these efforts, achieving high drug loadings exceeding 50 wt.% in PLGA particles with suitable hydrodynamic sizes for pulmonary delivery remains challenging.

IV.2. Objectives

The objective of this study was to explore a range of techniques and formulations intended for the encapsulation of colistin within polymeric micro- and nanoparticles. The ultimate goal was to assess the potential of these formulations for being used in pulmonary drug delivery and for the treatment of *P. aeruginosa* infections. Four different methods were proposed: (i) synthesis of PLGA nanoparticles single emulsion-solvent evaporation method; (ii) encapsulation through nanoprecipitation with miscible solvents, utilizing PLGA-poly(ethylene glycol) (PEG) as the encapsulating matrix; (iii) colistin nanocoacervation in hydroxypropyl methylcellulose (HPMC) using the antisolvent precipitation method followed by encapsulation within PLGA nanoparticles; and (iv) colistin encapsulation within PLGA microparticles using electrospraying.

IV.3. Experimental

IV.3.1. Synthesis and characterization of colistin loaded nano and microparticles

IV.3.1.1. Synthesis of unprotonated colistin

Colistin sulphate salt was initially dissolved in Milli-Q water to a final concentration of 20 mg/mL. The hydrophobic form of colistin was then achieved by gradually adding a 0.2 M NaOH solution while stirring the mixture. The addition of NaOH was continuous until the pH reached 11, as colistin contains five amine groups with an estimated pKa of ≈10 [316]. Consequently, the previously water-soluble colistin precipitated as a white insoluble solid. This solid was then filtered under vacuum and rinsed multiple times with Milli-Q water. Finally, the solid was dried under vacuum overnight, resulting in a synthesis yield of 60 wt.%.

IV.3.1.2. Synthesis of PLGA-colistin nanoparticles

PLGA-colistin nanoparticles (PLGA@COL NPs) were synthesized through the oil-in-water (o/w) single emulsion solvent evaporation method. Briefly, 50 mg of PLGA polymer, 150 mg of Pluronic-F68, and varying quantities of hydrophobic colistin (ranging from 12.5 mg to 50 mg) were dissolved in 5 mL of ethyl acetate. This organic phase was then emulsified with an aqueous phase of 10 mL of Milli-Q water via sonication for 25 seconds, utilizing an ultrasonic probe with a diameter of 0.13 inches and an amplitude set at 40% (Digital Sonifier 450, Branson, USA). The resulting o/w emulsion was stirred at 600 rpm for 3 h to facilitate the evaporation of ethyl acetate. The resulting nanoparticles were then washed through several centrifugation cycles (7500 rpm, 15 minutes) and finally dispersed in 2 mL of Milli-Q water.

IV.3.1.3. Synthesis of PLGA-PEG-colistin nanoparticles

Hydrophobic colistin was encapsulated in PLGA-PEG using the nanoprecipitation technique. Firstly, 5 mg of PLGA-PEG and varying quantities of hydrophobic colistin (ranging from 2.5 mg to 9 mg) were dispersed in 1 mL of acetone. This dispersion was slowly added drop by drop at a rate of 2 mL/h, utilizing a syringe pump (model PHD Ultra, Harvard Apparatus, Holliston, MA, USA) into 1 mL of Milli-Q water, while maintaining continuous stirring. When it was fully added, the acetone was allowed to evaporate by stirring at room temperature for 2 h, allowing the precipitation of the polymeric nanoparticles. The resulting nanoparticles (PLGA-PEG@COL NPs) were subsequently washed through centrifugation (10,000 rpm, 10 minutes) with Milli-Q water.

IV.3.1.4. Preparation of colistin nanoparticles

Colistin nanoparticles (CNPs) were synthesized using the anti-solvent precipitation method, which was adapted from a previously reported procedure [317]. This approach was chosen to obtain a high drug loading because the nanoparticles produced consist of a considerable proportion of the pure antibiotic. Firstly, 15 mg of hydrophobic colistin was mixed with 1.5 mL of PEG300 while heating and stirring. Simultaneously, an anti-solvent solution was prepared by combining 100 mg of HPMC in 3.5 mL of water. Next, the colistin-PEG300 mixture was quickly added into the HPMC solution, maintaining continuous stirring (400 rpm) and room temperature for 2 minutes. The resulting organic-to-aqueous phase ratio was 3/7, with HPMC accounting for 2 wt.% in the final mixture. The appearance of a stable opaque dispersion indicated the successful formation of colistin nanoparticles stabilized with HPMC. CNPs were then washed by various centrifugation cycles (13,000 rpm, 30 minutes) using Milli-Q water in order to remove the unreacted polymer. Lastly, the resulting CNPs were freeze-dried to produce a dry powder, suitable for storage and further use.

IV.3.1.5. PLGA-colistin microparticles electrospraying

PLGA-colistin microparticles (PLGA@COL MPs) were fabricated via the electrospray technique utilizing a Yflow 2.2 D500 electrospinner (Electrospinning Machines/R&D Microencapsulation, Valencia, Spain). The electrospinner featured an 8 cm diameter aluminium disc plate covered with aluminium foil as collector, as previously reported [318]. First, a mixture of PLGA (10 w/v) and hydrophobic colistin in DMF with varying colistin concentrations (10, 15, 20, 30 wt.% relative to the polymer mass) was prepared by agitating the solution overnight at room temperature. The PLGA-colistin mixture was loaded into a 10 mL syringe and then pumped through a 22-gauge needle acting as a spray nozzle using a syringe pump. The needle was positioned 30 cm away from the collector plate to allow the DMF solvent to evaporate effectively during the electrospraying process. The flow rate was set at 0.5 mL/h, with the collector set to -3.80 kV and the needle voltage ranging between +10.0 kV and +14.5 kV to establish a stable Taylor cone-jet. Microparticle formation occurred at room temperature, with relative humidity levels between 30% and 50%. The resulting microparticles were collected as a dry white powder by gently scraping them from the aluminium foil using a spatula.

IV.3.1.6. Nano and microparticles characterization

The hydrodynamic size of the resultant formulations was assessed through dynamic light scattering (DLS) using a Brookhaven 90Plus particle size analyser. For zeta potential measurements, the same equipment with ZetaPALS software was employed. The assays were conducted in a 1 mM KCl aqueous solution at a pH of 6, maintaining a stable temperature of 25 °C. The zeta potential values were ascertained by examining the electrophoretic mobility of the nanoparticles and subsequently applying the Smoluchowski equation. Transmission electron microscopy (TEM) images

were captured using a T20-FEI Tecnai thermionic microscope, operating at an acceleration voltage of 200 kV. Samples were deposited onto carbon-coated copper grids, air-dried at room temperature, and stained with a negative staining agent (3% phosphotungstic acid) to enhance the contrast of the polymeric particles. Morphological characterization of all the products was also conducted utilizing an Inspect F-50 Scanning Electron Microscope (SEM FEI, The Netherlands), with the samples previously coated with a palladium layer. The microscopy images were subjected to analysis using the open-source image processing software ImageJ to generate the corresponding histograms depicting particle size distribution.

IV.3.2. Aerodynamic particle diameter analysis

The aerodynamic particle size distribution of CNPs and PLGA@COL MPs was studied using a Next Generation Impactor (NGI) provided by Copley Scientific Limited in Nottingham, UK. This NGI was equipped with a TPK 2000 critical flow controller and a HCP5 vacuum pump (Copley HCP5, Nottingham, UK). To achieve the desired conditions, the flow rate was adjusted to generate a pressure drop of 4 kPa within the powder inhaler (Handihaler®, Boehringer Ingelheim, Germany), and the aspiration time was adjusted to intake 4 litres of air. In each test (N = 3), the inhaler was loaded with a size 3 hard gelatin capsule containing 21 ± 1 mg of the corresponding dry particles. Then, two cycles of aspiration were performed. After the particle emission, the material remaining within the capsule, the inhaler, the induction port and all the stages of the NGI, was collected. The mass of particles with an aerodynamic diameter less than 5 µm, expressed as a percentage of the total mass emitted and recovered, was defined as the fine particle fraction (FPF). The mass median aerodynamic diameter (MMAD) and FPF were calculated using previously established methods [319–321]. For colistin release studies, particles with aerodynamic diameters falling within the range of 3 to 5 µm were collected and kept for further use.

IV.3.3. Colistin loading and *in vitro* release

To evaluate drug release kinetics *in vitro*, 2 mg of CNPs with aerodynamic diameters ranging from 3 to 5 µm were dispersed into 12 mL of 0.1 M ammonium acetate buffer (pH 7). The resulting suspension was divided into aliquots and incubated for 24 hours (37 °C, 120 rpm). At specified time points, the tubes (with three replicates per time point) were subjected to centrifugation (13,000 rpm, 5 minutes), followed by the collection of the supernatants.

Subsequently, colistin concentration in the collected samples was determined using a validated LC-MS/MS method, as previously reported [307, 321–325]. A chromatographic analysis was carried out on an Alliance 2695 system (Waters, France) equipped with a Jupiter 300-Å column (5.0 µm, 50 mm length, 2.0-mm inner diameter; Waters, St.-Quentin en Yvelines, France). The mobile phase, delivered at a flow rate of 0.2 mL/min, consisted of a mixture of 0.1% (v/v) formic acid in acetonitrile and 0.1% (v/v) formic acid in water in a ratio of 25:75 (v/v). The mass spectrometer used was a

Micromass Quattro microAPI (Waters, France), operating in positive ion mode. Calibration standard curves were prepared using seven samples in ammonium acetate buffer, with colistin base concentrations ranging from 0.01 to 10 µg/mL.

To determine the encapsulation efficiency (EE) and drug loading (DL) of the colistin in all formulations, liquid-liquid extractions of the PLGA or PLGA-PEG polymers were conducted, using a 1:1 (v/v) mix of methylene chloride and 0.1% (v/v) formic acid in water. In the case of CNPs, complete dissolution of colistin in a solution containing 0.1% (v/v) formic acid in water was achieved over a 24-hour period. Subsequently, a similar LC-MS/MS method was used to quantify colistin in the 0.1% (v/v) formic acid in water phase. Controls containing a known amount of colistin demonstrated 100% recovery of colistin in both cases. The EE and DL in the different formulations were calculated using the same equations as in section **II.3.1**.

IV.3.4. *P. aeruginosa* loaded alginate beads preparation

PAO1 were embedded in alginate beads in order to simulate a biofilm following a previously reported procedure [326]. Initially, PAO1 cultures in MHB were cultured until reaching the exponential growth phase. Subsequently, the cultures were diluted to an OD_{600} of 0.3. A 1 mL aliquot of this suspension was washed by centrifugation with 0.9% (w/v) NaCl, followed by dispersion in 9 mL of 2% (w/v) alginate. This preparation was then emulsified with 100 mL of paraffin oil containing 0.01% (v/v) SPAN®60 using a mechanical stirrer (RZR-2021, Heidolph, France). For the gelation of the droplets containing the alginate, 20 mL of 0.1 M TRIS-HCl buffer at pH 7, containing 0.1 M $CaCl_2$, were added drop by drop to the emulsion while stirring continuously (1,300 rpm). Finally, the emulsion was allowed to cool for 1 h with an ice bath surrounding the beaker while stirring at 300 rpm. Once the alginate beads had formed, they were separated by centrifugation (5,000g for 10 minutes) and washed four times with 0.9% (w/v) NaCl.

IV.3.5. Antimicrobial activity of CNPs

Freshly prepared alginate beads containing PAO1 were dispersed in 5 mL MHB. Subsequently, 100 µL of this suspension was aliquoted into each well of white, flat-bottomed 96-well microplates (Greiner®, France). The bioluminescence in the wells was monitored over time until it reached an intensity of approximately 1,000 RLU. Once this intensity was reached, 100 µL of MHB solutions containing increasing concentrations of colistin and CNPs (ranging from 0.2 to 40 µg/mL) were added to the wells. The plates were then sealed with a transparent membrane to prevent evaporation, and luminescence readings were taken every 30 minutes for a duration of 24 hours at 37 °C using a microplate reader (Infinite 200 Pro, Tecan, France). After 24 hours, to release the bacteria from the alginate beads, the cultures were diluted in a citrate-bicarbonate buffer (comprising 0.02 M citric acid and 0.05 M Na_2CO_3) and incubated for 10 minutes at 37 °C on an orbital shaker (200 rpm). Subsequently, the

solubilized beads were serially diluted in a 0.9% (w/v) NaCl solution and plated onto MHA plates for bacterial quantification through colony formation counting.

IV.4. Results and discussion

IV.4.1. Synthesis and characterization of colistin-loaded nano and microparticles

The use of antibiotic-loaded nanoparticles for pulmonary delivery presents clear advantages compared to enteral delivery: It avoids first-pass metabolism and provides the opportunity to tune particle size and surface characteristics for precise targeting the lung parenchyma. This study explores the development of various polymeric nano- and microparticles designed for colistin encapsulation. To achieve desired particle sizes and high drug loadings, different synthesis methods were employed, including o/w emulsification, nanoprecipitation, coacervation, and electrospraying.

The o/w single emulsion solvent evaporation method proved effective in producing PLGA@COL NPs. Various concentrations of hydrophobic colistin in the synthesis procedure (12.5, 30 and 50 mg/mL) were used to optimize the drug loading. **Figure IV.1a** displays a SEM image of PLGA@COL NPs synthesized with 50 mg of hydrophobic colistin. The resulting PLGA@COL NPs exhibited a spherical shape, with a narrow particle size distribution of 105 ± 28 nm. The quantity of drug incorporated during the synthesis did not significantly impact the size and shape of the nanoparticles. TEM images of PLGA@COL NPs (**Figure IV.1b**) revealed also spherical and monodisperse nanoparticles. Interestingly, dark grey regions inside the particles, particularly prominent in samples with higher colistin concentrations, likely indicated the presence of precipitated colistin within them, stained by the contrast agent used for TEM. These grey areas disappeared in the images (**Figure IV.1c**) when the nanoparticles were incubated in an aqueous medium at a pH of 6–7, suggesting colistin solubilization and release. This phenomenon is attributed to colistin positive charge at neutral pH due to amine functional groups in its structure, rendering it soluble in water [327]. Using DLS, the hydrodynamic size of PLGA@COL NPs synthesized was determined to be 300 ± 60 nm. As depicted in **Table 3**, this methodology achieved a colistin loading of less than 2 wt.% (1.8 wt.% ± 0.6).

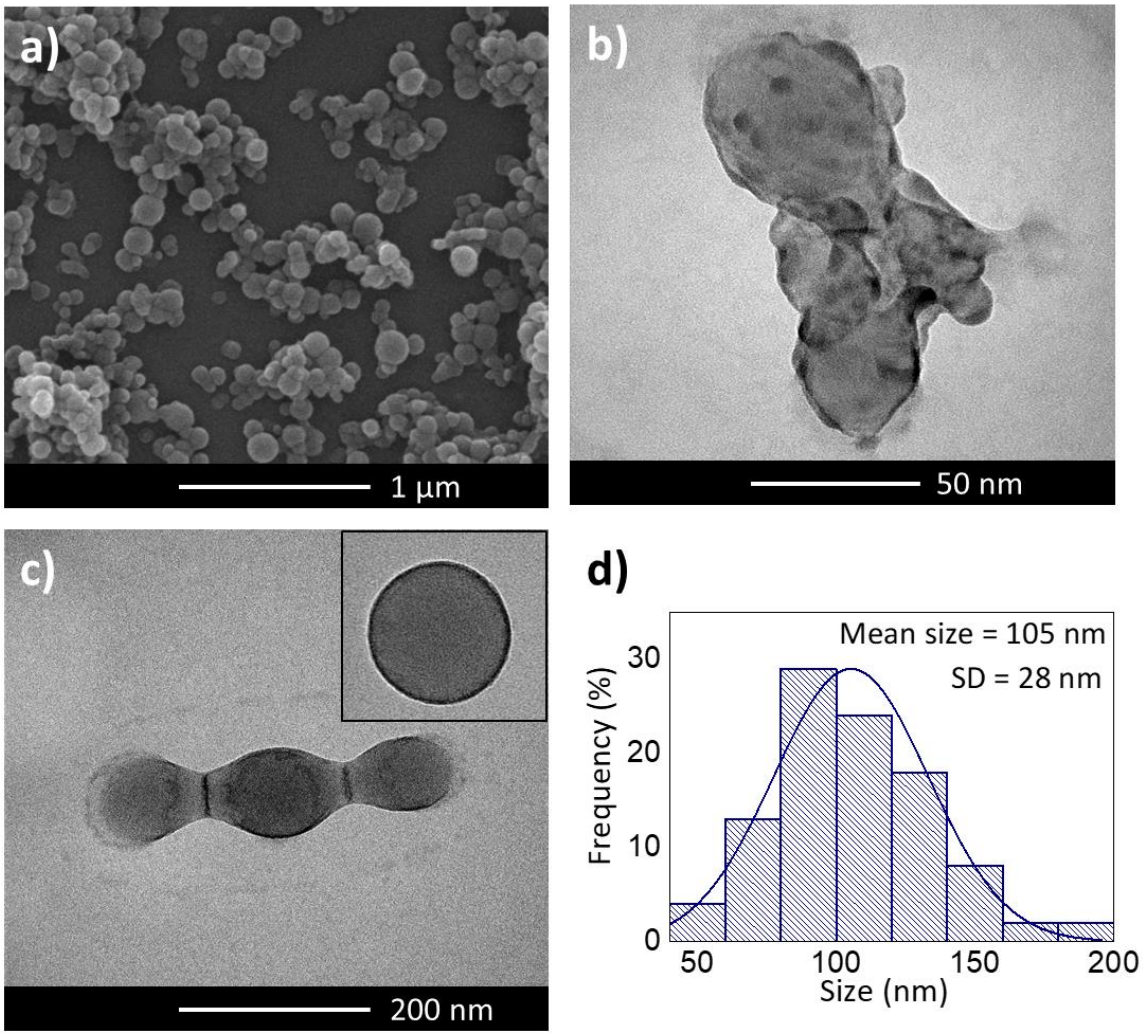

Figure IV.1: PLGA@COL nanoparticles characterization: SEM **(a)** and TEM **(b)** images of PLGA-colistin nanoparticles obtained by o/w emulsification using 50 mg of colistin. **c)** TEM images of PLGA-colistin nanoparticles after incubation in a medium with a pH adjusted to 6. **d)** Size distribution histogram retrieved from SEM measurements (N=100) of PLGA-colistin nanoparticles obtained by o/w emulsification.

Table 3: Size, encapsulation efficiency (EE), and drug loading (DL) data of the different formulations

	PLGA@COL NPs	**PLGA@CNPs NPs**	**PLGA-PEG@COL NPs**	**CNPs**	**PLGA@COL MPs**
Size (nm)	105 ± 28	114 ± 27	77 ± 20	20.5 ± 3.1	1900 ± 300
EE (%)	9.0 ± 3.08	1.5 ± 0.1	8.3 ± 4.5	26.0 ± 5.0	75 ± 20
DL (%)	1.8 ± 0.6	1.1 ± 0.1	5.3 ± 2.9	55.0 ± 5.0	15 ± 4

Single emulsion-solvent evaporation using PLGA in non-miscible solvents is a commonly employed and reliable methodology for antibiotic encapsulation. However, it has notable drawbacks, including the limited drug loading and the need for surfactants [313, 314, 328].

As introduced earlier, surface modification with specific PEGs can enhance the pulmonary biodistribution of carrier particles and improve their mucus penetration when administered through the pulmonary route [329]. For this reason, PLGA-PEG@COL NPs were prepared using the nanoprecipitation method. As in the previous procedure, various concentrations of colistin in the organic phase (2.5, 5, 7, and 9 mg/mL) were used during the optimization of the procedure. **Figure IV.2** depicts SEM and TEM images, as well as the size distribution histogram of the resulting nanoparticles using 9 mg/mL of colistin in the synthesis. PLGA-PEG@COL NPs exhibited mean sizes of 77 nm, smaller than those of PLGA@COL NPs obtained via emulsification. Using DLS, the hydrodynamic size for the nanoparticles with the highest colistin loading was 424 ± 55 nm, indicating potential incipient nanoparticle agglomeration. **Table 3** shows how this synthesis achieved a drug loading of 5.3 wt.%. ± 2.9.

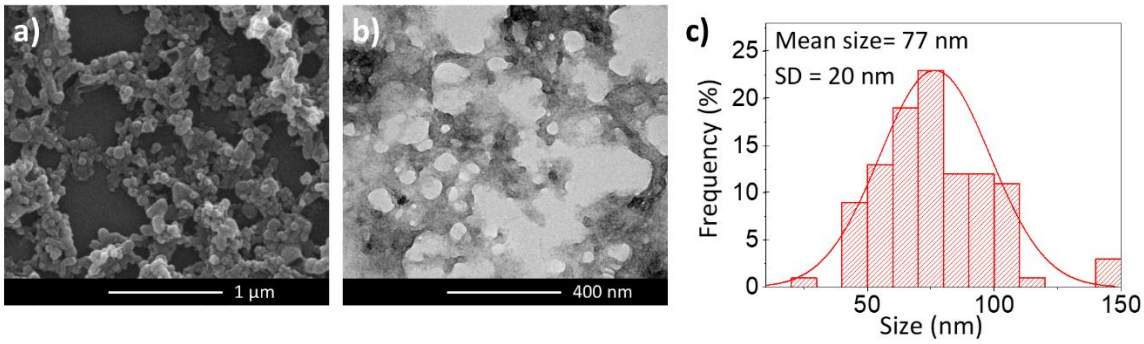

Figure IV.2: PLGA-PEG@COL nanoparticles characterization: SEM **(a)**, TEM **(b)** and size distribution histogram **(c)** of PLGA-PEG@COL NPs obtained by nanoprecipitation using 9 mg/mL of colistin.

Nanoprecipitation outperformed the o/w simple emulsion method in terms of colistin encapsulation. This improvement can be likely attributed to a reduced drug loss: In nanoprecipitation, the organic solvent swiftly diffuses into the aqueous phase, precipitating the water-insoluble polymer and entrapping the colistin. Furthermore, the higher vapor pressure of acetone (231 mmHg at 25 °C) in comparison to that of ethyl acetate (93 mmHg at 25 °C) facilitates the evaporation of the solvent in the former method, leading to rapid polymer precipitation and superior drug encapsulation.

With the objective of further enhance the colistin loading in the nanoparticles, the coacervation of hydrophobic colistin using the anti-solvent precipitation method was considered. In this methodology, after achieving supersaturation of colistin, nucleation begins, and particle growth follows depending on the availability of precursors. HPMC acts as a surface growth inhibitor at the drug nucleation sites, creating a diffusion barrier that effectively confines particle size to the nanoscale, preventing further growth. This methodology enables the synthesis of nanomaterials with high drug delivery capabilities [330].

The optimization process involved the variation of the amount of colistin used in the synthesis, with concentrations ranging from 4.2 to 15 mg. The most favourable

outcomes were observed when 15 mg of colistin were employed (**Figure IV.3a-c**). TEM images show the formation of CNPs with a mean diameter of 20.5 ± 3.1 nm (N = 100), resulting in a uniform particle size distribution. The hydrodynamic size of the dispersions containing CNPs, as measured by DLS, was 415 nm. The zeta potential value of CNPs, obtained at pH = 6, was approximately +1.71 ± 0.25 mV. These values were close to the isoelectric point and may explain the observed agglomeration of CNPs detected via DLS. As shown in **Table 3**, this formulation achieved a DL of 55 wt.%.

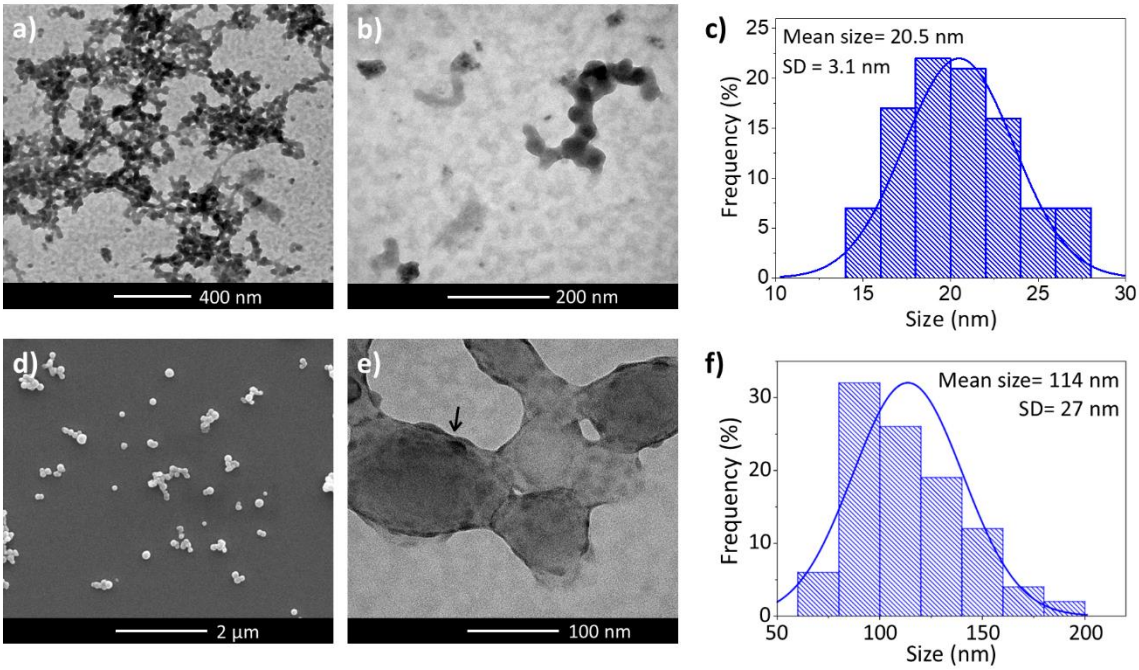

Figure IV.3: CNPs and PLGA@CNPs nanoparticles characterization: TEM **(a, b)** and size distribution histogram **(c)** of CNPs obtained by anti-solvent precipitation technique using 15 mg of colistin. SEM **(d)**, TEM **(e)** and size distribution histogram **(f)** of PLGA@CNPs NPs obtained by o/w emulsification.

The CNPs were used as drug delivery carriers for future assays, but they were also encapsulated in PLGA nanoparticles (PLGA@CNPs NPs) using the o/w single emulsion solvent evaporation method. To achieve this, 100 mg of prepared CNPs were dispersed in ethyl acetate and emulsified following the protocol previously described in this section. The results yielded monodisperse PLGA nanoparticles measuring 114 nm in size, loaded with CNPs (**Figure IV.3d-f**). However, the drug loading obtained (1.1 wt.% ± 0.1) was not significantly higher than that achieved by the PLGA@COL NPs methodology (see **Table 3**). This may be attributed to the potential loss of CNPs during the emulsion or the solvent evaporation stage.

Lastly, with the intention of producing particles on the microscale, the synthesis of PLGA@COL MPs via the electrospraying technique was studied. Initially, various concentrations of colistin were used within the organic solution containing the polymer to achieve high drug loadings while minimizing the particles polydispersity. The final optimized procedure used a combination of PLGA at 10% (w/v) and colistin sulphate at 20 wt.% (in relation to the PLGA mass) in DMF. The PLGA@COL MPs

produced exhibited a uniform size distribution, with a mean diameter of 1.9 ± 0.3 µm, as depicted in **Figure IV.4**.

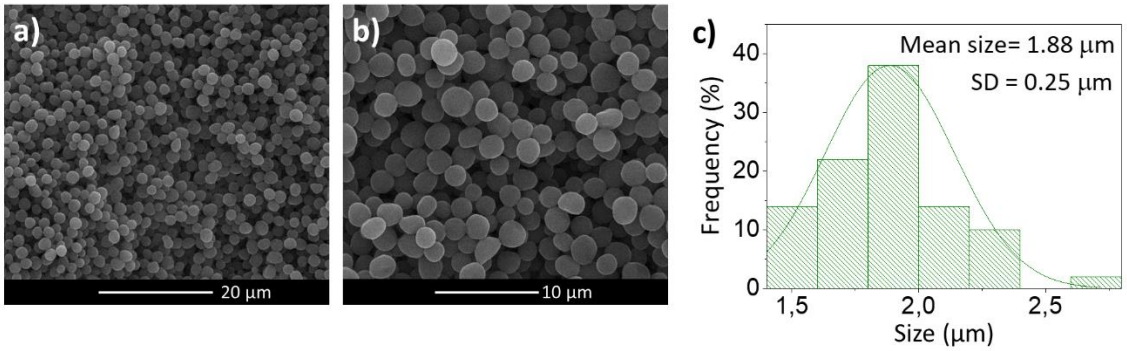

Figure IV.4: PLGA@COL microparticles characterization: SEM **(d, e)** and size distribution histogram **(f)** of PLGA@COL MPs obtained by electrospraying.

The EE and DL of the optimized methodologies were assessed using LC-MS/MS, and the results are summarized in Table 2. Notably, the highest drug loading values were achieved for CNPs, which contained 55.0 wt.% of colistin. Comparatively, PLGA@COL MPs produced via electrospraying exhibited higher colistin loadings than PLGA@COL NPs and PLGA-PEG@COL NPs. The electrosprayed microparticles achieved a drug loading of 15 wt.% in colistin, in line with previous reports on this encapsulation methodology [273, 331]. Meanwhile, the drug loading in the nanoparticles generated through the o/w emulsion and nanoprecipitation methods remained below 2 wt.%, consistent with previous reports [332, 333]. These results highlight electrospraying as a cost-effective alternative to emulsion or nanoprecipitation-based methods. Additionally, electrospraying operates at room temperature, eliminating the need to protect the polymer from thermal degradation, as required in emulsion-based techniques due to the high shear stress involved [334].

IV.4.2. Aerodynamic properties analysis

For the pulmonary administration of high doses (>10 mg) of common use drugs such as antibiotics, dry powder inhalers (DPIs) and nebulizers are the only suitable delivery methods. DPIs tend to have a higher patient compliance due to their convenience (shorter administration and device cleaning times, compact device size) [335, 336]. As a result, the potential of the formulated particles to serve as dry powders for inhalation was studied. Given that the electrosprayed PLGA@COL MPs and the CNPs resulted in the highest drug loading values, these two formulations were selected for further analysis. Their aerodynamic particle diameter was evaluated using a Next Generation Impactor (NGI) to categorize aerosol particles into size fractions. As previously mentioned, to optimize lung deposition, the aerodynamic size of inhaled particles should fall within the range of 1 to 5 µm [337, 338].

Throughout the aerosolization process within the NGI, it was observed that a substantial portion of the PLGA@COL MPs tended to accumulate in the induction port. This observation indicates that these particles generate aerosols characterized by

larger aerodynamic sizes, which renders them unsuitable for pulmonary delivery. Consistent with previous reports, it was observed that without the addition of dispersion modifiers or special surface coatings, a significant portion of the microparticles in dry powder inhalation PLGA formulations remained in the capsule and in the inhalation device [339]. This study did not explore the utilization of surface or intraparticle agents, such as plasticizers and anti-tacking components, as they could have compromised the final drug loading in the final aerosolizable pharmaceutical formulations.

In contrast, the aerodynamic properties observed for the CNPs in the NGI (**Figure IV.5**) indicate that this formulation is suitable for pulmonary delivery: It exhibited a mass median aerodynamic diameter (MMAD) of 3.3 ± 0.2 µm and a geometric standard deviation (GSD) of 2.4 ± 0.2 µm. The observed MMAD falls within the range of 1 to 5 µm, recognized as the breathable fraction of an aerosol. This range is considered appropriate for pulmonary drug delivery and standard respiratory treatments [340]. Particles with a MMAD between 1 and 3 µm tend to deposit more effectively in the deeper lung regions (bronchioles and alveoli) compared to those with a MMAD near 5 µm [341]. The fraction of inhaled fine particle mass (particles with an aerodynamic diameter below 5 µm) relative to the total particle mass in the assay was 32.6 ± 0.3%.

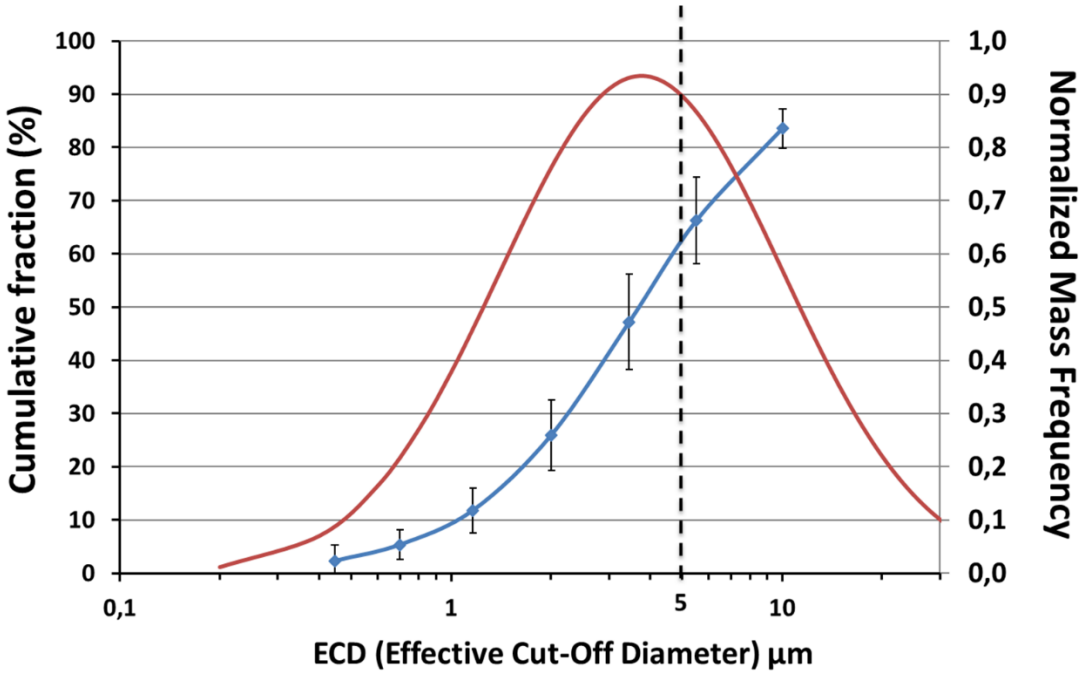

Figure IV.5: Cascade impactor results for the CNPs. In blue, the cumulative fraction of the particles mass versus the effective cut-off diameter. In red, frequency distribution of the particle masses.

In summary, the CNPs achieved the highest drug loading and demonstrated an appropriate aerodynamic diameter for pulmonary delivery. Taking this into consideration, it could be assumed that these nanoparticles may have formed

aggregates of micrometre-sized particles, possibly due to their significant surface reactivity, which promoted the development of supramolecular interactions. This was corroborated by SEM, as shown in the images in **Figure IV.6**.

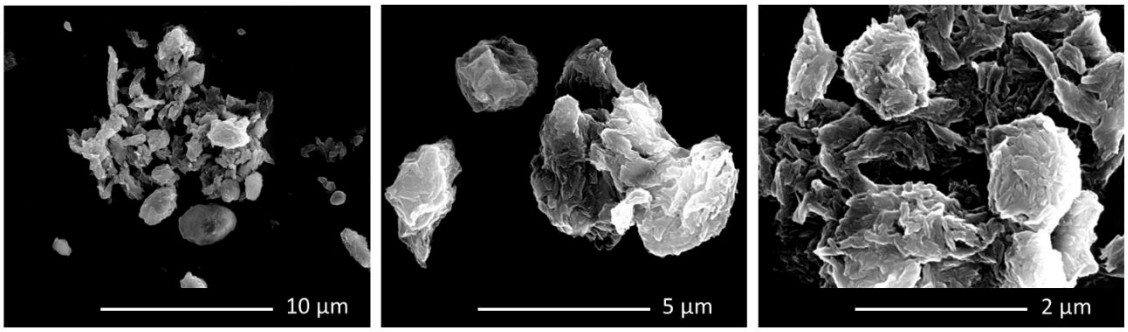

Figure IV.6: SEM micrographs acquired from aggregated CNPs.

Among the various formulations explored to produce colistin-loaded nanoparticles suitable for pulmonary delivery, the synthesis of CNPs emerged as the most advantageous, yielding the highest colistin loading (55.0 wt.%± 5.0) and the best aerodynamic properties. Due to their significant surface reactivity, which promoted the development of supramolecular interactions, these nanoparticles formed aggregates of micrometre-sized particles. From a pulmonary safety perspective, it is worth noting that the two polymers (HPMC and PEG) used to create the CNPs have well-established safety profiles in pulmonary drug delivery applications. Moreover, they are featured as excipients in certain commercially available formulations [342–344].

It is also worth considering that the transition from laboratory-scale production to industrial-scale manufacturing of nanomedicines presents significant challenges [345]. One of the scaling-up challenges in coacervation processes involves meeting safety standards regarding residual solvent levels (ICH Q3C (R6) impurity guideline) [346]. In this case, the organic solvent used, PEG 300, can be easily extracted with water and is authorized to be present at high concentrations in the final product. Lastly, to overcome scaling challenges and minimize batch-to-batch variations related to these formulation methods, microfluidic devices have demonstrated their potential to consistently produce nanoparticles through coacervation [347].

IV.4.3. Drug release and antimicrobial properties

The colistin content within the CNPs exhibited an immediate burst release profile when examined *in vitro* in an acetate buffer, releasing all of its colistin content within 10 min. This suggests the fast solubilization of colistin from the HPMC matrix. Although drug delivery systems based on HPMC are recognized for gradual drug release over time [348], it is likely that the highly water-soluble nanometric HPMC polymeric matrix (20.5 nm) plays a role in the observed burst release kinetics. These reduced-sized CNPs exhibit enhanced solubility, consistent with previous reports on similar nanometric coacervates [317]. Consequently, when CNPs come into contact with an aqueous

medium with the appropriate pH, they would release their encapsulated colistin promptly. This is a favourable characteristic as it quickens the drug bioavailability and helps preventing the presence of bacteria at sub-MIC concentrations, thereby reducing the risk of antimicrobial-resistant mutant selection.

In antimicrobial activity assays conducted with the biofilm model of *P. aeruginosa*, CNPs exhibited a slightly better antimicrobial activity compared to the hydrophilic free colistin (colistin sulphate salt) (**Figure IV.7**). Given the high drug loading of the CNPs (55.0 wt.%), the bactericidal activity of colistin against this bacterial model was significantly enhanced. At 5 μg/mL free colistin was unable to reduce the bacterial growth, however, the CNPs reduced by 4 log the number of colonies. At 5.5 μg/mL those nanoparticles reached the MBC whereas the free drug needed concentrations above 10 μg/mL to produce the same outcome.

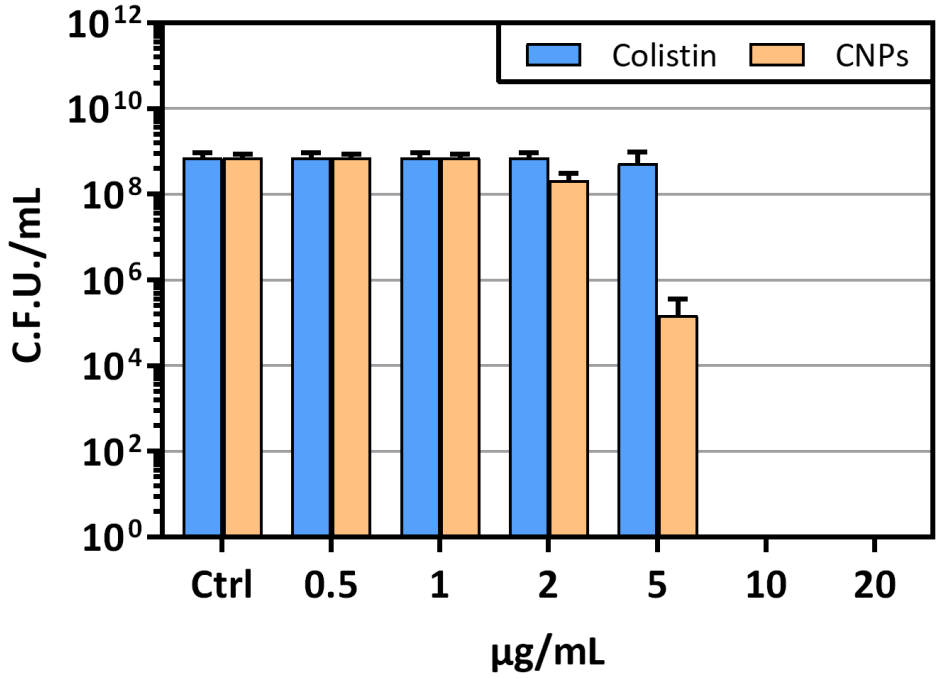

Figure IV.7: Antimicrobial activity of colistin sulphate and CNPs against PAO1 in alginate-beads biofilm model after 24 hours.

IV.5. Conclusions

Among the various synthesis explored to produce drug delivery formulations achieving high colistin loadings and having optimal aerodynamic properties for efficient pulmonary delivery, the nanocoacervation through the anti-solvent precipitation method emerges as the best choice. As demonstrated in this study, this methodology outperforms other alternatives, including single emulsion solvent evaporation, nanoprecipitation, and electrospraying.

The encapsulation of the unprotonated form of colistin within a HPMC matrix achieves remarkable drug loadings, reaching up to 55 wt.% ± 5 of colistin. The resulting nanoparticles exhibit a favourable mass median aerodynamic diameter of 3.3 ± 0.2 µm, rendering them well-suited for pulmonary delivery after aerosolization. Lastly, when compared to the free drug, these particles demonstrate enhanced antimicrobial efficacy in a biofilm model of the *P. aeruginosa* PAO1 strain, highlighting their potential as a promising solution for combating pulmonary bacterial infections.

CHAPTER V

Lysostaphin-loaded PLGA nanoparticles for targeted treatment of *Staphylococcus aureus* infections

Table of contents

Summary

The study presented in this chapter introduces a novel approach by encapsulating lysostaphin, an anti-staphylococci bacteriocin, within PLGA nanoparticles. The chapter assesses the antimicrobial activity of free LYS and LYS-loaded PLGA nanoparticles against different strains of *S. aureus* in planktonic, biofilm, and in a macrophagic intracellular infection model. GFP-expressing *S. aureus* was employed to facilitate traceability.

The results demonstrated a significant reduction in bacterial viability, both in planktonic and biofilm states, and in some cases, the complete eradication of bacteria. Notably, the *in vitro* intracellular infection model showcased the enhanced efficiency of the developed nanoparticles compared to free (i.e., non-encapsulated) bacteriocin treatment.

This research presents the first report on lysostaphin encapsulation within PLGA nanoparticles and offers potential avenues to enhance lysostaphin therapeutic efficacy against *S. aureus* infections.

The content of this chapter has been adapted from the following submitted work:

Landa, G.; Aguerri, L.; Irusta, S.; Mendoza, G.; Arruebo, M.

PLGA Nanoparticle-Encapsulated Lysostaphin for the Targeted Treatment of *Staphylococcus aureus* Infections.

Journal of Colloid and Interface Science, 2023, submitted.

V.1. Introduction

Bacteriocins, lytic enzymes of bacterial origin, serve as natural antimicrobial agents that play a crucial role in microbial competition and shaping bacterial populations [114]. Produced by bacteria as a defence mechanism against competing microorganisms, they exhibit bactericidal activity comparable to antibiotics, but with a very narrow spectrum of activity. This, coupled with their reported rarity in resistance development, make them a favourable option for antimicrobial therapy [115]. Lysostaphin (LYS), a well-studied bacteriocin, is a naturally occurring endopeptidase derived from *Staphylococcus simulans*. It possesses exceptional enzymatic activity by cleaving polyglycine bridges that serve as cross-linkers in the cell wall structure of *staphylococci* [118, 349]. *In vitro* investigations have demonstrated its potent bactericidal efficacy against *S. aureus* strains, even those exhibiting resistance to conventional antibiotics like MRSA [120, 350]. LYS displays superior efficacy compared to native human response against infection and broad-spectrum antibiotics like penicillin and vancomycin [351–353]. Furthermore, it exhibits a remarkable capability to effectively lyse both actively growing cells and cells in stationary growth phase, and it shows enhanced efficacy against bacterial biofilms [350, 354, 355]. The effectiveness of LYS and its therapeutic potential have been examined across diverse contexts, like animal models featuring systemic infections [356], wound infections [357], bone infections [358], endocarditis [359], mastitis [355], keratitis [360], and biofilm and implant-associated infections [361]. Additionally, clinical trials have been conducted to investigate the effectiveness of LYS in humans afflicted with persistent nasal colonization [362, 363]. Overall, these studies reveal the potential of LYS as a therapeutic agent against staphylococcal infections in diverse clinical scenarios.

Nevertheless, the clinical applicability of LYS encounters two primary challenges. Firstly, the loss of enzymatic activity under physiological conditions [364]. Secondly, the potential immunogenicity of LYS raises concerns regarding the development of immune responses and associated adverse reactions [365]. To overcome these challenges, a range of strategies have been explored. These strategies include PEGylation [366–368], glycosylation [369], inclusion in hydrogels [366], polymers [370], fusion with other proteins (Bovine serum albumin, Cell-penetrating peptides…) [371–375] or its encapsulation in nanocarriers such as liposomes [376].

Encapsulation of enzymes within polymeric particles offers a promising approach to preserve their stability and to ensure the sustained enzymatic activity required for effective therapeutic applications [377, 378]. By providing a protective environment, this platform may preserve and maintain the enzymatic functionality over extended periods of time [379, 380]. In this study, we present a novel approach for enhancing the efficacy of LYS by encapsulating it within PLGA nanoparticles.

Herein, the focus has been placed on evaluating the antimicrobial activity of LYS-loaded PLGA nanoparticles against *S. aureus* in both planktonic and sessile states, as

well as in an intracellular infection model in J774 murine macrophages. The elimination of intracellular bacterial persisters poses a significant challenge in infection management. Currently, this represents the first study on LYS encapsulation within PLGA nanoparticles. This research aims to provide insights into the potential of this formulation to enhance the therapeutic effectiveness of LYS, thereby addressing the difficulties associated with *S. aureus* infections.

V.2. Objectives

The objective of the work conducted in this chapter was firstly to investigate the potential of LYS encapsulation within PLGA nanoparticles as a novel approach to enhance the therapeutic efficacy of LYS for addressing the challenges associated with *S. aureus* infections. Secondly, to evaluate and compare the antimicrobial activity of free LYS and LYS-loaded PLGA nanoparticles against *S. aureus* in both planktonic and sessile states. Lastly, to assess the effectiveness of LYS-loaded PLGA nanoparticles in an intracellular infection model using J774 murine macrophages, particularly targeting the elimination of intracellular bacterial persisters.

These objectives aim to study the feasibility and effectiveness of utilizing PLGA nanoparticles as carriers for LYS, with the ultimate goal of improving the treatment of *S. aureus* infections in various clinical contexts.

V.3. Experimental

V.3.1. Synthesis of PLGA@LYS nanoparticles

To prepare the PLGA@LYS NPs, a LYS aqueous solution (2 mg/mL, 0.5 mL) was combined with TFE:DCM (1:4, 4.5 mL) in which PLGA (100 mg) had been previously dissolved. The resulting solution was added dropwise into a 5% (w/v) PVA aqueous solution. To form an emulsion, the mixture was sonicated using a probe with a diameter of 0.13 inches and an amplitude of 40%. The emulsion was allowed to stir at room temperature for 4 hours to allow DCM evaporation and the subsequent precipitation of the NPs. To remove the excess of PVA and unincorporated LYS, the resulting NPs were centrifuged at 13,000 rpm for 15 minutes and washed three times with ultrapure water.

V.3.2. Characterization of PLGA@LYS nanoparticles

Particle size and size distribution of PLGA@LYS NPs were measured by DLS using a Brookhaven 90Plus particle size analyzer. Zeta potential of the NPs was measured by electrophoretic mobility using the same instrument. The morphology of the NPs was visualized by SEM microscope after sputter coating the particles with Pd. Encapsulation efficiency (EE) and drug loading (DL) of LYS into PLGA NPs were determined by using a modified BCA Protein Assay Kit (Thermo Fisher Scientific). Briefly, the NPs were

suspended in an aqueous solution containing 0.1 M NaOH 0.5% (w/v) and stirred vigorously during 24 hours at 37 °C to hydrolyze completely the PLGA and release the LYS. Prior to the assay, the samples were sonicated for 15 minutes and then centrifuged 5 minutes at 13,000 rpm to collect the supernatants. LYS was quantified using a Varioskan LUX microplate reader (Thermo Fisher Scientific) at a wavelength of 595 nm. The EE and DL in the different formulations were calculated using the same equations as in section **II.3.1**.

To determine the drug release profile of LYS from the PLGA@LYS NPs, the samples were resuspended in a PBS buffer solution and incubated at 37 °C with constant agitation. At predefined time points, aliquots of the suspension were collected and centrifuged (5 minutes, 13,000 rpm) to obtain the supernatants. The amount of released LYS was quantified using the BCA assay. The percentage of released LYS was calculated with respect to the total amount of protein encapsulated in the NPs. The experiment was performed in triplicate.

V.3.3. Antimicrobial activity of LYS and PLGA@LYS nanoparticles

Different strains of *S. aureus* (ATCC 25923, GFP-expressing *S. aureus*, Newman (MSSA) and USA300 (MRSA)) were inoculated in 5 mL of TSB and incubated overnight at 37 °C with shaking. The culture was then diluted in fresh TSB to achieve an OD_{600}=0.006 (≈10^7 colony forming units (CFU)/mL) and transferred to a 96-well plate. Bacterial suspensions were then treated with increasing concentrations of free LYS (0.25-3 µg/mL) or PLGA@LYS NPs (10-100 µg/mL, to reach equivalent concentrations of the free antimicrobial peptide) and incubated at 37 °C for 24 hours with shaking. The antibacterial activity was evaluated by the serial dilution method followed by plating the treated samples on TSA plates. The experiments were carried out three times in triplicate.

V.3.4. Biofilm inhibition and eradication assays

S. aureus expressing GFP was inoculated in 5 mL of TSB and incubated at 37 °C with vigorous shaking overnight. The resulting culture was diluted in fresh TSB to attain a density of OD_{600}=0.006 (≈10^7 CFU/mL) and then transferred to 96-well plates. For the biofilm inhibition studies, cultures were treated at this point with increasing concentrations of free LYS (0.1-64 µg/mL) or PLGA@LYS NPs (5-2,000 µg/mL, to reach equivalent concentrations of the free antimicrobial peptide) and incubated at 37 °C for 24 hours without shaking. For the biofilm eradication studies, cultures were not treated and incubated at 37 °C for 24 hours with shaking to promote biofilm formation. Then, planktonic cells were removed by washing twice with PBS and the already formed mature biofilms were treated at the same conditions as the ones used in the inhibition studies. In both methodologies, after incubation, samples were washed twice with PBS prior quantifying the biofilm biomass by the Crystal Violet assay, to count bacterial colonies, and to study the biofilm morphology by confocal microscopy.

As mentioned, the evaluation of the biofilm biomass obtained was carried out by the Crystal Violet assay. First, cultures were fixed with 200 µL of 4% PFA in PBS for 15 min and then stained with 200 µL of 0.1% Crystal Violet in Milli Q water for another 15 minutes. After staining, the Crystal Violet in excess was removed by washing the wells with water up to 5 times. The fixed stained samples were solubilized with 200 µL of 33% acetic acid for 15 minutes. Lastly, the absorbance was measured at 570 nm using a microplate reader. Five replicas of each experimental group were tested. To count the bacterial colonies obtained, the biofilms were disrupted by sonication in a water bath for 5 minutes and collected. Finally, the dispersed biofilms were serially diluted in sterile PBS before plating them in TSA for CFU counting. The experiments were conducted three times in triplicate.

To observe the morphology of the biofilms, *S. aureus* GFP cultures were established using the same procedure described above, with the exception that bacteria were seeded onto microscope 8-cell culture chamber slides (Thermo Fisher Scientific). Then, the biofilms were stained with Calcofluor White at a concentration of 40 µg/mL for 20 minutes at room temperature. The stain in excess was removed by washing it three times with sterile PBS. Samples were then covered with coverslips and with a drop of mounting medium (Fluoromount-GTM, Thermo Fisher Scientific). The biofilms were observed using a confocal laser scanning microscope (Zeiss LSM 880; Zeiss, Germany) equipped with a 63x oil immersion objective. Z-stack images were acquired with a step size of 0.5 µm, and the images were analysed using the ZEN 3.3 software (Zeiss, Germany).

V.3.5. Cell cytotoxicity assays

The cytotoxic effects of LYS and PLGA@LYS NPs were evaluated using J774 murine macrophages. The macrophages were grown in DMEM High-Glucose supplemented with 10% FBS and 1% PSA, and were incubated in a humidified atmosphere at 37° C and 5% CO_2. The medium was replaced every 2-3 days and cells were passaged when they reached confluence. For the cytotoxicity assays, the cells were seeded in 96-well plates at a density of 18,000 cells/cm^2 and incubated overnight. Then, the culture medium was replaced with fresh DMEM containing varying concentrations of LYS (0.1-16 µg/mL) and PLGA@LYS NPs (60-1,000 µg/mL) and incubated for 24 hours. After incubation, cell viability was assessed using the Blue Cell® Viability Assay (Abnova). Briefly, the medium was replaced with 100 µL of fresh supplemented DMEM containing 10% of the reagent and incubated for 2 hours at 37 °C. The fluorescence was measured at excitation/emission wavelengths of 570/590 nm using a microplate reader. Control samples (non-treated samples) were also analysed (assigned with 100% viability). The experiments were performed in triplicate.

V.3.6. *In vitro* model of cell infection and treatment

The *in vitro* infection model was developed as we previously reported [247]. In brief, J774 macrophages were seeded in 6-well plates at a density of 18,000 cells/cm^2.

Before the infection assay, cells were washed twice with PBS and DMEM was renewed without PSA to avoid any interference with the infection.

To prepare *S. aureus* GFP, 5 mL of TSB was inoculated and incubated overnight at 37 °C with shaking. The bacteria were then cultured by centrifugation at 4,000 rpm for 5 minutes, washed with PBS, and resuspended in the same buffer to achieve an OD_{600}=0.006 (10^7 CFU/mL). To establish the co-culture of macrophages and *S. aureus* GFP, the bacterial cells were added to the macrophage culture at a multiplicity of infection (MOI) of 10:1. The co-culture was then centrifuged at 200 g for 5 minutes and incubated for 1 hour at 37 °C. Subsequently, the medium was discarded, and the cells were washed with PBS to remove non-phagocytized bacteria. To eliminate any remaining extracellular bacteria, the cells were then treated with 100 ppm gentamicin in DMEM for an additional hour.

Two different approaches were used for the treatment of the intracellular infection. In the first approach, macrophages were pre-treated with various concentrations of either LYS (1 and 5 µg/mL) or PLGA@LYS NPs (50 – 500 µg/mL) for 4 hours prior to the infection. In the second approach, already infected macrophages were treated with the same concentrations of LYS and PLGA@LYS NPs for 1 hour, replacing gentamicin. In both cases, non-infected and non-treated cells were used as controls. The schematic diagram of the two experimental processes is shown in **Figure V.1**. The rationale behind was to know if LYS in its free and encapsulated forms was able to prevent eukaryotic cells for being infected (pre-treatment approach) and to know if LYS in its free and encapsulated forms was able to eliminate intracellular infective persisters.

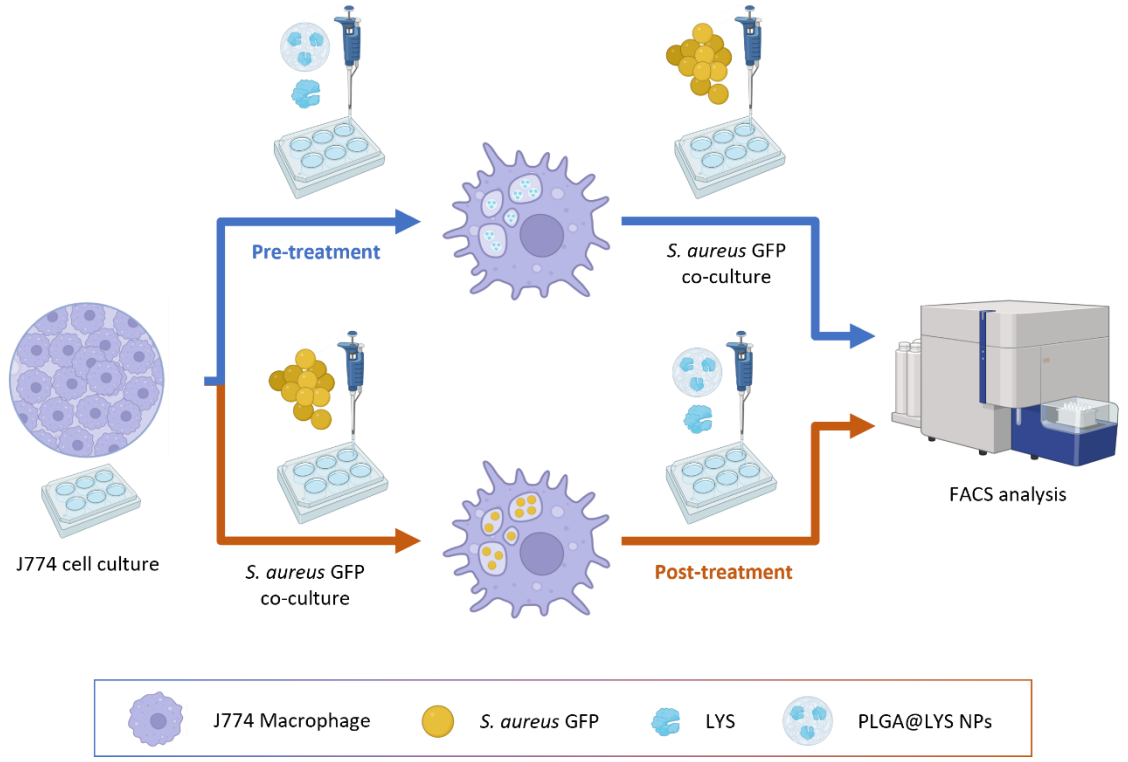

Figure V.1: Experimental methodologies following pre-treatment and post-treatment strategies.

To perform a quantitative analysis of the infection status in the co-culture, the cells underwent flow cytometry (FACS) analysis. To do this, the co-cultures were fixed with 4% PFA for 30 minutes at room temperature. Afterwards, cells were washed and collected to be analysed by FACS (Gallios flow cytometer, Beckman Coulter, USA). The cells within the co-culture were sorted based on their size and the level of GFP signal. Resulting data were analysed using the Flowing 2 software.

Additionally, confocal microscopy was used to observe the effects of LYS and PLGA@LYS NPs treatments against the intracellular *S. aureus* GFP infection in macrophages. For these experiments, the methodology followed was the same as described above though in order to facilitate microscopy analysis, a glass coverslip (Ø13 mm) was initially placed on the bottom of the multi-well plates before macrophages seeding. After cell fixation, the coverslips with the cells were incubated in the dark with Phalloidin 546 (1:200 in PBS-BSA-saponin solution) for 1 h at room temperature. Then, cells were rinsed with 1% PBS-BSA and distilled water. Afterwards, cells were washed with PBS 1x BSA 1%, and subsequently with a solution of saponin 0.1% in PBS 1x BSA 1%. The samples were then mounted on glass slides using DAPI-Fluoromount GTM (Thermo Fisher Scientific) and analysed using confocal microscopy with a 63x oil immersion objective. Z-stack images were acquired with a step size of 0.5 µm, and z-stack orthogonal projections were utilized to visualize the presence of bacteria inside the macrophages. The images were analysed using the ZEN 3.3 software.

V.3.7. Statistical analysis

In every bar graph, values are displayed as the mean ± SD. The statistical analysis of experimental data was performed using Prism 8 software. Three replicas were carried out for each experiment, and all experimental conditions were tested in triplicate unless otherwise specified. The statistical analysis in the antimicrobial activity experiments was performed using the Kruskal-Wallis test. For the intracellular infection assay, a one-way analysis of variance (ANOVA) was employed for conducting multiple comparisons along with a Dunnett's post-test. Statistically significant differences were identified when $p \leq 0.05$.

V.4. Results and Discussion

V.4.1. Physico-chemical characterization of PLGA@LYS NPs

Figure V.2a displays the SEM micrographs obtained for the PLGA@LYS NPs. All the images obtained showed a relatively homogeneous diameter in the particles and a spherical shape. PLGA@LYS NPs exhibited mean diameters of 153.76 ± 45.8 nm. **Figure V.2b** shows the unequivocal absorbance signal in the UV region (max 280 nm attributed to its proteinaceous nature) of the LYS when loaded within the PLGA@LYS NPs. The synthesis method was adapted from that of Wan et al. [380], who synthesized PLGA microparticles encapsulating LYS using the same polymer. The synthesis method optimization was initially performed in the absence of LYS, using Bovine serum albumin (BSA, a cost-effective model protein) instead of LYS. The differences in morphology between the PLGA@LYS NPs and the empty or BSA-loaded particles were not significant (results not shown). The encapsulation efficiency and drug loading were 47.38 ± 2.4 wt. % and 2.88 ± 0.7 wt. %, respectively. The release kinetics of LYS from the PLGA@LYS NPs were evaluated in saline buffer. The release profile (**Figure V.2c**) demonstrated a two-phase pattern: an initial burst release during the first 24 hours, followed by a prolonged and sustained release over a period of 7 days. At this point, 37.5 wt. % of the LYS content was released. Data was reasonably good fitted to the Peppas-Sahlin model indicating that LYS release was attributed to both Fickian diffusion and case II relaxations. The rapid protein release during the initial burst is advantageous as it makes LYS rapidly bioavailable to eradicate bacteria. Meanwhile, the sustained release maintains persistent concentration levels that last for days, preventing further bacterial growth and the possibility of re-infection.

This profile would be attributed to an initial release of the LYS present in the outmost part of the PLGA nanoparticles and a subsequent release of the LYS present in the solid matrix structure after hydrolysis and matrix erosion. Lin et al. reported the formulation of PLGA microparticles encapsulating LYS for pulmonary delivery [380]. Contrary to our work, those authors showed a burst release extended between 24 to 72 hours, eventually reaching 80% release rate after 7 days. According to the authors and the previous literature [381], this delayed burst release is attributed to an empty

microspherical structure present in their capsules, which is something not existent in the solid matrix nanoparticles synthesized in the current study.

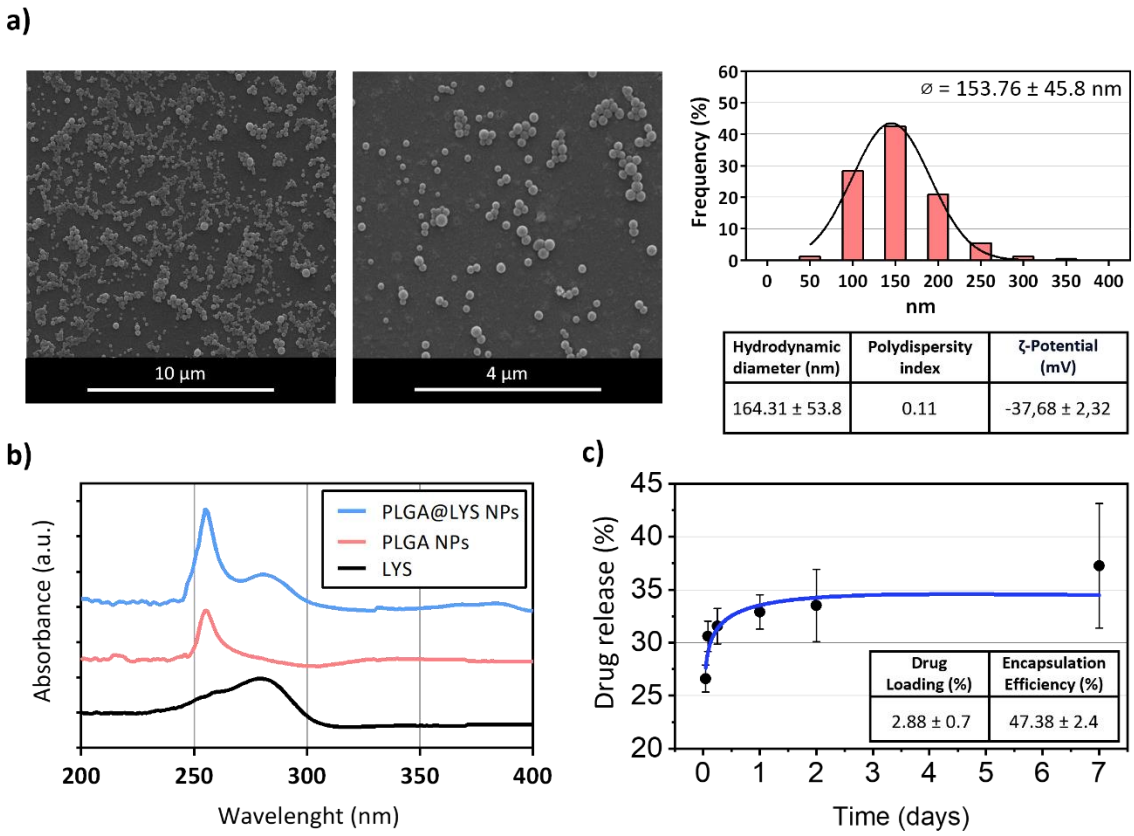

Figure V.2: Synthesis and characterization of PLGA@LYS NPs: **a)** SEM images of PLGA@LYS NPs and the frequency distribution of particle diameters. The table displays the results of DLS analysis and z-potential measurements at a pH of 6; **b)** UV-VIS identification of LYS in PLGA@LYS NPs; **c)** Drug release profile of LYS from PLGA@LYS NPs and its corresponding numerical fitting using the Peppas-Sahlin model. The inset table shows the percentages of drug loading and encapsulation efficiency data.

V.4.2. Antimicrobial activity

Free LYS showed a concentration-dependent antimicrobial activity against all tested *S. aureus* planktonic strains (**Figure V.3a**). LYS MBC varied among the different strains, being MRSA the most susceptible (1 µg/mL), which is a positive outcome. However, these differences in susceptibility between strains are not considered significant according to previous reports [382]. The LYS MIC and MBC against *S. aureus* GFP were determined to be 0.5 and 3 µg/mL, respectively. Given that MIC values for *S. aureus* GFP were in the same order as those observed for *S. aureus* WT and for MRSA, the former strain was used for the subsequent assays in order to take advantage of its easy visualization by confocal microscopy thanks to the expression of the GFP. The PLGA@LYS NPs also exhibited significant antimicrobial activity against planktonic *S. aureus* GFP strain, showing MIC and MBC values of 60 and 80 µg/mL (**Figure V.3b**). Considering the DL data (**Figure V.2c**), these values would correspond to approximately

1.73 and 2.3 µg/mL of encapsulated LYS. These values, while not identical to those observed for free LYS, indicate that LYS retained its bactericidal activity after the encapsulation process.

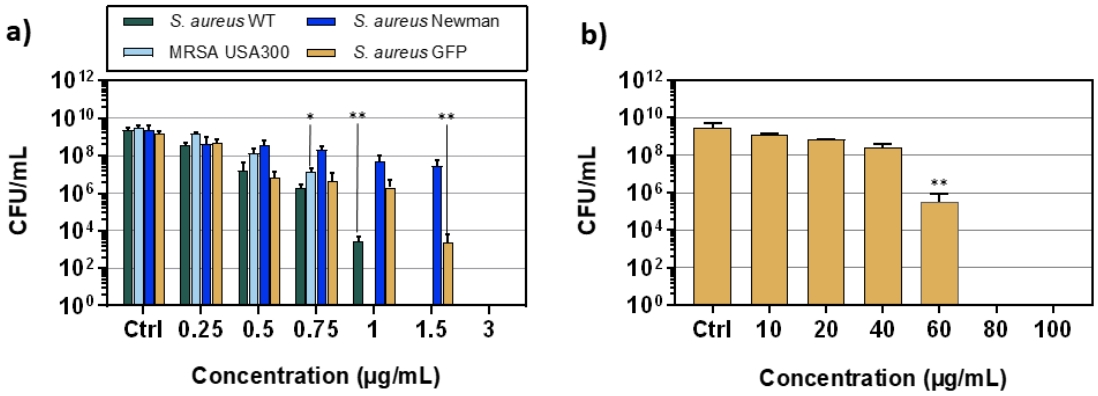

Figure V.3: Antimicrobial activity of LYS and PLGA LYS. The statistics analysis compare each treatment group to the control group (*p <0.05; **p <0.01; ***p <0.001). **a)** Antimicrobial activity of free LYS against various strains of *S. aureus* in planktonic state. **b)** Antimicrobial activity of PLGA@LYS NPs against *S. aureus* GFP in planktonic state.

On the other hand, neither free LYS nor PLGA@LYS NPs were able to completely eliminate the bacterial population in preformed mature biofilms (**Figure V.4a** and **b,** eradication assays), though a significant reduction in the bacterial load was attained at the highest concentrations assayed. On mature biofilms, the MIC was reached for the free LYS at 16 µg/mL while for the PLGA@LYS NPs was 2,000 µg/mL, which corresponds to a concentration of 57.6 µg/mL of encapsulated LYS. The higher concentration needed to inhibit biofilm formation when using PLGA@LYS NPs compared to the use of the free enzyme could be attributed to the difficulty for the NPs to diffuse and permeate thorough the exopolysaccharide composed biofilm. In agreement with the previous literature, the doses of antimicrobial needed to completely eradicate bacteria in mature biofilms are orders of magnitude superior to the ones needed when bacteria remain in their planktonic state [383].

In the analysis of biofilm biomass formation using the Crystal Violet assay (**Figure V.4c** and **d**), it was shown that the lowest concentration of LYS (0.1 µg/mL) was capable of inhibiting biofilm formation, while the PLGA@LYS NPs formulation required 500 µg/mL (14.4 µg/mL of encapsulated LYS) for a similar outcome. Nevertheless, considering the results of colony counting in these assays (**Figure V.4a** and **b**, inhibition assays), it should be noted that the absence of biomass due to the inhibition of biofilm formation does not always imply the complete elimination of the bacteria. For instance, even though 0.1 µg/mL of LYS was effective in preventing biofilm formation, there were still bacteria present in the cultures, even in those treated with 1 µg/mL. In contrast, for the case of PLGA@LYS NPs, the bacteria were eliminated with 200 µg/mL (5.76 µg/mL of encapsulated LYS), even though the presence of reduced biomass was still observed.

Additionally, it was observed that 8 µg/mL of LYS and 500 µg/mL of PLGA@LYS NPs (14.4 µg/mL of encapsulated LYS) were needed to significantly disperse and nearly eradicate an already stablished mature biofilm. However, as pointed out above, neither free LYS nor PLGA@LYS NPs could completely eliminate the bacteria present in the culture, as attested in the eradication data (**Figure V.4a** and **b**).

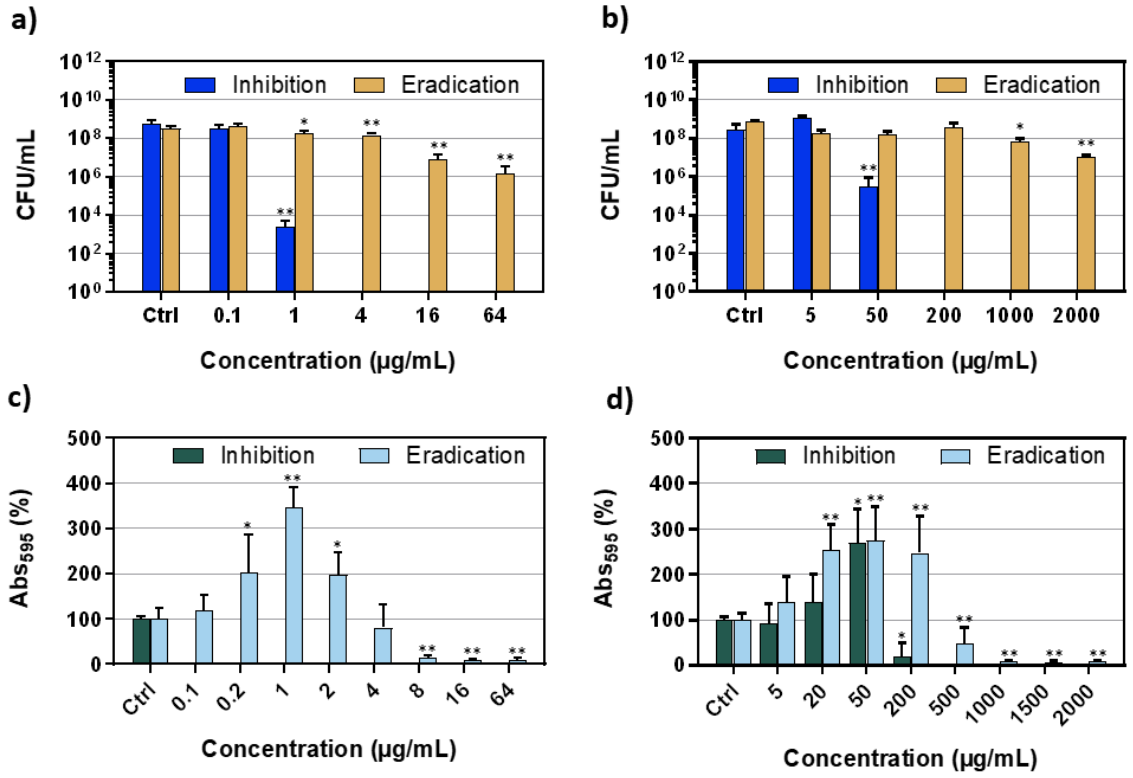

Figure V.4: Antimicrobial and antibiofilm activity of LYS and PLGA LYS. Colony count of *S. aureus* GFP in biofilm inhibition and eradication studies using free LYS **(a)** and PLGA@LYS NPs **(b)**. Biofilm inhibition and eradication activity of LYS **(c)** and PLGA@LYS NPs **(d)** using the crystal violet staining assay. The statistics analysis compares each treatment group to the control group (*p <0.05; **p <0.01; ***p <0.001).

It has been reported that LYS is capable of inhibit and eradicate *S. aureus* biofilms on artificial surfaces [384], a characteristic that has led to its recognition as a potential antimicrobial coating on clinical materials [385, 386]. Moreover, the encapsulation of LYS has shown the potential to enhance the anti-biofilm capacities of the molecule when compared to its free form [387]. This is likely attributed to the protective effect against trapping and inactivation of the molecule in the biofilm microenvironment, and its sustained release from the carrier. In our case, we do not see an enhancement in the antimicrobial action when using the encapsulated LYS in the short term, which is attributed to the sustained release of the antimicrobial compound. We postulate that the use of a sustained release system would aid in any prolonged duration of the antimicrobial action and successive applications of the free LYS would not be necessary when having the nanoparticulated system here described.

Figure V.4c and **d** also revealed that there was an effect in which the biofilm mass increased in the presence of low treatment concentrations, as antimicrobial exposure

can promote biofilm formation [388]. This phenomenon can occur when sublethal concentrations of antimicrobial agents are used, which can stimulate bacteria to form biofilms as a protective response against the selective pressure of antimicrobials.

Biofilm formation of *S. aureus* GFP was monitored using confocal microscopy and the Calcofluor White stain (**Figure V.5**).

Similar to previous assays, the capacity of free and encapsulated LYS to both inhibit and disperse the biofilm was evaluated. Cultures treated with PLGA NPs without LYS did not show significant changes compared to the control. The concentrations utilized for these assays were selected taking into consideration the PLGA@LYS NPs drug loading and the results depicted in **Figure V.4**.

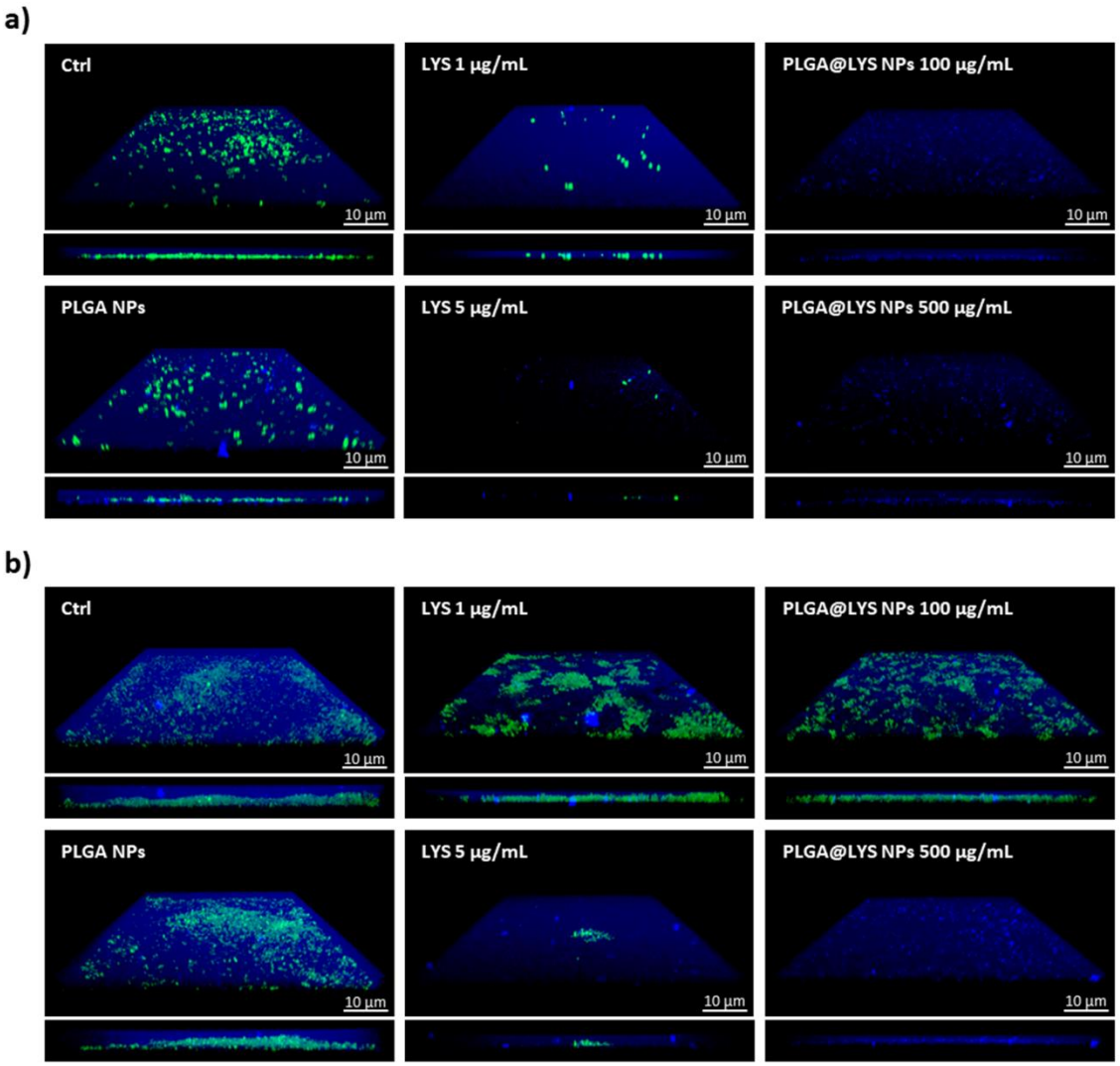

Figure V.5: Confocal laser scanning microscopy of *S. aureus* GFP biofilm cultures. Biofilm inhibition **(a)** and eradication **(b)** activities of LYS and PLGA@LYS NPs. Bacteria are depicted in green, whereas biofilm stains are depicted in blue. Images below were constructed from the z-stack acquisition.

In consonance with those results, both LYS and PLGA@LYS NPs formulations were more effective inhibiting the formation of biofilm rather than eradicating it. This situation was foreseeable since bacteria in inhibition assays started in a planktonic state and were in contact with the treatment since the beginning of the experiments hindering biofilm formation. Likewise, it was noticeable that a dose-dependent concentration in proposed treatments (free LYS or encapsulated one) led to a reduction in GFP expression and extracellular matrix labelling. Arguably, PLGA@LYS NPs treatments were more effective in reducing the GFP signal, both in the inhibition and eradication assays, in comparison with those using free LYS. A disparity seems evident between the results for LYS 5 µg/mL and PLGA@LYS NPs 500 µg/mL (14.4 µg/mL of LYS) concentrations in **Figure V.5b**, compared to the biofilm eradication data shown in **Figure V.4a** and **b**. Considering the CFU count, a much more present GFP expression would have been expected. However, it is important to note that GFP production could be hindered if bacteria are metabolically dormant, owing to biofilm formation, nutrient scarcity, or antimicrobial action [389, 390]. The results regarding biofilm formation observed in confocal microscopy support those obtained in the crystal violet assays (**Figure V.4c** and **d**).

V.4.3. Intracellular infection

To study the effects of the treatment of free LYS and PLGA@LYS NPs on a cell line infected with *S. aureus*, an intracellular infection model was developed using J774 macrophages infected with GFP-expressing *S. aureus*. This represents one of the most challenging scenarios where persister bacteria, named small colony variants, live intracellularly exhibiting phenotypic resistance against the action of antimicrobials and being responsible for chronic recurrent infections.

The cytotoxicity of LYS and PLGA@LYS NPs for J774 macrophages was previously assessed using the Blue Cell Viability Assay (**Figure V.6**). No concentration that previously demonstrated bactericidal activity caused a reduction below 80% viability at 24 hours, indicating that neither treatments could be classified as cytotoxic (according to ISO 10993-5) [391].

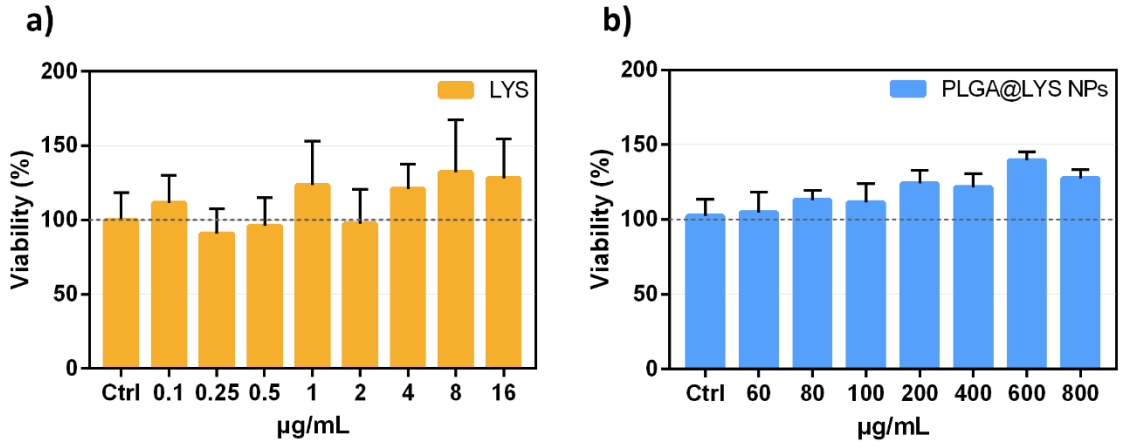

Figure V.6: J774 macrophages viability after 24 hours of incubation with rising concentrations of free LYS **(a)** and PLGA@LYS NPs **(b)** following the Blue Cell Viability Assay. Experimental conditions were tested in triplicate.

Figure V.7 depicts the results of employing free LYS and PLGA@LYS NPs to eradicate intracellular *S. aureus* GFP infection. **Figure V.7a** and **b** present the quantitative analysis conducted through FACS for the two strategies outlined in the methods section: pre-treatment (incubation with LYS and PLGA@LYS NPs prior to infection) and post-treatment (incubation after infection), respectively. The graphs illustrate that in both cases, around 40 to 50% of macrophages exhibited GFP+ fluorescence, indicating their uptake of a substantial infective bacterial load. With the addition of LYS and PLGA@LYS NPs, the percentage of GFP+ macrophages noticeably diminished.

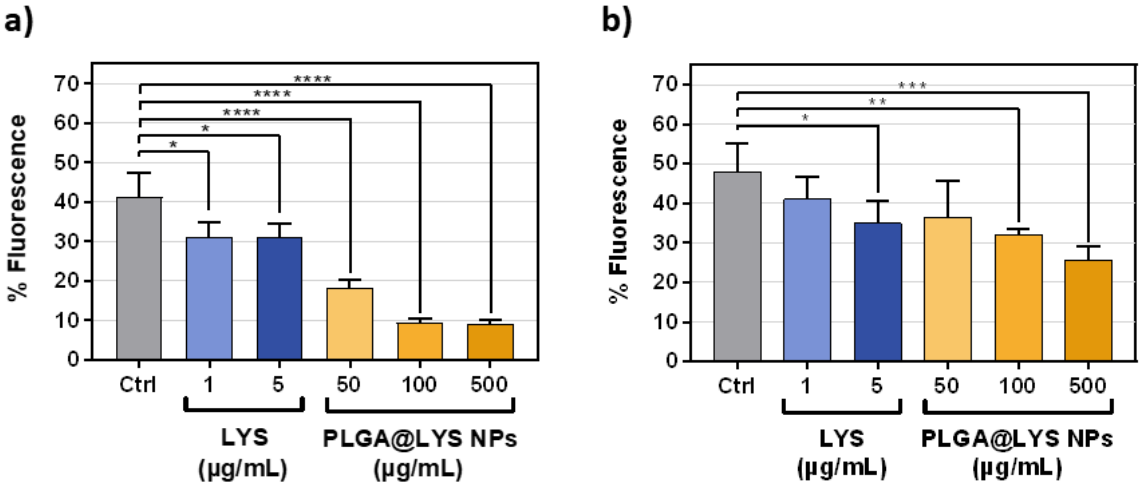

Figure V.7: Therapeutic activity of LYS and PLGA@LYS NPs in intracellular infection model. Flow cytometry analysis of the pre-treatment **(a)** and post treatment **(b)** assays. Graphs illustrate the percentage of macrophages in the culture exhibiting GFP signal. Data on graphs are expressed as mean ± SD of three independent experiments. The statistics compare each treatment group to the control group (*p <0.05; **p <0.01; ***p <0.001; ****p <0.0001).

In the case of the pretreatment strategy (**Figure V.7a**), the incubation of cells with free LYS resulted in the reduction of GFP+ macrophages to a 31%, regardless of the concentration used. However, when treated with 50 µg/mL PLGA@LYS NPs (1.44 µg/mL of LYS), GFP+ macrophages decreased to 18%, and the application of 100 and 500 µg/mL PLGA@LYS NPs (2.88 and 14.4 µg/mL of LYS), further lowered the count to 9%. These results highlight how LYS encapsulation enhances its antimicrobial capacity in the setting of an intracellular infection. The colocalization within the same intracellular compartment might be responsible for this high antimicrobial action observed in agreement with previous reports [392, 393]. These persisters have been reported to be localized in the late endosomal/lysosomal system in macrophages [393], having the ability to resist hydrolytic enzymes, bactericidal peptides, and the acidic pH [394]. Likewise, PLGA NPs are internalized by professional phagocytic cells such as macrophages and up-taken by receptor-mediated phagocytosis within the endosomal/lysosomal system [395]. Therefore, a co-localization of the nanoparticles in the same intracellular vesicle than the one where the infective small colony variants are located could be responsible for the enhanced antimicrobial action observed. In the post-treatment strategy (**Figure V.7b**), it was observed how the use of 1 and 5 µg/mL of LYS decreased the amount of GFP+ macrophages from 48% to 40 and 34%, respectively. Yet, the best outcome in this context was achieved with 500 µg/mL PLGA@LYS NPs (14.4 µg/mL of LYS), resulting in a 50% reduction of infected macrophages, and reaffirming how PLGA@LYS NPs is superior to free LYS. However, it should be noted that between the two strategies, the pretreatment approach (**Figure V.7b**) reduced the proportion of infected macrophages in the coculture in a more significant and prominent way.

Taking this final consideration into account, the pre-treatment strategy was chosen for a qualitative study using confocal microscopy. **Figure V.8** portrays J774 macrophages infected with *S. aureus* GFP. These images utilize an orthogonal projection via maximum intensity projection to showcase bacteria both inside and outside cells on the same plane. *S. aureus* GFP are shown in green, while cell nuclei are stained in blue with DAPI, and the cytoskeleton is highlighted in red using phalloidin 546.

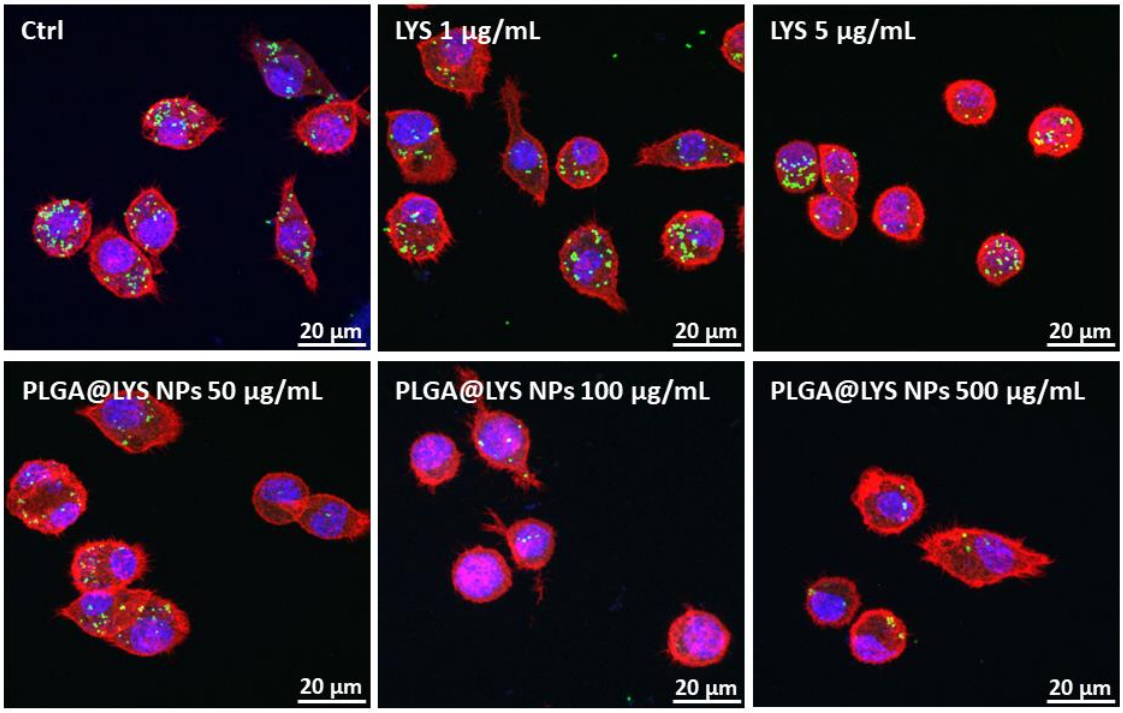

Figure V.8: Confocal laser scanning microscopy of pre-treatment assay. Bacteria are stained in green, while cell nuclei are stained with DAPI (blue) and cytoskeleton with phalloidin 546 (red).

The control image (infected cells with no treatment) displays the macrophages filled with green spots, suggesting a substantial load of metabolically active bacteria in the cytoplasm. The following images corroborate the outcomes from the quantitative analysis shown in **Figure V.7a**, highlighting how the amount of intracellular bacteria decreases more significantly and in a dose-dependent manner using PLGA@LYS NPs compared to the use of equivalent doses of the free bacteriocin.

It has been reported that the bactericidal activity of LYS cannot effectively target intracellular bacteria within the host [396, 397]. This limitation can be attributed to both its molecular size (~25kDa) and its degradation in the phagolysosome. In this case, the encapsulation of LYS within PLGA nanoparticles would promote phagocytosis and the uptake of the peptide by macrophages, while the polymeric matrix would safeguard it from degradation within the phagolysosome. Consequently, the intracellular concentration of LYS within the cell would be substantially increased when compared to using the peptide in its free form.

To address this same issue, Yang et al. [398] used mannose-modified exosomes as a drug delivery vehicle to deliver a combination of LYS and vancomycin, which effectively eradicated intracellular MRSA. The authors highlighted how the encapsulated formulation outperformed the free form both *in vitro* and *in vivo*. Along the same lines, Ali et al. [379] reported the development of PLGA nanoparticles incorporating the antimicrobial peptide SAAP-148, for the management of skin infection models. These particles exhibited the ability to permeate and eliminate intracellular *S. aureus* within 3D human skin models. Lastly, Dimer et al. [399]

encapsulated the antibiotic clarithromycin in PLGA nanocapsules for targeting intracellular *S. aureus*. This approach significantly reduced intracellular *S. aureus* by 1,000 times compared to the effect of the free drug. In RAW cells, treated bacteria shifted to non-acidic compartments. The nanocapsules demonstrated potential *in vivo* in wound models and zebrafish, indicating improved delivery to sub-epithelial tissues.

Based on the results obtained in the last part of our study, it can be concluded that the PLGA nanoencapsulation of LYS was very effective in enhancing the therapeutic efficacy of the bacteriocin to eradicate intracellular pathogens. This improvement was particularly evident with the pre-treatment strategy. Considering the background, this could be attributed to the promotion of phagocytosis, its safeguarding against phagolysosome arrest, and its facilitation of accumulation within the cell cytoplasm.

V.5. Conclusions

This study successfully encapsulated LYS, an anti-*Staphylococcus aureus* bacteriocin, within stable and monodisperse PLGA nanoparticles. The PLGA@LYS NPs obtained demonstrated a rapid initial burst of LYS release, followed by sustained release. This release kinetics is beneficial for biomedical applications, as it offers rapid initial availability of LYS to eliminate bacteria. The subsequent sustained release helps maintain persistent concentration levels, hindering potential further bacterial growth and reinfection.

Furthermore, it demonstrated enhanced antimicrobial activity in an intracellular infection model using murine macrophages, for both pre-treatment and post-treatment strategies. The *in vivo* limitations of applying free LYS can be overcome by encapsulating it within PLGA-based nanoparticles. This approach provides sustained release over time, reduces bacterial biomass, and eliminates intracellular small colony variants responsible for infection relapse episodes.

As a result, the developed nanoparticles represent a promising and innovative strategy against biofilm and intracellular infections caused by *S. aureus*.

CHAPTER VI

Point-of-care bacteria detection and eradication enabled by functionalized gold nanoparticles

Table of contents

Summary

This chapter details the development of a rapid optical whole-cell bacterial biosensor. This system utilized sialic acid-functionalized gold nanoparticles, taking advantage of the ability of pathogenic bacteria to integrate exogenous sialic acid. The interaction with bacteria caused the gold nanoparticles to aggregate, resulting in a detectable change in their surface plasmon resonance and optical spectra. This system allowed for the selective screening of Gram-positive wild type *S. aureus* (ATCC 25923) and MRSA USA300, as well as Gram-negative bacteria (*P. aeruginosa* ATCC 15442), by selecting the appropriate media.

Discrimination of bacterial pathogens was conducted in different media, including water, two different buffers, bacterial culture media, human serum, and human urine. High bacterial loads were required to provide a statistically significant optical pathogen identification in human serum, whereas it was not possible to detect the presence of bacteria at clinically relevant levels in urine.

The content of this chapter has been adapted from the following published work:

Landa, G.; Miranda-Calderón, L.G.; Sebastián, V.; Irusta, S.; Mendoza, G.; Arruebo, M.

Selective point-of-care detection of pathogenic bacteria using sialic acid functionalized gold nanoparticles.

Talanta, **2021**, Volume 234, 122644, https://doi.org/10.1016/j.talanta.2021.122644

VI.1. Introduction

In the diagnosis and treatment of bacterial infectious diseases, clinical microbiology laboratories make use of a wide range of bacterial identification techniques. These include traditional culture-based methods like the serial dilution, disk diffusion, Gram-staining, and the use of selective or chromogenic screening plates. More advanced methods, which offer greater sensitivity and automation, include Polymerase Chain Reaction (PCR), Enzyme-Linked Immunosorbent Assay (ELISA), Matrix-Assisted Laser Desorption Ionization-Time of Flight (MALDI-TOF) Mass Spectrometry, DNA microarrays, and Loop-Mediated Isothermal Amplification (LAMP) [400, 401]. However, culture-based methods can be time-consuming, and the more advanced automated and genotypic methods tend to be pricier and require specialized training. As a result, many of these methods are unsuitable for point-of-care (POC) testing. POC refers to the location where medical testing and treatment is provided directly to the patient. POC testing and diagnostics are designed to be performed quickly, without the need for sending samples to external facilities, enabling healthcare professionals to make prompt decisions that directly benefit the patient.

In the case of bacterial infections, it becomes crucial to develop POC diagnostic tools that are fast and can simultaneously analyse multiple pathogens. These tools would provide healthcare professionals with quick pathogen identification, allowing them to make informed decisions regarding the best antibiotic treatment. The ability to discriminate between Gram-positive and Gram-negative pathogens is especially important, as it would prevent the initiation of empirical treatments with suboptimal broad-spectrum antibiotics.

The prevalent POC biosensors used for screening bacterial infections and for conducting antimicrobial susceptibility tests comprise various technologies. These include immunochromatographic lateral flow biosensors, molecular diagnostic systems, microfluidic platforms, and nanotechnology-based methodologies. The latter category involves the use of metallic nanoparticles with fluorescent or magnetic properties, as well as other nanostructured materials that have been functionalized with specific recognition elements. These moieties can include moieties such as antibodies, peptides, antibiotics, aptamers, bacterial toxins, peptides, and more.

For example, Gao and colleagues [402] reported the successful detection of bacteria in human blood at a concentration of 10 CFU (colony forming units) per mL in under 2 hours. This achievement was made possible through the utilization of magnetic nanoparticles in conjunction with a conjugated complex consisting of vancomycin and fluorescein. In their study, vancomycin played a crucial role in facilitating multiple ligand-receptor interactions with the bacterial cell wall, while magnetic nanoparticles were employed to concentrate the bacteria found within whole blood samples. Additionally, fluorescence resonance energy transfer (FRET) has also been employed to facilitate the coupling of aptamer-functionalized gold

nanoparticles (utilized as acceptors) with upconversion nanoparticles (employed as donors). These nanoparticles were linked through the attachment of complementary DNA sequences, achieving a coordinated molecular interaction [403].

In this chapter, gold nanoparticles (AuNPs) have been modified with N-acetylneuraminic acid, the predominant form of sialic acid (SA) in human cells. SA is typically located as a terminal sugar on multiple glycoproteins, glycolipids, and proteoglycans. Genetic analyses have provided evidence that various strains of *S. aureus* and other *Staphylococci* utilize SA as a carbon, nitrogen, and energy source [404, 405]. Moreover, SA is also used to evade immune system recognition. Staphylococcal superantigen-like proteins, which require SA for their synthesis, bind to Toll-like receptors. These receptors are responsible for recognizing pathogens and trigger the production of proinflammatory cytokines and chemokines that attract phagocytic macrophages [406].

In this study, gold nanoparticles coated with sialic acid (SA-AuNPs) were employed to detect the presence of *S. aureus*. Considering the *S. aureus* natural uptake of SA, when these bacteria were present, they would interact with the SA coating of the SA-AuNPs. This interaction resulted in the aggregation of the gold nanoparticles, leading to the alteration of their surface plasmon resonance and their optical spectra. This system has the capability to detect both Gram-positive and Gram-negative bacteria and to differentiate between an MRSA strain and a wild-type *S. aureus*. Its performance was evaluated in water, two independent buffers, bacterial broth, human serum, and human urine. Poly (allylamine hydrochloride) (PAH)-functionalized gold nanoparticles (PAH-AuNPs) were introduced as a negative control to showcase the specificity of SA-AuNPs. PAH is a water-soluble linear cationic polyelectrolyte containing primary amine groups, which exhibit electrostatic binding affinity to negatively charged surfaces, such as the Gram-positive bacterial wall.

VI.2. Objectives

The objective of the study was to develop a rapid optical biosensor for whole-cell bacterial detection based on the optical properties of functionalized gold nanoparticles. For this purpose, two types of functionalization were considered: one involving a cationic polymer with a positive charge (PAH), and another related to the use of N-acetylneuraminic acid. The hypothesis behind the sensor system lays in the alteration of the optical properties of the nanoparticles upon contact with bacteria. This interaction would lead to the agglomeration of gold nanoparticles, resulting in a change in the optical spectrum that could be utilized to detect, quantify, and differentiate pathogenic bacteria in complex environments.

VI.3. Experimental

VI.3.1. Synthesis of gold nanoparticles

Gold nanoparticles conjugated with N-acetylneuraminic acid (SA-AuNPs) were synthesized as follows: 250 µL of a 0.02 M $HAuCl_4$ aqueous solution were combined with 10 mL of a 1.25 mM SA aqueous solution. This solution was then stirred (1,000 rpm) and heater to 80 °C. Shortly after, 35 µL of 1 M NaOH were introduced, and the reaction continued for 15 minutes. The formation of the gold colloids was attested as the solution colour transitioned from yellow to a deep red hue. Lastly, the solution was cooled in an ice bath and the Au NPs were washed twice with Mili-Q water through centrifugation cycles (10,000 rpm, 20 minutes).

Gold nanoparticles conjugated with PAH (PAH-AuNPs) were synthesized as follows: A 10 mL solution of 0.25% (w/v) PAH in water was prepared and mixed with 200 µL of 0.1 M $HAuCl_4$, and mechanically stirred for 10 minutes. Subsequently, 400 µL of a freshly dissolved aqueous solution of 0.02 M $NaBH_4$ was added and stirred for 45 minutes. The resulting red dispersion was then allowed to cool to room temperature and washed twice with Mili-Q water through centrifugation cycles (12,000 rpm, 20 minutes).

VI.3.2. Characterization of gold nanoparticles

The formation of Au NPs was monitored using UV–vis extinction spectroscopy (V-670 UV-VIS-NIR Jasco spectrophotometer). Analysis of the surface plasmon resonance (SPR) was carried out in the 400 to 700 nm range. Zeta potential values for the Au NPs suspensions were measured at neutral pH. The presence of organic components (SA or PAH) on the surface of the Au NPs was assessed via Fourier-transform infrared spectroscopy (FTIR) with a VERTEX 70v FTIR Spectrometer equipped with an ATR Golden Gate accessory. AuNPs suspension droplets were placed on coverslips and air-dried at RT for FTIR measurements.

The average size and morphology of the synthesized AuNPs were examined using TEM imaging. For TEM sample preparation, 10 µL of the Au NPs were applied onto a carbon-coated copper grid (300 mesh, Electron Microscopy Sciences) and allowed to dry at RT. Subsequently, 10 µL of a 3% (w/v) aqueous solution of phosphotungstic acid hydrate, a negative staining agent, were introduced in the samples to aid in the observation of organic moieties. TEM images were captured using a FEI Tecnai T20 electron microscope running at 200 kV. These images were subsequently analysed using the ImageJ software to determine the size distribution and morphology of the Au NPs. Additionally, high-angle annular dark-field scanning transmission electron microscopy (HAADF-STEM) images were obtained using a high-angle annular dark field detector in a FEI XFEG TITAN electron microscope, operating at 300 kV and equipped with a CETCOR Cs-probe corrector. Elemental analysis was performed using an energy-

dispersive X-ray spectroscopy (EDS) detector, which enabled EDS experiments in scanning mode.

To determine the quantity of SA on the surface of the SA-AuNPs, the particles were lyophilized and subjected to a thermogravimetric analysis. This involved the tracking of the weight loss as the sample was heated in air at a consistent rate of 10 °C per minute, up to a temperature of 1,000 ◦C. The analysis was conducted using a Mettler Toledo TGA/SDTA 851.

VI.3.3. Bacterial cultures

Bacterial liquid cultures were growth in TSB media, with overnight growth occurring at 37 ◦C while stirring at 150 rpm. This process extended from the initial inoculation to reaching the stationary growth phase, corresponding to a density of 10^9 CFU/mL. Subsequently, bacteria were washed with PBS through centrifugation (4,000 RPM, 10 minutes). They were finally re-suspended in HEPES buffer (0.1 M) to achieve a final cell density of 10^8 CFU/mL, for the following assays.

VI.3.4. Bactericidal action

The MIC and MBC of the AuNPs against *S. aureus* were determined through the serial dilution method. Bacterial suspensions were prepared at a concentration of 10^5 CFU/mL in fresh TSB media, which contained a range of AuNPs concentrations (5, 10, 25, 50, and 100 µg/mL). Following 24 hours of incubation at 37 ◦C with orbital shaking, the cultures were plated onto TSA plates, and the colony forming units (CFUs) were quantified after 24 additional hours of incubation. These measurements were conducted in triplicate and the results were averaged.

VI.3.5. Bactericidal detection

The bacterial detection assays involved diluting 20 µL of AuNPs suspensions in 160 µL of various media, including water, DPBS, HEPES, TSB, human serum, and human urine, to achieve a final concentration of 50 µg/mL. This concentration was chosen to ensure an optical signal visible to the naked eye upon bacterial detection. Next, 20 µL of the bacterial suspensions in HEPES buffer were added into the AuNPs solutions, resulting in a final bacterial concentration ranging from 10^5 to 10^7 CFU/mL. Control samples consisted of AuNPs dispersions (50 µg/mL) in different media in the absence of bacteria. Throughout the assay, the cultures were incubated at 37 °C with orbital stirring (150 rpm) to facilitate the interaction between bacteria and AuNPs. UV–vis spectroscopy analysis was conducted in a microplate reader (Multimode Synergy HT Microplate Reader; Biotek, USA) at various time points (1, 2, 4, 8, and 24 hours) to monitor changes in the optical SPR spectra of the AuNPs. All measurements and conditions were tested in triplicate.

Supramolecular interactions between AuNPs and bacteria were examined using SEM and TEM. Different suspensions of *S. aureus*, each containing 10^7 CFU/mL, were

prepared in TSB media containing AuNPs (50 µg/mL) and incubated for 1 hours at 37 °C with orbital stirring. After this incubation, the bacteria with AuNPs were washed three times with 10X PBS through centrifugation cycles (3,000 rpm, 10 minutes). Subsequently, they were resuspended and fixed using a 2.5% glutaraldehyde solution, in which the samples were incubated (2 h, RT).

For SEM samples preparation, the bacteria underwent further washes to eliminate the fixative agent before being filtered onto a 0.2-µm polycarbonate filter. These filters were subjected to dehydration using a series of graded ethanol concentrations, followed by drying at RT. Finally, the samples were placed on a microscope slide and coated with carbon using a Leica EM ACE200 sputter coater, as described in previous reports [407]. SEM and electron backscatter diffraction (EBSD) images were acquired using a FEI Inspect F50 electron microscope. For TEM samples preparation, similar bacterial suspensions were centrifuged to create pellets consisting of both bacteria and the attached AuNPs. These pellets were then stained with phosphotungstic acid hydrate (3% [w/v] in water) and incubated for 1 hour at room temperature. Subsequently, they were dehydrated through a series of graded ethanol concentrations and embedded in epoxy resin. Lastly, ultrathin sections of the samples were carefully cut using a diamond knife and a Leica EM UC7 ultramicrotome. TEM images were captured using a FEI Tecnai T20 electron microscope operating at 200 kV.

VI.3.6. Statistical analysis

Statistical data analysis was performed using a 2-way ANOVA test, followed by a Dunnett's multiple comparison test, conducted with GraphPad Prism 8 software. The error bars represent the mean plus standard deviation (*p-value < 0.05, **p < 0.01, ***p < 0.001, ****p < 0.0001).

VI.4. Results and discussion

VI.4.1. Synthesis and characterization of AuNPs

Developing simple POC sensors for the detection of pathogenic bacteria and differentiate between wild type *S. aureus* and MRSA, especially in resource-limited settings, is vital for guiding antibiotic treatments. In this chapter, AuNPs have been used as part of a colorimetric sensor to distinguish between Gram-positive and Gram-negative bacteria, as well as between *S. aureus* and MRSA in various media. Two distinct AuNPs were prepared for this purpose, one coated with a positively charged polyelectrolyte (PAH) and the other with SA on their surfaces. The latter choice was based on the preferential uptake of exogenous SA by *S. aureus* as a nutrient source.

Figure VI.1a and **b** showcase the morphology of AuNPs functionalized with PAH and SA, respectively. The magnified images offer a detailed view of the stained organic layers of PAH and SA, which are present on the AuNPs surface. The particle size analysis in **Figure VI.1c** reveals a Gaussian distribution centred at 12 nm for the PAH-

AuNPs and 20 nm for the SA-AuNPs. Zeta potential values measured at a neutral pH were +10.13 ± 1.56 mV for PAH-AuNPs and -13.21 ± 1.87 mV for SA-AuNPs. Both colloidal gold-based suspensions exhibited a SPR absorption peak at 520 nm (**Figure VI.1d**), a characteristic feature of these particles having this size and shape [408]. Isolated AuNPs absorb visible light through various mechanisms, including collective electron excitations generating SPR, electronic transitions between energy bands, and conduction electron scattering [409]. The latter becomes more prominent in cases of agglomeration or irreversible aggregation, resulting in a red-shift toward longer wavelengths and diminishing the AuNPs SPR. This shift is primarily attributed to electric dipole-dipole interactions and plasmon coupling among neighbouring particles in the aggregate [410]. This aggregation-dependent optical properties were employed by Lee et al. [411] to detect influenza virus in culture media using SA-AuNPs, capitalizing on the interaction between virions and SA receptors on target cells.

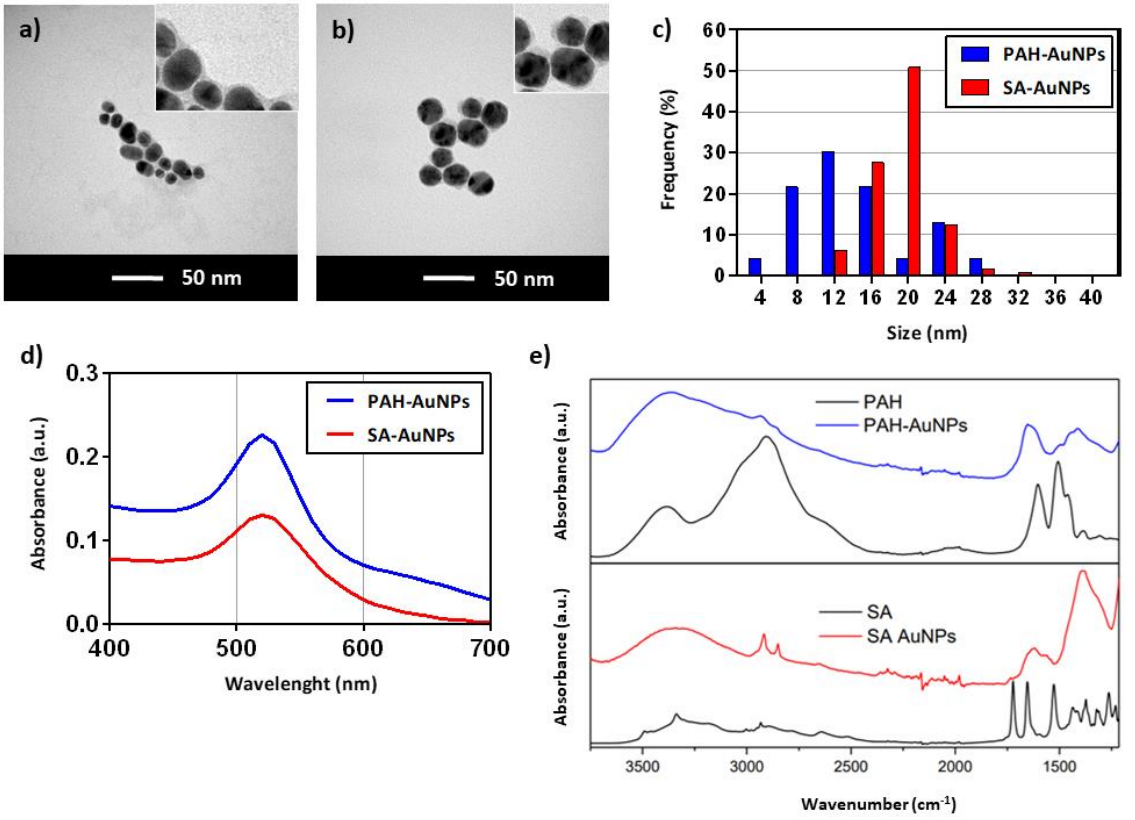

Figure VI.1: AuNPs characterization: **(a)** and **(b)** images of PAH-AuNPs and SA-AuNPs, respectively. Insets show high magnification images to appreciate the stained organic coating on the AuNPs surface. **c)** Size distribution of AuNPs. **d)** Absorption spectra of AuNPs. **e)** FTIR of AuNPs, PAH and SA.

FTIR analysis (**Figure VI.1e**) verified that both AuNPs synthesis methods yielded particles with characteristic bands attributed to SA and PAH. The absorbance peaks in the spectra of Au-functionalized samples were weaker and broader when compared with the spectra of pure organic molecules. This phenomenon can be attributed to the lower concentration of these compounds present in the samples, which is a commonly reported observation [412]. For the PAH-AuNPs, the spectrum displays a characteristic

band at 1603 cm^{-1} associated with the in-plane N–H bending of the organic molecule, appearing as a shoulder on the band attributed to the O–H bending of the adsorbed water [413]. In this range, the asymmetric vibration of the N–H group and a peak corresponding to the C–H bending (1387 cm^{-1}) are also evident. Overlapping with the broad band due to the O–H stretching of adsorbed water, two faint signals at 2926 and 2865 cm^{-1} confirm the presence of PAH on the AuNPs surface [414, 415]. In the IR spectrum of SA-AuNPs, the characteristic absorption stretching bands of the amide and hydroxyl groups are observed in the range of 3600-2900 cm^{-1}, along with peaks at 2917 and 2850 cm^{-1}, which can be attributed to C–H stretching [416]. Broad bands are noticeable in the regions associated with amide I and amide II stretching vibrations (1690–1590 and 1500-1580 cm^{-1}, respectively). Additionally, peaks at 1754 and 1722 cm^{-1}, linked to ester carbonyl stretching modes, are extremely faint and shifted to lower wavenumbers, indicating hydrogen bonding interactions, as reported in the literature [417]. In the 100-1500 cm^{-1} region, a broad band is observed due to the stretching of SA's C–O and C–OH groups [418].

The thermogravimetric analysis of SA-AuNPs (**Figure VI.2a**) indicated that, following the degradation of the organic compound, the remaining mass of gold accounts for 71.5 wt.%, signifying that 28.5 wt.% corresponds to SA. Further examination of the UV–vis spectrum for both SA and SA-AuNPs within the range of 190 nm to 700 nm (**Figure VI.2b**) revealed that only a 7.8 wt.% of the SA, initially introduced as a precursor during the synthesis, remained in the final dispersion of SA-AuNPs. This residual SA constitutes 27.9 wt.% of the final material, aligning well with the TGA findings.

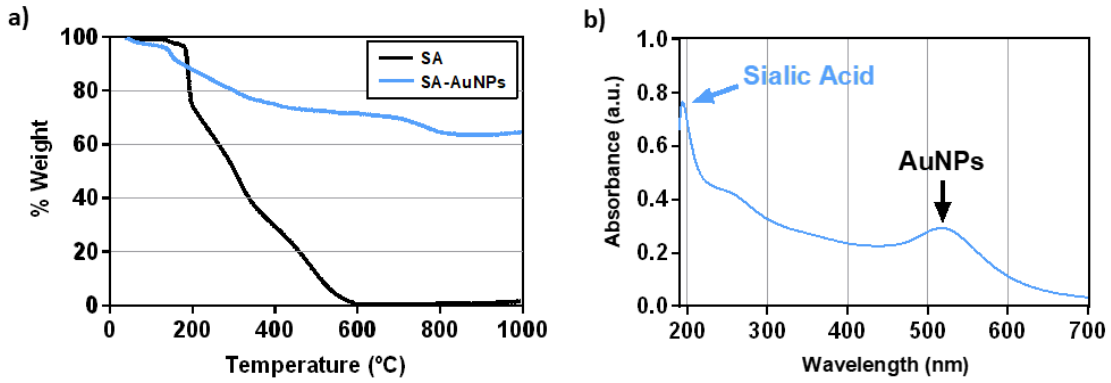

Figure VI.2: a) Thermogravimetric analysis of SA-AuNPs. **b)** Absorption spectra of SA-AuNPs (190-700 nm).

VI.4.2. Bacterial detection and interaction with Au NPs

Figure VI.3 depicts the colorimetric analysis of the interaction between the three bacterial species (*S. aureus*, MRSA, and *P. aeruginosa*) and the SA-AuNPs and PAH-AuNPs in different media. The quantification of the UV–vis absorbance ratio at 600 and 520 nm was used for the assessment of the agglomeration state of Au-NPs in the presence of bacteria. This was achieved by subtracting from the signal of the Au-NPs

with bacteria the signal of the bacteria alone. At 600 nm, the absorption of the culture media is negligible, and variations in optical density are primarily attributed to bacterial population growth.

When PAH-AuNPs were employed, statistically significant differences in the absorbance 600/520 ratio were observed in the presence of 10^7 CFU/mL bacteria in various media (water, PBS, and HEPES), as depicted in **Figure VI.3a**. However, in a complex medium such as TSB, the PAH-AuNPs failed to report the presence or absence of bacteria. In contrast, SA-AuNPs successfully detected both *S. aureus* and MRSA in this medium (**Figure VI.3b**), rendering distinct signals. Moreover, the presence of Gram-positive bacteria could be discerned with the naked eye (**Figure VI.3c**). Under visual inspection, it was observed that the introduction of SA-AuNPs to Gram-negative bacteria (*P. aeruginosa*) did not alter the characteristic pink colour of the culture medium. In contrast, when introduced to Gram-positive bacteria (either wild-type *S. aureus* or MRSA), the colour transitioned to yellow.

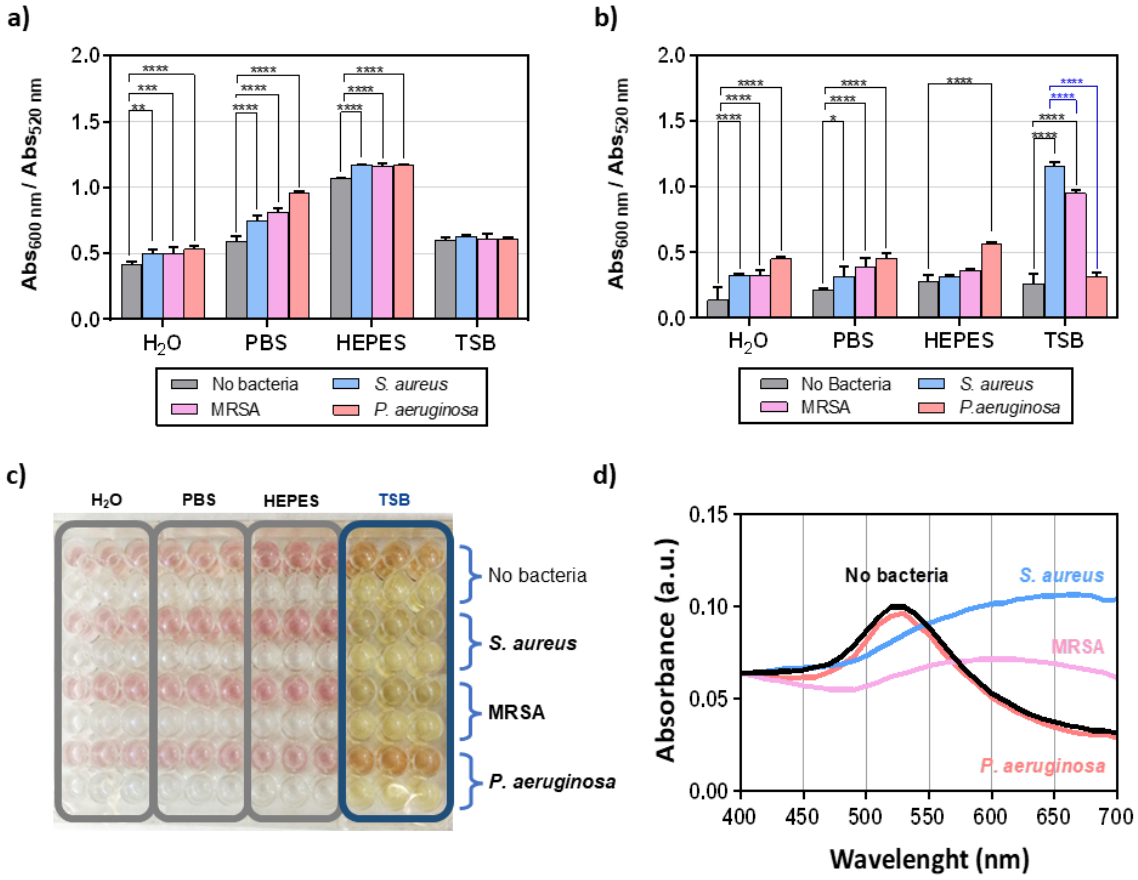

Figure VI.3: Response of AuNPs to the presence of bacteria. **(a)** and **(b)** show the Abs 600/Abs 520 nm ratio for PAH-AuNPs and SA-AuNPs, respectively, in the presence of various bacteria and in different media. Error bars indicate the standard deviation of the mean (*p < 0.05, **p < 0.01, ***p < 0.001, ****p < 0.0001). TSB incubation data from SA-AuNPs and statistical differences between *S. aureus* and other bacteria are indicated with a dashed line. **(c)** and **(d)** show the alteration in colour and absorption spectra of the SA-AuNPs in the presence of bacteria. In **(c)**, the first row displays the

optical signal of the medium containing the nanoparticles, and the second row illustrates the colour observed in the absence of nanoparticles.

The absorbance spectra of SA-AuNPs was analysed in the presence of wild-type *S. aureus*, MRSA, and *P. aeruginosa* in TSB, following background signal subtraction (**Figure VI.3d**). The initial sharp SPR peak at 520 nm observed in pristine NPs underwent a redshift, resulting in a broader peak across the visible spectrum. This shift indicates the agglomeration of AuNPs, which is likely caused by the bacterial uptake of SA as a nutrient for cell wall synthesis. As mentioned earlier, specific transporters on the cell wall facilitate the uptake of SA-NPs, leading to a reduction in interparticle spacing and increased scattering.

The statistical analysis of the Abs 600/520 Abs ratio with increasing bacterial concentrations allowed for the detection of bacterial loads ≥ 10^6 CFU/mL, as depicted in **Figure VI.4a**. Consequently, signals above this threshold could be distinguished with 1-log sensitivity. This analysis also could facilitate susceptibility testing due to the distinct signals observed for wild-type *S. aureus* and MRSA. However, the limit of detection in TSB was achieved only for bacterial loads exceeding 10^5 CFU/mL, which surpasses the typical bacterial counts encountered during bacteraemia (>50 CFU/mL) [419, 420]. For symptomatic urinary tract infections, bacterial loads exceeding 10^5 CFU per mL of urine are typically used for bacteriuria diagnosis [421]. Therefore, both serum and urine were assessed as suspension media to evaluate the optical sensor capability to detect bacteria. As shown in **Figure VI.4b**, it was observed that SA-AuNPs could discriminate between Gram-positive and Gram-negative bacteria and differentiate MRSA from wild-type *S. aureus* in TSB and serum. However, these bacterial loads were not detected in human urine at any of the tested pH levels. This phenomenon could be attributed to the presence of urea in urine, which had the capability to disrupt hydrogen bond interactions in host-guest chemistry [422].

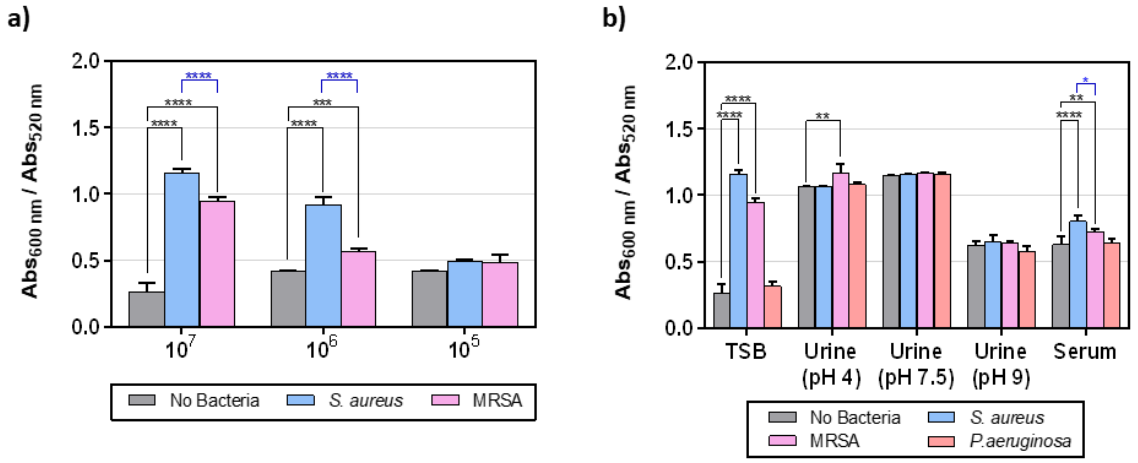

Figure VI.4: a) Abs 600/Abs 520 nm ratio of SA-AuNPs against different concentrations of *S. aureus* and MRSA in TSB. **b)** Abs 600/Abs 520 nm ratio of SA-AuNPs in presence of bacteria using human urine and serum as dispersive medium. Error bars indicate the standard deviation of the mean (*p < 0.05, **p < 0.01, ***p < 0.001, ****p < 0.0001).

As previously noted, *S. aureus* employs various enzymes, such as N-acetylneuraminate lyase, to break down SA as a source of carbon, nitrogen, and energy. The binding between MRSA N-acetylneuraminate lyase and the 2 R-diastereoisomer of SA has been attributed to hydrogen bonds [423]. Hence, the capacity of SA-AuNPs to bind effectively could be compromised in the presence of a hydrogen bonding inhibitor, such as urea. This supports the initial hypothesis that robust supramolecular interactions are responsible for the attachment between SA-AuNPs and *S. aureus*.

Additionally, the efficacy of the developed formulations in human serum was assessed using a bacterial load of 10^7 CFU/mL. Serum separation was easily achieved through conventional, minimally invasive blood withdrawal, followed by clotting and centrifugation. Even within the complex serum matrix containing monosaccharides, proteins, electrolytes, hormones, and more, it was possible to statistically detect the presence of *S. aureus* and MRSA using SA-AuNPs, which reported a distinct signal for both bacterial strains.

The distinct signals provided for different bacterial strains could be leveraged for an antibiotic susceptibility test in TSB, offering different signals for MRSA and *S. aureus* wild type. These differences between strains may be attributed to variations in cell wall composition. It has been reported that MRSA exhibits reduced peptidoglycan cross-linking compared to other *S. aureus* strains [424]. This reduction triggers a strong immune response and enhances pathogenicity by rendering MRSA resistant to intracellular elimination by immune cells. Additionally, MRSA differs from its wild-type counterpart in wall teichoic acid content within its envelope. These acids are covalently linked to the peptidoglycans present on the bacterial cell wall [425].

It was also observed that when using SA-AuNPs, the detection of Gram-negative bacteria *P. aeruginosa* was only possible in water, PBS, and HEPES, but not in TSB, human serum or urine. This difference may be partly due to the competition among various components present in TSB. Notably, *P. aeruginosa* exhibits time-dependent uptake of exogenous SA through a specific linkage, which enhances its pathogenicity [426]. However, the differences in results between *S. aureus* and *P. aeruginosa* may stem from the distinct nature of the outer membrane for Gram-negative bacteria, primarily composed of lipopolysaccharides surrounding a thin peptidoglycan cell wall, in contrast to Gram-positive bacteria, which lack an outer membrane but possess a thick peptidoglycan layer. Furthermore, different transporters for SA have been identified for Gram-positive and Gram-negative bacteria, with the latter relying on protein-mediated transport across the outer membrane, in addition to common porin-based transport. These differences may explain the observed variations [427].

The interaction between SA-AuNPs and bacteria is visually depicted in **Figure VI.5**. SEM images utilizing secondary and backscattered electrons reveal that bacterial wall are decorated with clusters of aggregated SA-AuNPs. Over time, the quantity of gold nanoparticles decorating the bacterial surface increased, leading to agglomeration, as

confirmed by the broad absorption peak observed during bacterial detection (**Figure VI.3**).

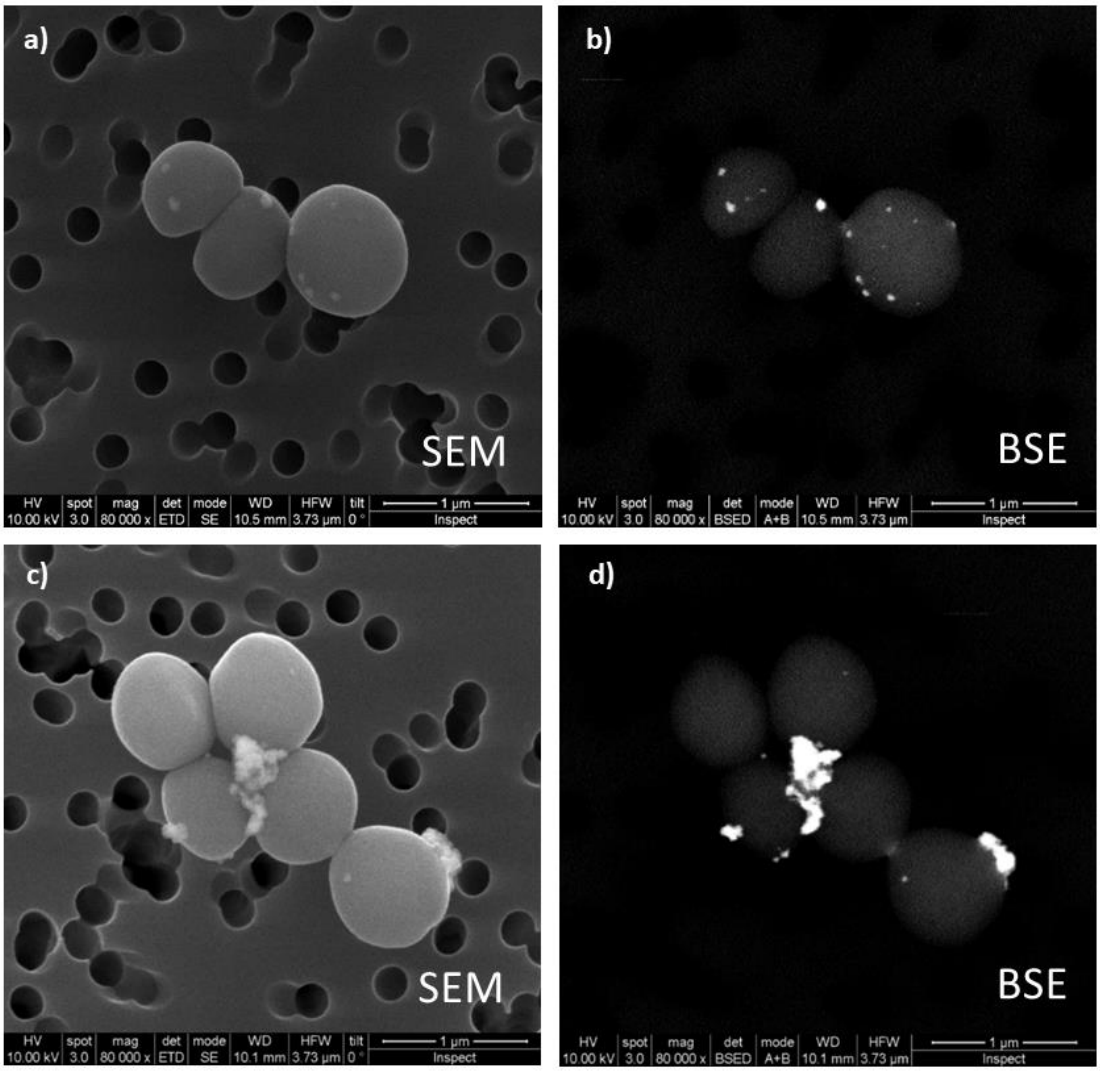

Figure VI.5: SEM and EBDS images of S. aureus before and after incubation with SA-AuNPs in TSB for 10 minutes **(a** and **b)** and 1 hour **(c** and **d)**.

Ultrathin sections of SA-AuNPs and bacteria were prepared using ultramicrotomy, stained, and subsequently analysed via TEM. TEM images in **Figure VI.6** illustrate individual nanoparticles situated on the bacterial surface. A time-dependent interaction was observed, with larger nanoparticle-based agglomerates forming over time when comparing the interactions at 10 minutes and 1 hour of contact. Backscattered SEM images (**Figure VI.5b** and **d**) and HAADF-STEM images (**Figure VI.6d** and **e**) provided evidence of the presence of AuNPs, evident through the heightened brightness of Au atoms (indicative of high electronic density). The crystalline structure of Au NPs remained intact throughout the incubation with *S. aureus* (**inset Figure VI.6e**). Additionally, EDS analysis of nanoparticles situated on the bacterial membrane validated the presence of Au nanoparticles (**Figure VI.6f**), as it revealed characteristic

energy signals associated with Au X-ray transitions, along with signals stemming from the Cu microscopy grid used as support.

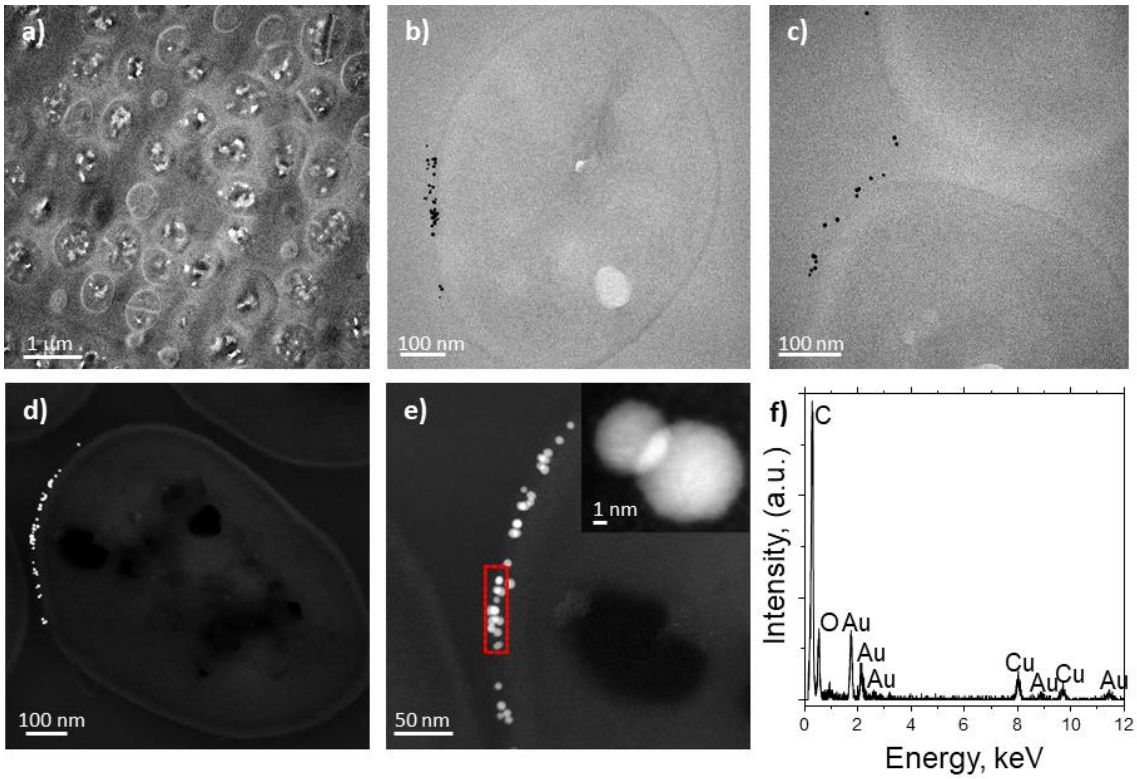

Figure VI.6: Electron microscopy analysis of *S. aureus* following incubation with SA-AuNPs. **(a)**, **(b)** and **(c)** show TEM images. **(d)** and **(e)** show HAADF-STEM images, and **(f)** energy-dispersive X-ray spectroscopy (EDS) analysis of the red dashed region outlined in **(e)**.

Notably, no NPs were detected inside the bacteria, indicating that SA interacts with the bacterial cell wall, likely following the exogenous incorporation of SA in various *S. aureus* strains (including MRSA). This incorporation has been reported to be facilitated by the chromosomal locus transporter (NanT gene) as part of their initial steps in catabolizing N-acetylneuraminic acid as a carbon source [404]. Importantly, the fact that staphylococcal murein sacculi cannot be penetrated by proteins suggests that 20 nm AuNPs, due to their size, are unlikely to pass through the 20–40 nm thick peptidoglycan layer, as seen in electron microscopy images.

To investigate potential bactericidal effects of SA-AuNPs and PAH-AuNPs during colorimetric detection assays, an assessment of their MIC and MBC was conducted. The MIC, defined as the concentration causing a 2-log reduction in visible bacterial growth after overnight incubation at 37 °C, as well as MBC values, were not attained for SA-AuNPs (**Figure VI.7a**). For PAH-AuNPs MIC and MBC were achieved at 5 and 25 µg/mL of PAH-AuNPs, respectively. As shown in **Figure VI.7b**, the growth of *S. aureus* varied depending on the culture medium, with different CFU counts observed (~10^9 CFU/mL in TSB and ~10^6 CFU/mL in serum) when reaching stationary phase.

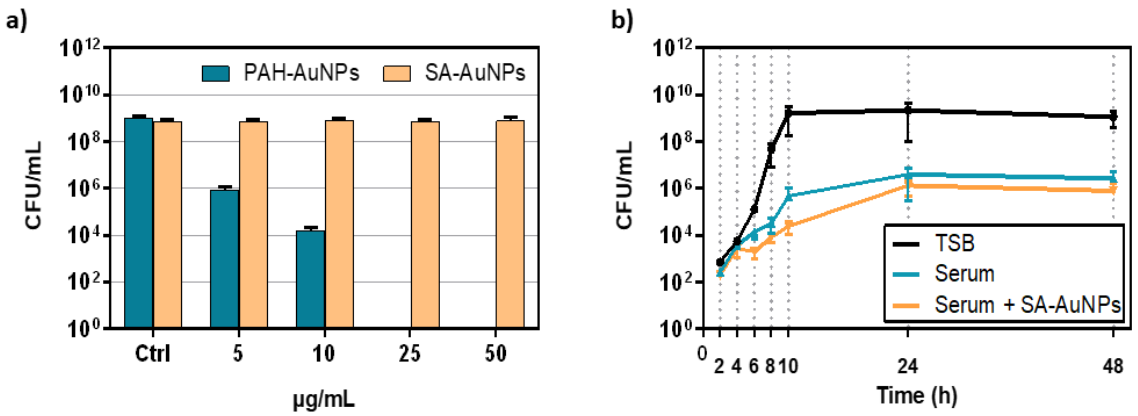

Figure VI.7: a) Antimicrobial activity of AuNPs against planktonic *S. aureus* in TSB after 24 hours. **b)** *S. aureus* growth kinetics in TSB and human serum in presence or absence of SA-AuNPs.

Previous studies have achieved success in detecting bacteria in clinical samples by monitoring the aggregation state of AuNPs. For instance, Yang et al. [40] employed gold nanoparticles surface-functionalized with D-alanine-D-alanine. Exploiting the bacterial uptake of the oligopeptide and measuring the red-shift in the optical spectrum of the AuNPs, they were able to detect the presence of various Gram-positive bacteria, achieving a detection limit of 3.2×10^2 CFU/mL for *S. aureus*. While their method effectively detected bacteria in clinical samples, it did not distinguish between Gram-positive and Gram-negative bacteria.

In contrast, Zhu et al. [428] devised a fast method for identifying bacterial LPS using AuNPs functionalized with two different DNA aptamers. AuNPs functionalized with an ethanolamine aptamer could bind to ethanolamine and recognize any type of LPS, causing AuNPs to aggregate in the presence of bacteria and induce a colour shift from red to blue. Similarly, AuNPs functionalized with an aptamer against *E. coli* O111: B4 LPS specifically targeted O111:B4 LPS, enabling differentiation between *E. coli* strains. This approach facilitated typing and detected LPS at concentrations ranging from 2.5 to 20 µg/mL.

It is worth noting that this strategy extends beyond the use of AuNPs. Shin et al. [429] developed a colorimetric assay based on the aggregation of blue-coloured polymeric nanobeads using vancomycin as a ligand. When these nanobeads were incubated with Gram-positive bacteria, the binding caused the appearance of blue precipitates, which were visible with the naked eye. Utilizing a filtration system to collect the precipitates during incubation, they attained a detection limit of 2.5×10^5 CFU/µL for Gram-positive bacteria.

VI.5. Conclusions

Pathogenic bacterial ability to incorporate exogenous sialic acid can be harnessed to aggregate sialic acid-functionalized gold nanoparticles. This allowed the detection of

bacterial presence by observing changes in the optical properties of the nanoparticles. In contrast, the functionalization of gold particles with a cationic polymer to induce aggregation on the bacterial surface based on charge differences did not yield the same results in detecting and differentiating bacterial species in complex media.

This detection system was developed through a straightforward colorimetric analysis of the SPR band in the visible spectrum of gold nanoparticles. In the presence of bacteria, the initially sharp SPR absorbance peak at 520 nm exhibited a noticeable redshift, evolving into a broad peak across the visible spectrum. This shift indicates nanoparticle agglomeration, a result of reduced interparticle spacing and increased scattering.

The system has the capability to distinguish between wild-type *S. aureus* and MRSA, a prevalent agent of nosocomial infections, and to differentiate between Gram-positive and Gram-negative bacteria. The differentiation between Gram-positive and Gram-negative bacteria can be attributed to variations in the outer membrane and bacterial wall composition. Furthermore, the distinct SA transporters identified for these bacterial types contribute to the discrimination. While the sensor effectively identified bacteria in TSB medium and serum samples, it faced challenges in detecting bacteriuria in urine. This limitation may stem from the disruption of hydrogen bonding between sialic acid and bacteria due to the presence of urea.

CHAPTER VII

General conclusions

VII. General conclusions

The primary purpose of this thesis was the development of nanostructured systems for the treatment and detection of bacterial infections. Following the research conducted and detailed in the preceding chapters, the most relevant conclusions are summarized below:

- Thymol (THY), farnesol nanoparticles (FAR NPs) and chlorhexidine (CHXD) treatment demonstrated significant bactericidal activity *in vitro* against *S. aureus* both in planktonic and sessile forms, especially those that in combination incorporated CHXD. The bactericidal activity was enhanced when combining different antimicrobials, as opposed to monotherapy. The combination of THY and FAR NPs successfully eradicated the bacteria in a mature biofilm when individual treatments could not. The combination of THY and CHXD halved the minimal bactericidal concentration (MBC) of CHXD against *S. aureus* biofilm. No direct correlation was observed between bacterial cell counts and the bioluminescence emitted by the bioluminescent *S. aureus* Xen36 in response to antimicrobial treatments, possibly due to the influence of other co-factors on bacterial metabolic activity.
- The *in vivo* studies highlighted the potential use of terpene-based compounds in conjunction with CHXD for improved wound treatment and enhanced healing. Treatments lacking CHXD were unable to validate their effectiveness *in vivo*. Combination therapy including CHXD and FAR NPs showed enhanced effectiveness over monotherapy, revealing an initial substantial reduction in bacterial counts. However, since not all pathogenic microorganisms were completely eradicated, bacterial regrowth occurred after the completion of the treatment.
- The monitoring of bacterial co-cultures with bioluminescent and wild type strains in order to develop a polymicrobial mixed biofilm was successful. Neither physical contact nor the presence of both bacterial species in the environment was necessary for *P. aeruginosa* to exert its anti-staphylococcal action.
- Within the mixed biofilm, the interplay between bacterial species granted *S. aureus* a survival advantage, enabling it to be less susceptible to the bactericidal action of CHXD and subsequently rising the MIC values for both THY and CHXD. We have corroborated, as other authors have shown a non-random spatial organization of the bacterial species in mixed biofilm forms.
- In the pursuit of encapsulating colistin for pulmonary delivery, the nanocoacervation of unprotonated colistin using the anti-solvent precipitation method stood out as the best choice. It achieved the highest drug loading at 55 wt.% ± 5.0, surpassing other synthesis methodologies like emulsion, nanoprecipitation, and electrospraying.

- The synthesized colistin nanoparticles aggregated into microparticles, showing optimal aerodynamic diameter for pulmonary administration (3.3 ± 0.2 µm). The colistin content in this formulation exhibited an immediate burst release profile when examined *in vitro*, making colistin rapidly bioavailable. Additionally, these particles showed increased antimicrobial effectiveness in a biofilm model of the *P. aeruginosa* PAO1 strain when compared to the effect of equivalent doses of the free drug, as they reduced the MBC of colistin by half, highlighting their potential as a promising solution for treating pulmonary bacterial infections.
- Lysostaphin (LYS), an anti-*Staphylococcus aureus* bacteriocin, was successfully encapsulated within stable and monodisperse poly(lactic-co-glycolic acid) (PLGA) nanoparticles. These PLGA@LYS nanoparticles displayed an initial burst release of LYS, followed by a gradual and sustained release. This release pattern is beneficial as it facilitates rapid bacterial elimination and maintains a steady concentration to prevent bacterial regrowth and reinfection.
- The encapsulated LYS retained its antimicrobial activity against *S. aureus* in both planktonic and sessile forms. Moreover, in an intracellular infection model using murine macrophages, it demonstrated enhanced antimicrobial activity when administered both before and after the infection, when compared to its free form. The most promising outcomes were achieved when pre-treating with 100 µg/mL of PLGA@LYS nanoparticles, resulting in a remarkable 77% reduction in the number of infected macrophages compared to the control group. Considering the drug loading data, this implies that encapsulated LYS is six times more effective than its free form in this scenario. These findings underscore the potential of LYS encapsulation as a promising strategy for combating *S. aureus* infections, both in extracellular and intracellular contexts.
- Bacterial detection using sialic acid-functionalized gold nanoparticles and is subsequent colorimetric analysis shows promise for differentiating bacterial species and strains through changes in the nanoparticles optical properties. The developed system effectively distinguishes between wild-type *S. aureus* and MRSA, and between Gram-positive and Gram-negative bacteria, by leveraging variations in bacterial membrane composition and sialic acid transporters.
- The sensor demonstrated robust performance in identifying bacteria within Tryptic Soy Broth medium and human serum samples. However, it encountered difficulties when detecting bacteriuria in urine, likely attributable to the presence of urea, which disrupts the hydrogen bonding between sialic acid and bacteria, consequently hindering the detection process.

CAPÍTULO VII

Conclusiones generales

VII. Conclusiones generales

Esta tesis ha tenido como objetivo principal el desarrollo de sistemas nanoestructurados para el tratamiento y la detección de infecciones bacterianas. A continuación, se resumen las conclusiones más relevantes tras la investigación detallada en los capítulos anteriores:

- El tratamiento con timol (THY), nanopartículas de farnesol (FAR NPs) y clorhexidina (CHXD) demostró una actividad bactericida significativa *in vitro* contra *S. aureus* tanto en su forma planctónica como sésil, especialmente cuando los tratamientos involucraban CHXD. La actividad bactericida de los tratamientos se potenció al combinar distintos agentes antimicrobianos en comparación con su aplicación individual. La combinación de THY y FAR NPs eliminó con éxito a *S. aureus* en un biofilm maduro, cuando los tratamientos individuales no fueron capaces de hacerlo. La combinación de THY y CHXD redujo a la mitad la concentración bactericida mínima (CBM) de la CHXD contra *S. aureus* en biofilm. No se observó una correlación directa entre el recuento de células bacterianas y la bioluminiscencia emitida por *S. aureus* Xen36 bioluminiscente en respuesta a los tratamientos antimicrobianos, posiblemente debido a la influencia de otros cofactores en la actividad metabólica bacteriana.
- Los estudios *in vivo* resaltaron el potencial uso de THY y FAR NPs junto con CHXD para el tratamiento de heridas tópicas infectadas y para facilitar su curación. Los tratamientos que no incluyeron CHXD no pudieron demostrar su efectividad en estudios *in vivo*. La terapia de combinación que incorporaba CHXD y FAR NPs mostró una efectividad mejorada en comparación con la monoterapia, revelando una reducción inicial sustancial en el recuento bacteriano. Sin embargo, dado que no se erradicaron por completo todas las bacterias, se observó una proliferación de estas en la herida después de la finalización del tratamiento.
- La monitorización de los co-cultivos empleando cepas bacterianas bioluminiscentes y *wild type* con el fin de desarrollar un biofilm mixto polimicrobiano se consiguió con éxito. Ni el contacto físico ni la presencia de ambas especies bacterianas en el entorno fueron necesarios para que la *P. aeruginosa* ejerciera su acción anti-estafilocócica.
- Además, dentro del biofilm mixto, la interacción entre las especies bacterianas otorgó a *S. aureus* ventajas para su supervivencia, siendo menos susceptible a la acción bactericida de CHXD y aumentando los valores de la concentración inhibitoria mínima (CIM) tanto para THY como para CHXD. Por último, se corroboró una organización no aleatoria de las especies bacterianas dentro de biofilm mixtos como se había descrito anteriormente.
- Con el objetivo de encapsular colistina para su administración pulmonar, la nanocoacervación de colistina no protonada mediante el método de precipitación con solventes inmiscibles destacó como la opción más eficaz de

las evaluadas. Logró la carga de fármaco más alta, alcanzando un 55% ± 5.0 en peso, superando a otras metodologías de síntesis como la emulsión, nanoprecipitación y el electrosprayado.

- Las nanopartículas de colistina sintetizadas agregaban de manera espontánea en micropartículas, mostrando un diámetro aerodinámico óptimo para su administración pulmonar (3.3 ± 0.2 µm). El contenido de colistina en esta formulación presentó un perfil de liberación inmediata cuando se evaluó *in vitro*, lo que la haría rápidamente biodisponible en el organismo. Además, en comparación con el fármaco libre, estas partículas redujeron la CBM de la colistina a la mitad en un modelo de biofilm de *P. aeruginosa* PAO1, resaltando su potencial para el tratamiento de infecciones bacterianas pulmonares.
- La lisostafina (LYS), una bacteriocina con actividad antimicrobiana frente al *S. aureus*, fue encapsulada exitosamente en nanopartículas estables y uniformes de poli(láctico-co-glicólico) (PLGA). Estas nanopartículas (PLGA@LYS NPs) presentaron una liberación inicial rápida de LYS, seguida de una liberación gradual y sostenida. Este patrón de liberación facilitaría la rápida eliminación de bacterias y a la vez mantendría una concentración constante de LYS para prevenir el crecimiento bacteriano y la reinfección.
- La LYS encapsulada retuvo su actividad antimicrobiana contra *S. aureus* en cultivos planctónicos y en biofilm. Además, en un modelo de infección intracelular de macrófagos murinos, demostró una mayor actividad antimicrobiana en comparación con su forma libre, ya fuese administrada tanto antes como después de la infección. Los resultados más prometedores se obtuvieron cuando se realizó un pretratamiento a los macrófagos con 100 µg/mL de PLGA@LYS NPs, lo que resultó en una notable reducción del 77% en el número de macrófagos infectados. Teniendo en cuenta los datos de carga de fármaco, esto implicaría que la LYS encapsulada es seis veces más efectiva que su forma libre en este escenario. Estos hallazgos subrayan el potencial de la encapsulación de LYS como una estrategia prometedora para combatir infecciones por *S. aureus*, tanto en contextos extracelulares como intracelulares.
- Las nanopartículas de oro funcionalizadas con ácido siálico y su subsiguiente análisis colorimétrico ofrecieron, mediante los cambios en las características ópticas de las nanopartículas, un sistema prometedor de cara a detectar y diferenciar especies y cepas bacterianas. Aprovechando las variaciones en la composición de la membrana bacteriana y los transportadores de ácido siálico, este sistema distinguiría con eficacia entre el *S. aureus wild type* y el *S. aureus* resistente a la meticilina (MRSA), así como entre bacterias Gram-positivas y Gram-negativas.
- El sensor desarrollado demostró una detección consistente en la identificación de bacterias en medio de cultivo y suero humano. Sin embargo, encontró dificultades en la detección de bacteriuria en la orina, posiblemente debido a la presencia de urea, que interfiere con la formación de enlaces por puentes de hidrógeno entre el ácido siálico y las bacterias.

APPENDICES

Table of contents

Appendix I: Supporting information

This section includes figures that are referenced throughout the chapters:

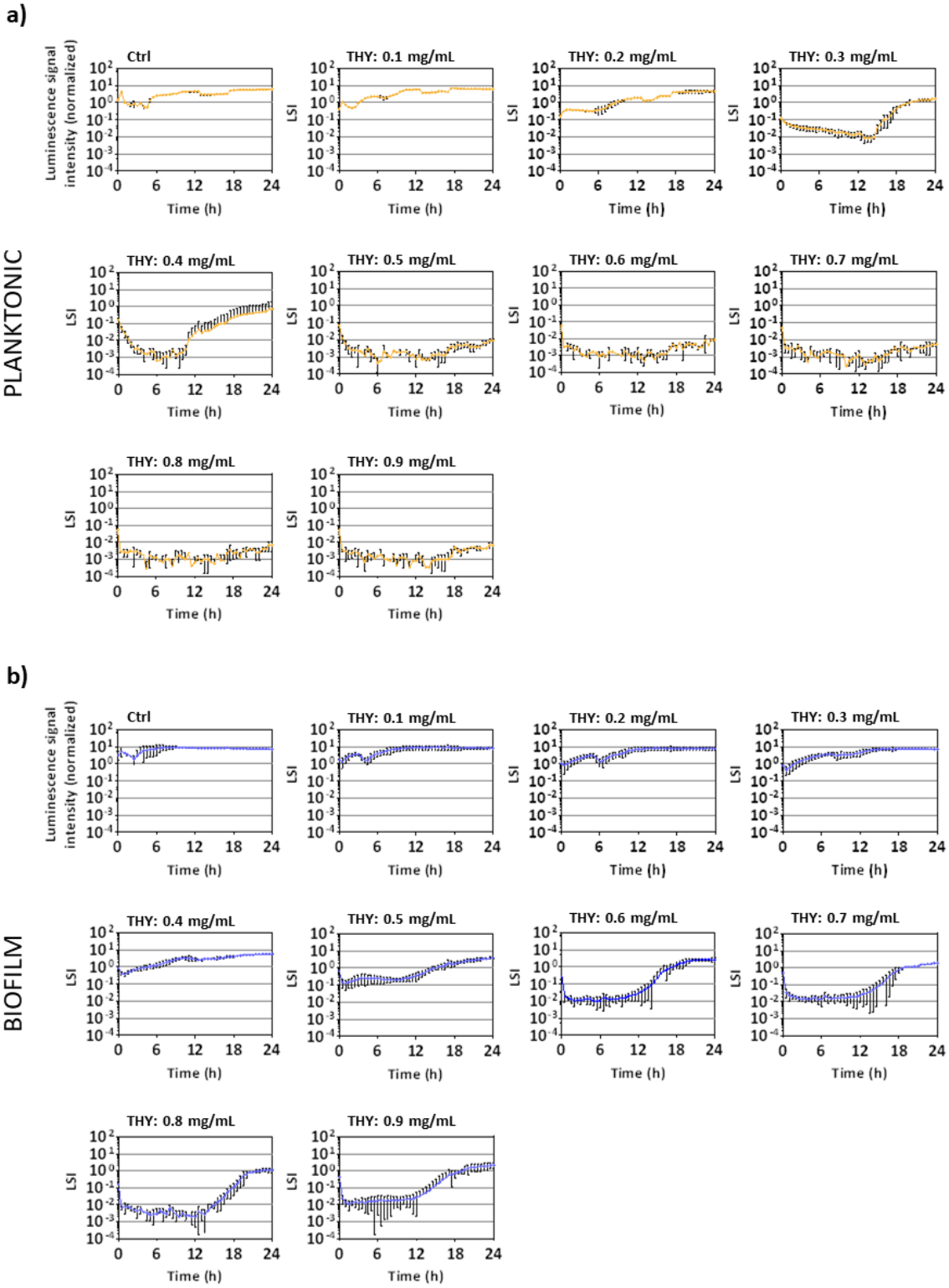

Appendix I.1: Luminescence signal intensity (LSI) over 24 hours of *S. aureus* Xen36 cultures, both in planktonic cultures **(a)** and biofilm **(b)**, after treatment with thymol (THY; 0.1-0.9 mg/mL).

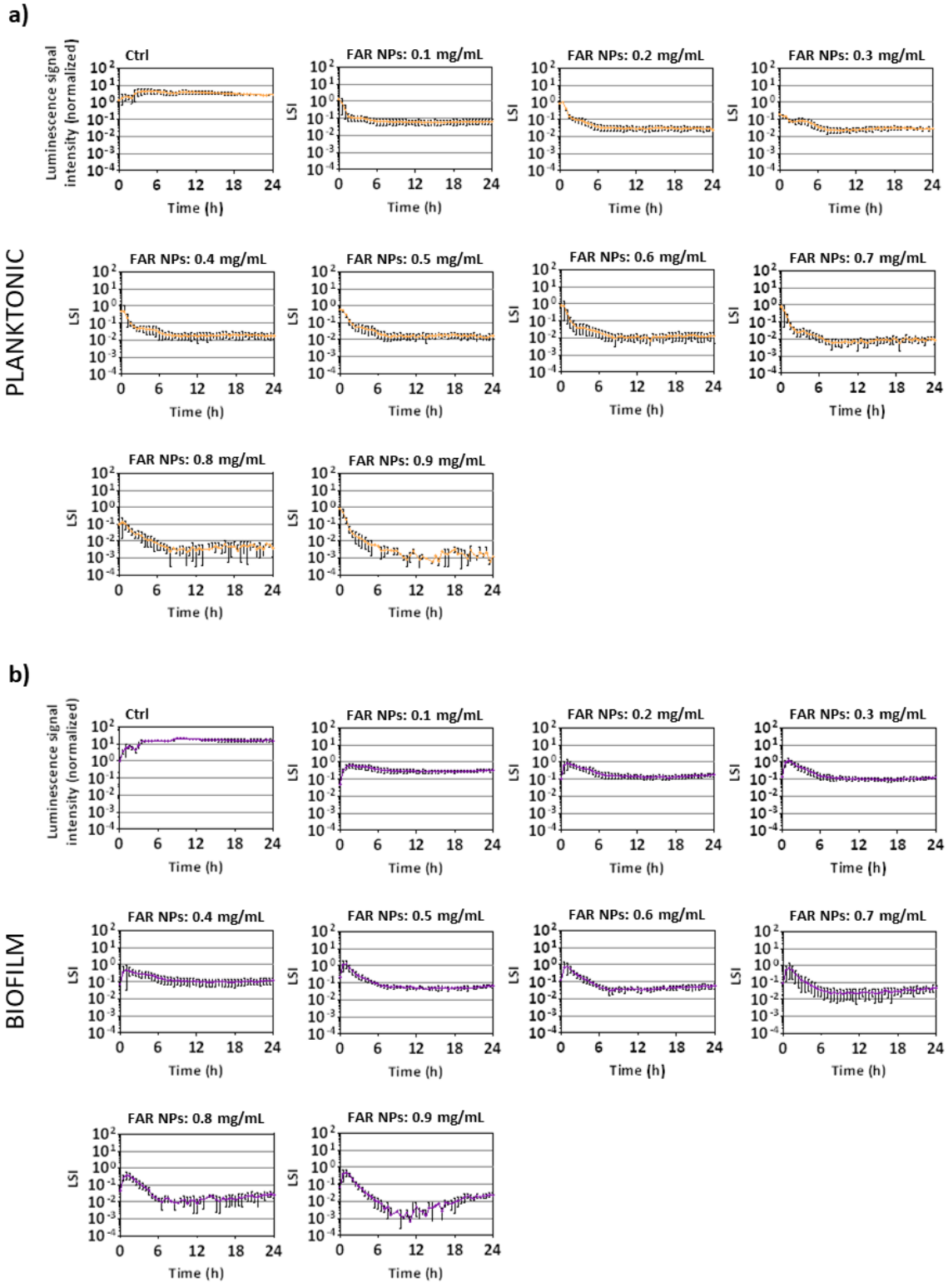

Appendix I.2: Luminescence signal intensity (LSI) over 24 hours of *S. aureus* Xen36 cultures, both in planktonic cultures **(a)** and biofilm **(b)**, after treatment with farnesol nanoparticles (FAR NPs; 0.1-0.9 mg/mL).

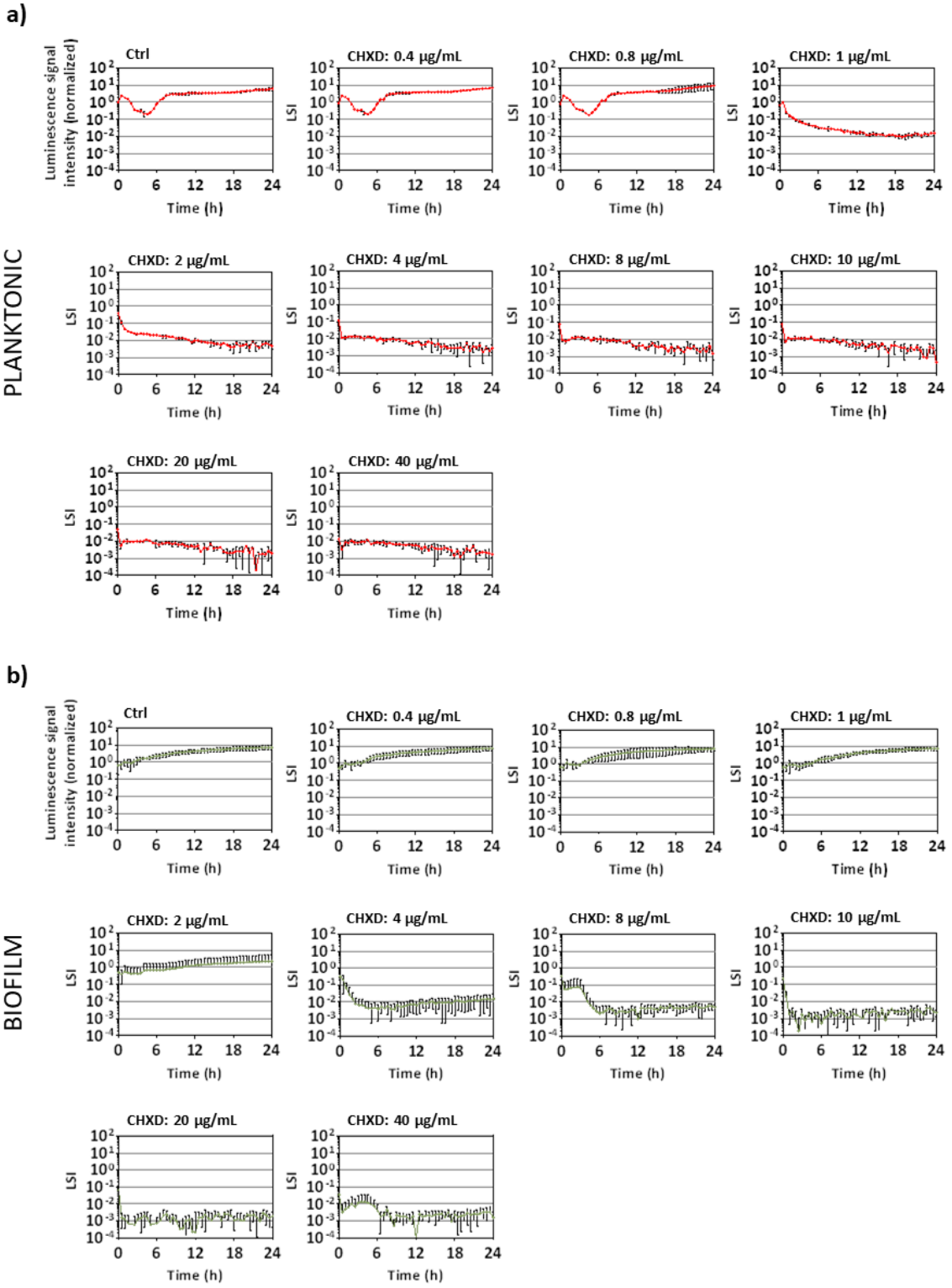

Appendix I.3: Luminescence signal intensity (LSI) over 24 hours of *S. aureus* Xen36 cultures, both in planktonic cultures **(a)** and biofilm **(b)**, after treatment with chlorhexidine (CHXD; 0.4-40 µg/mL).

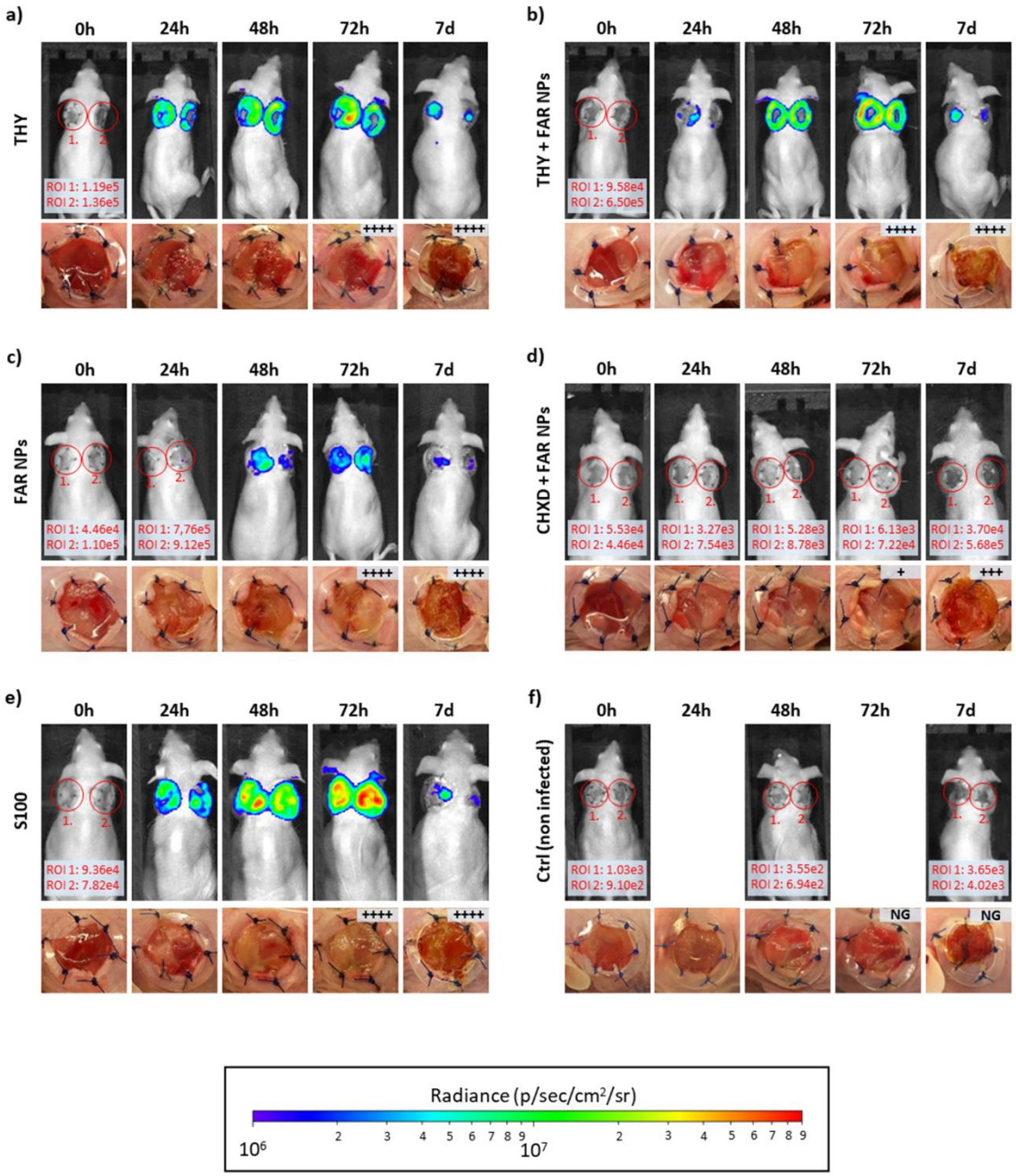

Appendix I.4: Luminescence signal of *S. aureus* Xen36 obtained in the *in vivo* model and morphological evaluation of the wounds at 24 hours, 48 hours, 72 hours, and 7 days after surgery and infection. Except for the non-infected control group **(f)**, all the depicted groups were infected and treated as follows: **a)** Treated with a free THY aqueous solution (1 mg/mL); **b)** Treated with FAR NPs suspension (10 mg/mL); **c)** Treated with a free THY aqueous solution (1 mg/mL) and FAR NPs suspension (10 mg/mL); **d)** Treated with free CHXD digluconate (1%) and FAR NPs suspension (10 mg/mL). **e)** Treated with unloaded S100 fibers (16 mg). **f)** Non-infected control group. Microbiological results regarding bacterial colony counting are reported as NG (no growth), and ranging from (+) indicating a low number of colonies to (++++) representing a massive culture.

Appendix II: Materials

This appendix comprises a structured summary, organized by chapters, of the materials, reagents, and suppliers essential for the completion of all the experimental procedures.

Chapter II:

- Eudragit® S100 was generously donated by Evonik Industries AG (Essen, Germany).
- Ethanol absolute and dimethylformamide were purchased from Panreac AppliChem (Barcelona, Spain).
- Labrafac® WL 1349 (caprylic/capric acid triglycerides) was provided by Gattefossé S.A. (Saint-Priest, France).
- Phospholipon® HS90 (hydrogenated lecithin) was provided by Lipoid Gmbh (Ludwigshafen, Germany).
- Solutol® HS15 (macrogol 15 hydroxystearate, polyoxyl 15 hydroxystearate; a mixture of free polyethylene glycol 660 and polyethylene glycol 660 hydroxystearate) was provided by BASF Pharma (Levallois-Perret, France).
- Dimethyl sulfoxide (>99%), phosphate-buffered saline (1x), thymol (>98.5%), (S)-(-)-limonene (food grade, ≥95%), naproxen sodium salt (98-102%), dichloromethane (>99%), farnesol (95%), phosphotungstic acid hydrate, Mueller-Hinton broth, Mueller-Hinton agar, chlorhexidine (≥99.5%), chlorhexidine digluconate (20% [w/v] aqueous solution) and sodium chloride (>99%) were purchased from Sigma-Aldrich (Darmstadt, Germany).
- *Staphylococcus aureus* ATCC 49525 Xen36 (*S. aureus* Xen36) was provided by Perkin-Elmer (Waltham, USA).

Chapter III

- Thymol (>98.5%) and chlorhexidine (≥99.5%) were purchased from Sigma-Aldrich (France).
- Mueller-Hinton broth and agar were also obtained from Sigma-Aldrich (France).
- Colistin sulfate salt was purchased from Sigma-Aldrich (France).
- *Staphylococcus aureus* ATCC 29213 strain was obtained from Ielab (Spain)
- *Staphylococcus aureus* strain ATCC 49525 Xen36 were obtained from Perkin-Elmer (USA).
- A *Staphylococcus aureus* strain expressing green fluorescence protein (GFP) was kindly provided by Dr. Cristina Prat, Institut d'Investigació en Ciències de la Salut Germans Trias i Pujol (IGTP, Spain).
- *Pseudomonas aeruginosa* PA01 ATCC 27853, *Pseudomonas aeruginosa* PA01 strain rendered bioluminescent by chromosomal integration of the LuxCDABE operon, and *Pseudomonas aeruginosa* PA01 (ATCC 27853)

transfected with mCTXtagBFP2, which expresses blue fluorescence protein (BFP), were supplied by Prof. Patrick Plesiat (Centre National de Référence de la résistance aux antibiotiques, Centre Hospitalier Universitaire de Besançon, France).

Chapter IV

- The bioluminescent *Pseudomonas aeruginosa* PAO1 strain, engineered to express the luxCDABE operon through chromosomal integration, was kindly provided by Professor Patrick Plesiat from the Centre National de Référence de la résistance aux antibiotiques, Centre Hospitalier Universitaire de Besançon, France.
- Mueller-Hinton Broth, Muelle-Hinton Agar, colistin sulfate salt, parafilm oil, sorbitan monooleate (SPAN®60), Trizma® hydrochloride, sodium bicarbonate, and calcium chloride were obtained from Sigma Aldrich, France.
- Mueller-Hinton agar, sodium citrate dihydrate and sodium bicarbonate were procured from Sigma Aldrich, France.

Chapter V:

- Poly(lactic-co-glycolic acid) 50:50 Resomer RG 502H was purchased from Evonik Industries AG (Essen, Germany).
- Lysostaphin from *Staphylococcus simulans*, 2,2,2-trifluoroethanol, dichloromethane, Mowiol® 4-88, bovine serum albumin, acetic acid, Calcofluor White, and Crystal Violet ACS reagent were supplied by Sigma Aldrich (Darmstadt, Germany).
- *Staphylococcus aureus* ATCC 25923 strain was obtained from Ielab (Alicante, Spain).
- GFP-expressing *Staphylococcus aureus* and two clinical strains (methicillin-susceptible *Staphylococcus aureus* Newman strain and methicillin-resistant *Staphylococcus aureus* USA300 strain were kindly donated by Dr. Cristina Prat (Institut d'Investigació en Ciències de la Salut Germans Trias i Pujol, Badalona, Spain).
- Paraformaldehyde 4% in PBS and Phalloidin-546 were obtained from Fisher Scientific (Waltham, USA).
- The Blue Cell® Viability Assay kit was purchased from Abnova (Taiwan), while saponin from Quillaja Bark pure and SDS for molecular biology were obtained from AppliChem (Germany).
- Fetal bovine serum was obtained from Gibco (Waltham, USA), while high-glucose Dulbecco's modified Eagle's medium (DMEM w/stable glutamine), antibiotic-antimycotic solution (penicillin-streptomycin-amphotericin B; PSA), and DPBS 1X buffer were acquired from Biowest (Nuaillé, France).

- Tryptone soy broth was obtained from Laboratorios Conda-Pronadisa SA (Madrid, Spain), and tryptone soy agar plates were purchased from Avantor VWR (Radnor, USA).

Chapter VI:

- *Staphylococcus aureus* ATCC 25923 (Ielab, Alicante, Spain) and the clinical strain Methicillin Resistant *Staphylococcus aureus* USA300 was kindly donated by Dr. Cristina Prat-Aymerich (Institut d'Investigació en Ciències de la Salut Germans Trias i Pujol, Badalona, Spain).
- *Pseudomonas aeruginosa* ATCC 27853, was also donated by Dr. Cristina Prat-Aymerich.
- Human serum and urine samples, along with data from study participants, were sourced from the Biobank of the Aragon Health System (BSSA, IACS). This Biobank is an integral part of the Spanish National Biobanks Network and follows established standard procedures. The collection and utilization of these samples received the required approvals from the Ethics and Scientific Committees of our University. To establish diverse physiological backgrounds, the pH levels of the urine samples were adjusted to three different values (4.5, 7.5, and 9) by incorporating acetic acid or sodium hydroxide.

Appendix III: References

1. Baker, R. E., Mahmud, A. S., Miller, I. F., Rajeev, M., Rasambainarivo, F., Rice, B. L., … Metcalf, C. J. E. (2022). Infectious disease in an era of global change. *Nature Reviews Microbiology*, *20*(4), 193–205. https://doi.org/10.1038/s41579-021-00639-z

2. Bloom, D. E., & Cadarette, D. (2019). Infectious Disease Threats in the Twenty-First Century: Strengthening the Global Response. *Frontiers in Immunology*, *10*. https://doi.org/10.3389/fimmu.2019.00549

3. Coates, M. M., Ezzati, M., Robles Aguilar, G., Kwan, G. F., Vigo, D., Mocumbi, A. O., … Bukhman, G. (2021). Burden of disease among the world's poorest billion people: An expert-informed secondary analysis of Global Burden of Disease estimates. *PLOS ONE*, *16*(8), e0253073. https://doi.org/10.1371/journal.pone.0253073

4. Boutayeb, A. (2010). The Burden of Communicable and Non-Communicable Diseases in Developing Countries. In *Handbook of Disease Burdens and Quality of Life Measures* (pp. 531–546). New York, NY: Springer New York. https://doi.org/10.1007/978-0-387-78665-0_32

5. World Health Organization (WHO). (2020). The top 10 causes of death.

6. Murray, C. J. L., Ikuta, K. S., Sharara, F., Swetschinski, L., Robles Aguilar, G., Gray, A., … Naghavi, M. (2022). Global burden of bacterial antimicrobial resistance in 2019: a systematic analysis. *The Lancet*, *399*(10325), 629–655. https://doi.org/10.1016/S0140-6736(21)02724-0

7. Marcia Metzgar Hobbs. (2019). *Lippincott® Illustrated Reviews: Microbiology*. (C. Cornelissen & M. Hobbs, Eds.) (4th ed.). LWW.

8. Bill, F., Foundation, M. G., Trust, W., & Care, S. (2022). Global mortality associated with 33 bacterial pathogens in 2019 : a systematic analysis for the Global Burden of Disease Study 2019, *400*, 2221–2248. https://doi.org/10.1016/S0140-6736(22)02185-7

9. Boucher, H. W., & Corey, G. R. (2008). Epidemiology of Methicillin-Resistant *Staphylococcus aureus*. *Clinical Infectious Diseases*, *46*(S5), S344–S349. https://doi.org/10.1086/533590

10. Chambers, H. F. (2001). The changing epidemiology of staphylococcus aureus? *Emerging Infectious Diseases*, *7*(2), 178–182. https://doi.org/10.3201/eid0702.010204

11. DeLeo, F. R., Otto, M., Kreiswirth, B. N., & Chambers, H. F. (2010). Community-associated meticillin-resistant Staphylococcus aureus. *The Lancet*, *375*(9725), 1557–1568. https://doi.org/10.1016/S0140-6736(09)61999-1

12. Tong, S. Y. C., Davis, J. S., Eichenberger, E., Holland, T. L., & Fowler, V. G. (2015). Staphylococcus aureus Infections: Epidemiology, Pathophysiology, Clinical Manifestations, and Management. *Clinical Microbiology Reviews*, *28*(3), 603–661. https://doi.org/10.1128/CMR.00134-14

13. Salgado-Pabón, W., Breshears, L., Spaulding, A. R., Merriman, J. A., Stach, C. S., Horswill, A. R., … Schlievert, P. M. (2013). Superantigens Are Critical for Staphylococcus aureus

Infective Endocarditis, Sepsis, and Acute Kidney Injury. *mBio*, *4*(4). https://doi.org/10.1128/mBio.00494-13

14. Conlon, B. P. (2014). *Staphylococcus aureus* chronic and relapsing infections: Evidence of a role for persister cells. *BioEssays*, *36*(10), 991–996. https://doi.org/10.1002/bies.201400080

15. Le, K. Y., & Otto, M. (2015). Quorum-sensing regulation in staphylococci—an overview. *Frontiers in Microbiology*, *6*. https://doi.org/10.3389/fmicb.2015.01174

16. Sikora, A., & Zahra, F. (2023, January). Nosocomial Infections. *StatPearls Publishing*.

17. Ikuta, K. S., Swetschinski, L. R., Robles Aguilar, G., Sharara, F., Mestrovic, T., Gray, A. P., … Naghavi, M. (2022). Global mortality associated with 33 bacterial pathogens in 2019: a systematic analysis for the Global Burden of Disease Study 2019. *The Lancet*, *400*(10369), 2221–2248. https://doi.org/10.1016/S0140-6736(22)02185-7

18. Qin, S., Xiao, W., Zhou, C., Pu, Q., Deng, X., Lan, L., … Wu, M. (2022). Pseudomonas aeruginosa: pathogenesis, virulence factors, antibiotic resistance, interaction with host, technology advances and emerging therapeutics. *Signal Transduction and Targeted Therapy*, *7*(1), 199. https://doi.org/10.1038/s41392-022-01056-1

19. Jurado-Martín, I., Sainz-Mejías, M., & McClean, S. (2021). Pseudomonas aeruginosa: An Audacious Pathogen with an Adaptable Arsenal of Virulence Factors. *International Journal of Molecular Sciences*, *22*(6), 3128. https://doi.org/10.3390/ijms22063128

20. Moradali, M. F., Ghods, S., & Rehm, B. H. A. (2017). Pseudomonas aeruginosa Lifestyle: A Paradigm for Adaptation, Survival, and Persistence. *Frontiers in Cellular and Infection Microbiology*, *7*. https://doi.org/10.3389/fcimb.2017.00039

21. Pang, Z., Raudonis, R., Glick, B. R., Lin, T.-J., & Cheng, Z. (2019). Antibiotic resistance in Pseudomonas aeruginosa: mechanisms and alternative therapeutic strategies. *Biotechnology Advances*, *37*(1), 177–192. https://doi.org/10.1016/j.biotechadv.2018.11.013

22. Lambert, M.-L., Suetens, C., Savey, A., Palomar, M., Hiesmayr, M., Morales, I., … Wolkewitz, M. (2011). Clinical outcomes of health-care-associated infections and antimicrobial resistance in patients admitted to European intensive-care units: a cohort study. *The Lancet Infectious Diseases*, *11*(1), 30–38. https://doi.org/10.1016/S1473-3099(10)70258-9

23. *Informe global de España Resumen provisional*. (2016).

24. Cox, G., & Wright, G. D. (2013). Intrinsic antibiotic resistance: Mechanisms, origins, challenges and solutions. *International Journal of Medical Microbiology*, *303*(6–7), 287–292. https://doi.org/10.1016/j.ijmm.2013.02.009

25. Martinez, J. L. (2014). General principles of antibiotic resistance in bacteria. *Drug Discovery Today: Technologies*, *11*, 33–39. https://doi.org/10.1016/j.ddtec.2014.02.001

26. Cosgrove, S. E. (2006). The Relationship between Antimicrobial Resistance and Patient Outcomes: Mortality, Length of Hospital Stay, and Health Care Costs. *Clinical Infectious Diseases*, *42*(Supplement_2), S82–S89. https://doi.org/10.1086/499406

27. Sydnor, E. R. M., & Perl, T. M. (2011). Hospital Epidemiology and Infection Control in Acute-Care Settings. *Clinical Microbiology Reviews*, *24*(1), 141–173. https://doi.org/10.1128/CMR.00027-10

28. Jim O'Neill. (2016). *Tackling drug-resistant infections globally: final report and recommendations*. London: Review on Antimicrobial Resistance.

29. Hutchings, M. I., Truman, A. W., & Wilkinson, B. (2019). Antibiotics: past, present and future. *Current Opinion in Microbiology*, *51*, 72–80. https://doi.org/10.1016/j.mib.2019.10.008

30. World Health Organization (WHO). (2015). *Global action plan on antimicrobial resistance*.

31. World Health Organization (WHO). (2021). *2021 antibacterial agents in clinical and preclinical development:*

32. Plackett, B. (2020). Why big pharma has abandoned antibiotics. *Nature*, *586*(7830), S50–S52. https://doi.org/10.1038/d41586-020-02884-3

33. Pagès, J.-M., James, C. E., & Winterhalter, M. (2008). The porin and the permeating antibiotic: a selective diffusion barrier in Gram-negative bacteria. *Nature Reviews Microbiology*, *6*(12), 893–903. https://doi.org/10.1038/nrmicro1994

34. García-Sureda, L., Doménech-Sánchez, A., Barbier, M., Juan, C., Gascó, J., & Albertí, S. (2011). OmpK26, a Novel Porin Associated with Carbapenem Resistance in Klebsiella pneumoniae. *Antimicrobial Agents and Chemotherapy*, *55*(10), 4742–4747. https://doi.org/10.1128/AAC.00309-11

35. Walsh, A. G., Matewish, M. J., Burrows, L. L., Monteiro, M. A., Perry, M. B., & Lam, J. S. (2000). Lipopolysaccharide core phosphates are required for viability and intrinsic drug resistance in Pseudomonas aeruginosa. *Molecular Microbiology*, *35*(4), 718–727. https://doi.org/10.1046/j.1365-2958.2000.01741.x

36. Guo, L., Lim, K. B., Poduje, C. M., Daniel, M., Gunn, J. S., Hackett, M., & Miller, S. I. (1998). Lipid A Acylation and Bacterial Resistance against Vertebrate Antimicrobial Peptides. *Cell*, *95*(2), 189–198. https://doi.org/10.1016/S0092-8674(00)81750-X

37. Fishovitz, J., Hermoso, J. A., Chang, M., & Mobashery, S. (2014). Penicillin-binding protein 2a of methicillin-resistant Staphylococcus aureus. *IUBMB life*, *66*(8), 572–7. https://doi.org/10.1002/iub.1289

38. Worthington, R. J., & Melander, C. (2013). Overcoming Resistance to β-Lactam Antibiotics. *The Journal of Organic Chemistry*, *78*(9), 4207–4213. https://doi.org/10.1021/jo400236f

39. Krause, K. M., Serio, A. W., Kane, T. R., & Connolly, L. E. (2016). Aminoglycosides: An Overview. *Cold Spring Harbor perspectives in medicine*, *6*(6). https://doi.org/10.1101/cshperspect.a027029

40. Du, D., Wang-Kan, X., Neuberger, A., van Veen, H. W., Pos, K. M., Piddock, L. J. V., & Luisi, B. F. (2018). Multidrug efflux pumps: structure, function and regulation. *Nature Reviews Microbiology*, *16*(9), 523–539. https://doi.org/10.1038/s41579-018-0048-6

41. Then, R. L. (1982). Mechanisms of Resistance to Trimethoprim, the Sulfonamides, and Trimethoprim-Sulfamethoxazole. *Clinical Infectious Diseases*, *4*(2), 261–269. https://doi.org/10.1093/clinids/4.2.261

42. C Reygaert, W. (2018). An overview of the antimicrobial resistance mechanisms of bacteria. *AIMS Microbiology*, *4*(3), 482–501. https://doi.org/10.3934/microbiol.2018.3.482

43. Magiorakos, A.-P., Srinivasan, A., Carey, R. B., Carmeli, Y., Falagas, M. E., Giske, C. G., … Monnet, D. L. (2012). Multidrug-resistant, extensively drug-resistant and pandrug-resistant bacteria: an international expert proposal for interim standard definitions for acquired resistance. *Clinical Microbiology and Infection*, *18*(3), 268–281. https://doi.org/10.1111/j.1469-0691.2011.03570.x

44. World Health Organization (WHO). (2017). *Prioritization of Pathogens to Guide Discovery, Research and Development of New Antibiotics for Drug-Resistant Bacterial Infections, Including Tuberculosis*. *WHO Bulletin* (Vol. 13).

45. Cassini, A., Högberg, L. D., Plachouras, D., Quattrocchi, A., Hoxha, A., Simonsen, G. S., … Hopkins, S. (2019). Attributable deaths and disability-adjusted life-years caused by infections with antibiotic-resistant bacteria in the EU and the European Economic Area in 2015: a population-level modelling analysis. *The Lancet Infectious Diseases*, *19*(1), 56–66. https://doi.org/10.1016/S1473-3099(18)30605-4

46. Zhen, X., Lundborg, C. S., Sun, X., Hu, X., & Dong, H. (2019). Economic burden of antibiotic resistance in ESKAPE organisms: a systematic review. *Antimicrobial Resistance & Infection Control*, *8*(1), 137. https://doi.org/10.1186/s13756-019-0590-7

47. Marturano, J. E., & Lowery, T. J. (2019). ESKAPE Pathogens in Bloodstream Infections Are Associated With Higher Cost and Mortality but Can Be Predicted Using Diagnoses Upon Admission. *Open Forum Infectious Diseases*, *6*(12). https://doi.org/10.1093/ofid/ofz503

48. Gould, I. M., Reilly, J., Bunyan, D., & Walker, A. (2010). Costs of healthcare-associated methicillin-resistant Staphylococcus aureus and its control. *Clinical Microbiology and Infection*, *16*(12), 1721–1728. https://doi.org/10.1111/j.1469-0691.2010.03365.x

49. Köck, R., Becker, K., Cookson, B., van Gemert-Pijnen, J. E., Harbarth, S., Kluytmans, J., … Friedrich, A. W. (2010). Methicillin-resistant Staphylococcus aureus (MRSA): burden of disease and control challenges in Europe. *Eurosurveillance*, *15*(41). https://doi.org/10.2807/ese.15.41.19688-en

50. Kourtis, A. P., Hatfield, ; Kelly, Baggs, J., Mu, ; Yi, See, I., Epson, E., … Cardo, D. (2017). *Morbidity and Mortality Weekly Report Vital Signs: Epidemiology and Recent Trends in Methicillin-Resistant and in Methicillin-Susceptible Staphylococcus aureus Bloodstream Infections-United States*. Retrieved from https://www.cdc.gov/mmwr

51. Flemming, H.-C., & Wingender, J. (2010). The biofilm matrix. *Nature Reviews Microbiology*, *8*(9), 623–633. https://doi.org/10.1038/nrmicro2415

52. Donlan, R. M., & Costerton, J. W. (2002). Biofilms: Survival Mechanisms of Clinically Relevant Microorganisms. *Clinical Microbiology Reviews*, *15*(2), 167–193. https://doi.org/10.1128/CMR.15.2.167-193.2002

53. Kostakioti, M., Hadjifrangiskou, M., & Hultgren, S. J. (2013). Bacterial Biofilms: Development, Dispersal, and Therapeutic Strategies in the Dawn of the Postantibiotic Era. *Cold Spring Harbor Perspectives in Medicine*, *3*(4), a010306–a010306. https://doi.org/10.1101/cshperspect.a010306

54. Lewis, K. (2008). Multidrug Tolerance of Biofilms and Persister Cells (pp. 107–131). https://doi.org/10.1007/978-3-540-75418-3_6

55. Stoodley, P., Sauer, K., Davies, D. G., & Costerton, J. W. (2002). Biofilms as Complex Differentiated Communities. *Annual Review of Microbiology*, *56*(1), 187–209. https://doi.org/10.1146/annurev.micro.56.012302.160705

56. Sauer, K., Stoodley, P., Goeres, D. M., Hall-Stoodley, L., Burmølle, M., Stewart, P. S., & Bjarnsholt, T. (2022). The biofilm life cycle: expanding the conceptual model of biofilm formation. *Nature Reviews Microbiology*, *20*(10), 608–620. https://doi.org/10.1038/s41579-022-00767-0

57. Miller, M. B., & Bassler, B. L. (2001). Quorum Sensing in Bacteria. *Annual Review of Microbiology*, *55*(1), 165–199. https://doi.org/10.1146/annurev.micro.55.1.165

58. Preda, V. G., & Săndulescu, O. (2019). Communication is the key: biofilms, quorum sensing, formation and prevention. *Discoveries*, *7*(3), e10. https://doi.org/10.15190/d.2019.13

59. Hassett, D. J., Ma, J.-F., Elkins, J. G., McDermott, T. R., Ochsner, U. A., West, S. E. H., … Iglewski, B. H. (1999). Quorum sensing in Pseudomonas aeruginosa controls expression of catalase and superoxide dismutase genes and mediates biofilm susceptibility to hydrogen peroxide. *Molecular Microbiology*, *34*(5), 1082–1093. https://doi.org/10.1046/j.1365-2958.1999.01672.x

60. Winson, M. K., Camara, M., Latifi, A., Foglino, M., Chhabra, S. R., Daykin, M., … Bycroft, B. W. (1995). Multiple N-acyl-L-homoserine lactone signal molecules regulate production of virulence determinants and secondary metabolites in Pseudomonas aeruginosa. *Proceedings of the National Academy of Sciences*, *92*(20), 9427–9431. https://doi.org/10.1073/pnas.92.20.9427

61. Sadovskaya, I., Vinogradov, E., Li, J., Hachani, A., Kowalska, K., & Filloux, A. (2010). High-level antibiotic resistance in Pseudomonas aeruginosa biofilm: the ndvB gene is involved in the production of highly glycerol-phosphorylated -(1->3)-glucans, which bind aminoglycosides. *Glycobiology*, *20*(7), 895–904. https://doi.org/10.1093/glycob/cwq047

62. Doroshenko, N., Tseng, B. S., Howlin, R. P., Deacon, J., Wharton, J. A., Thurner, P. J., … Stoodley, P. (2014). Extracellular DNA Impedes the Transport of Vancomycin in Staphylococcus epidermidis Biofilms Preexposed to Subinhibitory Concentrations of Vancomycin. *Antimicrobial Agents and Chemotherapy*, *58*(12), 7273–7282. https://doi.org/10.1128/AAC.03132-14

63. Billings, N., Ramirez Millan, M., Caldara, M., Rusconi, R., Tarasova, Y., Stocker, R., & Ribbeck, K. (2013). The Extracellular Matrix Component Psl Provides Fast-Acting Antibiotic Defense in Pseudomonas aeruginosa Biofilms. *PLoS Pathogens*, *9*(8), e1003526. https://doi.org/10.1371/journal.ppat.1003526

64. Helaine, S., & Kugelberg, E. (2014). Bacterial persisters: formation, eradication, and experimental systems. *Trends in Microbiology*, *22*(7), 417–424. https://doi.org/10.1016/j.tim.2014.03.008

65. Gefen, O., & Balaban, N. Q. (2009). The importance of being persistent: heterogeneity of bacterial populations under antibiotic stress. *FEMS Microbiology Reviews*, *33*(4), 704–717. https://doi.org/10.1111/j.1574-6976.2008.00156.x

66. Schaible, B., Taylor, C. T., & Schaffer, K. (2012). Hypoxia increases antibiotic resistance in Pseudomonas aeruginosa through altering the composition of multidrug efflux pumps. *Antimicrobial agents and chemotherapy*, *56*(4), 2114–8. https://doi.org/10.1128/AAC.05574-11

67. Savage, V. J., Chopra, I., & O'Neill, A. J. (2013). Staphylococcus aureus Biofilms Promote Horizontal Transfer of Antibiotic Resistance. *Antimicrobial Agents and Chemotherapy*, *57*(4), 1968–1970. https://doi.org/10.1128/AAC.02008-12

68. Olsen, I. (2015). Biofilm-specific antibiotic tolerance and resistance. *European Journal of Clinical Microbiology & Infectious Diseases*, *34*(5), 877–886. https://doi.org/10.1007/s10096-015-2323-z

69. Nickel, J. C., Ruseska, I., Wright, J. B., & Costerton, J. W. (1985). Tobramycin resistance of Pseudomonas aeruginosa cells growing as a biofilm on urinary catheter material. *Antimicrobial Agents and Chemotherapy*, *27*(4), 619–624. https://doi.org/10.1128/AAC.27.4.619

70. Marrie, T. J., Nelligan, J., & Costerton, J. W. (1982). A scanning and transmission electron microscopic study of an infected endocardial pacemaker lead. *Circulation*, *66*(6), 1339–1341. https://doi.org/10.1161/01.CIR.66.6.1339

71. Costerton, J. W., Stewart, P. S., & Greenberg, E. P. (1999). Bacterial Biofilms: A Common Cause of Persistent Infections. *Science*, *284*(5418), 1318–1322. https://doi.org/10.1126/science.284.5418.1318

72. Di Domenico, E., Farulla, I., Prignano, G., Gallo, M., Vespaziani, M., Cavallo, I., … Ensoli, F. (2017). Biofilm is a Major Virulence Determinant in Bacterial Colonization of Chronic Skin Ulcers Independently from the Multidrug Resistant Phenotype. *International Journal of Molecular Sciences*, *18*(5), 1077. https://doi.org/10.3390/ijms18051077

73. Assefa, M., & Amare, A. (2022). Biofilm-Associated Multi-Drug Resistance in Hospital-Acquired Infections: A Review. *Infection and Drug Resistance*, *Volume 15*, 5061–5068. https://doi.org/10.2147/IDR.S379502

74. MacDougall, C., & Polk, R. E. (2005). Antimicrobial Stewardship Programs in Health Care Systems. *Clinical Microbiology Reviews*, *18*(4), 638–656. https://doi.org/10.1128/CMR.18.4.638-656.2005

75. Aiesh, B. M., Nazzal, M. A., Abdelhaq, A. I., Abutaha, S. A., Zyoud, S. H., & Sabateen, A. (2023). Impact of an antibiotic stewardship program on antibiotic utilization , bacterial susceptibilities , and cost of antibiotics United States of America Infectious Diseases Society of America The Society for Healthcare Epidemiology of America. *Scientific Reports*, 1–9. https://doi.org/10.1038/s41598-023-32329-6

76. Huang, L.-J., Chen, S.-J., Hu, Y.-W., Liu, C.-Y., Wu, P.-F., Sun, S.-M., … Wang, F.-D. (2022). The impact of antimicrobial stewardship program designed to shorten antibiotics use on the incidence of resistant bacterial infections and mortality. *Scientific Reports*, *12*(1), 913. https://doi.org/10.1038/s41598-022-04819-6

77. Worthington, R. J., & Melander, C. (2013). Combination approaches to combat multidrug-resistant bacteria. *Trends in Biotechnology*, *31*(3), 177–184. https://doi.org/10.1016/j.tibtech.2012.12.006

78. Ejim, L., Farha, M. A., Falconer, S. B., Wildenhain, J., Coombes, B. K., Tyers, M., … Wright, G. D. (2011). Combinations of antibiotics and nonantibiotic drugs enhance antimicrobial efficacy. *Nature chemical biology*, *7*(6), 348–50. https://doi.org/10.1038/nchembio.559

79. Paul, M., Lador, A., Grozinsky-Glasberg, S., & Leibovici, L. (2014). Beta lactam antibiotic monotherapy versus beta lactam-aminoglycoside antibiotic combination therapy for sepsis. *Cochrane Database of Systematic Reviews*, *2018*(12). https://doi.org/10.1002/14651858.CD003344.pub3

80. Siriyong, T., Murray, R. M., Bidgood, L. E., Young, S. A., Wright, F., Parcell, B. J., … Coote, P. J. (2019). Dual β-lactam combination therapy for multi-drug resistant Pseudomonas aeruginosa infection: enhanced efficacy in vivo and comparison with monotherapies of penicillin-binding protein inhibition. *Scientific Reports*, *9*(1), 9098. https://doi.org/10.1038/s41598-019-45550-z

81. Bartash, R., & Nori, P. (2017). Beta-lactam combination therapy for the treatment of Staphylococcus aureus and Enterococcus species bacteremia: A summary and appraisal of the evidence. *International Journal of Infectious Diseases*, *63*, 7–12. https://doi.org/10.1016/j.ijid.2017.07.019

82. Papp-Wallace, K. M. (2019). The latest advances in β-lactam/β-lactamase inhibitor combinations for the treatment of Gram-negative bacterial infections. *Expert Opinion on Pharmacotherapy*, *20*(17), 2169–2184. https://doi.org/10.1080/14656566.2019.1660772

83. Stavri, M., Piddock, L. J. V., & Gibbons, S. (2007). Bacterial efflux pump inhibitors from natural sources. *Journal of Antimicrobial Chemotherapy*, *59*(6), 1247–1260. https://doi.org/10.1093/jac/dkl460

84. Lomovskaya, O., Warren, M. S., Lee, A., Galazzo, J., Fronko, R., Lee, M., … Lee, V. J. (2001). Identification and characterization of inhibitors of multidrug resistance efflux pumps in Pseudomonas aeruginosa: novel agents for combination therapy. *Antimicrobial agents and chemotherapy*, *45*(1), 105–16. https://doi.org/10.1128/AAC.45.1.105-116.2001

85. Kalle, A. M., & Rizvi, A. (2011). Inhibition of bacterial multidrug resistance by celecoxib, a cyclooxygenase-2 inhibitor. *Antimicrobial agents and chemotherapy*, *55*(1), 439–42. https://doi.org/10.1128/AAC.00735-10

86. Velikova, N., Mas, N., Miguel-Romero, L., Polo, L., Stolte, E., Zaccaria, E., … Wells, J. (n.d.). Broadening the antibacterial spectrum of histidine kinase autophosphorylation inhibitors via the use of ε-poly-L-lysine capped mesoporous silica-based nanoparticles.

Nanomedicine Nanotechnology, Biol. Med, *13*, 569–581. https://doi.org/10.1016/j.nano.2016.09.011.

87. Gotoh, Y., Eguchi, Y., Watanabe, T., Okamoto, S., Doi, A., & Utsumi, R. (2010). Two-component signal transduction as potential drug targets in pathogenic bacteria. *Current opinion in microbiology*, *13*(2), 232–9. https://doi.org/10.1016/j.mib.2010.01.008

88. Paluch, E. (2020). Prevention of biofilm formation by quorum quenching, 1871–1881.

89. Nafee, N., Husari, A., Maurer, C. K., Lu, C., Rossi, C. D., Steinbach, A., … Schneider, M. (n.d.). Antibiotic-free nanotherapeutics: Ultra-small, mucus-penetrating solid lipid nanoparticles enhance the pulmonary delivery and anti-virulence efficacy of novel quorum sensing inhibitors. *J. Control. Release*, *192*, 131–140. https://doi.org/10.1016/j.jconrel.2014.06.055.

90. Worthington, R. J., & Melander, C. (2013). Combination approaches to combat multidrug-resistant bacteria. *Trends in Biotechnology*, *31*(3), 177–184. https://doi.org/10.1016/j.tibtech.2012.12.006

91. Al-Hasan, M. N., Wilson, J. W., Lahr, B. D., Thomsen, K. M., Eckel-Passow, J. E., Vetter, E. A., … Baddour, L. M. (2009). β-Lactam and Fluoroquinolone Combination Antibiotic Therapy for Bacteremia Caused by Gram-Negative Bacilli. *Antimicrobial Agents and Chemotherapy*, *53*(4), 1386–1394. https://doi.org/10.1128/AAC.01231-08

92. Feyaerts, A. F., Luyten, W., & Van Dijck, P. (2020). Striking essential oil: tapping into a largely unexplored source for drug discovery. *Scientific Reports*, *10*(1), 2867. https://doi.org/10.1038/s41598-020-59332-5

93. Guan, R., Van Le, Q., Yang, H., Zhang, D., Gu, H., Yang, Y., … Peng, W. (2021). A review of dietary phytochemicals and their relation to oxidative stress and human diseases. *Chemosphere*, *271*, 129499. https://doi.org/10.1016/j.chemosphere.2020.129499

94. Atanasov, A. G., Waltenberger, B., Pferschy-Wenzig, E.-M., Linder, T., Wawrosch, C., Uhrin, P., … Stuppner, H. (2015). Discovery and resupply of pharmacologically active plant-derived natural products: A review. *Biotechnology Advances*, *33*(8), 1582–1614. https://doi.org/10.1016/j.biotechadv.2015.08.001

95. Savoia, D. (2012). Plant-derived antimicrobial compounds: alternatives to antibiotics. *Future Microbiology*, *7*(8), 979–990. https://doi.org/10.2217/fmb.12.68

96. Abreu, A. C., McBain, A. J., & Simões, M. (2012). Plants as sources of new antimicrobials and resistance-modifying agents. *Natural Product Reports*, *29*(9), 1007. https://doi.org/10.1039/c2np20035j

97. Cowan, M. M. (1999). Plant products as antimicrobial agents. *Clinical microbiology reviews*, *12*(4), 564–82. https://doi.org/10.1128/CMR.12.4.564

98. Subramani, R., Narayanasamy, M., & Feussner, K.-D. (2017). Plant-derived antimicrobials to fight against multi-drug-resistant human pathogens. *3 Biotech*, *7*(3), 172. https://doi.org/10.1007/s13205-017-0848-9

99. Khameneh, B., Iranshahy, M., Soheili, V., & Fazly Bazzaz, B. S. (2019). Review on plant antimicrobials: a mechanistic viewpoint. *Antimicrobial Resistance & Infection Control*, *8*(1), 118. https://doi.org/10.1186/s13756-019-0559-6

100. Holler, J. G., Christensen, S. B., Slotved, H.-C., Rasmussen, H. B., Guzman, A., Olsen, C.-E., … Molgaard, P. (2012). Novel inhibitory activity of the Staphylococcus aureus NorA efflux pump by a kaempferol rhamnoside isolated from Persea lingue Nees. *Journal of Antimicrobial Chemotherapy*, *67*(5), 1138–1144. https://doi.org/10.1093/jac/dks005

101. Guimarães, A. C., Meireles, L. M., Lemos, M. F., Guimarães, M. C. C., Endringer, D. C., Fronza, M., & Scherer, R. (2019). Antibacterial Activity of Terpenes and Terpenoids Present in Essential Oils. *Molecules*, *24*(13), 2471. https://doi.org/10.3390/molecules24132471

102. Nehme, R., Andrés, S., Pereira, R. B., Ben Jemaa, M., Bouhallab, S., Ceciliani, F., … Abdennebi-Najar, L. (2021). Essential Oils in Livestock: From Health to Food Quality. *Antioxidants*, *10*(2), 330. https://doi.org/10.3390/antiox10020330

103. Cheng, G., Hao, H., Xie, S., Wang, X., Dai, M., Huang, L., & Yuan, Z. (2014). Antibiotic alternatives: the substitution of antibiotics in animal husbandry? *Frontiers in Microbiology*, *5*. https://doi.org/10.3389/fmicb.2014.00217

104. Mahlapuu, M., Håkansson, J., Ringstad, L., & Björn, C. (2016). Antimicrobial Peptides: An Emerging Category of Therapeutic Agents. *Frontiers in Cellular and Infection Microbiology*, *6*. https://doi.org/10.3389/fcimb.2016.00194

105. Yeung, A. T. Y., Gellatly, S. L., & Hancock, R. E. W. (2011). Multifunctional cationic host defence peptides and their clinical applications. *Cellular and Molecular Life Sciences*, *68*(13), 2161–2176. https://doi.org/10.1007/s00018-011-0710-x

106. Yeaman, M. R., & Yount, N. Y. (2003). Mechanisms of Antimicrobial Peptide Action and Resistance. *Pharmacological Reviews*, *55*(1), 27–55. https://doi.org/10.1124/pr.55.1.2

107. Mookherjee, N., & Anderson, M. A. (n.d.). Antimicrobial host defence peptides : functions and clinical potential. *Nature Reviews Drug Discovery*. https://doi.org/10.1038/s41573-019-0058-8

108. Rima, M., Rima, M., Fajloun, Z., Sabatier, J., Bechinger, B., & Naas, T. (2021). Antimicrobial Peptides : A Potent Alternative to Antibiotics, 1–15.

109. Dijksteel, G. S., Ulrich, M. M. W., Middelkoop, E., & Boekema, B. K. H. L. (2021). Review: Lessons Learned From Clinical Trials Using Antimicrobial Peptides (AMPs). *Frontiers in Microbiology*, *12*. https://doi.org/10.3389/fmicb.2021.616979

110. Arnusch, C. J., Pieters, R. J., & Breukink, E. (2012). Enhanced Membrane Pore Formation through High-Affinity Targeted Antimicrobial Peptides. *PLoS ONE*, *7*(6), e39768. https://doi.org/10.1371/journal.pone.0039768

111. Fadaka, A. O., Sibuyi, N. R. S., Madiehe, A. M., & Meyer, M. (2021). Nanotechnology-Based Delivery Systems for Antimicrobial Peptides. *Pharmaceutics*, *13*(11), 1795. https://doi.org/10.3390/pharmaceutics13111795

112. Andrade, F. F., Silva, D., Rodrigues, A., & Pina-Vaz, C. (2020). Colistin update on its mechanism of action and resistance, present and future challenges. *Microorganisms*, *8*(11), 1–12. https://doi.org/10.3390/microorganisms8111716

113. Mahlapuu, M., Sidorowicz, A., Mikosinski, J., Krzyżanowski, M., Orleanski, J., Twardowska-Saucha, K., … Apelqvist, J. (2021). Evaluation of <scp>LL</scp> -37 in

healing of <scp>hard-to-heal</scp> venous leg ulcers: A multicentric prospective randomized <scp>placebo-controlled</scp> clinical trial. *Wound Repair and Regeneration*, *29*(6), 938–950. https://doi.org/10.1111/wrr.12977

114. Riley, M. A., & Wertz, J. E. (2002). Bacteriocins: Evolution, Ecology, and Application. *Annual Review of Microbiology*, *56*(1), 117–137. https://doi.org/10.1146/annurev.micro.56.012302.161024

115. Cotter, P. D., Ross, R. P., & Hill, C. (2013). Bacteriocins — a viable alternative to antibiotics? *Nature Reviews Microbiology*, *11*(2), 95–105. https://doi.org/10.1038/nrmicro2937

116. Simons, A., Alhanout, K., & Duval, R. E. (2020). Bacteriocins, Antimicrobial Peptides from Bacterial Origin: Overview of Their Biology and Their Impact against Multidrug-Resistant Bacteria. *Microorganisms*, *8*(5). https://doi.org/10.3390/microorganisms8050639

117. Soltani, S., Hammami, R., Cotter, P. D., Rebuffat, S., Biron, E., Drider, D., … Fliss, I. (2021). Bacteriocins as a new generation of antimicrobials : toxicity aspects and regulations, (August 2020), 1–24. https://doi.org/10.1093/femsre/fuaa039

118. Browder, H. P., Zygmunt, W. A., Young, J. R., & Tavormina, P. A. (1965). Lysostaphin: Enzymatic mode of action. *Biochemical and Biophysical Research Communications*, *19*(3), 383–389. https://doi.org/10.1016/0006-291X(65)90473-0

119. Wu, J. A., Kusuma, C., Mond, J. J., & Kokai-Kun, J. F. (2003). Lysostaphin Disrupts *Staphylococcus aureus* and *Staphylococcus epidermidis* Biofilms on Artificial Surfaces. *Antimicrobial Agents and Chemotherapy*, *47*(11), 3407–3414. https://doi.org/10.1128/AAC.47.11.3407-3414.2003

120. Kusuma, C. M., & Kokai-Kun, J. F. (2005). Comparison of Four Methods for Determining Lysostaphin Susceptibility of Various Strains of *Staphylococcus aureus*. *Antimicrobial Agents and Chemotherapy*, *49*(8), 3256–3263. https://doi.org/10.1128/AAC.49.8.3256-3263.2005

121. Motley, M. P., Banerjee, K., & Fries, B. C. (2019). Monoclonal antibody-based therapies for bacterial infections. *Current Opinion in Infectious Diseases*, *32*(3), 210–216. https://doi.org/10.1097/QCO.0000000000000539

122. Zurawski, D. V., & McLendon, M. K. (2020). Monoclonal Antibodies as an Antibacterial Approach Against Bacterial Pathogens. *Antibiotics*, *9*(4), 155. https://doi.org/10.3390/antibiotics9040155

123. Cavaco, M., Castanho, M. A. R. B., & Neves, V. (2022). The Use of Antibody-Antibiotic Conjugates to Fight Bacterial Infections. *Frontiers in Microbiology*, *13*. https://doi.org/10.3389/fmicb.2022.835677

124. Wang-Lin, S. xin, Zhou, C., Kamath, A. V., Hong, K., Koppada, N., Saad, O. M., … Deng, R. (2018). Minimal physiologically-based pharmacokinetic modeling of DSTA4637A, A novel THIOMAB^{TM} antibody antibiotic conjugate against *Staphylococcus aureus* , in a mouse model. *mAbs*, 1–13. https://doi.org/10.1080/19420862.2018.1494478

125. Wilcox, M. H., Gerding, D. N., Poxton, I. R., Kelly, C., Nathan, R., Birch, T., … Dorr, M.-B. (2017). Bezlotoxumab for Prevention of Recurrent *Clostridium difficile* Infection. *New England Journal of Medicine*, *376*(4), 305–317. https://doi.org/10.1056/NEJMoa1602615

126. Elusys Therapeutics, INC. (n.d.). Anthim (obiltoxaximab) Injection for the Treatment of Inhalational Anthrax. Retrieved July 15, 2023, from https://anthim.com/

127. Altun, E., Aydogdu, M. O., Chung, E., Ren, G., Homer-Vanniasinkam, S., & Edirisinghe, M. (2021). Metal-based nanoparticles for combating antibiotic resistance. *Applied Physics Reviews*, *8*(4). https://doi.org/10.1063/5.0060299

128. Slavin, Y. N., Asnis, J., Häfeli, U. O., & Bach, H. (2017). Metal nanoparticles: understanding the mechanisms behind antibacterial activity. *Journal of Nanobiotechnology*, *15*(1), 65. https://doi.org/10.1186/s12951-017-0308-z

129. Kotrange, H., Najda, A., Bains, A., Gruszecki, R., Chawla, P., & Tosif, M. M. (2021). Metal and Metal Oxide Nanoparticle as a Novel Antibiotic Carrier for the Direct Delivery of Antibiotics. *International Journal of Molecular Sciences*, *22*(17), 9596. https://doi.org/10.3390/ijms22179596

130. Abo-Shama, U. H., El-Gendy, H., Mousa, W. S., Hamouda, R. A., Yousuf, W. E., Hetta, H. F., & Abdeen, E. E. (2020). Synergistic and Antagonistic Effects of Metal Nanoparticles in Combination with Antibiotics Against Some Reference Strains of Pathogenic Microorganisms . *Infection and Drug Resistance*, *Volume 13*, 351–362. https://doi.org/10.2147/IDR.S234425

131. Bankier, C., Matharu, R. K., Cheong, Y. K., Ren, G. G., Cloutman-Green, E., & Ciric, L. (2019). Synergistic Antibacterial Effects of Metallic Nanoparticle Combinations. *Scientific Reports*, *9*(1), 16074. https://doi.org/10.1038/s41598-019-52473-2

132. Rai, M., Yadav, A., & Gade, A. (2009). Silver nanoparticles as a new generation of antimicrobials. *Biotechnology Advances*, *27*(1), 76–83. https://doi.org/10.1016/j.biotechadv.2008.09.002

133. Sondi, I., & Salopek-Sondi, B. (2004). Silver nanoparticles as antimicrobial agent: a case study on E. coli as a model for Gram-negative bacteria. *Journal of Colloid and Interface Science*, *275*(1), 177–182. https://doi.org/10.1016/j.jcis.2004.02.012

134. Ferdous, Z., & Nemmar, A. (2020). Health Impact of Silver Nanoparticles: A Review of the Biodistribution and Toxicity Following Various Routes of Exposure. *International Journal of Molecular Sciences*, *21*(7), 2375. https://doi.org/10.3390/ijms21072375

135. Haes, A. J., & Van Duyne, R. P. (2004). A unified view of propagating and localized surface plasmon resonance biosensors. *Analytical and Bioanalytical Chemistry*, *379*(7–8), 920–930. https://doi.org/10.1007/s00216-004-2708-9

136. Chen, H., Kou, X., Yang, Z., Ni, W., & Wang, J. (2008). Shape- and Size-Dependent Refractive Index Sensitivity of Gold Nanoparticles. *Langmuir*, *24*(10), 5233–5237. https://doi.org/10.1021/la800305j

137. Yuan, P., Ding, X., Yang, Y. Y., & Xu, Q. (2018). Metal Nanoparticles for Diagnosis and Therapy of Bacterial Infection. *Advanced Healthcare Materials*, *7*(13). https://doi.org/10.1002/adhm.201701392

138. Aponte, M., Murru, N., & Shoukat, M. (2020). Therapeutic, Prophylactic, and Functional Use of Probiotics: A Current Perspective. *Frontiers in Microbiology*, *11*. https://doi.org/10.3389/fmicb.2020.562048

139. Tegegne, B. A., & Kebede, B. (2022). Probiotics, their prophylactic and therapeutic applications in human health development: A review of the literature. *Heliyon*, *8*(6), e09725. https://doi.org/10.1016/j.heliyon.2022.e09725

140. Silva, D. R., Sardi, J. de C. O., Pitangui, N. de S., Roque, S. M., Silva, A. C. B. da, & Rosalen, P. L. (2020). Probiotics as an alternative antimicrobial therapy: Current reality and future directions. *Journal of Functional Foods*, *73*, 104080. https://doi.org/10.1016/j.jff.2020.104080

141. Tham, C. S.-C., Peh, K.-K., Bhat, R., & Liong, M.-T. (2012). Probiotic properties of bifidobacteria and lactobacilli isolated from local dairy products. *Annals of Microbiology*, *62*(3), 1079–1087. https://doi.org/10.1007/s13213-011-0349-8

142. Lee, J.-S., Chung, M.-J., & Seo, J.-G. (2013). In Vitro Evaluation of Antimicrobial Activity of Lactic Acid Bacteria against Clostridium difficile. *Toxicological Research*, *29*(2), 99–106. https://doi.org/10.5487/TR.2013.29.2.099

143. Buffie, C. G., Bucci, V., Stein, R. R., McKenney, P. T., Ling, L., Gobourne, A., … Pamer, E. G. (2015). Precision microbiome reconstitution restores bile acid mediated resistance to Clostridium difficile. *Nature*, *517*(7533), 205–208. https://doi.org/10.1038/nature13828

144. Lin, D. M., Koskella, B., & Lin, H. C. (2017). Phage therapy: An alternative to antibiotics in the age of multi-drug resistance. *World journal of gastrointestinal pharmacology and therapeutics*, *8*(3), 162–173. https://doi.org/10.4292/wjgpt.v8.i3.162

145. Yang, X., Haque, A., Matsuzaki, S., Matsumoto, T., & Nakamura, S. (2021). The Efficacy of Phage Therapy in a Murine Model of Pseudomonas aeruginosa Pneumonia and Sepsis. *Frontiers in Microbiology*, *12*. https://doi.org/10.3389/fmicb.2021.682255

146. Jault, P., Leclerc, T., Jennes, S., Pirnay, J. P., Que, Y.-A., Resch, G., … Gabard, J. (2019). Efficacy and tolerability of a cocktail of bacteriophages to treat burn wounds infected by Pseudomonas aeruginosa (PhagoBurn): a randomised, controlled, double-blind phase 1/2 trial. *The Lancet Infectious Diseases*, *19*(1), 35–45. https://doi.org/10.1016/S1473-3099(18)30482-1

147. Ferry, T., Leboucher, G., Fevre, C., Herry, Y., Conrad, A., Josse, J., … Mabrut, E. (2018). Salvage Debridement, Antibiotics and Implant Retention (“DAIR”) With Local Injection of a Selected Cocktail of Bacteriophages: Is It an Option for an Elderly Patient With Relapsing Staphylococcus aureus Prosthetic-Joint Infection? *Open Forum Infectious Diseases*, *5*(11). https://doi.org/10.1093/ofid/ofy269

148. Gigante, A., & Atterbury, R. J. (2019). Veterinary use of bacteriophage therapy in intensively-reared livestock. *Virology Journal*, *16*(1), 155. https://doi.org/10.1186/s12985-019-1260-3

149. Roach, D. R., & Donovan, D. M. (2015). Antimicrobial bacteriophage-derived proteins and therapeutic applications. *Bacteriophage*, *5*(3), e1062590. https://doi.org/10.1080/21597081.2015.1062590

150. Vargason, A. M., Anselmo, A. C., & Mitragotri, S. (2021). The evolution of commercial drug delivery technologies. *Nature Biomedical Engineering*, *5*(September). https://doi.org/10.1038/s41551-021-00698-w

151. Park, H., Otte, A., & Park, K. (2023). Evolution of Drug Delivery Systems: From 1950 to 2020 and Beyond, 53–65. https://doi.org/10.1016/j.jconrel.2021.12.030.Evolution

152. Park, K. (2014). Controlled drug delivery systems: Past forward and future back. *Journal of Controlled Release*, *190*, 3–8. https://doi.org/10.1016/j.jconrel.2014.03.054

153. National Nanotechnology Initiative. (n.d.). Retrieved August 1, 2023, from https://www.nano.gov/about-nni

154. Jia, Y., Jiang, Y., He, Y., Zhang, W., Zou, J., Magar, K. T., … He, W. (2023). Approved Nanomedicine against Diseases. *Pharmaceutics*, *15*(3), 774. https://doi.org/10.3390/pharmaceutics15030774

155. Poon, W., Kingston, B. R., Ouyang, B., Ngo, W., & Chan, W. C. W. (2020). A framework for designing delivery systems. *Nature Nanotechnology*, *15*(10), 819–829. https://doi.org/10.1038/s41565-020-0759-5

156. Waheed, S., Li, Z., Zhang, F., Chiarini, A., Armato, U., & Wu, J. (2022). Engineering nano - drug biointerface to overcome biological barriers toward precision drug delivery. *Journal of Nanobiotechnology*, *4*, 1–25. https://doi.org/10.1186/s12951-022-01605-4

157. Yun, Y. H., Lee, B. K., Park, K., & Lafayette, W. (2016). Controlled Drug Delivery: Historical perspective for the next generation, 2–7. https://doi.org/10.1016/j.jconrel.2015.10.005.Controlled

158. Blanco, E., Shen, H., & Ferrari, M. (2015). Principles of nanoparticle design for overcoming biological barriers to drug delivery. *Nature Biotechnology*, *33*(9), 941–951. https://doi.org/10.1038/nbt.3330

159. Baryakova, T. H., Pogostin, B. H., Langer, R., & McHugh, K. J. (2023). Overcoming barriers to patient adherence: the case for developing innovative drug delivery systems. *Nature Reviews Drug Discovery*, *22*(5), 387–409. https://doi.org/10.1038/s41573-023-00670-0

160. Chang, E. H., Harford, J. B., Eaton, M. A. W., Boisseau, P. M., Dube, A., Hayeshi, R., … Lee, D. S. (2015). Nanomedicine: Past, present and future – A global perspective. *Biochemical and Biophysical Research Communications*, *468*(3), 511–517. https://doi.org/10.1016/j.bbrc.2015.10.136

161. Zou, W., McAdorey, A., Yan, H., & Chen, W. (2023). Nanomedicine to overcome antimicrobial resistance: challenges and prospects. *Nanomedicine*, *18*(5), 471–484. https://doi.org/10.2217/nnm-2023-0022

162. Din, F. ud, Aman, W., Ullah, I., Qureshi, O. S., Mustapha, O., Shafique, S., & Zeb, A. (2017). Effective use of nanocarriers as drug delivery systems for the treatment of

selected tumors. *International Journal of Nanomedicine*, *Volume 12*, 7291–7309. https://doi.org/10.2147/IJN.S146315

163. Mitchell, M. J., Billingsley, M. M., Haley, R. M., Wechsler, M. E., Peppas, N. A., & Langer, R. (2021). Engineering precision nanoparticles for drug delivery. *Nature Reviews Drug Discovery*, *20*(2), 101–124. https://doi.org/10.1038/s41573-020-0090-8

164. Sundar, S., & Kumar Prajapati, V. (2012). Drug Targeting to Infectious Diseases by Nanoparticles Surface Functionalized with Special Biomolecules. *Current Medicinal Chemistry*, *19*(19), 3196–3202. https://doi.org/10.2174/092986712800784630

165. Dawidczyk, C. M., Kim, C., Park, J. H., Russell, L. M., Lee, K. H., Pomper, M. G., & Searson, P. C. (2014). State-of-the-art in design rules for drug delivery platforms: Lessons learned from FDA-approved nanomedicines. *Journal of Controlled Release*, *187*, 133–144. https://doi.org/10.1016/j.jconrel.2014.05.036

166. Wang, D.-Y., van der Mei, H. C., Ren, Y., Busscher, H. J., & Shi, L. (2020). Lipid-Based Antimicrobial Delivery-Systems for the Treatment of Bacterial Infections. *Frontiers in Chemistry*, *7*. https://doi.org/10.3389/fchem.2019.00872

167. Liu, Y., Shi, L., Su, L., van der Mei, H. C., Jutte, P. C., Ren, Y., & Busscher, H. J. (2019). Nanotechnology-based antimicrobials and delivery systems for biofilm-infection control. *Chemical Society Reviews*, *48*(2), 428–446. https://doi.org/10.1039/C7CS00807D

168. Allen, T. M., & Cullis, P. R. (n.d.). Liposomal drug delivery systems: From concept to clinical applications, Adv. *Drug Deliv. Rev*, *65*, 36–48. https://doi.org/10.1016/j.addr.2012.09.037.

169. Sercombe, L., Veerati, T., Moheimani, F., Wu, S. Y., Sood, A. K., & Hua, S. (n.d.). Advances and challenges of liposome assisted drug delivery. *Front. Pharmacol*, *6*, 1–13. https://doi.org/10.3389/fphar.2015.00286.

170. Deol, P., Khuller, G. K., & Joshi, K. (n.d.). Therapeutic efficacies of isoniazid and rifampin encapsulated in lung-specific stealth liposomes against Mycobacterium tuberculosis infection induced in mice., Antimicrob. *Agents Chemother*, *41*, 1211–1214. https://doi.org/10.1128/AAC.41.6.1211.

171. Wang, S., Yu, S., Lin, Y., Zou, P., Chai, G., Yu, H. H., … Zhou, Q. T. (n.d.). Co-Delivery of Ciprofloxacin and Colistin in Liposomal Formulations with Enhanced In Vitro Antimicrobial Activities against Multidrug Resistant Pseudomonas aeruginosa. *Pharm. Res*, *35*, 187. https://doi.org/10.1007/s11095-018-2464-8.

172. Pumerantz, A., Muppidi, K., Agnihotri, S., Guerra, C., Venketaraman, V., Wang, J., & Betageri, G. (n.d.). Preparation of liposomal vancomycin and intracellular killing of meticillin-resistant Staphylococcus aureus (MRSA)., Int. *J. Antimicrob. Agents*, *37*, 140–144. https://doi.org/10.1016/j.ijantimicag.2010.10.011.

173. Cipolla, D., Blanchard, J., & Gonda, I. (n.d.). Development of Liposomal Ciprofloxacin to Treat Lung Infections. *Pharmaceutics*, *8*, 6. https://doi.org/10.3390/pharmaceutics8010006.

174. Santos, R. S., Figueiredo, C., Azevedo, N. F., Braeckmans, K., & Smedt, S. C. D. (n.d.). Nanomaterials and molecular transporters to overcome the bacterial envelope barrier: Towards advanced delivery of antibiotics, Adv. *Drug Deliv. Rev*, *136–137*, 28–48. https://doi.org/10.1016/j.addr.2017.12.010.

175. Nicolosi, D., Scalia, M., Nicolosi, V. M., & Pignatello, R. (n.d.). Encapsulation in fusogenic liposomes broadens the spectrum of action of vancomycin against Gram-negative bacteria. *Int. J. Antimicrob. Agents*, *35*, 553–558. https://doi.org/10.1016/j.ijantimicag.2010.01.015.

176. Santos, R. S., Dakwar, G. R., Zagato, E., Brans, T., Figueiredo, C., Raemdonck, K., … Braeckmans, K. (n.d.). Intracellular delivery of oligonucleotides in Helicobacter pylori by fusogenic liposomes in the presence of gastric mucus. *Biomaterials*, *138*, 1–12. https://doi.org/10.1016/j.biomaterials.2017.05.029.

177. Mishra, V., Bansal, K. K., Verma, A., Yadav, N., Thakur, S., Sudhakar, K., & Rosenholm, J. M. (n.d.). Solid Lipid Nanoparticles: Emerging Colloidal Nano Drug Delivery Systems. *Pharm*, *10*. https://doi.org/10.3390/pharmaceutics10040191.

178. Eleraky, N. E., Allam, A., Hassan, S. B., & Omar, M. M. (n.d.). Nanomedicine fight against antibacterial resistance: An overview of the recent pharmaceutical innovations. *Pharmaceutics*, *12*, 1–51. https://doi.org/10.3390/pharmaceutics12020142.

179. Müller, R. H., Mäder, K., & Gohla, S. (n.d.). Solid lipid nanoparticles (SLN) for controlled drug delivery - a review of the state of the art., Eur. *J. Pharm. Biopharm. Off. J. Arbeitsgemeinschaft Fur Pharm. Verfahrenstechnik e.V*, *50*, 161–177. https://doi.org/10.1016/s0939-6411(00)00087-4.

180. Wang, Y., Wang, Z., Xu, C., Tian, H., & Chen, X. (n.d.). A disassembling strategy overcomes the EPR effect and renal clearance dilemma of the multifunctional theranostic nanoparticles for cancer therapy. *Biomaterials*, *197*, 284–293. https://doi.org/10.1016/j.biomaterials.2019.01.025.

181. Jones, M. N., Song, Y.-H., Kaszuba, M., & Reboiras, M. D. (n.d.). The Interaction of Phospholipid Liposomes with Bacteria and Their Use in the Delivery of Bactericides. *J. Drug Target*, *5*, 25–34. https://doi.org/10.3109/10611869708995855.

182. Ikeda, S., Zhang, Z., Kojima, M., Nakajima, M., & Fukuda, T. (n.d.). Evaluation of attachment and motion of bacteria-driven liposome based on antibody binding technique, Proc. - *IEEE Int. Conf. Robot. Autom*. https://doi.org/10.1109/ICRA.2011.5980579.

183. Ando, H., Lila, A. S. A., Kawanishi, M., Shimizu, T., Okuhira, K., Ishima, Y., & Ishida, T. (n.d.). Reactivity of IgM antibodies elicited by PEGylated liposomes or PEGylated lipoplexes against auto and foreign antigens. *J. Control. Release*, *270*, 114–119. https://doi.org/10.1016/j.jconrel.2017.12.002.

184. Rathnayake, K., Patel, U., Pham, C., McAlpin, A., Budisalich, T., & Jayawardena, S. N. (n.d.). Targeted Delivery of Antibiotic Therapy to Inhibit Pseudomonas aeruginosa Using Lipid-Coated Mesoporous Silica Core-Shell Nanoassembly, ACS Appl. *Bio Mater*, *3*, 6708–6721. https://doi.org/10.1021/acsabm.0c00622.

185. Fabani, M. M., Gargini, R., Taira, M. C., Iacono, R., & Alonso-Romanowski, S. (n.d.). Study of in vitro stability of liposomes and in vivo antibody response to antigen associated with liposomes containing GM1 after oral and subcutaneous immunization. *J. Liposome Res*, *12*, 13–27. https://doi.org/10.1081/lpr-120004772.

186. El-Say, K. M., & El-Sawy, H. S. (n.d.). Polymeric nanoparticles: Promising platform for drug delivery. *Int. J. Pharm*, *528*, 675–691. https://doi.org/10.1016/j.ijpharm.2017.06.052.

187. Bharatwaj, B., Wu, L., Whittum-Hudson, J. A., & Rocha, S. R. P. (n.d.). The potential for the noninvasive delivery of polymeric nanocarriers using propellant-based inhalers in the treatment of Chlamydial respiratory infections. *Biomaterials*, *31*, 7376–7385. https://doi.org/10.1016/j.biomaterials.2010.06.005.

188. Lai, P., Daear, W., Löbenberg, R., & Prenner, E. J. (n.d.). Overview of the preparation of organic polymeric nanoparticles for drug delivery based on gelatine, chitosan, poly(d,l-lactide-co-glycolic acid) and polyalkylcyanoacrylate., Colloids Surf. *B. Biointerfaces*, *118*, 154–163. https://doi.org/10.1016/j.colsurfb.2014.03.017.

189. Lu, H., Zhang, S., Wang, J., & Chen, Q. (2021). A Review on Polymer and Lipid-Based Nanocarriers and Its Application to Nano-Pharmaceutical and Food-Based Systems. *Frontiers in nutrition*, *8*, 783831. https://doi.org/10.3389/fnut.2021.783831

190. Rideau, E., Dimova, R., Schwille, P., Wurm, F. R., & Landfester, K. (2018). Liposomes and polymersomes: a comparative review towards cell mimicking. *Chemical Society Reviews*, *47*(23), 8572–8610. https://doi.org/10.1039/C8CS00162F

191. Sadler, K., & Tam, J. P. (n.d.). Peptide dendrimers: applications and synthesis. *Rev. Mol. Biotechnol*, *90*, 195–229. https://doi.org/10.1016/S1389-0352(01)00061-7.

192. Karthikeyan, R., Koushik, O., & Kumar, P. (n.d.). Dendrimeric Architecture for Effective Antimicrobial Therapy.

193. Jiang, G., Liu, S., Yu, T., Wu, R., Ren, Y., Mei, H. C., … Busscher, H. J. (n.d.). PAMAM dendrimers with dual-conjugated vancomycin and Ag-nanoparticles do not induce bacterial resistance and kill vancomycin-resistant Staphylococci. *Acta Biomater*, *123*, 230–243. https://doi.org/10.1016/j.actbio.2021.01.032.

194. Zhang, L., Pornpattananangku, D., Hu, C.-M. J., & Huang, C.-M. (n.d.). Development of nanoparticles for antimicrobial drug delivery., Curr. *Med. Chem*, *17*, 585–594. https://doi.org/10.2174/092986710790416290.

195. Combating multidrug-resistant Gram-negative bacteria with structurally nanoengineered antimicrobial peptide polymers. (n.d.). *Nat. Microbiol*, *1*. https://doi.org/10.1038/nmicrobiol.2016.162.

196. Hou, S., Zhou, C., Liu, Z., Young, A. W., Shi, Z., Ren, D., & Kallenbach, N. R. (n.d.). Antimicrobial dendrimer active against Escherichia coli biofilms., Bioorg. *Med. Chem. Lett*, *19*, 5478–5481. https://doi.org/10.1016/j.bmcl.2009.07.077.

197. Cano, A., Ettcheto, M., Espina, M., López-Machado, A., Cajal, Y., Rabanal, F., … Souto, E. B. (n.d.). State-of-the-art polymeric nanoparticles as promising therapeutic tools against

human bacterial infections. *J. Nanobiotechnology*, *18*, 1–24. https://doi.org/10.1186/s12951-020-00714-2.

198. Parisi, O. I., Scrivano, L., Sinicropi, M. S., & Puoci, F. (n.d.). Polymeric nanoparticle constructs as devices for antibacterial therapy., Curr. *Opin. Pharmacol*, *36*, 72–77. https://doi.org/10.1016/j.coph.2017.08.004.

199. Betancourt, T., Byrne, J. D., Sunaryo, N., Crowder, S. W., Kadapakkam, M., Patel, S., … Brannon-Peppas, L. (n.d.). PEGylation strategies for active targeting of PLA/PLGA nanoparticles. *J. Biomed. Mater. Res. A*, *91*, 263–276. https://doi.org/10.1002/jbm.a.32247.

200. Yu, N., Wang, X., Qiu, L., Cai, T., Jiang, C., Sun, Y., … Xiong, H. (n.d.). Bacteria-triggered hyaluronan/AgNPs/gentamicin nanocarrier for synergistic bacteria disinfection and wound healing application. *Chem. Eng. J*, *380*, 122582. https://doi.org/10.1016/j.cej.2019.122582.

201. Essa, D., Kondiah, P. P. D., Choonara, Y. E., & Pillay, V. (2020). The Design of Poly(lactide-co-glycolide) Nanocarriers for Medical Applications. *Frontiers in Bioengineering and Biotechnology*, *8*. https://doi.org/10.3389/fbioe.2020.00048

202. Martínez-Carmona, M., Gun'ko, Y. K., & Vallet-Regí, M. (n.d.). Mesoporous silica materials as drug delivery: "the nightmare" of bacterial infection. *Pharmaceutics*, *10*, 1–29. https://doi.org/10.3390/pharmaceutics10040279.

203. Xu, C., Lei, C., & Yu, C. (n.d.). Mesoporous Silica Nanoparticles for Protein Protection and Delivery, Front. *Chem*, *7*, 290. https://doi.org/10.3389/fchem.2019.00290.

204. Tu, J., Boyle, A. L., Friedrich, H., Bomans, P. H. H., Bussmann, J., Sommerdijk, N. A. J. M., … Kros, A. (n.d.). Mesoporous Silica Nanoparticles with Large Pores for the Encapsulation and Release of Proteins. *ACS Appl. Mater. Interfaces*, *8*, 32211–32219. https://doi.org/10.1021/acsami.6b11324.

205. Kuthati, Y., Sung, P.-J., Weng, C.-F., Mou, C.-Y., & Lee, C.-H. (n.d.). Functionalization of mesoporous silica nanoparticles for targeting, biocompatibility, combined cancer therapies and theragnosis. *J. Nanosci. Nanotechnol*, *13*, 2399–2430. https://doi.org/10.1166/jnn.2013.7363.

206. Wu, Z.-Y., Lee, C.-C., & Lin, H.-M. (n.d.). Hyaluronidase-Responsive Mesoporous Silica Nanoparticles with Dual-Imaging and Dual-Target Function. *Cancers (Basel*, *11*, 697. https://doi.org/10.3390/cancers11050697.

207. Muhammad, F., Guo, M., Qi, W., Sun, F., Wang, A., Guo, Y., & G. (n.d.). Zhu, pH-Triggered Controlled Drug Release from Mesoporous Silica Nanoparticles via Intracelluar Dissolution of ZnO Nanolids. *J. Am. Chem. Soc*, *133*, 8778–8781. https://doi.org/10.1021/ja200328s.

208. Effective reduction of biofilm through photothermal therapy by gold core@shell based mesoporous silica nanoparticles. (n.d.). *Microporous Mesoporous Mater*, *328*, 111489. https://doi.org/10.1016/j.micromeso.2021.111489.

209. Li, Y., Yan, Y., Wang, J., Li, L., & Tang, F. (2022). Preparation of silver nanoparticles decorated mesoporous silica nanorods with photothermal antibacterial property.

Colloids and Surfaces A: Physicochemical and Engineering Aspects, *648*, 129242. https://doi.org/10.1016/j.colsurfa.2022.129242

210. Reviews, C. (n.d.). Introduction to Metal − Organic Frameworks.

211. Lawson, H. D., Walton, S. P., & Chan, C. (n.d.). Metal-Organic Frameworks for Drug Delivery: A Design Perspective, ACS Appl. *Mater. Interfaces*, *13*, 7004–7020. https://doi.org/10.1021/acsami.1c01089.

212. Peng, S., Bie, B., Sun, Y., Liu, M., Cong, H., Zhou, W., … Zhou, X. (n.d.). Metal-organic frameworks for precise inclusion of single-stranded DNA and transfection in immune cells. *Nat. Commun*, *9*, 1–10. https://doi.org/10.1038/s41467-018-03650-w.

213. Wang, X., Lan, P. C., & Ma, S. (n.d.). Metal–Organic Frameworks for Enzyme Immobilization: Beyond Host Matrix Materials, ACS Cent. *Sci*, *6*, 1497–1506. https://doi.org/10.1021/acscentsci.0c00687.

214. Li, X., Semiramoth, N., Hall, S., Tafani, V., Josse, J., Laurent, F., … Gref, R. (n.d.). Compartmentalized Encapsulation of Two Antibiotics in Porous Nanoparticles: an Efficient Strategy to Treat Intracellular Infections. *Part. Part. Syst. Charact*, *36*, 1–9. https://doi.org/10.1002/ppsc.201800360.

215. Liang, M., Zhang, M., Yu, S., Wu, Q., Ma, K., Chen, Y., … Wang, F. (n.d.). Silver-Laden Black Phosphorus Nanosheets for an Efficient In Vivo Antimicrobial Application. *Small*, *1905938*, 1–11. https://doi.org/10.1002/smll.201905938.

216. Karakeçili, A., Topuz, B., Korpayev, S., & Erdek, M. (n.d.). Metal-organic frameworks for on-demand pH controlled delivery of vancomycin from chitosan scaffolds., Mater. *Sci. Eng. C. Mater. Biol. Appl*, *105*, 110098. https://doi.org/10.1016/j.msec.2019.110098.

217. Li, X., Qi, M., Li, C., Dong, B., Wang, J., Weir, M., … Xu, H. (n.d.). Novel nanoparticles of cerium-doped zeolitic imidazolate frameworks with dual benefits of antibacterial and anti-inflammatory functions against periodontitis. *J. Mater. Chem. B*, *7*. https://doi.org/10.1039/C9TB01743G.

218. A Zn azelate MOF: Combining antibacterial effect. (n.d.). *CrystEngComm*, *17*, 456–462. https://doi.org/10.1039/c4ce00885e.

219. Shen, M., Forghani, F., Kong, X., Liu, D., Ye, X., Chen, S., & Ding, T. (n.d.). Antibacterial applications of metal–organic frameworks and their composites. *Compr. Rev. Food Sci. Food Saf*, *19*, 1397–1419. https://doi.org/10.1111/1541-4337.12515.

220. Ghaffar, I., Imran, M., Perveen, S., Kanwal, T., Saifullah, S., Bertino, M. F., … Shah, M. R. (n.d.). Synthesis of chitosan coated metal organic frameworks (MOFs) for increasing vancomycin bactericidal potentials against resistant S. *aureus strain, Mater. Sci. Eng. C*, *105*. https://doi.org/10.1016/j.msec.2019.110111.

221. Chitosan-coated mesoporous MIL-100(Fe) nanoparticles as improved bio-compatible oral nanocarriers, Sci. (n.d.). *Rep*, *7*, 1–14. https://doi.org/10.1038/srep43099.

222. Cai, W., Gao, H., Chu, C., Wang, X., Wang, J., Zhang, P., … Chen, X. (n.d.). Engineering phototheranostic nanoscale metal-organic frameworks for multimodal imaging-guided cancer therapy. *ACS Appl. Mater. Interfaces*, *9*, 2040–2051. https://doi.org/10.1021/acsami.6b11579.

223. Burygin, G. L., Khlebtsov, B. N., Shantrokha, A. N., Dykman, L. A., Bogatyrev, V. A., & Khlebtsov, N. G. (n.d.). On the Enhanced Antibacterial Activity of Antibiotics Mixed with Gold Nanoparticles. *Nanoscale Res. Lett*, *4*, 794. https://doi.org/10.1007/s11671-009-9316-8.

224. Wang, L., Hu, C., & Shao, L. (n.d.). The antimicrobial activity of nanoparticles: Present situation and prospects for the future. *Int. J. Nanomedicine*, *12*, 1227–1249. https://doi.org/10.2147/IJN.S121956.

225. Yougbaré, S., Mutalik, C., Krisnawati, D. I., Kristanto, H., Jazidie, A., Nuh, M., … Kuo, T.-R. (n.d.). Nanomaterials for the Photothermal Killing of Bacteria. *Nanomater*, *10*. https://doi.org/10.3390/nano10061123.

226. Mao, C., Xiang, Y., Liu, X., Zheng, Y., Yeung, K. W. K., Cui, Z., … Wu, S. (2019). Local Photothermal/Photodynamic Synergistic Therapy by Disrupting Bacterial Membrane to Accelerate Reactive Oxygen Species Permeation and Protein Leakage. *ACS Applied Materials and Interfaces*, *11*(19), 17902–17914. research-article. https://doi.org/10.1021/acsami.9b05787

227. Design strategies of hybrid metallic nanoparticles for theragnostic applications. (n.d.). *Nanotechnology*, *24*, 432002. https://doi.org/10.1088/0957-4484/24/43/432002.

228. Wagner, A. M., Knipe, J. M., Orive, G., & Peppas, N. A. (2019). Quantum dots in biomedical applications. *Acta Biomaterialia*, *94*, 44–63. https://doi.org/10.1016/j.actbio.2019.05.022

229. Leevy, W. M., Lambert, T. N., Johnson, J. R., Morris, J., & Smith, B. D. (2008). Quantum dot probes for bacteria distinguish Escherichia coli mutants and permit in vivo imaging. *Chemical Communications*, (20), 2331. https://doi.org/10.1039/b803590c

230. Zhang, Y., & Clapp, A. (2011). Overview of Stabilizing Ligands for Biocompatible Quantum Dot Nanocrystals. *Sensors*, *11*(12), 11036–11055. https://doi.org/10.3390/s111211036

231. Krizanova, O., Penesova, A., Sokol, J., Hokynkova, A., Samadian, A., & Babula, P. (2022). Signaling pathways in cutaneous wound healing. *Frontiers in physiology*, *13*, 1030851. https://doi.org/10.3389/fphys.2022.1030851

232. Mirhaj, M., Labbaf, S., Tavakoli, M., & Seifalian, A. (2022). An Overview on the Recent Advances in the Treatment of Infected Wounds: Antibacterial Wound Dressings. *Macromolecular Bioscience*, *22*(7), 2200014. https://doi.org/10.1002/mabi.202200014

233. Ullah, A., Jang, M., Khan, H., Choi, H. J., An, S., Kim, D., … Kim, G. M. (2021). Microneedle array with a pH-responsive polymer coating and its application in smart drug delivery for wound healing. *Sensors and Actuators B: Chemical*, *345*, 130441. https://doi.org/10.1016/j.snb.2021.130441

234. Wei, M., Jiang, Q., Niu, N., Dong, L., Wang, L., Chen, W., … Wang, J. (2019). *Reduction of biofilm in chronic wounds by antibacterial protease combined with silver dressing*. *Int J Clin Exp Med* (Vol. 12). Retrieved from www.ijcem.com/

235. Jian, H.-J., Anand, A., Lai, J.-Y., Unnikrishnan, B., Chang, H.-T., Harroun, S. G., & Huang, C.-C. (2023). In Situ Hybridization of Polymeric Curcumin to Arginine-Derived Carbon

Quantum Dots for Synergistic Treatment of Bacterial Infections. *ACS Applied Materials & Interfaces*, *15*(22), 26457–26471. https://doi.org/10.1021/acsami.3c04316

236. Jian, H.-J., Yu, J., Li, Y.-J., Unnikrishnan, B., Huang, Y.-F., Luo, L.-J., … Huang, C.-C. (2020). Highly adhesive carbon quantum dots from biogenic amines for prevention of biofilm formation. *Chemical Engineering Journal*, *386*, 123913. https://doi.org/10.1016/j.cej.2019.123913

237. Li, Y.-J., Wei, S.-C., Chu, H.-W., Jian, H.-J., Anand, A., Nain, A., … Lai, J.-Y. (2022). Poly-quercetin-based nanoVelcro as a multifunctional wound dressing for effective treatment of chronic wound infections. *Chemical Engineering Journal*, *437*, 135315. https://doi.org/10.1016/j.cej.2022.135315

238. Huanbutta, K., Sittikijyothin, W., & Sangnim, T. (2019). Development and Characterization of Bilayer Wound Healing Patch Nanofiber Fabricated by Electrospinning. *Journal of Nano Research*, *59*, 46–56. https://doi.org/10.4028/www.scientific.net/jnanor.59.46

239. Parham, S., Kharazi, A. Z., Bakhsheshi-Rad, H. R., Kharaziha, M., Ismail, A. F., Sharif, S., … Berto, F. (2022). Antimicrobial Synthetic and Natural Polymeric Nanofibers as Wound Dressing: A Review. *Advanced Engineering Materials*, *24*(6), 2101460. https://doi.org/10.1002/adem.202101460

240. Zamani, M., Prabhakaran, M. P., & Ramakrishna, S. (2013). Advances in drug delivery via electrospun and electrosprayed nanomaterials. *International journal of nanomedicine*, *8*, 2997–3017. https://doi.org/10.2147/IJN.S43575

241. García-Salinas, S., Evangelopoulos, M., Gámez-Herrera, E., Arruebo, M., Irusta, S., Taraballi, F., … Tasciotti, E. (2020). Electrospun anti-inflammatory patch loaded with essential oils for wound healing. *International Journal of Pharmaceutics*, *577*, 119067. https://doi.org/10.1016/j.ijpharm.2020.119067

242. Vitanza, L., Maccelli, A., Marazzato, M., Scazzocchio, F., Comanducci, A., Fornarini, S., … Longhi, C. (2019). Satureja montana L. essential oil and its antimicrobial activity alone or in combination with gentamicin. *Microbial Pathogenesis*, *126*, 323–331. https://doi.org/10.1016/j.micpath.2018.11.025

243. Pires, A. L. R., de Azevedo Motta, L., Dias, A. M. A., de Sousa, H. C., Moraes, Â. M., & Braga, M. E. M. (2018). Towards wound dressings with improved properties: Effects of poly(dimethylsiloxane) on chitosan-alginate films loaded with thymol and beta-carotene. *Materials Science and Engineering: C*, *93*, 595–605. https://doi.org/10.1016/j.msec.2018.08.005

244. Gámez, E., Mendoza, G., Salido, S., Arruebo, M., & Irusta, S. (2019). Antimicrobial Electrospun Polycaprolactone-Based Wound Dressings: An In Vitro Study About the Importance of the Direct Contact to Elicit Bactericidal Activity. *Advances in wound care*, *8*(9), 438–451. https://doi.org/10.1089/wound.2018.0893

245. Gámez, E., Elizondo-Castillo, H., Tascon, J., García-Salinas, S., Navascues, N., Mendoza, G., … Irusta, S. (2020). Antibacterial Effect of Thymol Loaded SBA-15 Nanorods Incorporated in PCL Electrospun Fibers. *Nanomaterials (Basel, Switzerland)*, *10*(4), 616. https://doi.org/10.3390/nano10040616

246. Gámez-Herrera, E., García-Salinas, S., Salido, S., Sancho-Albero, M., Andreu, V., Pérez, M., … Mendoza, G. (2020). Drug-eluting wound dressings having sustained release of antimicrobial compounds. *European Journal of Pharmaceutics and Biopharmaceutics*, *152*, 327–339. https://doi.org/10.1016/j.ejpb.2020.05.025

247. Garcia-Salinas, S., Gámez, E., Landa, G., Arruebo, M., Irusta, S., & Mendoza, G. (2020). Antimicrobial Wound Dressings against Fluorescent and Methicillin-Sensitive Intracellular Pathogenic Bacteria. *ACS Applied Materials & Interfaces*, *12*(46), 51302–51313. https://doi.org/10.1021/acsami.0c17043

248. García-Salinas, S., Gámez, E., Asín, J., de Miguel, R., Andreu, V., Sancho-Albero, M., … Arruebo, M. (2020). Efficiency of Antimicrobial Electrospun Thymol-Loaded Polycaprolactone Mats In Vivo. *ACS Applied Bio Materials*, *3*(5), 3430–3439. https://doi.org/10.1021/acsabm.0c00419

249. Wu, Y. C., Wu, G. X., Huang, H. H., & Kuo, S. M. (2019). Liposome-encapsulated farnesol accelerated tissue repair in third-degree burns on a rat model. *Burns*, *45*(5), 1139–1151. https://doi.org/10.1016/j.burns.2019.01.010

250. Kaneko, M., Togashi, N., Hamashima, H., Hirohara, M., & Inoue, Y. (2011). Effect of farnesol on mevalonate pathway of Staphylococcus aureus. *The Journal of Antibiotics*, *64*(8), 547–549. https://doi.org/10.1038/ja.2011.49

251. Oliveira, D., Borges, A., Saavedra, M. J., Borges, F., & Simões, M. (2022). Screening of Natural Molecules as Adjuvants to Topical Antibiotics to Treat Staphylococcus aureus from Diabetic Foot Ulcer Infections. *Antibiotics (Basel, Switzerland)*, *11*(5), 620. https://doi.org/10.3390/antibiotics11050620

252. Fernandes, R. A., Monteiro, D. R., Arias, L. S., Fernandes, G. L., Delbem, A. C. B., & Barbosa, D. B. (2018). Virulence Factors in Candida albicans and Streptococcus mutans Biofilms Mediated by Farnesol. *Indian journal of microbiology*, *58*(2), 138–145. https://doi.org/10.1007/s12088-018-0714-4

253. Barot, T., Rawtani, D., Kulkarni, P., Hussain, C. M., & Akkireddy, S. (2020). Physicochemical and biological assessment of flowable resin composites incorporated with farnesol loaded halloysite nanotubes for dental applications. *Journal of the Mechanical Behavior of Biomedical Materials*, *104*, 103675. https://doi.org/10.1016/j.jmbbm.2020.103675

254. Valcourt, C., Buyck, J. M., Grégoire, N., Couet, W., Marchand, S., & Tewes, F. (2021). Lipid Nanoparticles Loaded with Farnesol or Geraniol to Enhance the Susceptibility of E. coli MCR-1 to Colistin. *Pharmaceutics*, *13*(11), 1849. https://doi.org/10.3390/pharmaceutics13111849

255. Sousa, F. L., Horta, S., Santos, M., Rocha, S. M., & Trindade, T. (2012). Release behavior of trans,trans-farnesol entrapped in amorphous silica capsules. *Results in pharma sciences*, *2*, 52–56. https://doi.org/10.1016/j.rinphs.2012.07.001

256. Yenice Gürsu, B. (2020). Potential antibiofilm activity of farnesol-loaded poly(DL-lactide-co-glycolide) (PLGA) nanoparticles against Candida albicans. *Journal of Analytical Science and Technology*, *11*(1). https://doi.org/10.1186/s40543-020-00241-7

257. Nowacka, M., Kowalewska, A., & Kręgiel, D. (2020). Farnesol-Containing Macromolecular Systems for Antibiofilm Strategies. *Surfaces*, *3*(2), 197–210. https://doi.org/10.3390/surfaces3020015

258. Wu, G.-X., Wang, Y.-W., Wu, C.-S., Lin, Y.-H., Hung, C.-H., Huang, H.-H., & Kuo, S.-M. (2021). Therapeutic Efficacy of Sesquiterpene Farnesol in Treatment of Cutibacterium acnes-Induced Dermal Disorders. *Molecules*, *26*(18), 5723. https://doi.org/10.3390/molecules26185723

259. Rueda-Fernández, M., Melguizo-Rodríguez, L., Costela-Ruiz, V. J., de Luna-Bertos, E., Ruiz, C., Ramos-Torrecillas, J., & Illescas-Montes, R. (2022). Effect of the most common wound antiseptics on human skin fibroblasts. *Clinical and experimental dermatology*, *47*(8), 1543–1549. https://doi.org/10.1111/ced.15235

260. Jain, A. K., Agarwal, A., Agrawal, H., & Agrawal, G. P. (2012). Double-liposome-based dual-drug delivery system as vectors for effective management of peptic ulcer. *Journal of Liposome Research*, *22*(3), 205–214. https://doi.org/10.3109/08982104.2012.655284

261. Pietsch, F., Heidrich, G., Nordholt, N., & Schreiber, F. (2021). Prevalent Synergy and Antagonism Among Antibiotics and Biocides in Pseudomonas aeruginosa. *Frontiers in microbiology*, *11*, 615618. https://doi.org/10.3389/fmicb.2020.615618

262. Phillips, P. L., Yang, Q., Davis, S., Sampson, E. M., Azeke, J. I., Hamad, A., & Schultz, G. S. (2015). Antimicrobial dressing efficacy against mature *Pseudomonas aeruginosa* biofilm on porcine skin explants. *International Wound Journal*, *12*(4), 469–483. https://doi.org/10.1111/iwj.12142

263. Burgess, K., Li, H., Abo-Zeid, Y., Fatimah, & Williams, G. R. (2018). The Effect of Molecular Properties on Active Ingredient Release from Electrospun Eudragit Fibers. *Pharmaceutics*, *10*(3), 103. https://doi.org/10.3390/pharmaceutics10030103

264. Turanlı, Y., & Acartürk, F. (2021). Fabrication and characterization of budesonide loaded colon-specific nanofiber drug delivery systems using anionic and cationic polymethacrylate polymers. *Journal of Drug Delivery Science and Technology*, *63*, 102511. https://doi.org/10.1016/j.jddst.2021.102511

265. Ramamoorthy, M., & Rajiv, S. (2015). In-vitro release of fragrant l-carvone from electrospun poly(ϵ-caprolactone)/wheat cellulose scaffold. *Carbohydrate Polymers*, *133*, 328–336. https://doi.org/10.1016/j.carbpol.2015.07.015

266. Sun, L., Ouyang, J., Zeng, F., & Wu, S. (2022). An AIEgen-based oral-administration nanosystem for detection and therapy of ulcerative colitis via 3D-MSOT/NIR-II fluorescent imaging and inhibiting NLRP3 inflammasome. *Biomaterials*, *283*, 121468. https://doi.org/10.1016/j.biomaterials.2022.121468

267. Miranda-Calderon, L., Yus, C., Landa, G., Mendoza, G., Arruebo, M., & Irusta, S. (2022). Pharmacokinetic control on the release of antimicrobial drugs from pH-responsive electrospun wound dressings. *International Journal of Pharmaceutics*, *624*, 122003. https://doi.org/10.1016/j.ijpharm.2022.122003

268. Dikić, J., Lukić, I., Pajnik, J., Pavlović, J., Hrenović, J., & Rajić, N. (2021). Antibacterial activity of thymol/carvacrol and clinoptilolite composites prepared by supercritical

solvent impregnation. *Journal of Porous Materials*, *28*(5), 1577–1584. https://doi.org/10.1007/s10934-021-01107-y

269. Milovanovic, S., Markovic, D., Aksentijevic, K., Stojanovic, D. B., Ivanovic, J., & Zizovic, I. (2016). Application of cellulose acetate for controlled release of thymol. *Carbohydrate Polymers*, *147*, 344–353. https://doi.org/10.1016/j.carbpol.2016.03.093

270. Liu, X., Ma, X., Kun, E., Guo, X., Yu, Z., & Zhang, F. (2018). Influence of lidocaine forms (salt vs. freebase) on properties of drug–eudragit® L100-55 extrudates prepared by reactive melt extrusion. *International Journal of Pharmaceutics*, *547*(1–2), 291–302. https://doi.org/10.1016/j.ijpharm.2018.06.009

271. Daghighi, S., Sjollema, J., Harapanahalli, A., Dijkstra, R. J. B., van der Mei, H. C., & Busscher, H. J. (2015). Influence of antibiotic pressure on bacterial bioluminescence, with emphasis on Staphylococcus aureus. *International Journal of Antimicrobial Agents*, *46*(6), 713–717. https://doi.org/10.1016/j.ijantimicag.2015.09.007

272. Hall, C. W., & Mah, T.-F. (2017). Molecular mechanisms of biofilm-based antibiotic resistance and tolerance in pathogenic bacteria. *FEMS Microbiology Reviews*, *41*(3), 276–301. https://doi.org/10.1093/femsre/fux010

273. Aragón, J., Feoli, S., Irusta, S., & Mendoza, G. (2019). Composite scaffold obtained by electro-hydrodynamic technique for infection prevention and treatment in bone repair. *International Journal of Pharmaceutics*, *557*, 162–169. https://doi.org/10.1016/j.ijpharm.2018.12.002

274. Karpanen, T. J., Worthington, T., Hendry, E. R., Conway, B. R., & Lambert, P. A. (2008). Antimicrobial efficacy of chlorhexidine digluconate alone and in combination with eucalyptus oil, tea tree oil and thymol against planktonic and biofilm cultures of Staphylococcus epidermidis. *Journal of Antimicrobial Chemotherapy*, *62*(5), 1031–1036. https://doi.org/10.1093/jac/dkn325

275. Filoche, S. K., Soma, K., & Sissons, C. H. (2005). Antimicrobial effects of essential oils in combination with chlorhexidine digluconate. *Oral Microbiology and Immunology*, *20*(4), 221–225. https://doi.org/10.1111/j.1399-302x.2005.00216.x

276. Inoue, Y., Shiraishi, A., Hada, T., Hirose, K., Hamashima, H., & Shimada, J. (2004). The antibacterial effects of terpene alcohols on Staphylococcus aureus and their mode of action. *FEMS Microbiology Letters*, *237*(2), 325–331. https://doi.org/10.1111/j.1574-6968.2004.tb09714.x

277. Jabra-Rizk, M. A., Meiller, T. F., James, C. E., & Shirtliff, M. E. (2006). Effect of farnesol on Staphylococcus aureus biofilm formation and antimicrobial susceptibility. *Antimicrobial agents and chemotherapy*, *50*(4), 1463–1469. https://doi.org/10.1128/AAC.50.4.1463-1469.2006

278. Sato, T., Watanabe, T., Mikami, T., & Matsumoto, T. (2004). Farnesol, a Morphogenetic Autoregulatory Substance in the Dimorphic Fungus Candida albicans, Inhibits Hyphae Growth through Suppression of a Mitogen-Activated Protein Kinase Cascade. *Biological and Pharmaceutical Bulletin*, *27*(5), 751–752. https://doi.org/10.1248/bpb.27.751

279. Togashi, N., Hamashima, H., Shiraishi, A., Inoue, Y., & Takano, A. (2010). Antibacterial Activities Against*Staphylococcus aureus*of Terpene Alcohols With Aliphatic Carbon

Chains. *Journal of Essential Oil Research*, *22*(3), 263–269. https://doi.org/10.1080/10412905.2010.9700321

280. Koo, H. (2003). Inhibition of Streptococcus mutans biofilm accumulation and polysaccharide production by apigenin and tt-farnesol. *Journal of Antimicrobial Chemotherapy*, *52*(5), 782–789. https://doi.org/10.1093/jac/dkg449

281. Bandara, H. M. H. N., Herpin, M. J., Kolacny, D., Harb, A., Romanovicz, D., & Smyth, H. D. C. (2016). Incorporation of Farnesol Significantly Increases the Efficacy of Liposomal Ciprofloxacin against *Pseudomonas aeruginosa* Biofilms *in Vitro*. *Molecular Pharmaceutics*, *13*(8), 2760–2770. https://doi.org/10.1021/acs.molpharmaceut.6b00360

282. Yung, D. B. Y., Sircombe, K. J., & Pletzer, D. (2021). Friends or enemies? The complicated relationship between *Pseudomonas aeruginosa* and *Staphylococcus aureus*. *Molecular Microbiology*, *116*(1), 1–15. https://doi.org/10.1111/mmi.14699

283. Pastar, I., Nusbaum, A. G., Gil, J., Patel, S. B., Chen, J., Valdes, J., … Davis, S. C. (2013). Interactions of Methicillin Resistant Staphylococcus aureus USA300 and Pseudomonas aeruginosa in Polymicrobial Wound Infection. *PLoS ONE*, *8*(2), e56846. https://doi.org/10.1371/journal.pone.0056846

284. Pastar, I., Nusbaum, A. G., Gil, J., Patel, S. B., Chen, J., Valdes, J., … Davis, S. C. (2013). Interactions of Methicillin Resistant Staphylococcus aureus USA300 and Pseudomonas aeruginosa in Polymicrobial Wound Infection. *PLoS ONE*, *8*(2), e56846. https://doi.org/10.1371/journal.pone.0056846

285. Baldan, R., Cigana, C., Testa, F., Bianconi, I., De Simone, M., Pellin, D., … Cirillo, D. M. (2014). Adaptation of Pseudomonas aeruginosa in Cystic Fibrosis Airways Influences Virulence of Staphylococcus aureus In Vitro and Murine Models of Co-Infection. *PLoS ONE*, *9*(3), e89614. https://doi.org/10.1371/journal.pone.0089614

286. Biswas, L., Biswas, R., Schlag, M., Bertram, R., & Götz, F. (2009). Small-Colony Variant Selection as a Survival Strategy for *Staphylococcus aureus* in the Presence of *Pseudomonas aeruginosa*. *Applied and Environmental Microbiology*, *75*(21), 6910–6912. https://doi.org/10.1128/AEM.01211-09

287. Hoffman, L. R., Déziel, E., D'Argenio, D. A., Lépine, F., Emerson, J., McNamara, S., … Miller, S. I. (2006). Selection for *Staphylococcus aureus* small-colony variants due to growth in the presence of *Pseudomonas aeruginosa*. *Proceedings of the National Academy of Sciences*, *103*(52), 19890–19895. https://doi.org/10.1073/pnas.0606756104

288. Biswas, L., Biswas, R., Schlag, M., Bertram, R., & Götz, F. (2009). Small-Colony Variant Selection as a Survival Strategy for *Staphylococcus aureus* in the Presence of *Pseudomonas aeruginosa*. *Applied and Environmental Microbiology*, *75*(21), 6910–6912. https://doi.org/10.1128/AEM.01211-09

289. Leid, J. G., Willson, C. J., Shirtliff, M. E., Hassett, D. J., Parsek, M. R., & Jeffers, A. K. (2005). The Exopolysaccharide Alginate Protects *Pseudomonas aeruginosa* Biofilm Bacteria from IFN-γ-Mediated Macrophage Killing. *The Journal of Immunology*, *175*(11), 7512–7518. https://doi.org/10.4049/jimmunol.175.11.7512

290. DeLeon, S., Clinton, A., Fowler, H., Everett, J., Horswill, A. R., & Rumbaugh, K. P. (2014). Synergistic Interactions of Pseudomonas aeruginosa and Staphylococcus aureus in an *In Vitro* Wound Model. *Infection and Immunity*, *82*(11), 4718–4728. https://doi.org/10.1128/IAI.02198-14

291. Gounani, Z., Şen Karaman, D., Venu, A. P., Cheng, F., & Rosenholm, J. M. (2020). Coculture of P. aeruginosa and S. aureus on cell derived matrix - An in vitro model of biofilms in infected wounds. *Journal of Microbiological Methods*, *175*, 105994. https://doi.org/10.1016/j.mimet.2020.105994

292. Woods, P. W., Haynes, Z. M., Mina, E. G., & Marques, C. N. H. (2019). Maintenance of S. aureus in Co-culture With P. aeruginosa While Growing as Biofilms. *Frontiers in Microbiology*, *9*. https://doi.org/10.3389/fmicb.2018.03291

293. DeLeon, S., Clinton, A., Fowler, H., Everett, J., Horswill, A. R., & Rumbaugh, K. P. (2014). Synergistic Interactions of Pseudomonas aeruginosa and Staphylococcus aureus in an *In Vitro* Wound Model. *Infection and Immunity*, *82*(11), 4718–4728. https://doi.org/10.1128/IAI.02198-14

294. Kumar, A., & Ting, Y. P. (2015). Presence of <scp> *P* </scp> *seudomonas aeruginosa* influences biofilm formation and surface protein expression of <scp> *S* </scp> *taphylococcus aureus*. *Environmental Microbiology*, *17*(11), 4459–4468. https://doi.org/10.1111/1462-2920.12890

295. Hotterbeekx, A., Kumar-Singh, S., Goossens, H., & Malhotra-Kumar, S. (2017). In vivo and In vitro Interactions between Pseudomonas aeruginosa and Staphylococcus spp. *Frontiers in Cellular and Infection Microbiology*, *7*. https://doi.org/10.3389/fcimb.2017.00106

296. Lightbown, J. W., & Jackson, F. L. (1956). Inhibition of cytochrome systems of heart muscle and certain bacteria by the antagonists of dihydrostreptomycin: 2-alkyl-4-hydroxyquinoline *N* -oxides. *Biochemical Journal*, *63*(1), 130–137. https://doi.org/10.1042/bj0630130

297. Williams, P., & Cámara, M. (2009). Quorum sensing and environmental adaptation in Pseudomonas aeruginosa: a tale of regulatory networks and multifunctional signal molecules. *Current Opinion in Microbiology*, *12*(2), 182–191. https://doi.org/10.1016/j.mib.2009.01.005

298. Kessler, E., Safrin, M., Olson, J. C., & Ohman, D. E. (1993). Secreted LasA of Pseudomonas aeruginosa is a staphylolytic protease. *The Journal of biological chemistry*, *268*(10), 7503–8.

299. Billings, N., Ramirez Millan, M., Caldara, M., Rusconi, R., Tarasova, Y., Stocker, R., & Ribbeck, K. (2013). The Extracellular Matrix Component Psl Provides Fast-Acting Antibiotic Defense in Pseudomonas aeruginosa Biofilms. *PLoS Pathogens*, *9*(8), e1003526. https://doi.org/10.1371/journal.ppat.1003526

300. Serra, R., Grande, R., Butrico, L., Rossi, A., Settimio, U. F., Caroleo, B., … de Franciscis, S. (2015). Chronic wound infections: the role of *Pseudomonas aeruginosa* and *Staphylococcus aureus*. *Expert Review of Anti-infective Therapy*, *13*(5), 605–613. https://doi.org/10.1586/14787210.2015.1023291

301. Pouget, C., Dunyach-Remy, C., Magnan, C., Pantel, A., Sotto, A., & Lavigne, J.-P. (2022). Polymicrobial Biofilm Organization of Staphylococcus aureus and Pseudomonas aeruginosa in a Chronic Wound Environment. *International Journal of Molecular Sciences*, *23*(18), 10761. https://doi.org/10.3390/ijms231810761

302. Kirketerp-Møller, K., Jensen, P. Ø., Fazli, M., Madsen, K. G., Pedersen, J., Moser, C., … Bjarnsholt, T. (2008). Distribution, Organization, and Ecology of Bacteria in Chronic Wounds. *Journal of Clinical Microbiology*, *46*(8), 2717–2722. https://doi.org/10.1128/JCM.00501-08

303. Ahn, J.-M., Kassees, K., Lee, T.-K., Manandhar, B., & Yousif, A. M. (2017). 6.03 - Strategy and Tactics for Designing Analogs: Biochemical Characterization of the Large Molecules☆. In S. Chackalamannil, D. Rotella, & S. E. B. T.-C. M. C. I. I. I. Ward (Eds.), (pp. 66–115). Oxford: Elsevier. https://doi.org/https://doi.org/10.1016/B978-0-12-409547-2.12413-8

304. Rello, J., Solé-Lleonart, C., Rouby, J.-J., Chastre, J., Blot, S., Poulakou, G., … Roberts, J. A. (2017). Use of nebulized antimicrobials for the treatment of respiratory infections in invasively mechanically ventilated adults: a position paper from the European Society of Clinical Microbiology and Infectious Diseases. *Clinical Microbiology and Infection*, *23*(9), 629–639. https://doi.org/10.1016/j.cmi.2017.04.011

305. Schuster, A., Haliburn, C., Döring, G., & Goldman, M. H. (2013). Safety, efficacy and convenience of colistimethate sodium dry powder for inhalation (Colobreathe DPI) in patients with cystic fibrosis: a randomised study. *Thorax*, *68*(4), 344–350. https://doi.org/10.1136/thoraxjnl-2012-202059

306. Bergen, P. J., Li, J., Rayner, C. R., & Nation, R. L. (2006). Colistin Methanesulfonate Is an Inactive Prodrug of Colistin against *Pseudomonas aeruginosa*. *Antimicrobial Agents and Chemotherapy*, *50*(6), 1953–1958. https://doi.org/10.1128/aac.00035-06

307. Boisson, M., Grégoire, N., Cormier, M., Gobin, P., Marchand, S., Couet, W., & Mimoz, O. (2017). Pharmacokinetics of nebulized colistin methanesulfonate in critically ill patients. *Journal of Antimicrobial Chemotherapy*, *72*(9), 2607–2612. https://doi.org/10.1093/jac/dkx167

308. Tsuji, B. T., Pogue, J. M., Zavascki, A. P., Paul, M., Daikos, G. L., Forrest, A., … Kaye, K. S. (2019). International Consensus Guidelines for the Optimal Use of the Polymyxins: Endorsed by the American College of Clinical Pharmacy (ACCP), European Society of Clinical Microbiology and Infectious Diseases (ESCMID), Infectious Diseases Society of America (IDSA), International Society for Anti-infective Pharmacology (ISAP), Society of Critical Care Medicine (SCCM), and Society of Infectious Diseases Pharmacists (SIDP). *Pharmacotherapy: The Journal of Human Pharmacology and Drug Therapy*, *39*(1), 10–39. https://doi.org/10.1002/phar.2209

309. Miller, D. P., Tarara, T. E., & Weers, J. G. (2021). Targeting of Inhaled Therapeutics to the Small Airways: Nanoleucine Carrier Formulations. *Pharmaceutics*, *13*(11), 1855. https://doi.org/10.3390/pharmaceutics13111855

310. Dünnhaupt, S., Kammona, O., Waldner, C., Kiparissides, C., & Bernkop-Schnürch, A. (2015). Nano-carrier systems: Strategies to overcome the mucus gel barrier. *European*

Journal of Pharmaceutics and Biopharmaceutics, *96*, 447–453. https://doi.org/10.1016/j.ejpb.2015.01.022

311. Guichard, M.-J., Leal, T., & Vanbever, R. (2017). PEGylation, an approach for improving the pulmonary delivery of biopharmaceuticals. *Current Opinion in Colloid & Interface Science*, *31*, 43–50. https://doi.org/10.1016/j.cocis.2017.08.001

312. Schneider, C. S., Xu, Q., Boylan, N. J., Chisholm, J., Tang, B. C., Schuster, B. S., … Hanes, J. (2017). Nanoparticles that do not adhere to mucus provide uniform and long-lasting drug delivery to airways following inhalation. *Science Advances*, *3*(4). https://doi.org/10.1126/sciadv.1601556

313. D'Angelo, I., Casciaro, B., Miro, A., Quaglia, F., Mangoni, M. L., & Ungaro, F. (2015). Overcoming barriers in Pseudomonas aeruginosa lung infections: Engineered nanoparticles for local delivery of a cationic antimicrobial peptide. *Colloids and Surfaces B: Biointerfaces*, *135*, 717–725. https://doi.org/https://doi.org/10.1016/j.colsurfb.2015.08.027

314. Nanjo, Y., Ishii, Y., Kimura, S., Fukami, T., Mizoguchi, M., Suzuki, T., … Yamaguchi, K. (2013). Effects of slow-releasing colistin microspheres on endotoxin-induced sepsis. *Journal of Infection and Chemotherapy*, *19*(4), 683–690. https://doi.org/10.1007/s10156-012-0544-y

315. Shi, M., Kretlow, J. D., Nguyen, A., Young, S., Scott Baggett, L., Wong, M. E., … Mikos, A. G. (2010). Antibiotic-releasing porous polymethylmethacrylate constructs for osseous space maintenance and infection control. *Biomaterials*, *31*(14), 4146–4156. https://doi.org/https://doi.org/10.1016/j.biomaterials.2010.01.112

316. Ma, Z., Wang, J., Nation, R. L., Li, J., Turnidge, J. D., Coulthard, K., & Milne, R. W. (2009). Renal Disposition of Colistin in the Isolated Perfused Rat Kidney. *Antimicrobial Agents and Chemotherapy*, *53*(7), 2857–2864. https://doi.org/10.1128/aac.00030-09

317. Alejo, T., Uson, L., Landa, G., Prieto, M., Yus Argón, C., Garcia-Salinas, S., … Arruebo, M. (2021). Nanogels with High Loading of Anesthetic Nanocrystals for Extended Duration of Sciatic Nerve Block. *ACS applied materials & interfaces*, *13*(15), 17220–17235. https://doi.org/10.1021/acsami.1c00894

318. Gámez-Herrera, E., García-Salinas, S., Salido, S., Sancho-Albero, M., Andreu, V., Pérez, M., … Mendoza, G. (2020). Drug-eluting wound dressings having sustained release of antimicrobial compounds. *European Journal of Pharmaceutics and Biopharmaceutics*, *152*, 327–339. https://doi.org/10.1016/j.ejpb.2020.05.025

319. Gaspar, M. C., Sousa, J. J. S., Pais, A. A. C. C., Cardoso, O., Murtinho, D., Serra, M. E. S., … Olivier, J.-C. (2015). Optimization of levofloxacin-loaded crosslinked chitosan microspheres for inhaled aerosol therapy. *European Journal of Pharmaceutics and Biopharmaceutics*, *96*, 65–75. https://doi.org/10.1016/j.ejpb.2015.07.010

320. Lamy, B., Serrano, D. R., O'Connell, P., Couet, W., Marchand, S., Healy, A. M., & Tewes, F. (2019). Use of leucine to improve aerodynamic properties of ciprofloxacin-loaded maltose microparticles for inhalation. *European Journal of Pharmaceutical Research*, *1*(1), 02–11. https://doi.org/10.34154/2019-ejpr.01(01).pp-02-11/euraass

321. Tewes, F., Brillault, J., Gregoire, N., Olivier, J.-C., Lamarche, I., Adier, C., … Marchand, S. (2020). Comparison between Colistin Sulfate Dry Powder and Solution for Pulmonary Delivery. *Pharmaceutics*, *12*(6), 557. https://doi.org/10.3390/pharmaceutics12060557

322. Gobin, P., Lemaître, F., Marchand, S., Couet, W., & Olivier, J.-C. (2010). Assay of Colistin and Colistin Methanesulfonate in Plasma and Urine by Liquid Chromatography-Tandem Mass Spectrometry. *Antimicrobial Agents and Chemotherapy*, *54*(5), 1941–1948. https://doi.org/10.1128/aac.01367-09

323. Marchand, S., Gobin, P., Brillault, J., Baptista, S., Adier, C., Olivier, J.-C., … Couet, W. (2010). Aerosol Therapy with Colistin Methanesulfonate: a Biopharmaceutical Issue Illustrated in Rats. *Antimicrobial Agents and Chemotherapy*, *54*(9), 3702–3707. https://doi.org/10.1128/aac.00411-10

324. Gontijo, A. V. L., Brillault, J., Grégoire, N., Lamarche, I., Gobin, P., Couet, W., & Marchand, S. (2014). Biopharmaceutical Characterization of Nebulized Antimicrobial Agents in Rats: 1. Ciprofloxacin, Moxifloxacin, and Grepafloxacin. *Antimicrobial Agents and Chemotherapy*, *58*(7), 3942–3949. https://doi.org/10.1128/aac.02818-14

325. Boisson, M., Jacobs, M., Grégoire, N., Gobin, P., Marchand, S., Couet, W., & Mimoz, O. (2014). Comparison of Intrapulmonary and Systemic Pharmacokinetics of Colistin Methanesulfonate (CMS) and Colistin after Aerosol Delivery and Intravenous Administration of CMS in Critically Ill Patients. *Antimicrobial Agents and Chemotherapy*, *58*(12), 7331–7339. https://doi.org/10.1128/aac.03510-14

326. Torres, B. G. S., Awad, R., Marchand, S., Couet, W., & Tewes, F. (2019). In vitro evaluation of Pseudomonas aeruginosa chronic lung infection models: Are agar and calcium-alginate beads interchangeable? *European Journal of Pharmaceutics and Biopharmaceutics*, *143*, 35–43. https://doi.org/10.1016/j.ejpb.2019.08.006

327. Dubashynskaya, N. V, & Skorik, Y. A. (2020). Polymyxin Delivery Systems: Recent Advances and Challenges. *Pharmaceuticals*, *13*(5), 83. https://doi.org/10.3390/ph13050083

328. d'Angelo, I., Quaglia, F., & Ungaro, F. (2015). PLGA carriers for inhalation: where do we stand, where are we headed? *Therapeutic Delivery*, *6*(10), 1139–1144. https://doi.org/10.4155/tde.15.37

329. Muralidharan, P., Mallory, E., Malapit, M., Hayes, D., & Mansour, H. (2014). Inhalable PEGylated Phospholipid Nanocarriers and PEGylated Therapeutics for Respiratory Delivery as Aerosolized Colloidal Dispersions and Dry Powder Inhalers. *Pharmaceutics*, *6*(2), 333–353. https://doi.org/10.3390/pharmaceutics6020333

330. Mohammad, I. S., Hu, H., Yin, L., & He, W. (2019). Drug nanocrystals: Fabrication methods and promising therapeutic applications. *International Journal of Pharmaceutics*, *562*, 187–202. https://doi.org/10.1016/j.ijpharm.2019.02.045

331. Yus, C., Irusta, S., Sebastian, V., & Arruebo, M. (2020). Controlling Particle Size and Release Kinetics in the Sustained Delivery of Oral Antibiotics Using pH-Independent Mucoadhesive Polymers. *Molecular Pharmaceutics*, *17*(9), 3314–3327. https://doi.org/10.1021/acs.molpharmaceut.0c00408

332. Andreu, V., Larrea, A., Rodriguez-fernandez, P., & Alfaro, S. (2019). microparticles for the oral treatment of Mycobacterium tuberculosis, (July 2018).

333. Gheffar, C., Le, H., Jouenne, T., Schaumann, A., Corbière, A., Vaudry, D., … Karakasyan, C. (2020). Antibacterial Activity of Ciprofloxacin-Loaded Poly(lactic-co-glycolic acid)-Nanoparticles Against *Staphylococcus aureus*. *Particle & Particle Systems Characterization*, *38*(1). https://doi.org/10.1002/ppsc.202000253

334. In Pyo Park, P., & Jonnalagadda, S. (2006). Predictors of glass transition in the biodegradable poly-lactide and poly-lactide-co-glycolide polymers. *Journal of Applied Polymer Science*, *100*(3), 1983–1987. https://doi.org/10.1002/app.22135

335. Westerman, E. M., Le Brun, P. P. H., Touw, D. J., Frijlink, H. W., & Heijerman, H. G. M. (2004). Effect of nebulized colistin sulphate and colistin sulphomethate on lung function in patients with cystic fibrosis: a pilot study. *Journal of Cystic Fibrosis*, *3*(1), 23–28. https://doi.org/10.1016/j.jcf.2003.12.005

336. Dolovich, M. B., & Dhand, R. (2011). Aerosol drug delivery: developments in device design and clinical use. *The Lancet*, *377*(9770), 1032–1045. https://doi.org/10.1016/s0140-6736(10)60926-9

337. Edwards, D. A., Hanes, J., Caponetti, G., Hrkach, J., Ben-Jebria, A., Eskew, M. Lou, … Langer, R. (1997). Large Porous Particles for Pulmonary Drug Delivery. *Science*, *276*(5320), 1868–1872. https://doi.org/10.1126/science.276.5320.1868

338. Malamatari, M., Charisi, A., Malamataris, S., Kachrimanis, K., & Nikolakakis, I. (2020). Spray Drying for the Preparation of Nanoparticle-Based Drug Formulations as Dry Powders for Inhalation. *Processes*, *8*(7), 788. https://doi.org/10.3390/pr8070788

339. Scherließ, R., & Janke, J. (2021). Preparation of Poly-Lactic-Co-Glycolic Acid Nanoparticles in a Dry Powder Formulation for Pulmonary Antigen Delivery. *Pharmaceutics*, *13*(8), 1196. https://doi.org/10.3390/pharmaceutics13081196

340. Healy, A. M., Amaro, M. I., Paluch, K. J., & Tajber, L. (2014). Dry powders for oral inhalation free of lactose carrier particles. *Advanced Drug Delivery Reviews*, *75*, 32–52. https://doi.org/10.1016/j.addr.2014.04.005

341. Carvalho, T. C., Peters, J. I., & Williams, R. O. (2011). Influence of particle size on regional lung deposition – What evidence is there? *International Journal of Pharmaceutics*, *406*(1), 1–10. https://doi.org/https://doi.org/10.1016/j.ijpharm.2010.12.040

342. Klonne, D. R., Dodd, D. E., Losco, P. E., Troup, C. M., & Tyler, T. R. (1989). Two-Week Aerosol Inhalation Study on Polyethylene Glycol (Peg) 3350 in F-344 Rats. *Drug and Chemical Toxicology*, *12*(1), 39–48. https://doi.org/10.3109/01480548908999141

343. Mahri, S., Rondon, A., Wilms, T., Bosquillon, C., & Vanbever, R. (2021). Biodistribution and elimination pathways of PEGylated recombinant human deoxyribonuclease I after pulmonary delivery in mice. *Journal of Controlled Release*, *329*, 1054–1065. https://doi.org/10.1016/j.jconrel.2020.10.034

344. Popov, T. A., Åberg, N., Emberlin, J., Josling, P., Ilyina, N. I., Nikitin, N. P., & Church, M. (2017). Methyl-cellulose powder for prevention and management of nasal symptoms.

Expert Review of Respiratory Medicine, *11*(11), 885–892. https://doi.org/10.1080/17476348.2017.1375408

345. Operti, M. C., Bernhardt, A., Grimm, S., Engel, A., Figdor, C. G., & Tagit, O. (2021). PLGA-based nanomedicines manufacturing: Technologies overview and challenges in industrial scale-up. *International Journal of Pharmaceutics*, *605*, 120807. https://doi.org/10.1016/j.ijpharm.2021.120807

346. Tang, Y., Scher, H. B., & Jeoh, T. (2020). Industrially scalable complex coacervation process to microencapsulate food ingredients. *Innovative Food Science & Emerging Technologies*, *59*, 102257. https://doi.org/10.1016/j.ifset.2019.102257

347. Shepherd, S. J., Issadore, D., & Mitchell, M. J. (2021). Microfluidic formulation of nanoparticles for biomedical applications. *Biomaterials*, *274*, 120826. https://doi.org/10.1016/j.biomaterials.2021.120826

348. Li, C. L., Martini, L. G., Ford, J. L., & Roberts, M. (2005). The use of hypromellose in oral drug delivery. *Journal of Pharmacy and Pharmacology*, *57*(5), 533–546. https://doi.org/10.1211/0022357055957

349. Schindler, C. A., & Schuhardt, V. T. (1964). LYSOSTAPHIN: A NEW BACTERIOLYTIC AGENT FOR THE STAPHYLOCOCCUS. *Proceedings of the National Academy of Sciences*, *51*(3), 414–421. https://doi.org/10.1073/pnas.51.3.414

350. Wu, J. A., Kusuma, C., Mond, J. J., & Kokai-Kun, J. F. (2003). Lysostaphin Disrupts *Staphylococcus aureus* and *Staphylococcus epidermidis* Biofilms on Artificial Surfaces. *Antimicrobial Agents and Chemotherapy*, *47*(11), 3407–3414. https://doi.org/10.1128/AAC.47.11.3407-3414.2003

351. Dixon, R. E., Goodman, J. S., & Koenig, M. G. (1968). Lysostaphin: an enzymatic approach to staphylococcal disease. 3. Combined lysostaphin-methicillin therapy of established staphylococcal abscesses in mice. *The Yale journal of biology and medicine*, *41*(1), 62–8.

352. Placencia, F. X., Kong, L., & Weisman, L. E. (2009). Treatment of Methicillin-Resistant Staphylococcus aureus in Neonatal Mice: Lysostaphin Versus Vancomycin. *Pediatric Research*, *65*(4), 420–424. https://doi.org/10.1203/PDR.0b013e3181994a53

353. Bastos, M. do C. de F., Coutinho, B. G., & Coelho, M. L. V. (2010). Lysostaphin: A Staphylococcal Bacteriolysin with Potential Clinical Applications. *Pharmaceuticals*, *3*(4), 1139–1161. https://doi.org/10.3390/ph3041139

354. Shah, A., Mond, J., & Walsh, S. (2004). Lysostaphin-coated catheters eradicate Staphylococccus aureus challenge and block surface colonization. *Antimicrobial agents and chemotherapy*, *48*(7), 2704–7. https://doi.org/10.1128/AAC.48.7.2704-2707.2004

355. Ceotto-Vigoder, H., Marques, S. L. S., Santos, I. N. S., Alves, M. D. B., Barrias, E. S., Potter, A., … Bastos, M. C. F. (2016). Nisin and lysostaphin activity against preformed biofilm of *Staphylococcus aureus* involved in bovine mastitis. *Journal of Applied Microbiology*, *121*(1), 101–114. https://doi.org/10.1111/jam.13136

356. Kokai-Kun, J. F., Chanturiya, T., & Mond, J. J. (2007). Lysostaphin as a treatment for systemic Staphylococcus aureus infection in a mouse model. *Journal of Antimicrobial Chemotherapy*, *60*(5), 1051–1059. https://doi.org/10.1093/jac/dkm347

357. Desbois, A. P., Gemmell, C. G., & Coote, P. J. (2010). In vivo efficacy of the antimicrobial peptide ranalexin in combination with the endopeptidase lysostaphin against wound and systemic meticillin-resistant Staphylococcus aureus (MRSA) infections. *International Journal of Antimicrobial Agents*, *35*(6), 559–565. https://doi.org/10.1016/j.ijantimicag.2010.01.016

358. Johnson, C. T., Sok, M. C. P., Martin, K. E., Kalelkar, P. P., Caplin, J. D., Botchwey, E. A., & García, A. J. (2019). Lysostaphin and BMP-2 co-delivery reduces *S. aureus* infection and regenerates critical-sized segmental bone defects. *Science Advances*, *5*(5). https://doi.org/10.1126/sciadv.aaw1228

359. Climo, M. W., Patron, R. L., Goldstein, B. P., & Archer, G. L. (1998). Lysostaphin Treatment of Experimental Methicillin-Resistant *Staphylococcus aureus* Aortic Valve Endocarditis. *Antimicrobial Agents and Chemotherapy*, *42*(6), 1355–1360. https://doi.org/10.1128/AAC.42.6.1355

360. Dajcs, J. J., Thibodeaux, B. A., Girgis, D. O., Shaffer, M. D., Delvisco, S. M., & O'Callaghan, R. J. (2002). Immunity to lysostaphin and its therapeutic value for ocular MRSA infections in the rabbit. *Investigative ophthalmology & visual science*, *43*(12), 3712–6.

361. Xue, B., Zhang, C., Wang, Y., Wang, J., Zhang, J., Lu, M., … Huang, Q. (2014). A Novel Controlled-Release System for Antibacterial Enzyme Lysostaphin Delivery Using Hydroxyapatite/Chitosan Composite Bone Cement. *PLoS ONE*, *9*(12), e113797. https://doi.org/10.1371/journal.pone.0113797

362. Quickel, K. E., Selden, R., Caldwell, J. R., Nora, N. F., & Schaffner, W. (1971). Efficacy and Safety of Topical Lysostaphin Treatment of Persistent Nasal Carriage of *Staphylococcus aureus*. *Applied Microbiology*, *22*(3), 446–450. https://doi.org/10.1128/am.22.3.446-450.1971

363. Jayakumar, J., Kumar, V. A., Biswas, L., & Biswas, R. (2021). Therapeutic applications of lysostaphin against *Staphylococcus aureus*. *Journal of Applied Microbiology*, *131*(3), 1072–1082. https://doi.org/10.1111/jam.14985

364. Drayton, M., Kizhakkedath, J. N., & Strau, S. K. (2020). Towards robust delivery of antimicrobial peptides to combat bacterial resistance. *Molecules*, *25*(13), 1–24. https://doi.org/10.3390/molecules25133048

365. Daley, M. J., & Oldham, E. R. (1992). Lysostaphin: immunogenicity of locally administered recombinant protein used in mastitis therapy. *Veterinary Immunology and Immunopathology*, *31*(3–4), 301–312. https://doi.org/10.1016/0165-2427(92)90017-K

366. Johnson, C. T., Wroe, J. A., Agarwal, R., Martin, K. E., Guldberg, R. E., Donlan, R. M., … García, A. J. (2018). Hydrogel delivery of lysostaphin eliminates orthopedic implant infection by *Staphylococcus aureus* and supports fracture healing. *Proceedings of the National Academy of Sciences*, *115*(22). https://doi.org/10.1073/pnas.1801013115

367. Walsh, S., Shah, A., & Mond, J. (2003). Improved Pharmacokinetics and Reduced Antibody Reactivity of Lysostaphin Conjugated to Polyethylene Glycol. *Antimicrobial Agents and Chemotherapy*, *47*(2), 554–558. https://doi.org/10.1128/AAC.47.2.554-558.2003

368. Resch, G., Moreillon, P., & Fischetti, V. A. (2011). PEGylating a bacteriophage endolysin inhibits its bactericidal activity. *AMB Express*, *1*(1), 29. https://doi.org/10.1186/2191-0855-1-29

369. Huang, C.-Y., Hsu, J.-T., Chung, P.-H., Cheng, W. T.-K., Jiang, Y.-N., & Ju, Y.-T. (2013). Site-Specific N-Glycosylation of Caprine Lysostaphin Restricts its Bacteriolytic Activity Toward *Staphylococcus Aureus*. *Animal Biotechnology*, *24*(2), 129–147. https://doi.org/10.1080/10495398.2012.760469

370. Lin, X., He, J., Li, W., Qi, Y., Hu, H., Zhang, D., … Zhou, M. (2021). Lung-Targeting Lysostaphin Microspheres for Methicillin-Resistant *Staphylococcus aureus* Pneumonia Treatment and Prevention. *ACS Nano*, *15*(10), 16625–16641. https://doi.org/10.1021/acsnano.1c06460

371. Cui, F., Li, G., Huang, J., Zhang, J., Lu, M., Lu, W., … Huang, Q. (2011). Development of chitosan-collagen hydrogel incorporated with lysostaphin (CCHL) burn dressing with anti-methicillin-resistant Staphylococcus aureus and promotion wound healing properties. *Drug Delivery*, *18*(3), 173–180. https://doi.org/10.3109/10717544.2010.509363

372. Grishin, A. V., Shestak, N. V., Lavrova, N. V., Lyashchuk, A. M., Popova, L. I., Strukova, N. V., … Lunin, V. G. (2019). Fusion of Lysostaphin to an Albumin Binding Domain Prolongs Its Half-Life and Bactericidal Activity in the Systemic Circulation. *Molecules*, *24*(16), 2892. https://doi.org/10.3390/molecules24162892

373. Becker, S. C., Roach, D. R., Chauhan, V. S., Shen, Y., Foster-Frey, J., Powell, A. M., … Donovan, D. M. (2016). Triple-acting Lytic Enzyme Treatment of Drug-Resistant and Intracellular Staphylococcus aureus. *Scientific Reports*, *6*(1), 25063. https://doi.org/10.1038/srep25063

374. Wang, Z., Kong, L., Liu, Y., Fu, Q., Cui, Z., Wang, J., … Sun, J. (2018). A Phage Lysin Fused to a Cell-Penetrating Peptide Kills Intracellular Methicillin-Resistant Staphylococcus aureus in Keratinocytes and Has Potential as a Treatment for Skin Infections in Mice. *Applied and Environmental Microbiology*, *84*(12). https://doi.org/10.1128/AEM.00380-18

375. Röhrig, C., Huemer, M., Lorgé, D., Luterbacher, S., Phothaworn, P., Schefer, C., … Schmelcher, M. (2020). Targeting Hidden Pathogens: Cell-Penetrating Enzybiotics Eradicate Intracellular Drug-Resistant Staphylococcus aureus. *mBio*, *11*(2). https://doi.org/10.1128/mBio.00209-20

376. Hajiahmadi, F., Alikhani, M. Y., Shariatifar, H., Arabestani, M. R., & Ahmadvand, D. (2019). The bactericidal effect of lysostaphin coupled with liposomal vancomycin as a dual combating system applied directly on methicillin-resistant Staphylococcus aureus infected skin wounds in mice . *International Journal of Nanomedicine*, *Volume 14*, 5943–5955. https://doi.org/10.2147/IJN.S214521

377. Mohamad, N. R., Marzuki, N. H. C., Buang, N. A., Huyop, F., & Wahab, R. A. (2015). An overview of technologies for immobilization of enzymes and surface analysis techniques for immobilized enzymes. *Biotechnology & Biotechnological Equipment*, *29*(2), 205–220. https://doi.org/10.1080/13102818.2015.1008192

378. Blanco, D., & Alonso, M. J. (1998). Protein encapsulation and release from poly(lactide-co-glycolide) microspheres: effect of the protein and polymer properties and of the co-encapsulation of surfactants. *European Journal of Pharmaceutics and Biopharmaceutics*, *45*(3), 285–294. https://doi.org/10.1016/S0939-6411(98)00011-3

379. Ali, M., van Gent, M. E., de Waal, A. M., van Doodewaerd, B. R., Bos, E., Koning, R. I., … Nibbering, P. H. (2023). Physical and Functional Characterization of PLGA Nanoparticles Containing the Antimicrobial Peptide SAAP-148. *International Journal of Molecular Sciences*, *24*(3), 2867. https://doi.org/10.3390/ijms24032867

380. Lin, X., He, J., Li, W., Qi, Y., Hu, H., Zhang, D., … Zhou, M. (2021). Lung-Targeting Lysostaphin Microspheres for Methicillin-Resistant *Staphylococcus aureus* Pneumonia Treatment and Prevention. *ACS Nano*, *15*(10), 16625–16641. https://doi.org/10.1021/acsnano.1c06460

381. Zhang, G.-H., Hou, R.-X., Zhan, D.-X., Cong, Y., Cheng, Y.-J., & Fu, J. (2013). Fabrication of hollow porous PLGA microspheres for controlled protein release and promotion of cell compatibility. *Chinese Chemical Letters*, *24*(8), 710–714. https://doi.org/10.1016/j.cclet.2013.05.011

382. Huber, M. M., & Huber, T. W. (1989). Susceptibility of methicillin-resistant Staphylococcus aureus to lysostaphin. *Journal of Clinical Microbiology*, *27*(5), 1122–1124. https://doi.org/10.1128/jcm.27.5.1122-1124.1989

383. Hirt, H., & Gorr, S.-U. (2013). Antimicrobial Peptide GL13K Is Effective in Reducing Biofilms of Pseudomonas aeruginosa. *Antimicrobial Agents and Chemotherapy*, *57*(10), 4903–4910. https://doi.org/10.1128/AAC.00311-13

384. Wu, J. A., Kusuma, C., Mond, J. J., & Kokai-Kun, J. F. (2003). Lysostaphin disrupts Staphylococcus aureus and Staphylococcus epidermidis biofilms on artificial surfaces. *Antimicrobial agents and chemotherapy*, *47*(11), 3407–14. https://doi.org/10.1128/AAC.47.11.3407-3414.2003

385. Shah, A., Mond, J., & Walsh, S. (2004). Lysostaphin-Coated Catheters Eradicate *Staphylococccus aureus* Challenge and Block Surface Colonization. *Antimicrobial Agents and Chemotherapy*, *48*(7), 2704–2707. https://doi.org/10.1128/AAC.48.7.2704-2707.2004

386. Taş, B. A., Berksun, E., Taş, C. E., Ünal, S., & Ünal, H. (2022). Lysostaphin-Functionalized Waterborne Polyurethane/Polydopamine Coatings Effective against *S. Aureus* Biofilms. *ACS Applied Polymer Materials*, *4*(6), 4298–4305. https://doi.org/10.1021/acsapm.2c00254

387. Johnson, C. T., Wroe, J. A., Agarwal, R., Martin, K. E., Guldberg, R. E., Donlan, R. M., … García, A. J. (2018). Hydrogel delivery of lysostaphin eliminates orthopedic implant infection by *Staphylococcus aureus* and supports fracture healing. *Proceedings of the National Academy of Sciences*, *115*(22). https://doi.org/10.1073/pnas.1801013115

388. Kaplan, J. B. (2011). Antibiotic-Induced Biofilm Formation. *The International Journal of Artificial Organs*, *34*(9), 737–751. https://doi.org/10.5301/ijao.5000027

389. Nasser, A., Jahanbakhshi, S., Soltan Dallal, M. M., Banar, M., Sattari-Maraji, A., & Azimi, T. (2023). Staphylococcus aureus Dormancy: Waiting for Insurgency. *Current Pharmaceutical Biotechnology*, *24*(15), 1898–1915. https://doi.org/10.2174/1389201024666230411110002

390. Resch, A., Rosenstein, R., Nerz, C., & Götz, F. (2005). Differential Gene Expression Profiling of *Staphylococcus aureus* Cultivated under Biofilm and Planktonic Conditions. *Applied and Environmental Microbiology*, *71*(5), 2663–2676. https://doi.org/10.1128/AEM.71.5.2663-2676.2005

391. ISO 10993-5:2009 Biological evaluation of medical devices — Part 5: Tests for in vitro cytotoxicity. (n.d.).

392. Andreu, V., Larrea, A., Rodriguez-Fernandez, P., Alfaro, S., Gracia, B., Lucía, A., … Arruebo, M. (2019). Matryoshka-type gastro-resistant microparticles for the oral treatment of *Mycobacterium tuberculosis*. *Nanomedicine*, *14*(6), 707–726. https://doi.org/10.2217/nnm-2018-0258

393. Lacoma, A., Usón, L., Mendoza, G., Sebastián, V., Garcia-Garcia, E., Muriel-Moreno, B., … Prat, C. (2020). Novel intracellular antibiotic delivery system against *Staphylococcus aureus* : cloxacillin-loaded poly(<scp>d</scp> , <scp>l</scp> -lactide-co-glycolide) acid nanoparticles. *Nanomedicine*, *15*(12), 1189–1203. https://doi.org/10.2217/nnm-2019-0371

394. Schröder, A., Kland, R., Peschel, A., von Eiff, C., & Aepfelbacher, M. (2006). Live cell imaging of phagosome maturation in Staphylococcus aureus infected human endothelial cells: small colony variants are able to survive in lysosomes. *Medical Microbiology and Immunology*, *195*(4), 185–194. https://doi.org/10.1007/s00430-006-0015-0

395. Behzadi, S., Serpooshan, V., Tao, W., Hamaly, M. A., Alkawareek, M. Y., Dreaden, E. C., … Mahmoudi, M. (2017). Cellular uptake of nanoparticles: journey inside the cell. *Chemical Society Reviews*, *46*(14), 4218–4244. https://doi.org/10.1039/C6CS00636A

396. Barkema, H. W., Schukken, Y. H., & Zadoks, R. N. (2006). Invited Review: The Role of Cow, Pathogen, and Treatment Regimen in the Therapeutic Success of Bovine Staphylococcus aureus Mastitis. *Journal of Dairy Science*, *89*(6), 1877–1895. https://doi.org/10.3168/jds.S0022-0302(06)72256-1

397. Oldham, E. R., & Daley, M. J. (1991). Lysostaphin: Use of a Recombinant Bactericidal Enzyme as a Mastitis Therapeutic. *Journal of Dairy Science*, *74*(12), 4175–4182. https://doi.org/10.3168/jds.S0022-0302(91)78612-8

398. Yang, X., Xie, B., Peng, H., Shi, G., Sreenivas, B., Guo, J., … He, Y. (2021). Eradicating intracellular MRSA via targeted delivery of lysostaphin and vancomycin with mannose-modified exosomes. *Journal of Controlled Release*, *329*, 454–467. https://doi.org/10.1016/j.jconrel.2020.11.045

399. Anversa Dimer, F., de Souza Carvalho-Wodarz, C., Goes, A., Cirnski, K., Herrmann, J., Schmitt, V., … Lehr, C.-M. (2020). PLGA nanocapsules improve the delivery of

clarithromycin to kill intracellular Staphylococcus aureus and Mycobacterium abscessus. *Nanomedicine: Nanotechnology, Biology and Medicine*, *24*, 102125. https://doi.org/10.1016/j.nano.2019.102125

400. Leonard, H., Colodner, R., Halachmi, S., & Segal, E. (2018). Recent Advances in the Race to Design a Rapid Diagnostic Test for Antimicrobial Resistance. *ACS Sensors*, *3*(11), 2202–2217. https://doi.org/10.1021/acssensors.8b00900

401. Khan, Z. A., Siddiqui, M. F., & Park, S. (2019). Current and Emerging Methods of Antibiotic Susceptibility Testing. *Diagnostics*, *9*(2), 49. https://doi.org/10.3390/diagnostics9020049

402. Gao, J., Li, L., Ho, P.-L., Mak, G. C., Gu, H., & Xu, B. (2006). Combining Fluorescent Probes and Biofunctional Magnetic Nanoparticles for Rapid Detection of Bacteria in Human Blood. *Advanced Materials*, *18*(23), 3145–3148. https://doi.org/10.1002/adma.200601058

403. Jin, B., Wang, S., Lin, M., Jin, Y., Zhang, S., Cui, X., … Lu, T. J. (2017). Upconversion nanoparticles based FRET aptasensor for rapid and ultrasenstive bacteria detection. *Biosensors and Bioelectronics*, *90*, 525–533. https://doi.org/10.1016/j.bios.2016.10.029

404. Olson, M. E., King, J. M., Yahr, T. L., & Horswill, A. R. (2013). Sialic Acid Catabolism in Staphylococcus aureus. *Journal of Bacteriology*, *195*(8), 1779–1788. https://doi.org/10.1128/jb.02294-12

405. Plumbridge, J., & Vimr, E. (1999). Convergent Pathways for Utilization of the Amino Sugars *N*. *Journal of Bacteriology*, *181*(1), 47–54. https://doi.org/10.1128/jb.181.1.47-54.1999

406. Yokoyama, R., Itoh, S., Kamoshida, G., Takii, T., Fujii, S., Tsuji, T., & Onozaki, K. (2012). Staphylococcal Superantigen-Like Protein 3 Binds to the Toll-Like Receptor 2 Extracellular Domain and Inhibits Cytokine Production Induced by Staphylococcus aureus, Cell Wall Component, or Lipopeptides in Murine Macrophages. *Infection and Immunity*, *80*(8), 2816–2825. https://doi.org/10.1128/iai.00399-12

407. Jabłoński, A., Matczak, K., Koceva-Chyła, A., Durka, K., Steverding, D., Jakubiec-Krześniak, K., … Kowalski, K. (2017). Cymantrenyl-Nucleobases: Synthesis, Anticancer, Antitrypanosomal and Antimicrobial Activity Studies. *Molecules*, *22*(12), 2220. https://doi.org/10.3390/molecules22122220

408. Link, S., & El-Sayed, M. A. (1999). Size and Temperature Dependence of the Plasmon Absorption of Colloidal Gold Nanoparticles. *The Journal of Physical Chemistry B*, *103*(21), 4212–4217. https://doi.org/10.1021/jp984796o

409. Noguez, C. (2007). Surface Plasmons on Metal Nanoparticles: The Influence of Shape and Physical Environment. *The Journal of Physical Chemistry C*, *111*(10), 3806–3819. https://doi.org/10.1021/jp066539m

410. Lee, C., Wang, P., Gaston, M. A., Weiss, A. A., & Zhang, P. (2017). Plasmonics-Based Detection of Virus Using Sialic Acid Functionalized Gold Nanoparticles. *Methods in molecular biology (Clifton, N.J.)*, *1571*, 109–116. https://doi.org/10.1007/978-1-4939-6848-0_7

411. Lee, C., Gaston, M. A., Weiss, A. A., & Zhang, P. (2013). Colorimetric viral detection based on sialic acid stabilized gold nanoparticles. *Biosensors and Bioelectronics*, *42*(1), 236–241. https://doi.org/10.1016/j.bios.2012.10.067

412. Sakellari, G. I., Hondow, N., & Gardiner, P. H. E. (2020). Factors Influencing the Surface Functionalization of Citrate Stabilized Gold Nanoparticles with Cysteamine, 3-Mercaptopropionic Acid or l-Selenocystine for Sensor Applications. *Chemosensors*, *8*(3), 80. https://doi.org/10.3390/chemosensors8030080

413. Sarwar, M. S., Huang, Q., Ghaffar, A., Abid, M. A., Zafar, M. S., Khurshid, Z., & Latif, M. (2020). A Smart Drug Delivery System Based on Biodegradable Chitosan/Poly(allylamine hydrochloride) Blend Films. *Pharmaceutics*, *12*(2), 131. https://doi.org/10.3390/pharmaceutics12020131

414. Zhao, Z., Li, Q., Gong, J., Li, Z., & Zhang, J. (2020). A poly(allylamine hydrochloride)/poly(styrene sulfonate) microcapsule-coated cotton fabric for stimulus-responsive textiles. *RSC Advances*, *10*(30), 17731–17738. https://doi.org/10.1039/d0ra02474k

415. Zucolotto, V., Ferreira, M., Cordeiro, M. R., Constantino, C. J. L., Balogh, D. T., Zanatta, A. R., … Oliveira, O. N. (2003). Unusual Interactions Binding Iron Tetrasulfonated Phthalocyanine and Poly(allylamine hydrochloride) in Layer-by-Layer Films. *The Journal of Physical Chemistry B*, *107*(16), 3733–3737. https://doi.org/10.1021/jp027573d

416. Singh, P., Ren, X., He, Y., Wu, L., Wang, C., Li, H., … Zhang, J. (2020). Fabrication of β-cyclodextrin and sialic acid copolymer by single pot reaction to site specific drug delivery. *Arabian Journal of Chemistry*, *13*(1), 1397–1405. https://doi.org/10.1016/j.arabjc.2017.11.011

417. Bou Khalil, M., Kates, M., & Carrier, D. (2000). FTIR Study of the Monosialoganglioside GM_1 in Perdeuterated Dimyristoylglycerophosphocholine ($DMPC_{d54}$) Multilamellar Bilayers: Spectroscopic Evidence of a Significant Interaction between Ca^{2+} Ions and the Sialic Acid Moiety of GM_1. *Biochemistry*, *39*(11), 2980–2988. https://doi.org/10.1021/bi9923104

418. Elayabharathi, T., Vinoliya Josephine Mary, J., & Mary Mettilda Bai, S. (2020). Characterization of a novel O-acetyl sialic acid specific lectin from the hemolymph of the marine crab, Atergatis integerrimus (Lamarck, 1818). *Fish & Shellfish Immunology*, *106*, 1131–1138. https://doi.org/https://doi.org/10.1016/j.fsi.2020.07.039

419. Opota, O., Jaton, K., & Greub, G. (2015). Microbial diagnosis of bloodstream infection: towards molecular diagnosis directly from blood. *Clinical Microbiology and Infection*, *21*(4), 323–331. https://doi.org/10.1016/j.cmi.2015.02.005

420. Yagupsky, P., & Nolte, F. S. (1990). Quantitative aspects of septicemia. *Clinical microbiology reviews*, *3*(3), 269–279. https://doi.org/10.1128/CMR.3.3.269

421. Hay, A. D., Birnie, K., Busby, J., Delaney, B., Downing, H., Dudley, J., … Butler, C. C. (2016). The Diagnosis of Urinary Tract infection in Young children (DUTY): a diagnostic prospective observational study to derive and validate a clinical algorithm for the diagnosis of urinary tract infection in children presenting to primary care with an acute

illness. *Health technology assessment (Winchester, England)*, *20*(51), 1–294. https://doi.org/10.3310/hta20510

422. Volz, N., & Clayden, J. (2011). The Urea Renaissance. *Angewandte Chemie International Edition*, *50*(51), 12148–12155. https://doi.org/10.1002/anie.201104037

423. North, R. A., Watson, A. J. A., Pearce, F. G., Muscroft-Taylor, A. C., Friemann, R., Fairbanks, A. J., & Dobson, R. C. J. (2016). Structure and inhibition of *N* -acetylneuraminate lyase from methicillin-resistant *Staphylococcus aureus*. *FEBS Letters*, *590*(23), 4414–4428. https://doi.org/10.1002/1873-3468.12462

424. Müller, S., Wolf, A. J., Iliev, I. D., Berg, B. L., Underhill, D. M., & Liu, G. Y. (2015). Poorly Cross-Linked Peptidoglycan in MRSA Due to mecA Induction Activates the Inflammasome and Exacerbates Immunopathology. *Cell Host & Microbe*, *18*(5), 604–612. https://doi.org/10.1016/j.chom.2015.10.011

425. Mistretta, N., Brossaud, M., Telles, F., Sanchez, V., Talaga, P., & Rokbi, B. (2019). Glycosylation of Staphylococcus aureus cell wall teichoic acid is influenced by environmental conditions. *Scientific Reports*, *9*(1). https://doi.org/10.1038/s41598-019-39929-1

426. Khatua, B., Ghoshal, A., Bhattacharya, K., Mandal, C., Saha, B., Crocker, P. R., & Mandal, C. (2009). Sialic acids acquired by*Pseudomonas aeruginosa*are involved in reduced complement deposition and siglec mediated host-cell recognition. *FEBS Letters*, *584*(3), 555–561. https://doi.org/10.1016/j.febslet.2009.11.087

427. Thomas, G. H. (2016). Sialic acid acquisition in bacteria-one substrate, many transporters. *Biochemical Society transactions*, *44*(3), 760–765. https://doi.org/10.1042/BST20160056

428. Zhu, L., Li, S., Shao, X., Feng, Y., Xie, P., Luo, Y., … Xu, W. (2019). Colorimetric detection and typing of E. coli lipopolysaccharides based on a dual aptamer-functionalized gold nanoparticle probe. *Microchimica Acta*, *186*(2). https://doi.org/10.1007/s00604-018-3212-9

429. Shin, C., Lee, H. N., Ryu, J. S., & Chung, H. J. (2018). Rapid naked-eye detection of Gram-positive bacteria by vancomycin-based nano-aggregation. *RSC Advances*, *8*(44), 25094–25103. https://doi.org/10.1039/c8ra03540g

Appendix IV: Published scientific papers & participations in conferences

Published scientific papers

IV.1. "*Antimicrobial Wound Dressings against Fluorescent and Methicillin-Sensitive Intracellular Pathogenic Bacteria*". García-Salinas, S.; Gámez, E.; **Landa, G.**; Arruebo, M.; Irusta, S.; Mendoza, G. ACS Applied Materials & Interfaces, **2020**, 12 (46), 51302-51313, https://doi.org/10.1021/acsami.0c17043.

IV.2. "*Nanogels with High Loading of Anesthetic Nanocrystals for Extended Duration of Sciatic Nerve Block*". Alejo, T.; Usón, L.; **Landa, G.**; Prieto, M.; Yus, C.; García-Salinas, S.; de Miguel, R.; Rodríguez-Largo, A.; Irusta, S.; Sebastián, V.; Mendoza, G.; Arruebo, M. ACS Applied Materials & Interfaces, **2021**, 13 (15), 17220-17235, https://doi.org/10.1021/acsami.1c00894.

IV.3. "*Selective point-of-care detection of pathogenic bacteria using sialic acid functionalized gold nanoparticles*". **Landa, G.**; Miranda-Calderón, L.G.; Sebastián, V.; Irusta, S.; Mendoza, G.; Arruebo, M. Talanta, **2021**, Volume 234, 122644, https://doi.org/10.1016/j.talanta.2021.122644

IV.4. "*Pharmacokinetic control on the release of antimicrobial drugs from pH-responsive electrospun wound dressings*". Miranda-Calderón, L.G.; Yus, C.; **Landa, G.**; Mendoza, G.; Arruebo, M.; Irusta, S. International Journal of Pharmaceutics, **2022**, Volume 624, 122003, https://doi.org/10.1016/j.ijpharm.2022.122003.

IV.5. *Light activated pulsatile drug delivery for prolonged peripheral nerve block*". Prieto, M.; Usón, L.; García-Salinas, S.; Yus, C.; **Landa, G.**; Alejo, T.; Lujan, L.; Pérez, M.; Irusta, S.; Sebastián, V.; Mendoza, G.; Arruebo, M. Biomaterials, **2022**, Volume 283, 121453, https://doi.org/10.1016/j.biomaterials.2022.121453.

IV.6. *"Colistin-loaded aerosolizable particles for the treatment of bacterial respiratory infections*". **Landa, G.**; Alejo, T.; Sauzet, T.; Laroche, J.; Sebastián, V.; Tewes, F.; Arruebo, M. International Journal of Pharmaceutics, **2023**, Volume 635, 122732, https://doi.org/10.1016/j.ijpharm.2023.122732

IV.7. *"Real-time in vivo monitoring of the antimicrobial action of combination therapies in the management of infected topical wounds***"**. **Landa, G.**; Miranda-Calderón, L.G.; Gómez, A.; Pérez, M.; Sebastián, V.; Arruebo, M.; Lamarche, I.; Tewes, F.; Irusta, S.; Mendoza, G. International Journal of Pharmaceutics, **2023**, Volume 646, 123502, https://doi.org/10.1016/j.ijpharm.2023.123502

IV.8. "*Combinatorial wound dressings loaded with synergistic antibiotics in the treatment of chronic infected wounds*". Miranda-Calderón, L.G.; Yus, C.; Remírez de

Ganuza, C.; Paesa, M.; **Landa, G.**; Tapia, E.; Pérez, E.; Pérez, M.; Sebastián, V.; Irusta, S.; Mendoza, G.; Arruebo, M. Chemical Engineering Journal, **2023**, 146679, https://doi.org/10.1016/j.cej.2023.146679

IV.9. "*PLGA nanoparticle-encapsulated lysostaphin for the targeted treatment of Staphylococcus aureus Infections***"**. **Landa, G.**; Aguerri, L.; Irusta, S.; Mendoza, G.*; Arruebo, M. Journal of Colloid and Interface Science. Submitted.

Conference Presentations and Posters

IV.10. "*Optical detection based on gold nanocomposites for the real-time monitoring of pathogenic bacteria infection progression*". **Landa, G.**; Miranda-Calderón, L.G.; Mendoza, G.; Arruebo, M.; Irusta, S.; XIIIth Spanish-Portuguese Conference on Controlled Drug Delivery, Santiago de Compostela, Spain, **22-24th January 2020**.

IV.11. "*Selective point-of-care detection of pathogenic bacteria using sialic acid functionalized gold nanoparticles*". **Landa, G.**; Miranda-Calderón, L.G.; Sebastián, V.; Irusta, S.; Mendoza, G.; Arruebo, M. XXII Congreso Argentino de Fisicoquímica y Química Inorgánica, La Plata, Argentina, **19-29th April 2021**.

IV.12. "*On the development of polymicrobial biofilm models to understand the complex microbiome of infected chronic wounds and their successful antimicrobial treatment*". **Landa, G.**; Irusta, S.; Mendoza, G.; Arruebo, M.; Tewes, F. 32nd European Congress of Clinical Microbiology & Infectious Diseases, Lisbon, Portugal, **23-26th April 2022**.

IV.13. "*Development of nanostructured systems containing essential oils with antimicrobial activity for the treatment of topical infected wounds*". **Landa, G.**; Miranda-Calderón, L.G.; Sebastián, V.; Irusta, S.; Mendoza, G.; Arruebo, M.; Tewes, F. XXXIX Reunión Bienal de la Sociedad Española de Química, Zaragoza, España, **25-29th June 2023**.